Nature-inspired Biomaterials Discovery for Tendon Tissue Engineering

Document status and date:
Published: 09/06/2021

Document Version:
Publisher's PDF, also known as Version of Record (includes final page, issue and volume numbers)

Please check the document version of this publication:

• A submitted manuscript is the version of the article upon submission and before peer-review. There can be important differences between the submitted version and the official published version of record. People interested in the research are advised to contact the author for the final version of the publication, or visit the DOI to the publisher's website.
• The final author version and the galley proof are versions of the publication after peer review.
• The final published version features the final layout of the paper including the volume, issue and page numbers.

Link to publication

Download date: 04. Oct. 2023

Nature-inspired Biomaterials Discovery

for

Tendon Tissue Engineering

by

Aysegul Dede Eren

Eindhoven, 2021

Nature inspired biomaterials discovery for tendon tissue engineering

PhD Thesis, Eindhoven University of Technology, Eindhoven, the Netherlands

Cover design: Aysegul Dede Eren & Egemen Deniz Eren

Nature-inspired Biomaterials Discovery for Tendon Tissue Engineering

PROEFSCHRIFT

ter verkrijging van de graad van doctor aan de
Technische Universiteit Eindhoven, op gezag van de
rector magnificus prof.dr.ir. F.P.T. Baaijens, voor een
commissie aangewezen door het College voor
Promoties, in het openbaar te verdedigen
op donderdag 9 Juni 2021 om 16:00 uur

door

Aysegul Dede Eren

Geboren te Turkije

Dit proefschrift is goedgekeurd door de promotoren en de samenstelling van de promotiecommissie is als volgt:

Voorzitter: prof. Dr. Keita Ito

Promotor: prof. Dr. Jan de Boer

Copromotor: dr. Jasper Foolen

Leden: prof. Dr. Patricia Dankers

prof. Dr. Carlijn Bouten

prof. Dr. Cornelis Storm

prof. Dr. Stephen Badylak (University of Pittsburgh)

dr. Pieter Emans (Maastricht University)

Adviseurs: dr. Bert van Rietbergen

Table of Content

Chapter I

General Introduction

A recapitulation of tendon tissue, its physiology, histological and mechanical changes that tendon undergoes upon damage and current treatment techniques are introduced in this chapter. We briefly discuss tenocyte phenotype cycle and outline of this thesis.

Chapter I

A connecting hand: Tendon

Tendons are one of the most dense fibrous musculoskeletal connective tissues in the body. They surround the body by attaching muscles to bones and together with ligaments, which are another type of fibrous connective tissues attaching bones to bones, help joint stabilization, allow body movement, and provide stability [1,2].

Tendon structure

Overall, tendon tissue is hypocellular and hypovascular with a rich extracellular matrix. It is composed of a highly organized hierarchical organization of type I collagen. Triple-helical type I collagen molecules assemble into fibrils, followed by the formation of fibers and fascicles, which ultimately form a tendon unit as illustrated at Fig.1[2]. The diameter of collagen fibrils can vary between 50 nm to 200 nm and can be millimeters in length, and fiber diameter can be between 50 μm to 100 μm[3]. The collagen bundles are covered by layers called endotenon, epitenon and paratenon which allow lessor or no friction formation [4]. The organization of collagen fibers and their intermolecular cross-linking combined with non-collagenous ECM gives the tendon tensile strength. This mechanical strength is vital for the maintenance of tissue homeostasis by residing cells. Predominantly, tendons are loaded along their long axis and transmit muscle contraction forces to bones.
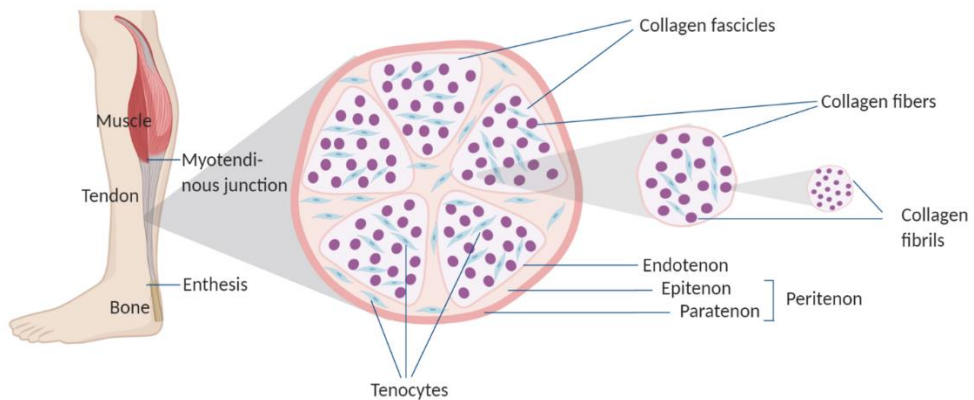
Figure 1. Schematic representation of the organization of tendon. *The hierarchical assembly of collagen fibrils to collagen fibers forms collagen fascicles, which ultimately form a tendon unit. Tendon fibroblasts, tenocytes, are placed between collagen fibers and possess elongated morphology.*

Biochemical and biomechanical properties of tendon

Collagen makes up the bulk of the structural components of both tendon and ligament ECM, (approximately 70-80 % of dry weight [5]) and of the different types of collagens, collagen type I is the most predominant collagen type in both tendons (approximately

95%) [3] and ligaments[6]. In addition to collagen type I, distribution of collagen type II, III, IV, V, and VI in tendons differs based on tendon's physiological state as well as spatial location[7] (e.g. type II in the cartilaginous zones, collagen type III in reticular fibers of blood vessels). In addition to the collagenous ECM, there is also a variety of non-collagenous proteins that contribute to tendon homeostasis. For instance, small leucine-rich proteoglycans (SLRPs) play essential roles in cell signaling, ECM assembly and turnover by interacting with collagens and fibronectin[8]. Decorin and biglycan are among the core ECM proteins and with a high affinity to bind collagen, they promote fibril arrangement and fibrillogenesis and ultimately tendon integrity [9]. Another vital ECM protein is tenascin-C which plays important roles in collagen fibril organization and healing [10]. Elastin, which makes up ~2 % of tendon ECM [8] provides mechanical strength and resistance.

Owing to its inherent function, as well as biochemical composition, tendons possess high mechanical strength, flexibility and due to its viscoelastic structure, tendons display stress relaxation and creep [11]. The physiological strain value for tendon is 4%, and upon stretch, tendon acts elastically and thus returns to the unloaded state without any damage occurring [11]. Above 4% of strain microscopic damages, and strains between 8% to 10% macroscopic damages take place[11]. Mechanical strength of tendon depends on several factors such as tissue thickness and collagen content. In general, an area of 1 cm^2 of tendon is able to bear 500 to 1000 kg and this is particularly important because, during jumping or weight-lifting, loads applied to tendon become very high [11]. Therefore, considering the amount and the rate of loads that are applied to them, tendon injuries are not the rarest type of injury among the musculoskeletal tissues.

Host cells: Tenocytes

The tendon ECM is produced by residing cells, predominantly tendon fibroblast also referred to as tenocytes. Tenocytes lie between collagen fibers in the longitudinal rows [12] and are morphologically spindle-shaped cells [13]. Their main function is to recognize and respond to biochemical and biomechanical changes in ECM, and in return, maintain tendon homeostasis. The mechanosensitive nature of tenocytes enabled them to respond to such changes by the formation and degradation of matrix proteins [13]. The ability to sense and give such responses is taking place via a process called mechanotransduction, which involves the interactions between extracellular matrix proteins, cell surface receptors, the internal actin cytoskeleton, and signaling molecules [13].

In addition to their spindle-shaped (elongated) morphology, several phenotypical gene/protein expression markers are also used to characterize tenocytes. Namely, 1) Scleraxis is a transcription factor and mainly detected in tendon cell precursor populations as well as in later stages, 2) Tenomodulin involved in cell proliferation,

differentiation, and collagen fibril maturation, 3) Tenascin-C, 4) Decorin, 5) Biglycan and 6) Collagen type I and type III are among the routinely used tenocyte markers. An important note is that many of these markers such as scleraxis, tenomodulin and collagen I are also used to identify ligament fibroblasts and overall elongated cell morphology is also used to identify the ligament fibroblasts [14].

Tenocytes produce their ECM based on environmental signals, and these environmental signals in return feed onto tenocyte phenotype. One of the important signals that tenocytes are exposed to are in the form of soluble factors such as growth factors. Transforming growth factor-β (TGF-β) is an important growth factor that contributes to tenocyte differentiation, migration, proliferation as well as tissue repair [15]. Similarly, insulin-like growth factor-1 (IGF-1), Platelet-derived growth factor (PDGF) and basic fibroblast growth factor (bFGF) are involved in the regulation of tenocyte function with respect to cell proliferation, migration and differentiation ultimately affecting tendon homeostasis and repair[15,16].

The overall mechanical signals (biomechanical, e.g. mechanical loading, shear stress, surface topography and biophysical, e.g. stiffness) are another element of the tenocyte function-ECM-tenocyte function cycle. In fact, mechanical loading is one of the vital forces for healthy tendon during development [13,17,18]. Mechanical forces at physiological levels are also required to maintain a healthy tendon homeostasis[13]. It is important to indicate that tenocytes can respond to mechanical stimulation as a signal that can lead to the production of different growth factors (e.g. TGF-β1) [17,19], which results in the synthesis of collagen type I [20], whose amount can indicate the health status of the tendon itself. These examples not only addresses the role of mechanical stimulation or growth factors on tenocyte function but also illustrates the dynamic conversations between tenocytes and signals exerting on them and ultimately how this mechanism contributes to tendon homeostasis. The disruptions in this conversation can lead to tissue injury and degeneration.

Tendon injuries and ruptures

Despite their mechanical strength and stability, tendon and ligament injuries and ruptures are still one of the most common musculoskeletal injury types worldwide. They make up of roughly 50% of the 33 million musculoskeletal injuries reported in United States [15] and approximately 30% of the general practice consultations about musculoskeletal pain are related to tendon-ligament disorders [2]. In the UK, soft tissue related disorders are the third most common rheumatologic condition [21]. The etiology of tendon injuries or ruptures is largely unknown yet it is agreed that several factors such as gender, age and physical condition can influence the prevalence of injuring tendons [22]. The prevalence of the occurrence of tendinopathy is 15% in elite athletes and 30–50% in people aged 60 [23].

Tendinopathy

There are different names to refer to the pathogenic process in tendon tissue. The term tendinitis refers to an acute inflammation to the tendon as a result of small ruptures[24]. Tendinosis is a structural and compositional time-dependent change that leads to tendon architectural degeneration of non-inflammatory origin[24]. Tendinopathy is an umbrella term to describe overall diseases/disorders/injuries in the tendon; naturally, tendinopathy will also be used throughout this chapter to refer to overall tendon injuries.

Tendinopathy can have multiple origins; interactions between intrinsic and extrinsic factors play an important role especially in chronic tendinopathy [25]. Chronic tendon injuries are caused by repetitive and excessive microtrauma overtime whilst acute tendon injuries occur after one overloading event yet it is also debated that acute tendon injuries have an underlying chronic impairment [26]. Overuse of tendons commonly damages patellar tendon, Achilles tendon, and underlie tennis elbow and rotator cuff injuries[13]. Additionally, several factors such as gender, age, the physical condition can influence the type and prevalence of tendinopathy [11]. Overall, excessive physical activity and loading of tendons are considered the number one cause of pathological degradation and when combined with intrinsic factors the risk of developing tendinopathy increase. There are different hypothesis to explain how excessive loads cause tendinopathy. For instance, during excessive loading, the formation of free radicals and oxidative stress due to perfusion of ischemia [27] and increased heat [11] leads tenocyte apoptosis, which ultimately results in tendon ECM degeneration. Another hypothesis is that the amount and the frequency of the loads lead to imbalance of the cytokines (e.g. interleukins, prostaglandin) and enzymes (e.g. matrix metalloproteinases (MMPs) and tissue inhibitors of metalloproteinases (TIMPs)), which are released by cells, that regulate the ECM network and remodelling [28].

Histological changes in tendinopathy

One of the most predominant microscopic changes is observed in the collagen fibers. Their orientation is disrupted and fiber diameter and overall density decline [29]. Additionally, collagen fibers display uneven and irregular crimping patterning as well as and increased waviness in contrast to the normal tight, parallel, bundled look in the healthy tendon [29]. Furthermore, increased neovascularization and interfibrillar glycosaminoglycans, hypercellularity, tissue degeneration (e.g. hypoxic, hyaline, fibrinoid and lipoid) and calcification are among the histological changes that tendinopathic tissue display [7]. Furthermore, the ratio of collagen type III to type I increases. Finally, the presence of tissue inflammation at the different stages of repetitive tendon microtrauma is seen [28,30,31].

In addition to the changes at the tissue level, at cellular level differences are observed. Firstly, tenocytes become more round with enlarged lysosomes, more proliferative and apoptotic [31]. These changes can also affect the function of gap junctions and ultimately alter cell-cell communication and nociception transmission [32]. Additionally, in tenocytes, the expression of inflammation markers and tissue degradation increase [33,34]. For instance, in an Achilles tendinopathy, decreased levels of MMP-3, 10 and TIMP-3; and increased levels of MMP-23 and MMP-1 was reported [35].

Tendon repair and regeneration

Healing starts upon tissue damage and it can take place via intrinsic and extrinsic mechanisms [36]. Repair via intrinsic mechanisms occurs via cell proliferation of the residing fibroblasts and synthesis of new ECM, repair via extrinsic mechanisms occurs via migration of inflammatory cells and fibroblasts from the surrounding tissues [37,38].

Tendon healing is composed of three stages: 1) Inflammation-immediate inflammatory response upon injury, 2) Repair-repair is characterized by an increase in fibroblasts and new ECM synthesis and 3) Remodeling [38]. However, depending on the severity of the injury, the remodeling process can take up to a year, and re-occurrence and re-injury is still a high risk [39]. Proper repair and tissue regeneration is not the strongest suit of tendon tissue: remodeling results in a structurally, biochemically and mechanically inferior tissue. In healed tendon, the collagen matrix becomes disorganized, the ratio or type II collagen to type I remains high which overall results in an impaired scar tissue [38]. This leads to a reduction in mobility, and increased pain and morbidity and makes tendons weaker and prone to re-ruptures and tears [37,38,40]. Re-rupture rate is especially higher in the rotator cuff (reported to be as high as 94% of the cases [41]), Achilles tendon [42] and patellar tendon[43].

Current treatments for tendinopathy

Pain management, physical therapy, corticosteroids and extracorporeal shock wave therapy are among the options for tendon injury treatments as the first line of treatment [21,38,44]. For some injuries, such as patellar tendinopathy corticosteroid therapy can also be used [45]. Surgery is often used as the last option when complications in tendon persist after non-operative options [45]. In the conventional surgical treatments, necrotic, degenerated tissue is removed and healthy ends sutured together [38]. However, the remaining tendon is generally shorter, plastically deformed and hence mechanically less strong compared to the healthy tendon. For this reason, commercial or non-commercial scaffolds are being used in the clinics for tendon repair. Among these, use of autografts is fairly limited due the availability and donor-site complications. In the United States in 2000, the treatment costs for tendon and ligament injuries were estimated to be $30 billion per year [46,47]. For this reason, allografts and xenografts became popular sources

of tendon grafts; however, the complications in provoking immune system and hence tissue rejection remains a the problem. Nonetheless, considering the demand in the market, different biological and synthetic scaffolds are also being produced in the last 25 years [47]. When the efficiency of the available tendon and ACL grafts was evaluated in 2009 by Chen and colleagues, the common problem was the weak mechanical properties and long-term biocompatibility [47]. Therefore, there is stills an unmet clinical need.

Future of tendinopathy treatments: meeting the unmet clinical need

Advances in molecular biology and imaging led us to develop new strategies to enhance tendon healing. In particular, tissue engineering and regenerative medicine opened new doors and broaden our horizons to engineer and produce new biomaterials. For tendon tissue what we know is that "The Biomaterial" should 1) Support host cell invasion, proliferation and differentiation, 2) Biochemically and biomechanically stable and similar to a healthy tendon, 3) Integrate with the host tendon without any complications.

However, finding the suitable biomaterial that checks out the marks mentioned above is only one side of the coin. We researchers are still discovering the underlying mechanisms behind the tendinopathy. To that extend, by benefiting from the advancements in materials science, in vitro systems are being engineered in order to mimic tendon with respect to surface topography, stiffness or mechanical stimulations. These systems will allow us to model tendinopathy in vitro by enabling research on the relation between tenocyte phenotype and its surrounding ECM.

Outline of this thesis

Understanding the story of the life of a tenocyte is one of the keys to producing useful materials for tendon tissue regeneration. Yet, the story of tenocyte is not very simple and not one line. When sitting in its beautiful collagen ECM, tenocytes receive signals from it and respond to these signals that result in the expression of certain genes that are translated into proteins. These proteins, in turn, function in the maintenance of the ECM that in return provides new or old signals back to the tenocyte (Fig. 2). Therefore, in the making of the graft to be used in tendon tissue regeneration, we should have an understanding on tenocyte shape and how it reflects its transcriptome and proteome that contributes to the formation of functional tendon ECM. The main focus of the research described in this thesis was to determine how cell shape is affected by its ECM, how the cell shape reflects its downstream signaling pathways in the regulation of genes and proteins and finally finding a biomaterial, which meets with the three criteria mentioned above, to be used in tendon tissue engineering. In order to achieve this, we turned to Mother Nature and inspired by it, when developing in vitro tools.

Chapter I

We use **chapter II** as a review article to describe the conversation between tenocyte phenotype with its ECM. Throughout **chapter II,** we use Fig. 2 as a tool to illustrate and highlight the relevance of cell shape to its phenotypical markers and we emphasize how the changes in vivo reflect tenocyte phenotype and vice versa. We ultimately describe the use and the relevance of the in vitro tools to study the causality between cell shape and its phenotypical markers via mechanotransduction pathways, namely integrin signaling and cytoskeletal organizations. We believe that this information is very vital to generate new in vivo and in vitro approaches on tendon healing and regeneration. To follow up that, in **chapter III,** as a review article, we stressed the importance of using omics tools to study cell-biomaterial interactions. Considering the big amount of transcriptomic and proteomics data, which allow looking to the problem from a broader picture, we believe that the paradigm shift from traditional experimental sciences to omics-based sciences will help us to produce better understanding and solutions for tendinopathy.

The history of the research on the relation between cell morphology, its phenotypical markers and their ECM goes back to 1970s. However, for the last 40 years, this relation remains a mystery in many ways. Therefore, we use **chapter IV** and **chapter V** to elaborate on this phenomenon in tenocytes. We first identified the shape parameters that are used to define an "elongated cell", namely aspect ratio or eccentricity, compactness and solidity, and characterized the tenocyte cell shape during in vitro culture. In **chapter IV, we** show that via self-agglomeration of collagen molecules during evaporation, three different surface topographies, namely isotropic, concentric and radial, on the same samples are formed. We used this approach to explore the effect of different surface topographies on cell shape. We found that tenocytes align between concentric ring and display increase cell elongation, compared to radial and isotropic regions. We further investigated the effect of the topography on tenocyte proliferation and found no significant difference despite a decreasing trend in the isotropic region. Self-agglomerated collagens bear great potential to study the effect of biomechanics with respect to surface topography pushing cells to different shapes, but also allow investigating the role of biochemistry due to the presence of collagen itself in the substrate. In **chapter V**, we dive into the relationship between cell shape and phenotypical markers more in detail. In this chapter, we first show that tenocytes lose their elongated shape and phenotypical markers decline during in vitro subculture. In order to study the relation between tenocyte shape and phenotypical markers, we produced a tendon-mimetic material that can push tenocytes to an elongated shape and further stop and even promote the expression of tenocyte transcription factor SCX that is lost during in vitro subculture. In **chapter V**, we indicate that the increased levels of SCX are positively correlated with elongated shape, making our point on cell shape-

phenotypical marker relation, and ultimately indicating the relevance of "tenocyte phenotype cycle" (Fig. 2).
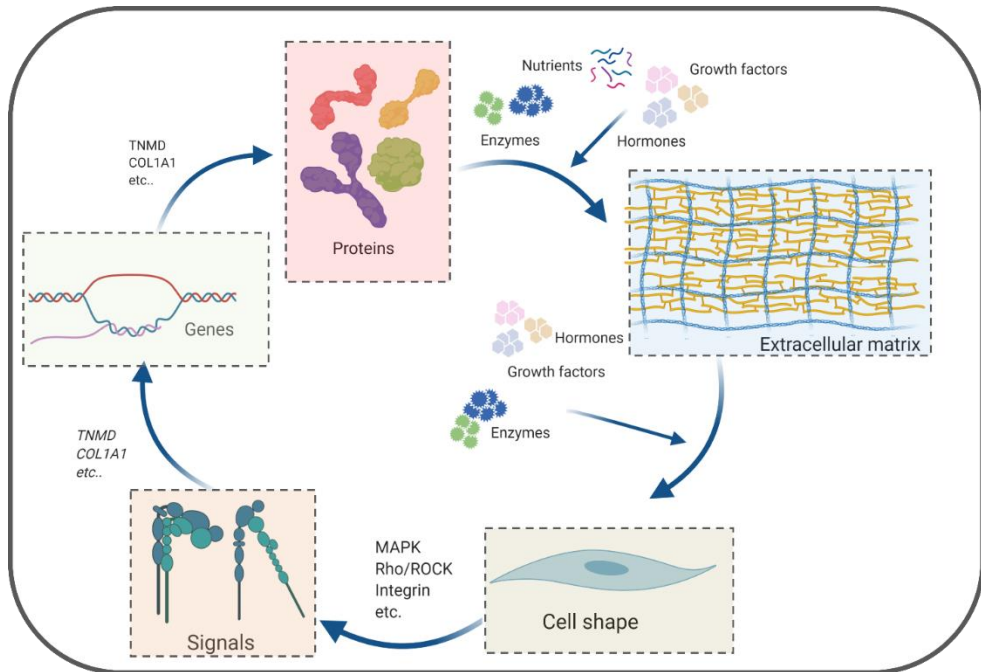
Figure 2. Tenocyte phenotype cycle. *Elongated shaped tenocytes produce signals such as Mitogen-activated protein kinase (MAPK), Rho/ Rho-associated protein kinase (ROCK) or integrin, resulting in the transcription of marker genes. This led to the translation of proteins involved in the regulation/formation of functional tendon extracellular matrix (ECM), enzymes, growth factors, hormones. Ultimately, tendon ECM effects the tenocyte shape and network continues in this fashion.*

In **chapter VI**, we delve deeper into defining the influence of cell shape on the regulation of integrin signaling and focal adhesion maturation. To investigate this, we manipulated the shape of human mesenchymal stem cells with two approaches; one is using ultraviolet photo patterning as a method to create adhesive islands, the other is soft embossing to generate surface topography. By using these methods, we performed a screen to correlate cell area with focal adhesion number and size per cell. In order to support our reasoning on the involvement of focal adhesions and integrin signaling, we took a transcriptomics approach to compare the differentially expressed genes and the pathways that they regulate between cells on flat surface and topographies. We further explored the same phenomena to explore the link between focal adhesion maturation

and cell area in both human mesenchymal stem cells and tenocytes. The results reported in **chapter VI** present important insights into how focal adhesion maturation is affected by the cell area.

Finding a biomaterial to be used in tendon regeneration has attracted many researchers due to the necessity of such material in clinics. Currently, available materials that are used in clinics are either not of tendon origin (such as collagen obtained from the dermis), or obtained as allografts or autografts. However, in research, the potential of other materials such as silk fibers, collagen electrospun fibers and decellularized tissues has been demonstrated in *in vivo* animal experiments. Of these options, decellularization, which is a method to remove the cellular component of a given tissue and using the remaining intact ECM as a graft material, steps forward because the source tissue can be a tendon, and its cell is obtained from animals, therefore increasing the availability of the tissue once ready for clinics. Since decellularized tissues have been used in regenerative medicine for the past 25 years, in **chapter VII,** we used decellularization as a tool to produce tendons that can be used in tendon regenerative medicine. Our results showed that the decellularization method that we present in **chapter VII** possess biomechanical and biochemical properties of a native tendon, and support cell proliferation in vitro. We also display its potential in *in vivo* by implanting it into rabbit knee. After six weeks, the decellularized tendon was invaded with host cells and the animal did not display any signs of lameness.

However, when we look around, we can observe that nature offers many more engineering geniuses. For instance in the world of plants, in addition to the current applications in materials science, a diverse set of material properties is hidden and waiting to be explored for tissue engineering and regenerative medicine applications. Therefore, in **chapter VIII**, we discuss the current approach on tissue engineering and emphasize that there is more to be inspired and use, such as plant-based scaffolds.

References

1. Benjamin, M., and Ralphs, J.R. Tendons and ligaments - An overview. Histol Histopathol. **12**, 1135, 1997.

2. Nourissat, G., Berenbaum, F., and Duprez, D. Tendon injury: From biology to tendon repair. Nat Rev Rheumatol . Nature Publishing Group, **11**, 223, 2015.

3. Screen, H.R.C., Berk, D.E., Kadler, K.E., Ramirez, F., and Young, M.F. Tendon functional extracellular matrix. J Orthop Res. **33**, 793, 2015.

4. Zheng, Z., Lipman, K., Wang, C., Ting, K., and Soo, C. Tendinopathy: injury, repair, and current exploration. Drug Des Devel Ther. **Volume 12**, 591, 2018.

5. Rumian, A.P., Wallace, A.M., and Birch, H.L. Tendons and Ligaments Are Anatomically Distinct But Overlap in Molecular and Morphological Features— A Comparative Study in an Ovine Model. Orthop Res Soc. **25**, 1121, 2007.

6. C. B. Frank. Ligament structure, physiology and function. J Musculoskel Neuron Interact. **4**, 199, 2004.

7. Fan, W., Michael, N., and Denitsa, D. Tendon injuries: basic science and new repair proposals. Gen Orthop. **2**, 211, 2017.

8. Taye, N., Karoulias, S.Z., and Hubmacher, D. The "other" 15–40%: The Role of Non-Collagenous Extracellular Matrix Proteins and Minor Collagens in Tendon. J Orthop Res. John Wiley & Sons, Ltd, **38**, 23, 2020.

9. Orgel, J.P.R.O., Eid, A., Antipova, O., Bella, J., and Scott, J.E. Decorin core protein (decoron) shape complements collagen fibril surface structure and mediates its binding. PLoS One. **4**, 2009.

10. Riley, G.P., Harrall, R.L., Cawston, T.E., Hazleman, B.L., and Mackie, E.J. Tenascin-C and human tendon degeneration. Am J Pathol. **149**, 933, 1996.

11. Sharma, P., and Maffulli, N. Tendon injury and tendinopathy: Healing and repair. J Bone Jt Surg - Ser A. **87**, 187, 2005.

12. Kjær, M. Role of Extracellular Matrix in Adaptation of Tendon and Skeletal Muscle to Mechanical Loading. Physiol Rev. **84**, 649, 2004.

13. Galloway, M.T., Lalley, A.L., and Shearn, J.T. The role of mechanical loading in tendon development, maintenance, injury, and repair. J Bone Jt Surg - Ser A. **95**, 1620, 2013.

14. Ban, H.Y., Shin, J.W., Chun, S.I., Kang, Y.G., Wu, Y., Kim, J.E., et al. Distinguishing tendon and ligament fibroblasts based on 1H nuclear magnetic resonance spectroscopy. Tissue Eng Regen Med. **13**, 677, 2016.

15. James, R., Kesturu, G., Balian, G., and Chhabra, A.B. Tendon: Biology, Biomechanics, Repair, Growth Factors, and Evolving Treatment Options. J

Hand Surg Am. **33**, 102, 2008.

16. Molloy, T., Wang, Y., and Murrell, G.A.C. The roles of growth factors in tendon and ligament healing. Sport Med. **33**, 381, 2003.

17. Henderson, J.H., and Carter, D.R. Mechanical induction in limb morphogenesis: The role of growth-generated strains and pressures. Bone. **31**, 645, 2002.

18. Kalson, N.S., Holmes, D.F., Herchenhan, A., Lu, Y., Starborg, T., and Kadler, K.E. Slow stretching that mimics embryonic growth rate stimulates structural and mechanical development of tendon-like tissue in vitro. Dev Dyn. **240**, 2520, 2011.

19. Vermeulen, S., Roumans, N., Honig, F., Carlier, A., Hebels, D., Dede Eren, A., et al. Mechanotransduction is a context-dependent activator of TGF-β signaling in mesenchymal stem cells. Biomaterials. **259**, 2020.

20. Heinemeier, K., Langberg, H., Olesen, J.L., and Kjaer, M. Role of TGF-β1 in relation to exercise-induced type I collagen synthesis in human tendinous tissue. J Appl Physiol. **95**, 2390, 2003.

21. Riley, G. Tendinopathy - From basic science to treatment. Nat Clin Pract Rheumatol. **4**, 82, 2008.

22. Maganaris, C.N., Narici, M. V., Almekinders, L.C., and Maffulli, N. Biomechanics and Pathophysiology of Overuse Tendon Injuries. Sport Med. **34**, 1005, 2012.

23. Ilaltdinov, A.W., Gong, Y., Leong, D.J., Gruson, K.I., Zheng, D., Fung, D.T., et al. Advances in the development of gene therapy, noncoding RNA, and exosome-based treatments for tendinopathy. Ann N Y Acad Sci. 1, 2020.

24. Bass, E. Tendinopathy: Why the difference between tendinitis and tendinosis matters. Int J Ther Massage Bodyw Res Educ Pract. **5**, 14, 2012.

25. Seitz, A.L., McClure, P.W., Finucane, S., Boardman, N.D., and Michener, L.A. Mechanisms of rotator cuff tendinopathy: Intrinsic, extrinsic, or both? Clin Biomech. Elsevier Ltd, **26**, 1, 2011.

26. Maganaris, C.N., Narici, M. V, Almekinders, L.C., and Maffulli, N. Biomechanics and Pathophysiology of Overuse Tendon Injuries. Sport Med . **34**, 1005, 2012.

27. Wang, M.X., Wei, A., Yuan, J., Clippe, A., Bernard, A., Knoops, B., et al. Antioxidant enzyme peroxiredoxin 5 is upregulated in degenerative human tendon. Biochem Biophys Res Commun. **284**, 667, 2001.

28. Battery, L., and Maffulli, N. Inflammation in overuse tendon injuries. Sports Med Arthrosc. **19**, 213, 2011.

29. Maffulli, N., Wong, J., and Almekinders, L.C. Types and epidemiology of

tendinopathy. Clin Sports Med. **22**, 675, 2003.

30. D'Addona, A., Maffulli, N., Formisano, S., and Rosa, D. Inflammation in tendinopathy. Surgeon . Elsevier Ltd, **15**, 297, 2017.

31. Millar, N.L., Murrell, G.A.C., and Mcinnes, I.B. Inflammatory mechanisms in tendinopathy - towards translation. Nat Rev Rheumatol . Nature Publishing Group, **13**, 110, 2017.

32. Rio, E., Moseley, L., Purdam, C., Samiric, T., Kidgell, D., Pearce, A.J., et al. The pain of tendinopathy: Physiological or pathophysiological? Sport Med. **44**, 9, 2014.

33. Dean, B.J.F., Dakin, S.G., Millar, N.L., and Carr, A.J. Review: Emerging concepts in the pathogenesis of tendinopathy. Surgeon . Elsevier Ltd, **15**, 349, 2017.

34. Ireland, D., Harrall, R., Curry, V., Holloway, G., Hackney, R., Hazleman, B., et al. Multiple changes in gene expression in chronic human Achilles tendinopathy. Matrix Biol. **20**, 159, 2001.

35. Jones, G.C., Corps, A.N., Pennington, C.J., Clark, I.M., Edwards, D.R., Bradley, M.M., et al. Expression profiling of metalloproteinases and tissue inhibitors of metalloproteinases in normal and degenerate human Achilles tendon. Arthritis Rheum. **54**, 832, 2006.

36. Liu, C.-F., Aschbacher-Smith, L., Barthelery, N.J., Dyment, N., Butler, D., and Wylie, C. What we should know before using tissue engineering techniques to repair injured tendons: a developmental biology perspective. Tissue Eng Part B Rev. **17**, 165, 2011.

37. Keller, T.C., Hogan, M. V, Kesturu, G., James, R., Balian, G., and Chhabra, A.B. Growth/differentiation factor-5 modulates the synthesis and expression of extracellular matrix and cell-adhesion-related molecules of rat Achilles tendon fibroblasts. Connect Tissue Res. England, **52**, 353, 2011.

38. Walden, G., Liao, X., Donell, S., Raxworthy, M.J., Riley, G.P., and Saeed, A. A Clinical, Biological, and Biomaterials Perspective into Tendon Injuries and Regeneration. Tissue Eng Part B Rev . **23**, 44, 2017.

39. Gajhede-Knudsen, M., Ekstrand, J., Magnusson, H., and Maffulli, N. Recurrence of Achilles tendon injuries in elite male football players is more common after early return to play: an 11-year follow-up of the UEFA Champions League injury study. Br J Sports Med. **47**, 763 LP, 2013.

40. Correia, S.I., Pereira, H., Silva-Correia, J., Van Dijk, C.N., Espregueira-Mendes, J., Oliveira, J.M., et al. Current concepts: tissue engineering and regenerative medicine applications in the ankle joint. J R Soc Interface. **11**, 20130784, 2014.

41. Kim, H.M., Galatz, L.M., Das, R., Havlioglu, N., Rothermich, S.Y., and

Thomopoulos, S. The role of transforming growth factor beta isoforms in tendon-to-bone healing. Connect Tissue Res. England, **52**, 87, 2011.

42. Yammine, K., and Assi, C. Efficacy of repair techniques of the Achilles tendon: A meta-analysis of human cadaveric biomechanical studies. Foot . Elsevier Ltd, **30**, 13, 2017.

43. Mine, T., Tanaka, H., Taguchi, T., Ihara, K., Moriwaki, T., and Kawai, S. Patellar tendon rupture and marked joint instability after total knee arthroplasty. Arch Orthop Trauma Surg. **124**, 267, 2004.

44. Andres, B.M., and Murrell, G.A.C. Treatment of tendinopathy: What works, what does not, and what is on the horizon. Clin Orthop Relat Res. **466**, 1539, 2008.

45. Everhart, J.S., Cole, D., Sojka, J.H., Higgins, J.D., Magnussen, R.A., Schmitt, L.C., et al. Treatment Options for Patellar Tendinopathy: A Systematic Review. Arthrosc - J Arthrosc Relat Surg. Arthroscopy Association of North America, **33**, 861, 2017.

46. Meislin, R.J., Sperling, J.W., and Stitik, T.P. Persistent shoulder pain: epidemiology, pathophysiology, and diagnosis. Am J Orthop (Belle Mead NJ). United States, **34**, 5, 2005.

Chapter II

The loop of phenotype: dynamic reciprocity links tenocyte morphology to tendon tissue homeostasis

C ells and their surrounding extracellular matrix (ECM) are engaged in dynamic reciprocity to maintain tissue homeostasis: cells deposit ECM, which in turn presents the signals that define cell identity. This loop of phenotype is obvious for biochemical signals, such as collagens, which are produced by and presented to cells, but the role of biomechanical signals is also increasingly recognised. In addition, cell shape goes hand in hand with cell function and tissue homeostasis. Aberrant cell shape and ECM is seen in pathological conditions, and control of cell shape in micro-fabricated platforms disclose the causal relationship between cell shape and cell function, often mediated by mechanotransduction. In this manuscript, we discuss the loop of phenotype for tendon tissue homeostasis. We describe cell shape and ECM organisation in normal and diseased tissue, how ECM composition influences tenocyte shape, and how that leads to the activation of signal transduction pathways and ECM deposition. We further describe the use of technologies to control cell shape to elucidate the link between cell shape and its phenotypical markers and focus on the causal role of cell shape in the loop of phenotype.

Chapter II

Introduction

The human body contains an estimated 37 trillion cells[1] which greatly vary in shape. Neurons are long cells with thin extensions[2], whereas erythrocytes possess a discoid shape, are flat, round and very small[3]. Smooth muscle cells are elongated[4] and epithelial cells can be flat, cuboidal or columnar[5]. Cells shape is often related to its function.

Many cell types secrete an extracellular matrix (ECM) and are embedded in it, and are thus exposed to a plethora of biochemical (e.g. growth factors, cytokines, collagens) and biomechanical signals (stretching, shear stress, stiffness and surface topography), which are in turn affecting cell shape. This results in activation of signal transduction pathways that are directly or indirectly leading to expression of genes or proteins involved in ECM homeostasis. This very ECM, in turn, provides biochemical and biomechanical signals to cells. The interdependence between cell phenotype and ECM properties is referred to as dynamic reciprocity. In this manuscript we wish to emphasize that reciprocal dynamics are often not direct but includes signal transduction, control of gene transcription, protein translation and extracellular deposition. To emphasize the circular nature of this series of causes and consequences, we use the term *"loop of phenotype"* (Fig. 1) in this manuscript. Our lab is particularly interested in the role that cell shape plays in the loop of phenotype, because disruptions in it, such as through overloading, impairment in signal transduction or mutation in ECM genes, can result in change in both cell shape and ECM composition. For instance, cirrhotic cardiomyopathy results from aberrant β-adrenergic receptor signalling[6] resulting in collagen accumulation, disordered cardiomyocyte arrangement and severe disarray of myofibrils[7]. Mutations in the gene encoding collagen type I causes the disease osteogenesis imperfecta which is associated with a decrease in collagen fibre diameter, changes in collagen crosslinking and increase in the production of osteoid[8] and osteoclastogenesis.

In this manuscript, we focus on tendon homeostasis, because we are interested in the relation between tenocyte cell shape and function. When the components of the tendon loop of phenotype change (e.g. through mechanical stimulation or changes in the structural organization), tenocyte phenotype changes rapidly. Elongated healthy tenocytes can become rounder, which is associated with a decline of phenotypical markers expression, as seen in tendinopathy[9–11] and upon *in vitro* tenocyte culture[12–16]. In this review, we will discuss the phenotypical loop and elaborate on the role of cell shape in signal transduction that governs tendon homeostasis, and aberrations that lead to tendinopathy and phenotypical decline in *in vitro* cell culture platforms.
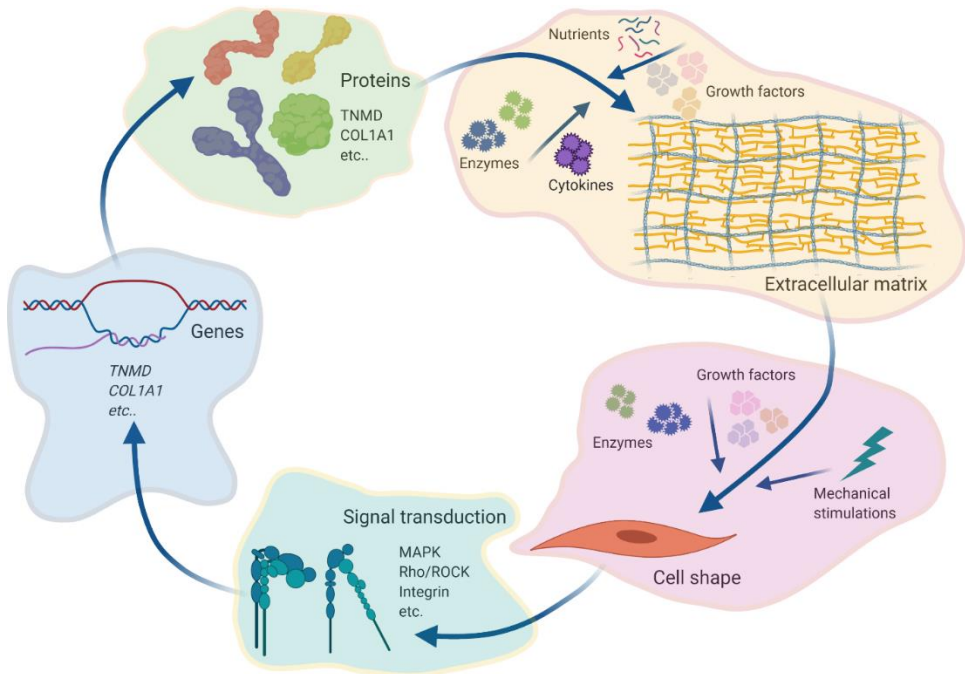
Figure 1. Loop of phenotype. *Extracellular matrix with its components (e.g. biomechanical or biochemical composition) dictate cell shape. The cell shape, in turn, leads to the activation of certain signals (e.g. Rho/ROCK pathway etc.), which results in transcription of direct or indirect target genes and translation of corresponding proteins. Translated proteins can be cytokines, nutrients, enzymes or growth factors, which, then contribute to the properties of the extracellular matrix, completing the loop.*

Tendon tissue homeostasis *in vivo*

Tendon genes

Tendon tissue is the product of proteins secreted by tendon fibroblasts, or tenocytes. As such, tendon tissue architecture is for a large part the result of the tenogenic gene expression profile, which is why we enter the loop at the level of gene expression in tenocytes. The genes encoding tenomodulin (*TNMD*)[17] and tendon ECM proteins such as collagen type I (*COL1*)[18] are actively transcribed in tenocytes. Differences in the expression levels of tenogenic genes underlies the differences in biochemical and mechanical properties of different types of tendon and ligaments. For instance, Achilles and patellar tendon display higher tensile strength and express more collagen type I compared to ligament tissues[19]. Genes encoding matrix metalloproteinases (MMPs)[20], which are involved in matrix remodelling as well as the genes encoding certain growth factors, which are needed for tendon tissue homeostasis such as *TGFβ2*[21], are also

expressed by tenocytes. Another class of genes expressed in tenocytes are those that encode transcription factors that regulate the expression of tendon genes, such as early growth response factor (EGR-1)[22], scleraxis (*SCX*)[23] and mohawk (*MKX*)[24]. *SCX* is considered to be a master regulator of tenogenic differentiation, for instance it regulates the expression of *COL1*[25,26] and *TNMD*[27,28]. The role of *Scx* in regulation of the expression of *Col1* is clear in *Scx* knock-down tenocytes[29,30] and stem cells[31,32]. When *Scx* is knocked down using short hairpin RNAs, foetal equine tenocytes [30] and embryonic stem cells fail to form tendons[31]. Similarly, in *Scx* deficient mice, tendons display a hypoplastic phenotype and partial or complete loss of tendons and disruptions in mechanical properties and less organized tendon matrix [27,33,34]. In fact, in *Scx* null mice, not only tendon growth is blunted, but also tendon-related ECM genes and protein expression is reduced even in mechanically loaded tendons[35], acknowledging the involvement of *Scx* in tendon homeostasis in response to mechanical stimulation. *Mkx* is another revelant transcription factor for tendon physiology and development. In *Mkx* knockout mice, overall tendon mass is reduced, while the diameter of collagen fibrils and expression of *Col1* is diminished compared to wild type mice [24]. The transcription factor Egr-1 can induce the expression of *Scx*[36] and *Col1*[37], and mutations in *Egr-1* leads to a reduced number of collagen fibrils[38]. EGR-1 knockdown leads to decreased expression of SCX and downstream matrix proteins, while leaving MKX levels unaffected[39]. *Fos* is another transcription factor that promotes early differentiation of stem cells in rat Achilles tendon [40]. Overexpression of *Fos* results in increased gene expression of *Scx, Mkx, Tnmd, Egr-1* and *Col-1* and when *Fos* was knocked-out, gene expression of *Mkx, Tnmd* and *Col-1* declined in tendon stem cells [40], emphasizing the role of *Fos* in the regulation of tenocyte marker genes and further tendon ECM. Of interest, both FOS and EGR-1 show elevated expression levels early upon mechanical stimulation[41], thereby connecting upstream extracellular effectors in the phenotypical loop with the expression of matrix genes.

Signals activating the transcription of tenogenic genes

In order to find out how tenogenic transcription factors and its cognate genes are activated, we move anti-clockwise in the loop of phenotype and look at the signal transduction pathways that impinge on the promoter of the genes regulating tendon ECM protein expression. In tenocytes, there are several signal transduction pathways that, when activated, induce the expression of tenocyte markers, which is excellently reviewed by Lavagnino *et al.* [42]. Of interest, calcium signaling can activate the MAPK pathway[43], leading downstream to an activation of EGR-1[44]. PI3K/protein kinase B and ERK pathways are also able to induce collagen synthesis[45], as are integrin mediated signaling, G-protein coupled membrane receptors, receptor tyrosine kinases (RTKs),

mitogen-activated protein kinases (MAPKs), stretch-activated ion channels and Hippo signaling [49, 52].

Collagen type I synthesis in tenocytes is also induced upon activation of transforming growth factor beta (TGF-β)[47,48] and basic fibroblast growth factor (bFGF)[49]. TGF-β signaling is essential for tendon development and maintaining tendon homeostasis[50]. In *Smad3* deficient mice, which is an essential mediator of TGF-β signaling, organization of tendon matrix is disrupted and protein expression of COL1 and TN-C and gene expression of *Col1*, *Tnmd* and *Mkx* is significantly decreased compared to wild type animals[51]. More interestingly, SCX expression is dependent on TGF-B stimulation[52], and *via* performing immunoprecipitation experiments, physical interaction between *Scx* and *Mkx* with *Smad3* is reported[51]. Many tenogenic genes are under the control of mechanotransduction pathways, which we will discuss next.

Mechanotransduction as a tendinogenic signal

Mechanical loading strongly affects tendon gene and protein expression, which becomes very clear when the loop is compromised by alterations in mechanical stimulation of cells or tissues. For instance, when mice underwent no-running, moderate and intensive running treadmill regimens, in both patellar and Achilles tendon moderate running led to an increase in gene expression of *Col1* and *Tnmd* and non-tenocyte related genes including *Sox9, Runx* and *Osterix* remained unchanged, compared to control and intense running[53]. In humans, frequent weight-bearing exercises leads to 20-30% larger tendons [54,55]. Rats exposed to short-term resistance training show increased expression of *Col1* [56]. Physiological levels of mechanical loading have been associated with anabolic effects on tendon physiology, for instance by increased collagen synthesis *via* TGF-β signaling and IGF-1 [46,57–60]. Blood samples and dialysate samples from peritendon tissue after 1 hour of uphill treadmill running by human subjects showed increase levels of TGF-β1 and pro-peptides for type I collagen (PICP), indicative of increased collagen accumulation[61]. In another experiment rats were exposed to different loading regimens, and an increase in the collagen levels was linked to increased levels of lysyl oxidase, which elevates collagen crosslinking and TGF-β1 levels[62]. Bhavani Thampatty and James Wang excellently reviewed and summarized *in vivo* studies using treadmill to demonstrate impact of mechanical loading on tendon homeostasis [63].

The role of mechanical loading in tendon homeostasis is ambivalent, with anabolic effects of physiological mechanical loading, and the induction of tendinopathic lesions with supra-physiological loading. The role of TGF-β1 and other growth factors on this process is under investigation. For instance, in tendinopathy, *TGF-β1* was found to be higher in tenocytes in patellar tendinosis compared to healthy counterparts[64]. In another report, expression of *TGFβ R1* in human diseased rotator cuff tendons was significantly

declined in diseased tendons, whilst *TGFβ R2* was increased[65]. This also suggest that the level of mechanical loading is an aspect to be considered when analyzing the loop of phenotype.

ECM composition influences mechanical properties and gene expression

The effect of mechanical loading on tendon tissue homeostasis demonstrated that mechanical signals are perceived by tenocytes and translated into different gene and protein expression profiles. Mechanical loading is transmitted to the cells through the ECM, and ECM composition indeed has a strong effect on the transmittance of mechanical loading. Tendons and ligaments are very strong. For instance, a tendon with an area of 1 cm^2 can bear a load of 500 to 1000 kg[66]. Depending on the type and location of the tendon, mechanical properties vary. Frequently loaded tendons are exposed to high tensile loads and hence display high tensile strength compared to tendons that are exposed to less tensile loads[67]. Tendon strength is related to its thickness as well as collagen content. Healthy tendon tissue is formed by hierarchical assembly of triple-helical type I collagen molecules into collagen fibrils, and fibers form the base of the tendon structure[68] (Fig 2). Roughly 95% of the dry weight of a tendon is collagen type I. Collagen types III, V, XI, XII, and XIV account for the other 5%[18]. In addition, tendon ECM contains non-collagenous molecules such as proteoglycans, glycoproteins, and glycoconjugates. These are involved in the regulation of collagen self-assembly and mechanical stability and strength [69].
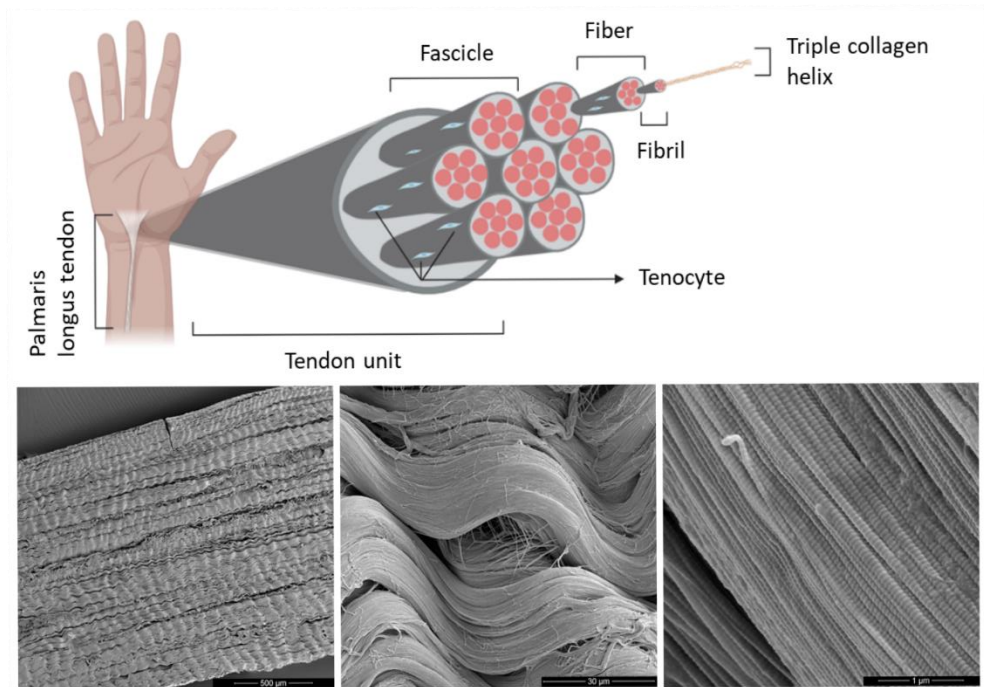
Figure 2. *Illustration of a healthy tendon. Top panel: Tendon connects muscles to bones. It is composed of highly organized and aligned collagen fibers. Essentially, type I collagen triple helices assemble into collagen fibrils that assemble into collagen fibers. Fibers form fascicles and together they form a tendon unit. Tenocytes (blue) are observed between collagen fibers and fascicles. Bottom panel: SEM images of tendon from low magnification (right) to high magnification (left).*

In tendinopathic lesions, a switch is observed from collagen type I to type III and collagen fiber diameter and organization decrease, which is associated with an increased amount of ground substances[70], a gel-like substance in the extracellular space containing component of ECM except for collagen[71]. In addition, neovascularization is observed, the abundance of glycoproteins increases[72] and the white color of healthy tendon becomes grey or brown [73,74]. Inevitably, mechanical properties change along with the biochemical changes. For instance, in insertional Achilles tendinopathy in humans, compared to healthy tendons, higher stiffness and lower transition strain was reported [75,76]. Interestingly, in a study which is conducted with 22 Achilles tendinopathy, 17 patellar tendinopathy, and 28 healthy control individuals, lower shear wave velocity was observed in the distal insertion site of Achilles tendon but higher at the mid-tendon compared to healthy controls[77]. Higher shear wave velocity was observed in in both regions of the tendon in patellar tendinopathy patients. Furthermore, in Achilles and

patellar tendon tendinopathy, lower and higher elastic modulus, respectively, was reported.

Gene expression changes when the composition and integrity of tendon ECM is compromised, as is seen in tendinopathic lesions. By subjecting mouse Achilles tendons to axial cyclic compressive loading for 3 weeks, tendinopathic lesions were induced, resulting in decreased expression of *Col1* and *Col3*[78]. Jelinsky and colleagues performed a transcriptome analysis of healthy human tendons and tendon with tendinopathic lesions [79]. Many genes were differentially expressed including genes encoding disintegrin and metalloprotease 12 (*ADAM12*), tenascin C (*TNC*), periostin (osteoblast specific factor) *(POSTN)*, and interleukin 13 receptor alpha 2 (*IL13RA2*), WNT1 inducible signaling pathway protein 1 (*WISP1*), Laminin, alpha 4 (*LAMA4*) and insulin-like growth factor binding protein 3 (*IGFBP3*) [79]. In a rat tendinopathy model, which is created by injection of collagenase, gene expression of *Tnmd, Scx* and *Col1a1* was significantly reduced[80]. Similarly in horses suffering from acute and chronic tendon disease, gene expression of fibro-chondrogenic genes such as collagen-II, -IX,-X, -XI, SOX9 was increased[81,82].

In tendinopathy, tenocytes also express genes and proteins that are involved in degradation of both matrix and non-matrix proteins, called matrix metalloproteinases (MMPs). They are involved in tissue repair, remodeling, wound healing and tissue homeostasis[83]. Expression of enzymes that regulate collagen breakdown such as *MMP2, MMP9, MMP14, MMP13,* and *MMP19* and metalloproteinase inhibitor-2 (*TIMP2*) is higher in tendinopathy compared to healthy tendons[79,84,8586]. Expression of MMPs was hypothesized to be regulated by the JAK/STAT signal transduction pathway, which activates IL-4R and IL-13RA2[87], and induce the activity of MMP9 and MMP14[88]. Similar results reported by Thorpe and co-workers further indicated that the expression of inflammation (cyclooxygenase-2 and interleukin-6) and matrix degradation markers (MMP-13) increases in tendinopathic lesions[89]. Some hereditary diseases influence tendon structure, which are excellently summarized by Vaughn and colleagues[90]. For instance, a guanine-thymine dinucleotide repeat polymorphism within the tenascin-C gene is reported to be associated with Achilles tendinopathy[91]. Similarly, a significant association of GDF5 rs143383[92], MMP3 rs679620, rs591058, and rs650108 polymorphisms[93] and TIMP2 rs4789932 and MMP3 rs679620[94] variants are among the genetic factors that are associated with tendinopathy. Collectively, these data show that changed composition of the ECM results in differential gene expression in tenocytes.

Tenocyte shape and its phenotype are related

Previously, we have seen that mechanical forces can be transmitted through the ECM and that its composition can alter the gene expression profile of tenocytes. Here, we associate ECM composition with cell shape, which next to mechanical forces provides a biomechanical context. In healthy tendons, tenocytes have an elongated shape which is caused by contact guidance of the collagen fibers to which they attach. The diameter and anisotropic organization of collagen fibers transmit the topographical cues and mechanical signals to tenocytes[95]. The long projections of tenocytes, which slide through the well-organized collagen fibrils in the healthy tendon, are absent in tendinopathy. Tenocytes in the damaged regions display rounder nuclei compared to healthy counterparts [10,96]. These observations suggest that cells shape, and tenocyte phenotype are causally related which is in line with a vast body of literature describing the relation between a cell's shape and its phenotype. Micro-fabricated systems such as nano- and micro topographies[97] and adhesive islands[98,99] can manipulate cell shape and have led to the dissection of cell shape related signal transduction pathways. Many molecular mechanisms have been described, ranging from the activation of stretch-activated ion channels to membrane curvature sensing BAR domain proteins and direct effects of mechanical loading on nuclear processes[100]. However, it is the signal cascade that links ECM, integrin, focal adhesions, Rho, ROCK, actin and actin-dependent transcription factors, which has achieved most attention and where we can assess causality between changes to the ECM, cell shape and cell fate. A schematic of this pathway and the relation between its components is depicted in Figure 3 and below we focus on integrin/actin-mediated signaling and tenocyte phenotype.
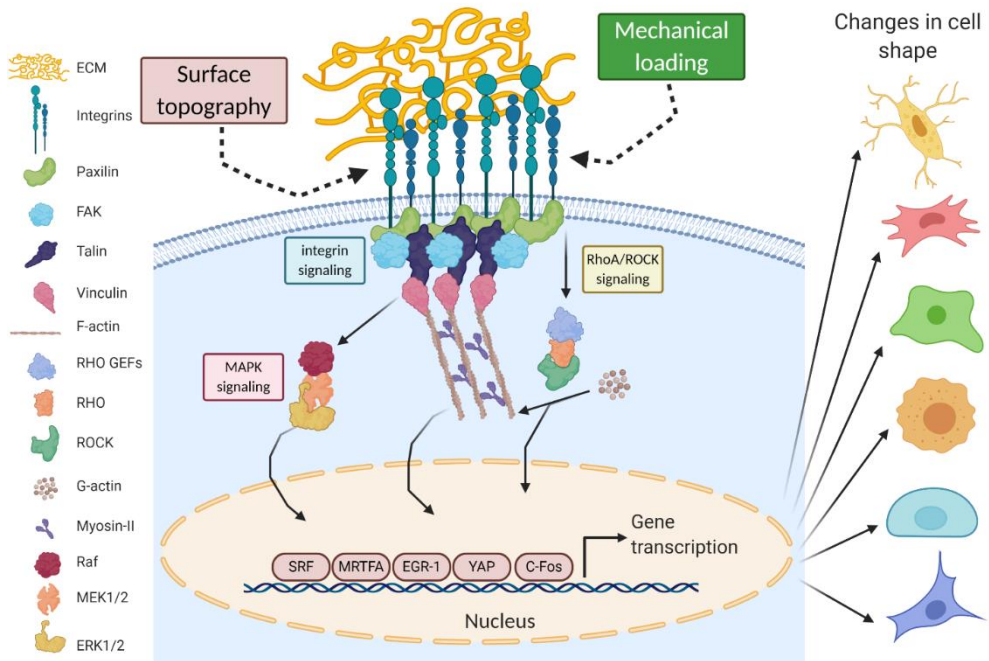
Figure 3. Overview of signal transduction pathways involved in the regulation of cell shape. *Integrins are transmembrane receptors crucial that bind to ECM proteins and initiate activation of downstream signalling pathways. Integrins organize in focal adhesion, which are composed of many proteins (Paxillin, Talin, FAK, Vinculin to name a few) and affect various processes such as cell spreading and migration. Its activity influences further activity of Rho/ROCK signalling, which is the main regulator of the polymerization of G-actin to F-actin, and MAPK/ERK pathways. Activity of focal adhesions, in return, can also be regulated by Rho/ROCK signalling and create a feedback loop that interconnects the actin machinery with integrin and focal adhesion signalling. The signalling pathways result in the activation of actin-sensitive transcription factors and subsequent changes in gene expression.*

Tenocyte shape and phenotype manipulation

As mentioned before, tenocyte shape is associated with either a healthy or tendinopathic phenotype. Changes in tenocyte shape and phenotype are also observed *in vitro* and this is most outspoken when tenocytes are isolated from their native tissue and put in culture. Within days, cell shape changes from the typical elongated high aspect ratio to more flattened spread out morphology typical of cultured fibroblasts. Nuclei become rounder, the actin cytoskeleton more spread and more actin stress fibers are

observed[12,13]. Concomitantly, the expression of *ColIII* increases and *Scx, Tnmd* and *ColI* expression decrease [12,14,101]. Integrin expression changes from high integrin beta 6 (*Itgβ6*) and integrin beta 4 (*Itgβ4*) expression in native tissue to high integrin alpha 11 (*Itga11*), integrin beta 1 (*Itgβ1*) and integrin alpha V (*Itgav*) in 2D cultures[16]. Collectively the change in gene and protein expression is referred to as dedifferentiation, a phenomenon observed in most cells that are transferred from the body into a culture dish.

To investigate the shape-phenotype relationship, many engineering strategies have been used in which the authors manipulate cell shape in vitro to enforce an elongated morphology. Anisotropic fibers[102–107], micro/nano grooves[108–111], tendon biomimetics[12,112,113] and mechanical loading[114–117] are used to create elongated stem cells[102–105,109,112,113,118] and tenocytes[12,106–108]. The consensus of most if not all these papers is that the tenocyte phenotype is favoured by experimental conditions that favour high aspect ratio. For instance, Kishore and co-workers used electrochemically aligned collagen threads (ELAC) to elongate cell shape and observed increased expression of tenogenic marker genes *SCX, TNMD* and *TNC* in human mesenchymal stem cells [107]. Elongated cell morphology was also achieved by imprinting of tendon topography into biomaterials. The elongated cell morphology on tendon-biomimetic topographies concurred with increased SCX levels in rat tenocytes and in TNMD in human mesenchymal stem cells [12,113]. Similar results were reported for human[106] and porcine[108] tenocytes: when dedifferentiated tenocytes are pushed to an elongated shape, expression of tenogenic marker genes increased. On our TopoChip platform, we also observed a clear correlation between *Scx* expression in rat tenocytes and elongated cell shape[119].

Tenogenic surfaces affect focal adhesion formation. For instance in one report, human mesenchymal stem cell were grown on nano-patterned surfaces and smaller focal adhesions were observed on nano-pattern surfaces compared to flat surfaces[120]. After 10 and 15 days of culture, relative to flat surface, patterned surfaces leads to an increase in tenocyte marker genes, such as *COL1, TNMD* and *SCX* as well as integrins *ITGB* and *ITGB5* [120]. Our own unpublished data supports this. We also observe that both rat tenocytes and human mesenchymal stem cells on surfaces with tenogenic potential are associated with smaller focal adhesion and suggests that tenogenesis is associated with low adherence. The opposite conclusion was reached based on an experiment in which mesenchymal stem cells were exposed to stretching. When the activity of FAK was completely inhibited, mesenchymal stem cells regressed to a circular shape and expression of *COL1A1, SCX* and *TNC* decreased[121]. To complicate matters, the relation between focal adhesion formation and tenogenic phenotype is reciprocal. When *Scx* expression was knocked down in mechanically-loaded equine tenocytes, cytosolic staining of vinculin decreased and longer vinculin-containing focal adhesions were

observed compared to controls[29]. This might be related to a decrease in collagen deposition influencing focal adhesion formation, yet additional research is required to elucidate the exact mechanisms. In the same study, transcriptomics analysis revealed that cytoskeletal organization, cell-matrix adhesion, ECM receptor interactions and focal adhesions are among the top downregulated biological processes in *Scx* knockdown tenocytes (Fig. 4). The reports described above seem to contradict each other but do point to crosstalk between the integrin mediated adhesion machinery and the tenogenic differentiation program. The next paragraph will focus on the role of actin cytoskeleton signalling, a crucial factor in cell shape regulation and the tenogenic phenotype.
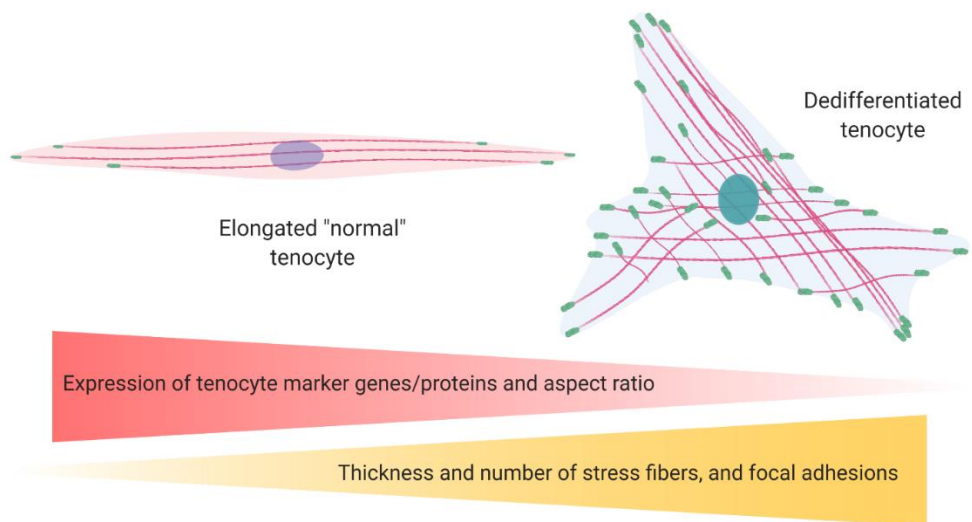
Figure 4. Relation between tenocyte phenotype with its cytoskeletal organization and focal adhesions. *In an elongated tenocyte (with a high aspect ratio), tenocytes have higher expression of tenogenic marker genes/proteins as well as smaller number/size of focal adhesions. Upon dedifferentiation, cell area increase and aspect ratio and expression of tenogenic marker genes/proteins decline. Furthermore, amount and thickness of stress fibres and focal adhesions increase.*

Actin cytoskeleton and Rho-ROCK signalling influence tenocyte gene transcription

A brief recap teaches us that the correlation between the tenogenic gene expression program and cell shape is very clear. The relation between focal adhesion and stress

fibre formation is clearly described in the literature as well[122]. Mature focal adhesions and stress fibre formation go hand in hand[123]. Tenogenic gene expression, focal adhesion abundance and activity and stress fibre formation is less clear. Actin filaments are the major component of the cell cytoskeleton, globular (G-actin) actin assembles into stress fibres that connect to focal adhesions and exert force and tension in and between cells and to the ECM[124]. Rho/ROCK signalling regulates polymerization of G-actin to filamentous (F-actin) and promotes actomyosin contractility, which leads to more mature focal adhesions[125].

Based on the above, one would assume that proteins that positively affect stress fibre formation and focal adhesion formation, such as Rho kinase and ROCK, have a negative effect on tenogenic gene expression and inhibitors of these proteins should result in increased expression of tenocyte markers. However, the opposite is observed in several articles[126–128]. For instance Maharam *et al.* inhibited the activity of ROCK, actin and myosin by treating human mesenchymal cells with the respective inhibitors Y-27632, Latrunculin A and blebbistatin, and demonstrated that not only elongated cell morphology enabled by silk scaffolds was destroyed, but also gene expression of *SCX* and *COL1A1* declined[129]. Similarly, treating the same cells with cytochalasin D, which inhibits actin polymerization, elongated cell morphology and protein expression of SCX and TNMD declined[129]. Another study to link the cell shape with differentiation of stem cells and involvement of ROCK signalling was performed by Calari *et al*[127]. They first reported that tenogenic differentiation was induced in cells on 3D collagen–glycosaminoglycan scaffolds, cells adapted an elongated shape, but ROCK activity was higher compared to isotropic controls. Furthermore, treatment with blebbistatin increased cell circularity and gene expression of *COL1A1* and *SCX* declined[127]. We reported decreased *SCX* expression in human mesenchymal stem cells cultured on tenogenic surface topographies upon inhibition of either Rho, ROCK and myosin [60]. In the same paper we demonstrate how Rho/ROCK signalling synergizes with TGF-β signalling on these tenogenic surfaces. Furthermore, we have unpublished data showing that upon blocking the same pathway, tenocytes on a tenogenic surface topography displayed decreased levels of TNMD protein levels as well as the expected changes in cell shape. Together, these studies demonstrate that elongated cells with fewer focal adhesions have fewer stress fibres pointing towards reduced Rho/ROCK signalling. However completely abolishing signalling induced by the physical environment through inhibitors negatively impacts tenogenic expression. Time dynamics might also be of importance here as we have demonstrated in a previous study where we found an increased presence of F-Actin, SRF and EGR-1 during the initial stages of MSC attachment on micro-topographies, after which F-actin stress fibres decreased. This also coincided with initial higher SCX levels, after which it declined over time[60].

The story is further complicated by the fact that the coupling between Rho and ROCK is ambiguous. For instance, in one study, attachment and spreading of endothelial cells was restricted, in which elevated activity of RhoA and reduced activity of myosin II and ROCK was observed[130]. Similarly, when porcine tenocytes were cultured on aligned microgrooves, higher levels of RhoA-GTP, decreased ROCK activity and increased TNMD expression was reported[108]. Treatment of these cells with the ROCK inhibitor Y27632 on a flat surface resulted in attenuated stress fibres and increased levels of TNMD on flat surfaces [108].

It is known that ROCK can be activated independent from Rho, and Rho can also phosphorylate FAK in the absence of stress fibers[131]. Similarly, PAK and MLCK, serine/threonine-protein kinases that regulate myosin II activity, can precede the ROCK activation[130,132]. The road from ECM, via integrin and F-actin to tenogenic gene expression may be clear, but the role that F-actin modifying proteins play in it is a topic of further investigation.

Actin-sensitive transcription factors regulate the expression of tenogenic marker genes

Actin- and mechano-sensitive transcription factors are important mediators in translating ECM signals into cell shape response. For instance, the levels of EGR-1 was elevated after 2 hours in tenocytes on micro topographies[13] and mechanical stimulation[22] which can also be related with the activity of RhoA *via* ERK and SRF signalling[133] and ultimately tenocyte phenotype. Furthermore, when EGR-1 is overexpressed in cells on flat surfaces, expression of *Scx* and *Tnmd* increased[22] and non-tenocyte differentiation (adipogenic, osteogenic and chondrogenic) differentiation was inhibited *via* the BMP12/Smad1/5/8 signalling pathway[134]. We observed increased levels SRF and EGR-1 in topography-induced tenogenic differentiation of human mesenchymal stem cells [60].

Previously, it has been shown that when smooth muscle cells are mechanically stretched, activator protein 1 (AP-1), which is dimeric transcription factors composed of Jun, Fos or ATF (activating transcription factor) subunits[135], FosB subunit is activated, which in turn induces expression of tenascin C[136]. Similarly, AP-1 has a binding site in the promotor for collagen type I[137], and gene expression of *Fos* is elevated upon mechanical stimulation of tendon stem cells [138], tenocytes[119] or by surface topography in human mesenchymal stem cells[60], indicating the involvement of Fos and AP-1 in tenocyte phenotype.

Another important set of transcriptional activators, YAP (Yes-associated protein) and TAZ (transcriptional coactivator with PDZ binding motif) are in the Hippo pathway,

which is also activated by the modulations in actin cytoskeleton *via* F-actin. YAP/TAZ are dominantly located in the cytoplasm and upon activation, they translocate the nucleus[139,140]. Subcellular localization and activity of YAP/TAZ changes based on substrate rigidity and topography[141–143], cytoskeletal remodelling[144,145] and stretching[144], therefore, its nuclear translocation is linked with cytoskeletal tension. When human adipose-derived mesenchymal stem cells were forced into an elongated shape *via* magnetic stimulation, YAP/TAZ was predominantly observed in the nucleus even after 11 days, which is also the time point in which the expression of *SCX* and *TNMD* display significant elevation compared to static cell culture[146]. Also, nuclear translocation of YAP in murine tenocytes upon cyclic stretching results in elevation of proteins levels of decorin[147], which is an important proteoglycan involved in tendon homeostasis[148]. Of interest, we mentioned before that TGF-β/Smad2/3 signalling is essential for both tendon development and homeostasis. Also here, TGF-β/Smad2/3 signalling can be mechano-regulated *via* nuclear translocation of phosphorylated smad2[149] and smad3[150] in tenocytes. This might be regulated through TAZ as shown for embryonic stem cells[151], however if this mechanism occurs in tenocytes still needs to be confirmed. Overall, the literature supports the notion that mechanical stimulation induces the tenogenic phenotype and indicate the role of mechanosensing and cytoskeletal organization on tenogenic differentiation.

Conclusion

Tendon tissue is dynamic: it continuously adapts to the mechanical stress it undergoes. What makes tenocytes and tendon tissue special is that the cells that make the matrix are also affected from them. That is very different from, for example, a neuron or a hormone-producing cell. Their response to a stimulus, an electrical pulse or the secretion of a hormone has no direct effect on their own gene expression profile. This is, however, the case with tenocytes, and therefore permanent damage to tendon tissue, for example during aging or trauma, also leads to permanent differences in the gene expression profile of the cells that make the matrix. This in turn influences the matrix and that in turn the tenocytes. This interdependence can lead to non-functional tendon tissue such as in a tendinopathic lesion being maintained.

Reciprocity also offers opportunities. Mechanical loading, growth factor supplementation, stem cell differentiation, gene therapy and small molecule interference are all tools that can be used to regain control of the loop of phenotype. We need to understand the physiology of tendon tissue and the pathophysiology of tendon lesions well. This requires more insight into the interaction between ECM and cells in vivo, and into the signal transduction pathways that control the expression of tendon genes. With a better understanding of the loop of phenotype we will be able to improve tendon therapy.

References

1. Bianconi, E., Piovesan, A., Facchin, F., Beraudi, A., Casadei, R., Frabetti, F., et al. An estimation of the number of cells in the human body. Ann Hum Biol. England, **40**, 463, 2013.

2. Sandell, J.H., and Masland, R.H. Shape and distribution of an unusual retinal neuron. J Comp Neurol . John Wiley & Sons, Ltd, **280**, 489, 1989.

3. Canham, P.B. The minimum energy of bending as a possible explanation of the biconcave shape of the human red blood cell. J Theor Biol . **26**, 61, 1970.

4. Owens, G.K. Regulation of differentiation of vascular smooth muscle cells. Physiol Rev . American Physiological Society, **75**, 487, 1995.

5. Welling, L.W., and Welling, D.J. Shape of epithelial cells and intercellular channels in the rabbit proximal nephron. Kidney Int . **9**, 385, 1976.

6. Baik, S.K., Fouad, T.R., and Lee, S.S. Cirrhotic cardiomyopathy. Orphanet J Rare Dis . BioMed Central, **2**, 15, 2007.

7. Chayanupatkul, M., and Liangpunsakul, S. Cirrhotic cardiomyopathy: review of pathophysiology and treatment. Hepatol Int . **8**, 308, 2014.

8. Etich, J., Leßmeier, L., Rehberg, M., Sill, H., Zaucke, F., Netzer, C., et al. Osteogenesis imperfecta—pathophysiology and therapeutic options. Mol Cell Pediatr . **7**, 9, 2020.

9. Tom, S., Parkinson, J., Ilic, M.Z., Cook, J., Feller, J.A., and Handley, C.J. Changes in the composition of the extracellular matrix in patellar tendinopathy. Matrix Biol . Elsevier B.V./International Society of Matrix Biology, **28**, 230, 2009.

10. Pingel, J., Lu, Y., Starborg, T., Fredberg, U., Langberg, H., Nedergaard, A., et al. 3-D ultrastructure and collagen composition of healthy and overloaded human tendon: Evidence of tenocyte and matrix buckling. J Anat. **224**, 548, 2014.

11. Jelinsky, S.A., Rodeo, S.A., Li, J., Gulotta, L. V, Archambault, J.M., and Seeherman, H.J. Regulation of gene expression in human tendinopathy. BMC Musculoskelet Disord. **12**, 86, 2011.

12. Dede Eren, A., Vasilevich, A., Eren, E.D., Sudarsanam, P., Tuvshindorj, U., de Boer, J., et al. Tendon-derived biomimetic surface topographies induce phenotypic maintenance of tenocytes in vitro. Tissue Eng Part A . 2020.

13. Vermeulen, S., Vasilevich, A., Tsiapalis, D., Roumans, N., Vroemen, P., Beijer, N.R.M., et al. Identification of topographical architectures supporting the phenotype of rat tenocytes. Acta Biomater. **83**, 2019.

14. Yao, L., Bestwick, C.S., Bestwick, L.A., Maffulli, N., and Aspden, R.M.

Phenotypic drift in human tenocyte culture. Tissue Eng. **12**, 1843, 2006.

15. Taylor, S.E., Vaughan-Thomas, A., Clements, D.N., Pinchbeck, G., MacRory, L.C., Smith, R.K., et al. Gene expression markers of tendon fibroblasts in normal and diseased tissue compared to monolayer and three dimensional culture systems. BMC Musculoskelet Disord. **10**, 1, 2009.

16. Mueller, A.J., Tew, S.R., Vasieva, O., Clegg, P.D., and Canty-Laird, E.G. A systems biology approach to defining regulatory mechanisms for cartilage and tendon cell phenotypes. Sci Rep . Nature Publishing Group, **6**, 1, 2016.

17. Qi, J., Dmochowski, J.M., Banes, A.N., Tsuzaki, M., Bynum, D., Patterson, M., et al. Differential expression and cellular localization of novel isoforms of the tendon biomarker tenomodulin. J Appl Physiol. United States, **113**, 861, 2012.

18. Screen, H.R.C., Berk, D.E., Kadler, K.E., Ramirez, F., and Young, M.F. Tendon functional extracellular matrix. J Orthop Res. **33**, 793, 2015.

19. Kharaz, Y.A. The molecular and cellular differences between tendons and ligaments. 2015.

20. Jelinsky, S.A., Rodeo, S.A., Li, J., Gulotta, L. V., Archambault, J.M., and Seeherman, H.J. Regulation of gene expression in human tendinopathy. BMC Musculoskelet Disord . BioMed Central Ltd, **12**, 86, 2011.

21. Gumucio, J.P., Sugg, K.B., and Mendias, C.L. TGF-β superfamily signaling in muscle and tendon adaptation to resistance exercise. Exerc Sport Sci Rev . **43**, 93, 2015.

22. Gaut, L., Robert, N., Delalande, A., Bonnin, M.A., Pichon, C., and Duprez, D. EGR1 regulates transcription downstream of mechanical signals during tendon formation and healing. PLoS One. **11**, 1, 2016.

23. Schweitzer, R., Chyung, J.H., Murtaugh, L.C., Brent, A.E., Rosen, V., Olson, E.N., et al. Analysis of the tendon cell fate using Scleraxis, a specific marker for tendons and ligaments. Development. **128**, 3855, 2001.

24. Ito, Y., Toriuchi, N., Yoshitaka, T., Ueno-Kudoh, H., Sato, T., Yokoyama, S., et al. The Mohawk homeobox gene is a critical regulator of tendon differentiation. Proc Natl Acad Sci U S A. **107**, 10538, 2010.

25. Espira, L., Lamoureux, L., Jones, S.C., Gerard, R.D., Dixon, I.M.C., and Czubryt, M.P. The basic helix–loop–helix transcription factor scleraxis regulates fibroblast collagen synthesis. J Mol Cell Cardiol . **47**, 188, 2009.

26. Léjard, V., Brideau, G., Blais, F., Salingcarnboriboon, R., Wagner, G., Roehrl, M.H.A., et al. Scleraxis and NFATc regulate the expression of the pro-alpha1(I) collagen gene in tendon fibroblasts. J Biol Chem. United States, **282**, 17665, 2007.

27. Shukunami, C., Takimoto, A., Nishizaki, Y., Yoshimoto, Y., Tanaka, S., Miura,

S., et al. Scleraxis is a transcriptional activator that regulates the expression of Tenomodulin, a marker of mature tenocytes and ligamentocytes. Sci Rep . Springer US, **8**, 1, 2018.

28. Shukunami, C., Takimoto, A., Oro, M., and Hiraki, Y. Scleraxis positively regulates the expression of tenomodulin, a differentiation marker of tenocytes. Dev Biol. **298**, 234, 2006.

29. Nichols, A.E.C., Settlage, R.E., Werre, S.R., and Dahlgren, L.A. Novel roles for scleraxis in regulating adult tenocyte function. BMC Cell Biol. BMC Cell Biology, **19**, 1, 2018.

30. Paterson, Y.Z., Evans, N., Kan, S., Cribbs, A., Henson, F.M.D., and Guest, D.J. The transcription factor scleraxis differentially regulates gene expression in tenocytes isolated at different developmental stages. Mech Dev . **163**, 103635, 2020.

31. Bavin, E.P., Atkinson, F., Barsby, T., and Guest, D.J. Scleraxis Is Essential for Tendon Differentiation by Equine Embryonic Stem Cells and in Equine Fetal Tenocytes. Stem Cells Dev . Mary Ann Liebert, Inc., publishers, **26**, 441, 2016.

32. Chen, W., Tang, H., Zhou, M., Hu, C., Zhang, J., and Tang, K. Dexamethasone inhibits the differentiation of rat tendon stem cells into tenocytes by targeting the scleraxis gene. J Steroid Biochem Mol Biol . **152**, 16, 2015.

33. Yoshimoto, Y., Takimoto, A., Watanabe, H., Hiraki, Y., Kondoh, G., and Shukunami, C. Scleraxis is required for maturation of tissue domains for proper integration of the musculoskeletal system. Sci Rep. Nature Publishing Group, **7**, 1, 2017.

34. Murchison, N.D., Price, B.A., Conner, D.A., Keene, D.R., Olson, E.N., Tabin, C.J., et al. Regulation of tendon differentiation by scleraxis distinguishes force-transmitting tendons from muscle-anchoring tendons. Development . **134**, 2697 LP, 2007.

35. Gumucio, J.P., Schonk, M.M., Kharaz, Y.A., Comerford, E., and Mendias, C.L. Scleraxis is required for the growth of adult tendons in response to mechanical loading. JCI Insight . The American Society for Clinical Investigation, **5**, 2020.

36. Gaut, L., Robert, N., Delalande, A., Bonnin, M.-A., Pichon, C., and Duprez, D. EGR1 Regulates Transcription Downstream of Mechanical Signals during Tendon Formation and Healing. PLoS One . Public Library of Science, **11**, e0166237, 2016.

37. Wu, Y.-F., Wang, H.-K., Chang, H.-W., Sun, J., Sun, J.-S., and Chao, Y.-H. High glucose alters tendon homeostasis through downregulation of the AMPK/Egr1 pathway. Sci Rep . **7**, 44199, 2017.

38. Lejard, V., Blais, F., Guerquin, M.J., Bonnet, A., Bonnin, M.A., Havis, E., et al.

EGR1 and EGR2 involvement in vertebrate tendon differentiation. J Biol Chem. **286**, 5855, 2011.

39. Guerquin, M.-J., Charvet, B., Nourissat, G., Havis, E., Ronsin, O., Bonnin, M.-A., et al. Transcription factor EGR1 directs tendon differentiation and promotes tendon repair. J Clin Invest . 2013/07/25. American Society for Clinical Investigation, **123**, 3564, 2013.

40. Chen, J., Zhang, E., Zhang, W., Liu, Z., Lu, P., Zhu, T., et al. Fos Promotes Early Stage Teno-Lineage Differentiation of Tendon Stem/Progenitor Cells in Tendon. Stem Cells Transl Med. **6**, 2009, 2017.

41. Eliasson, P., Andersson, T., Hammerman, M., and Aspenberg, P. Primary gene response to mechanical loading in healing rat Achilles tendons. J Appl Physiol. **114**, 1519, 2013.

42. Lavagnino, M., Wall, M.E., Little, D., Banes, A.J., Guilak, F., and Arnoczky, S.P. Tendon mechanobiology: Current knowledge and future research opportunities. J Orthop Res . 2015/04/27. **33**, 813, 2015.

43. White, C.D., and Sacks, D.B. Regulation of MAP kinase signaling by calcium. Methods Mol Biol. United States, **661**, 151, 2010.

44. Schwachtgen, J.L., Houston, P., Campbell, C., Sukhatme, V., and Braddock, M. Fluid shear stress activation of egr-1 transcription in cultured human endothelial and epithelial cells is mediated via the extracellular signal-related kinase 1/2 mitogen-activated protein kinase pathway. J Clin Invest . **101**, 2540, 1998.

45. Disser, N.P., Sugg, K.B., Talarek, J.R., Sarver, D.C., Rourke, B.J., and Mendias, C.L. Insulin-like growth factor 1 signaling in tenocytes is required for adult tendon growth. FASEB J . John Wiley & Sons, Ltd, **33**, 12680, 2019.

46. Heinemeier, K.M., and Kjaer, M. In vivo investigation of tendon responses to mechanical loading. **11**, 115, 2011.

47. Klein, M.B., Yalamanchi, N., Pham, H., Longaker, M.T., and Chan, J. Flexor tendon healing in vitro: Effects of TGF-β on tendon cell collagen production. J Hand Surg Am . **27**, 615, 2002.

48. Kaji, D.A., Howell, K.L., Balic, Z., Hubmacher, D., and Huang, A.H. Tgfβ signaling is required for tenocyte recruitment and functional neonatal tendon regeneration. Elife . eLife Sciences Publications, Ltd, **9**, e51779, 2020.

49. Wang, X.T., Liu, P.Y., Xin, K.-Q., and Tang, J.B. Tendon Healing In Vitro: bFGF Gene Transfer to Tenocytes by Adeno-Associated Viral Vectors Promotes Expression of Collagen Genes. J Hand Surg Am . **30**, 1255, 2005.

50. Pryce, B.A., Watson, S.S., Murchison, N.D., Staverosky, J.A., Dünker, N., and Schweitzer, R. Recruitment and maintenance of tendon progenitors by TGFbeta signaling are essential for tendon formation. Development. **136**, 1351, 2009.

51.   Berthet, E., Chen, C., Butcher, K., Schneider, R.A., Alliston, T., and Amirtharajah, M. Smad3 binds Scleraxis and Mohawk and regulates tendon matrix organization. J Orthop Res Off Publ Orthop Res Soc. **31**, 1475, 2013.

52.   Havis, E., Bonnin, M.-A., Olivera-Martinez, I., Nazaret, N., Ruggiu, M., Weibel, J., et al. Transcriptomic analysis of mouse limb tendon cells during development. Development . **141**, 3683 LP, 2014.

53.   Zhang, J., and Wang, J.H.-C. The Effects of Mechanical Loading on Tendons - An In Vivo and In Vitro Model Study. PLoS One . Public Library of Science, **8**, e71740, 2013.

54.   Rosager, S., Aagaard, P., Dyhre-Poulsen, P., Neergaard, K., Kjaer, M., and Magnusson, S.P. Load-displacement properties of the human triceps surae aponeurosis and tendon in runners and non-runners. Scand J Med Sci Sports . John Wiley & Sons, Ltd, **12**, 90, 2002.

55.   Kongsgaard, M., Aagaard, P., Kjaer, M., and Magnusson, S.P. Structural Achilles tendon properties in athletes subjected to different exercise modes and in Achilles tendon rupture patients. J Appl Physiol . American Physiological Society, **99**, 1965, 2005.

56.   Olesen, J.L., Heinemeier, K.M., Haddad, F., Langberg, H., Flyvbjerg, A., Kjær, M., et al. Expression of insulin-like growth factor I, insulin-like growth factor binding proteins, and collagen mRNA in mechanically loaded plantaris tendon. J Appl Physiol . American Physiological Society, **101**, 183, 2006.

57.   Heinemeier, K., Langberg, H., Olesen, J.L., and Kjaer, M. Role of TGF-β1 in relation to exercise-induced type I collagen synthesis in human tendinous tissue. J Appl Physiol. **95**, 2390, 2003.

58.   Mendias, C.L., Gumucio, J.P., and Lynch, E.B. Mechanical loading and TGF-β change the expression of multiple miRNAs in tendon fibroblasts. J Appl Physiol. **113**, 56, 2012.

59.   Sharir, A., and Zelzer, E. Tendon homeostasis: The right pull. Curr Biol . Elsevier Ltd, **21**, R472, 2011.

60.   Vermeulen, S., Roumans, N., Honig, F., Carlier, A., Hebels, D.G.A.J., Eren, A.D., et al. Mechanotransduction is a context-dependent activator of TGF-β signaling in mesenchymal stem cells. Biomaterials. **259**, 2020.

61.   Heinemeier, K., Langberg, H., Olesen, J.L., and Kjaer, M. Role of TGF-β1 in relation to exercise-induced type I collagen synthesis in human tendinous tissue. J Appl Physiol . American Physiological Society, **95**, 2390, 2003.

62.   Heinemeier, K.M., Olesen, J.L., Haddad, F., Langberg, H., Kjaer, M., Baldwin, K.M., et al. Expression of collagen and related growth factors in rat tendon and skeletal muscle in response to specific contraction types. J Physiol . 2007/05/31.

Blackwell Science Inc, **582**, 1303, 2007.

63.   Thampatty, B.P., and Wang, J.H.C. Mechanobiology of young and aging tendons: In vivo studies with treadmill running. J Orthop Res. **36**, 557, 2018.

64.   Molloy, T.J., Kemp, M.W., Wang, Y., and Murrell, G.A.C. Microarray analysis of the tendinopathic rat supraspinatus tendon: Glutamate signaling and its potential role in tendon degeneration. J Appl Physiol. **101**, 1702, 2006.

65.   Goodier, H.C.J., Carr, A.J., Snelling, S.J.B., Roche, L., Wheway, K., Watkins, B., et al. Comparison of transforming growth factor beta expression in healthy and diseased human tendon. Arthritis Res Ther . **18**, 48, 2016.

66.   Sharma, P., and Maffulli, N. Tendon Injury and Tendinopathy: Healing and Repair. JBJS . **87**, 2005.

67.   Maganaris, C.N., and Narici, M. V. Mechanical Properties of Tendons.

68.   Screen, H.R.C., Berk, D.E., Kadler, K.E., Ramirez, F., and Young, M.F. Tendon functional extracellular matrix. J Orthop Res. **33**, 793, 2015.

69.   J.H., Y., and J., H. Tendon proteoglycans: Biochemistry and function. J Musculoskelet Neuronal Interact . **5**, 22, 2005.

70.   Benazzo, F., Stennardo, G., and Valli, M. Achilles and patellar tendinopathies in athletes: pathogenesis and surgical treatment. Bull Hosp Jt Dis . **54**, 236—240, 1996.

71.   Docheva, D., Müller, S.A., Majewski, M., and Evans, C.H. Biologics for tendon repair. Adv. Drug Deliv. Rev. 2015.

72.   Cook, J.L., Khan, K.M., and Purdam, C. Achilles tendinopathy. Man Ther . **7**, 121, 2002.

73.   Khan, K.M., Cook, J.L., Bonar, F., Harcourt, P., and Astrom, M. Histopathology of common tendinopathies. Update and implications for clinical management. Sports Med. New Zealand, **27**, 393, 1999.

74.   Xu, Y., and Murrell, G.A.C. The basic science of tendinopathy. Clin Orthop Relat Res. **466**, 1528, 2008.

75.   Bah, I., Kwak, S.T., Chimenti, R.L., Richards, M.S., Ketz, J.P., Samuel Flemister, A., et al. Mechanical changes in the Achilles tendon due to insertional Achilles tendinopathy. J Mech Behav Biomed Mater . Elsevier, **53**, 320, 2016.

76.   Child, S., Hons, B., Bryant, A.L., Hons, B., Clark, R.A., Hons, B., et al. Mechanical Properties of the Achilles Tendon Aponeurosis Are Altered in Athletes With Achilles Tendinopathy. 1885, 2010.

77.   Coombes, B.K., Tucker, K., Vicenzino, B., Vuvan, V., Mellor, R., Heales, L., et al. Achilles and patellar tendinopathy display opposite changes in elastic properties: A shear wave elastography study. Scand J Med Sci Sports . John

Wiley & Sons, Ltd, **28**, 1201, 2018.

78.   Fleischhacker, V., Klatte-Schulz, F., Minkwitz, S., Schmock, A., Rummler, M., Seliger, A., et al. In Vivo and In Vitro Mechanical Loading of Mouse Achilles Tendons and Tenocytes-A Pilot Study. Int J Mol Sci . MDPI, **21**, 1313, 2020.

79.   Jelinsky, S.A., Rodeo, S.A., Li, J., Gulotta, L. V, Archambault, J.M., and Seeherman, H.J. Regulation of gene expression in human tendinopathy. BMC Musculoskelet Disord . BioMed Central Ltd, **12**, 86, 2011.

80.   Rui, Y.F., Lui, P.P.Y., Wong, Y.M., Tan, Q., and Chan, K.M. Altered fate of tendon-derived stem cells isolated from a failed tendon-healing animal model of tendinopathy. Stem Cells Dev. **22**, 1076, 2013.

81.   Nourissat, G., Berenbaum, F., and Duprez, D. Tendon injury: From biology to tendon repair. Nat Rev Rheumatol . Nature Publishing Group, **11**, 223, 2015.

82.   Clegg, P.D., Strassburg, S., and Smith, R.K. Cell phenotypic variation in normal and damaged tendons. Int J Exp Pathol. **88**, 227, 2007.

83.   Nagase, H., Visse, R., and Murphy, G. Structure and function of matrix metalloproteinases and TIMPs. Cardiovasc Res . **69**, 562, 2006.

84.   Alfredson, H., Lorentzon, M., Bäckman, S., Bäckman, A., and Lerner, U.H. cDNA-arrays and real-time quantitative PCR techniques in the investigation of chronic Achilles tendinosis. J Orthop Res Off Publ Orthop Res Soc. United States, **21**, 970, 2003.

85.   Chaudhury, S., and Carr, A.J. Lessons we can learn from gene expression patterns in rotator cuff tears and tendinopathies. J Shoulder Elb Surg . **21**, 191, 2012.

86.   J, P., U, F., K, Q., JO, L., P, S., K, H., et al. Local biochemical and morphological differences in human Achilles tendinopathy: a case control study. BMC Musculoskelet Disord .

87.   Lang, R., Patel, D., Morris, J.J., Rutschman, R.L., and Murray, P.J. Shaping gene expression in activated and resting primary macrophages by IL-10. J Immunol. United States, **169**, 2253, 2002.

88.   Fujisawa, T., Joshi, B., Nakajima, A., and Puri, R.K. A novel role of interleukin-13 receptor alpha2 in pancreatic cancer invasion and metastasis. Cancer Res. United States, **69**, 8678, 2009.

89.   Thorpe, C.T., Chaudhry, S., Lei, I.I., Varone, A., Riley, G.P., Birch, H.L., et al. Tendon overload results in alterations in cell shape and increased markers of inflammation and matrix degradation. Scand J Med Sci Sport. **25**, e381, 2015.

90.   Vaughn, N.H., Stepanyan, H., Gallo, R.A., and Dhawan, A. Genetic factors in tendon injury: A systematic review of the literature. Orthop J Sport Med. **5**, 1,

2017.

91.   Mokone, G.G., Gajjar, M., September, A. V, Schwellnus, M.P., Greenberg, J., Noakes, T.D., et al. The guanine-thymine dinucleotide repeat polymorphism within the tenascin-C gene is associated with achilles tendon injuries. Am J Sports Med. United States, **33**, 1016, 2005.

92.   Posthumus, M., Collins, M., Cook, J., Handley, C.J., Ribbans, W.J., Smith, R.K.W., et al. Components of the transforming growth factor-beta family and the pathogenesis of human Achilles tendon pathology--a genetic association study. Rheumatology (Oxford). England, **49**, 2090, 2010.

93.   Raleigh, S.M., van der Merwe, L., Ribbans, W.J., Smith, R.K.W., Schwellnus, M.P., and Collins, M. Variants within the MMP3 gene are associated with Achilles tendinopathy: possible interaction with the COL5A1 gene. Br J Sports Med. England, **43**, 514, 2009.

94.   El Khoury, L., Ribbans, W.J., and Raleigh, S.M. MMP3 and TIMP2 gene variants as predisposing factors for Achilles tendon pathologies: Attempted replication study in a British case-control cohort. Meta gene . Elsevier, **9**, 52, 2016.

95.   Wang, J.H.C., Guo, Q., and Li, B. Tendon biomechanics and mechanobiology - A mini review of basic concepts and recent advancements. J Hand Ther . Hanley & Belfus, **25**, 133, 2012.

96.   Steinmann, S., Pfeifer, C.G., Brochhausen, C., and Docheva, D. Spectrum of Tendon Pathologies : Triggers , Trails and End-State. 1, 2020.

97.   Ermis, M., Antmen, E., and Hasirci, V. Micro and Nanofabrication methods to control cell-substrate interactions and cell behavior: A review from the tissue engineering perspective. Bioact Mater . **3**, 355, 2018.

98.   Liu, W.F., and Chen, C.S. Engineering biomaterials to control cell function. Mater Today . **8**, 28, 2005.

99.   Weng, S., and Fu, J. Synergistic regulation of cell function by matrix rigidity and adhesive pattern. Biomaterials . **32**, 9584, 2011.

100. Haftbaradaran Esfahani, P., and Knöll, R. Cell shape: effects on gene expression and signaling. Biophys Rev . **12**, 895, 2020.

101. Mazzocca, A.D., Chowaniec, D., McCarthy, M.B., Beitzel, K., Cote, M.P., McKinnon, W., et al. In vitro changes in human tenocyte cultures obtained from proximal biceps tendon: Multiple passages result in changes in routine cell markers. Knee Surgery, Sport Traumatol Arthrosc. **20**, 1666, 2012.

102. Yin, Z., Chen, X., Chen, J.L., Shen, W.L., Hieu Nguyen, T.M., Gao, L., et al. The regulation of tendon stem cell differentiation by the alignment of nanofibers. Biomaterials . Elsevier Ltd, **31**, 2163, 2010.

103. Tu, T., Shen, Y., Wang, X., Zhang, W., Zhou, G., Zhang, Y., et al. Tendon ECM modified bioactive electrospun fibers promote MSC tenogenic differentiation and tendon regeneration. Appl Mater Today . Elsevier Ltd, **18**, 100495, 2020.

104. Zhou, K., Feng, B., Wang, W., Jiang, Y., Zhang, W., Zhou, G., et al. Nanoscaled and microscaled parallel topography promotes tenogenic differentiation of asc and neotendon formation in vitro. Int J Nanomedicine. **13**, 3867, 2018.

105. Popielarczyk, T.L., Nain, A.S., and Barrett, J.G. Aligned nanofiber topography directs the tenogenic differentiation of mesenchymal stem cells. Appl Sci. **7**, 2017.

106. Schoenenberger, A.D., Foolen, J., Moor, P., Silvan, U., and Snedeker, J.G. Substrate fiber alignment mediates tendon cell response to inflammatory signaling. Acta Biomater . Acta Materialia Inc., **71**, 306, 2018.

107. Kishore, V., Bullock, W., Sun, X., Scott, W., Dyke, V., and Akkus, O. Tenogenic differentiation of human MSCs induced by the topography of electrochemically aligned collagen threads. Biomaterials . Elsevier Ltd, **33**, 2137, 2012

108. Zhu, J., Li, J., Wang, B., Zhang, W.J., Zhou, G., Cao, Y., et al. The regulation of phenotype of cultured tenocytes by microgrooved surface structure. Biomaterials . Elsevier Ltd, **31**, 6952, 2010. Available from: http://dx.doi.org/10.1016/j.biomaterials.2010.05.058

109. Shi, Y., Zhou, K., Zhang, W., Zhang, Z., Zhou, G., Cao, Y., et al. Microgrooved topographical surface directs tenogenic lineage specific differentiation of mouse tendon derived stem cells. Biomed Mater. IOP Publishing, **12**, 2017.

110. Chaudhary, J.K., and Rath, P.C. Microgrooved-surface topography enhances cellular division and proliferation of mouse bone marrow-derived mesenchymal stem cells. PLoS One. **12**, 1, 2017.

111. Dede Eren, A., Eren, E.D., Wilting, T.J.S., de Boer, J., Gelderblom, H., and Foolen, J. Self-agglomerated collagen patterns govern cell behaviour. Sci Rep . **11**, 1516, 2021.

112. Tang, S.W., Yuen, W., Kaur, I., Pang, S.W., Voelcker, N.H., and Lam, Y.W. Capturing instructive cues of tissue microenvironment by silica bioreplication. Acta Biomater . Elsevier Ltd, **102**, 114, 2020.

113. Tong, W.Y., Shen, W., Yeung, C.W.F., Zhao, Y., Cheng, S.H., Chu, P.K., et al. Functional replication of the tendon tissue microenvironment by a bioimprinted substrate and the support of tenocytic differentiation of mesenchymal stem cells. Biomaterials . Elsevier Ltd, **33**, 7686, 2012.

114. Jiang, Y., Liu, H., Li, H., Wang, F., Cheng, K., Zhou, G., et al. A proteomic analysis of engineered tendon formation under dynamic mechanical loading in vitro. Biomaterials . Elsevier Ltd, **32**, 4085, 2011.

115. Neidlinger-Wilke, C., Grood, E.S., Wang, J.H.C., Brand, R.A., and Claes, L. Cell alignment is induced by cyclic changes in cell length: Studies of cells grown in cyclically stretched substrates. J Orthop Res. **19**, 286, 2001.

116. Wang, J., Jia, F., Yang, G., Yang, S., Campbell, B., Stone, D., et al. Cyclic Mechanical Stretching of Human Tendon Fibroblasts Increases the Production of Prostaglandin E 2 and Levels of Cyclooxygenase Expression: A Novel In Vitro Model Study. Connect Tissue Res . **44**, 128, 2003.

117. Chen, X., Yin, Z., Chen, J.L., Shen, W.L., Liu, H.H., Tang, Q.M., et al. Force and scleraxis synergistically promote the commitment of human ES cells derived MSCs to tenocytes. Sci Rep. **2**, 1, 2012.

118. Dede Eren, A., Sinha, R., Eren, E.D., Huipin, Y., Gulce-Iz, S., Valster, H., et al. Decellularized Porcine Achilles Tendon Induces Anti-inflammatory Macrophage Phenotype In Vitro and Tendon Repair In Vivo. J Immunol Regen Med . Elsevier, **8**, 100027, 2020.

119. Vermeulen, S., Vasilevich, A., Tsiapalis, D., Roumans, N., Vroemen, P., Beijer, N.R.M., et al. Identification of topographical architectures supporting the phenotype of rat tenocytes. Acta Biomater. Acta Materialia Inc., **83**, 277, 2019.

120. Iannone, M., Ventre, M., Formisano, L., Casalino, L., Patriarca, E.J., and Netti, P.A. Nanoengineered surfaces for focal adhesion guidance trigger mesenchymal stem cell self-organization and tenogenesis. Nano Lett. **15**, 1517, 2015.

121. Xu, B., Song, G., Ju, Y., Li, X., Song, Y., and Watanabe, S. RhoA / ROCK , Cytoskeletal Dynamics , and Focal Adhesion Kinase are Required for Mechanical Stretch-Induced Tenogenic Differentiation of Human Mesenchymal Stem Cells. J Cell Physiol. 2722, 2011.

122. Parsons, J.T., Horwitz, A.R., and Schwartz, M.A. Cell adhesion: Integrating cytoskeletal dynamics and cellular tension. Nat Rev Mol Cell Biol . Nature Publishing Group, **11**, 633, 2010.

123. Tojkander, S., Gateva, G., and Lappalainen, P. Actin stress fibers - Assembly, dynamics and biological roles. J Cell Sci. **125**, 1855, 2012.

124. Ohashi, K., Fujiwara, S., and Mizuno, K. Roles of the cytoskeleton, cell adhesion and rho signalling in mechanosensing and mechanotransduction. J Biochem. **161**, 245, 2017.

125. Seo, C.H., Furukawa, K., Montagne, K., Jeong, H., and Ushida, T. The effect of substrate microtopography on focal adhesion maturation and actin organization via the RhoA/ROCK pathway. Biomaterials . Elsevier Ltd, **32**, 9568, 2011.

126. Madhurakkat Perikamana, S.K., Lee, J., Ahmad, T., Kim, E.M., Byun, H., Lee, S., et al. Harnessing biochemical and structural cues for tenogenic differentiation of adipose derived stem cells (ADSCs) and development of an in vitro tissue interface mimicking tendon-bone insertion graft. Biomaterials. **165**, 79, 2018.

127. Caliari, S.R., and Harley, B.A.C. Structural and biochemical modification of a collagen scaffold to selectively enhance MSC tenogenic, chondrogenic, and osteogenic differentiation. Adv Healthc Mater. **3**, 1086, 2014.

128. Yin, Z., Chen, X., Song, H. xin, Hu, J. jie, Tang, Q. mei, Zhu, T., et al. Electrospun scaffolds for multiple tissues regeneration invivo through topography dependent induction of lineage specific differentiation. Biomaterials . Elsevier Ltd, **44**, 173, 2015.

129. Maharam, E., Yaport, M., Villanueva, N.L., Akinyibi, T., Laudier, D., He, Z., et al. Rho/Rock signal transduction pathway is required for MSC tenogenic differentiation. Bone Res. **3**, 2015.

130. Bhadriraju, K., Yang, M., Alom Ruiz, S., Pirone, D., Tan, J., and Chen, C.S. Activation of ROCK by RhoA is regulated by cell adhesion, shape, and cytoskeletal tension. Exp Cell Res. **313**, 3616, 2007.

131. Flinn, H.M., and Ridley, A.J. Rho stimulates tyrosine phosphorylation of focal adhesion kinase, p130 and paxillin. J Cell Sci. England, **109 (Pt 5**, 1133, 1996.

132. Totsukawa, G., Yamakita, Y., Yamashiro, S., Hartshorne, D.J., Sasaki, Y., and Matsumura, F. Distinct roles of ROCK (Rho-kinase) and MLCK in spatial regulation of MLC phosphorylation for assembly of stress fibers and focal adhesions in 3T3 fibroblasts. J Cell Biol . The Rockefeller University Press, **150**, 797, 2000.

133. McBeath, R., Pirone, D.M., Nelson, C.M., Bhadriraju, K., and Chen, C.S. Cell Shape, Cytoskeletal Tension, and RhoA Regulate Stem Cell Lineage Commitment. Dev Ceel. **6**, 483, 2004.

134. Tao, X., Liu, J., Chen, L., Zhou, Y., and Tang, K. EGR1 induces tenogenic differentiation of tendon stem cells and promotes rabbit rotator cuff repair. Cell Physiol Biochem. **35**, 699, 2015.

135. Karin, M., Liu, Z. g, and Zandi, E. AP-1 function and regulation. Curr Opin Cell Biol. England, **9**, 240, 1997.

136. Ramachandran, A., Gong, E.M., Pelton, K., Ranpura, S.A., Mulone, M., Seth, A., et al. FosB Regulates Stretch-Induced Expression of Extracellular Matrix Proteins in Smooth Muscle. Am J Pathol . Elsevier, **179**, 2977, 2011.

137. Lin, C.-H., Yu, M.-C., Tung, W.-H., Chen, T.-T., Yu, C.-C., Weng, C.-M., et al. Connective tissue growth factor induces collagen I expression in human lung fibroblasts through the Rac1/MLK3/JNK/AP-1 pathway. Biochim Biophys Acta. Netherlands, **1833**, 2823, 2013.

138. Popov, C., Burggraf, M., Kreja, L., Ignatius, A., Schieker, M., and Docheva, D. Mechanical stimulation of human tendon stem/progenitor cells results in upregulation of matrix proteins, integrins and MMPs, and activation of p38 and

ERK1/2 kinases. BMC Mol Biol . **16**, 6, 2015.

139. Dupont, S. Role of YAP/TAZ in cell-matrix adhesion-mediated signalling and mechanotransduction. Exp Cell Res. United States, **343**, 42, 2016.

140. Codelia, V.A., Sun, G., and Irvine, K.D. Regulation of YAP by mechanical strain through Jnk and Hippo signaling. Curr Biol. **24**, 2012, 2014.

141. Halder, G., Dupont, S., and Piccolo, S. Transduction of mechanical and cytoskeletal cues by YAP and TAZ. Nat Rev Mol Cell Biol . Nature Publishing Group, **13**, 591, 2012.

142. Schroeder, M.C., and Halder, G. Regulation of the Hippo pathway by cell architecture and mechanical signals. Semin Cell Dev Biol . Elsevier Ltd, **23**, 803, 2012.

143. Dupont, S., Morsut, L., Aragona, M., Enzo, E., Giulitti, S., Cordenonsi, M., et al. Role of YAP/TAZ in mechanotransduction. Nature. Nature Publishing Group, **474**, 179, 2011.

144. Aragona, M., Panciera, T., Manfrin, A., Giulitti, S., Michielin, F., Elvassore, N., et al. A mechanical checkpoint controls multicellular growth through YAP/TAZ regulation by actin-processing factors. Cell . Elsevier Inc., **154**, 1047, 2013.

145. Calvo, F., Ege, N., Grande-Garcia, A., Hooper, S., Jenkins, R.P., Chaudhry, S.I., et al. Mechanotransduction and YAP-dependent matrix remodelling is required for the generation and maintenance of cancer-associated fibroblasts. Nat Cell Biol. Nature Publishing Group, **15**, 637, 2013.

146. Tomás, A.R., Gonçalves, A.I., Paz, E., Freitas, P., Domingues, R.M.A., and Gomes, M.E. Magneto-mechanical actuation of magnetic responsive fibrous scaffolds boosts tenogenesis of human adipose stem cells. Royal Society of Chemistry, 18255, 2019.

147. Hayashi, N., Sato, T., Yumoto, M., Kokabu, S., Fukushima, Y., Kawata, Y., et al. Cyclic stretch induces decorin expression via yes-associated protein in tenocytes: A possible mechanism for hyperplasia in masticatory muscle tendon-aponeurosis hyperplasia. J Oral Maxillofac Surgery, Med Pathol . **31**, 175, 2019.

148. Robinson, K.A., Sun, M., Barnum, C.E., Weiss, S.N., Huegel, J., Shetye, S.S., et al. Decorin and biglycan are necessary for maintaining collagen fibril structure, fiber realignment, and mechanical properties of mature tendons. Matrix Biol. **64**, 81, 2017.

149. Maeda, T., Sakabe, T., Sunaga, A., Sakai, K., Rivera, A.L., Keene, D.R., et al. Conversion of Mechanical Force into TGF-β-Mediated Biochemical Signals. Curr Biol . Elsevier, **21**, 933, 2011.

150. Jones, E.R., Jones, G.C., Legerlotz, K., and Riley, G.P. Cyclical strain modulates

metalloprotease and matrix gene expression in human tenocytes via activation of TGFβ. Biochim Biophys Acta - Mol Cell Res . **1833**, 2596, 2013.

151.   Varelas, X., Sakuma, R., Samavarchi-Tehrani, P., Peerani, R., Rao, B.M., Dembowy, J., et al. TAZ controls Smad nucleocytoplasmic shuttling and regulates human embryonic stem-cell self-renewal. Nat Cell Biol. England, **10**, 837, 200

Chapter III

High-throughput methods in the discovery and study of biomaterials and materiobiology

The complex interaction of cells with biomaterials (i.e., materiobiology) plays an increasingly pivotal role in the development of novel implants, biomedical devices, and tissue engineering scaffolds to treat diseases, aid in the restoration of bodily functions, construct healthy tissues or regenerate diseased ones. However, the conventional approaches are incapable of screening the huge amount of potential material parameter combinations to identify the optimal cell responses, and involves a combination of serendipity and many series of trial-and-error experiments. For advanced tissue engineering and regenerative medicine, highly efficient and complex bioanalysis platforms are expected to explore the complex interaction of cells with biomaterials using combinatorial approaches that offer desired complex microenvironments during healing, development, and homeostasis. In this review, we first introduce materiobiology and its high-throughput screening (HTS). Then, we present an in-depth of the recent progress of 2D/3D HTS platforms (i.e., gradient and microarray) in the principle, preparation, their screening for materiobiology, and combination with other advanced technologies. The Compendium for Biomaterial Transcriptomics and high content imaging, computational simulations, and their translation towards commercial and clinical uses are highlighted. In the final section, current challenges and future perspectives are discussed. High-throughput experimentation within the field of materiobiology enables the elucidation of the relationships between biomaterial properties and biological behaviour, and thereby serves a potential tool for accelerating the development of high-performance biomaterials.

Compendium for Biomaterial Transcriptomics-cBiT

A major factor in terms of studying cell-material interactions is the variance between different laboratories using not only different material preparations and characterizations as a biomaterial analogue, also the variations in cell types, culture conditions, the specific type of cell behaviour, and the analysis approach. To truly come to the core parameters that drive cell behaviour, which is induced by physicochemical properties of biomaterials or used biochemical stimulation, a more unified approach and general comprehension needs to be created concerning the complete development route and analysis phase. This general comprehension can only be achieved when data from various sources with defined analysis data and biological approaches is shared and available for reuse. For this purpose, cBiT [1] has been created to facilitate the sharing of results from the biointerface field ranging from various methodologies for material preparation and characterization as described in the previous sections as well as performing generalized biological assessments, outcomes, and high-content imaging in a standardized fashion, which is the focus of this section.

Measuring Biological Outcome: Gene Expression

Measuring gene expression is one of the widely used ways to evaluate how cells respond to biomaterials, because it gives a snapshot of cellular activity at the molecular scale. There are several methods by which gene expression can be measured, and each has its advantages and challenges. In this section, we will focus on the basic mechanism of gene expression and the relevance of the different measurement techniques. Furthermore, we will summarize gene expression measurement tools, and how they have been implemented to understand biomaterial-cell interactions.

Relevance of Gene Expression in Research

Genes are the basic unit of the genome sequence, which encodes a set of functional products, proteins, and ultimately dictates cell phenotype and function. For this reason, gene expression levels are measured in many areas of biological research, such as oncology [2–5] and developmental biology [6–9]. In addition, gene expression levels have been measured in biomaterials research to determine whether the engineered biomaterial is capable of inducing stem cell differentiation [10–12], or can support the phenotype of differentiated cells for prospective tissue engineering applications [13–15]. To make conclusions regarding the compatibility of the biomaterial, researchers select specific "marker" genes based on their scientific question. Marker genes can be used to identify cell types or cell phenotypes. For instance, ALP has been used in bone tissue engineering to assess early osteogenic differentiation [16]. When the expression of ALP upregulated *in vitro*, it indicates that the biomaterial has potential osteoinductive

properties *in vivo*. For some tissues, there are more than one marker gene. For instance, in tendon tissue engineering, the combination of the expression of three or four genes, including *scleraxis* gene *(SCX)* and *tenomodulin (TNMD),* are used to determine the tenogenic capacity of the engineered biomaterial [17,18]. Furthermore, marker genes can be used to show the activity of a signaling pathway that regulates the response of a cell to the biomaterial; and can provide valuable insights into the fundamentals of cell-biomaterial interactions [19,20]. Hence, information obtained from gene expression data can then be used to modify and specifically tailor the biomaterial.

Regulation of gene expression

When a cell receives signals from its environment, it can respond to it by changing its shape and proliferation rate, differentiating into another cell type, maintaining its phenotype, or dying. These signals can be small molecules (Fig.1 (1)), or the surface topography (Fig.1 (2)), and surface chemistry (Fig.1 (3)) of a biomaterial. They are then transmitted to the nucleus through certain biological pathways. In the nucleus, there are intermediary elements such as transcription factors and enzymes, both of which regulate the gene expression (Fig.1 (4)). Transcription factors are transcriptional activator proteins that bind to the DNA sequence, and stimulate the expression of target genes (Fig.1 (5)). Enzymes, such as RNA polymerase, are involved in the production of messenger RNA (mRNA) that can be considered as a copy of the gene. Afterward, genes are converted into proteins, and ultimately result in cellular response, such as proliferation, apoptosis, or differentiation (Fig.1 (6)). In the gene expression regulatory machine, there are also repressors that regulate the gene expression process by binding to a specific DNA sequence or other transcription factors, and inhibit gene expression.

Gene expression can also be controlled through epigenetic regulation mechanisms, such as DNA methylation and histone modifications. Measurement of DNA methylation (the process of gene methylation) provides information on the epigenetic make-up of a cell, which can indicate how the particular biomaterial affects gene expression. For instance, Schellenberg *et al.* investigated the DNA methylation profiles of mesenchymal stem cells cultured on TCP or on PDMS [21]. They showed that matrix elasticity does not have a major impact on DNA methylation profiles, but that it influences differentiation towards adipogenic and osteogenic lineage. This information is vital, as it emphasizes the relevance of matrix elasticity when designing a biomaterial with which cells will directly interact. Similar to DNA methylation, histone (the proteins in cell nuclei that DNA is rolled over) acetylation and deacetylation are involved in gene expression regulation by changing the accessibility of DNA to transcription factors. Downing *et al.* reported that biophysical cues provided by parallel microgrooves decreased histone deacetylase activity, and therefore, lead to increased histone H3 acetylation and methylation [22]. They concluded that a change in cell morphology is responsible for

modulation of the epigenetic state of cells. Hence, understanding the regulation of gene expression can help to manipulate cellular states or cellular differentiation.
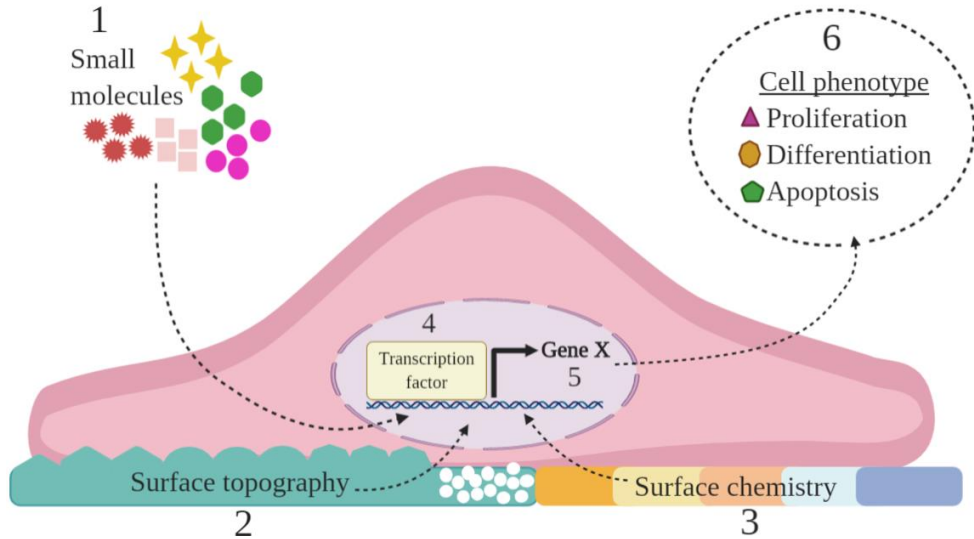

Figure 1. *Cells receive external stimuli, such as small molecules (1), or the surface topography (2) and surface chemistry (3) of a material, and produce a response via signaling pathways. The pathways can, in turn, lead to the production of transcription enhancers, such as transcription factors (4) that enable the expression of certain genes (5). This gene expression can lead to different cell phenotypes (6) such as proliferation, differentiation, or cell death.*

Methods to Measure Gene Expression

Since the discovery of DNA, scientists have been developing different methods to measure gene expression. Each method has advantages and challenges, but the selection of the appropriate tool can provide valuable information. In this section, we describe the commonly used gene expression measurement tools, their advantages, and limitations, and finally, give examples from biomaterials research.

Fluorescence *in situ* hybridization (FISH)

The presence of a biomaterial not only affects the gene expression of the cells that are in direct contact with it, but also that of the cells in the vicinity. It is, therefore, important to understand gene expression in the context of the spatial organization of cells within the tissue. FISH allows quantification of both *in vitro* and *in vivo* spatial gene expression, which makes it a very useful technique. For instance, Zreiqat *et al.* investigated the

expression of osteoblastic genes in hBM-MSCs that were cultured on pure titanium and titanium alloy [23]. They used FISH to quantify the gene expression, and found that there was an increase in the expression of osteoblastic genes on the cells cultured on pure titanium and titanium alloy compared to TCP plates. In order to confirm the validity of their results, they performed quantitative immunohistochemistry to measure the expression of corresponding proteins. Their results provided initial information on how small differences in the surface chemistry and structure of biomaterials can induce osteogenic differentiation. Similarly, Knabe *et al.* showed the effect of bioactive glass-ceramics on the expression of osteogenic genes and corresponding proteins by performing Q-FISH and immunohistochemistry, respectively [24]. They reported that glass-ceramics could be regarded as potential bone substitutes.

Although it is a useful technique, FISH does have several limitations. Firstly, the optimization of samples, multiplexing, and the number of cells and materials to be used in the detection all require a lot of time and effort. Secondly, in order to detect the gene expression, histological slides are prepared out of the material or tissue, and this requires extra handling of the samples. Therefore, FISH is not as straightforward as other gene expression methods. However, this technique is very useful for identifying the spatial gene expression in particular.

Quantitative polymerase chain reaction (qPCR)

When investigating the overall expression of the target gene under certain conditions, qPCR is the most frequently used technique. As it is commonly used in biological research, sample preparation and data analysis methods are well-defined for qPCR. Therefore, performing qPCR requires less optimization and eliminates limitations in sample handling.

In biomaterials research, qPCR can be used to answer various biological questions. In our recent study, we employed qPCR to measure the expression of ALP, OCN and OPN genes in order to identify the surface topographies that can induce osteogenic differentiation [25]. Here, we reported that certain surface topographies induce osteogenic differentiation more than others *in vitro*; and these selected surfaces are capable of osteogenic differentiation *in vivo*. In addition, qPCR can be performed to understand and evaluate the initial biological response of a cell to a material. For instance, Kato *et al.* investigated the gene expression of *Heat-Shock Protein* (*HSP*) *70*, *90,* and *47* in HeLa S3 cells cultured on different materials, such as TCP, silicone, tetrafluoroethylene-hexafluoropropylene copolymer, and cellulose [26]. Their results showed that *HSP 70* mRNA can be used as a marker for the investigation of cell-polymer interactions. In another study, the same group investigated the expression of the oncogenes *c-myc, c-fos*, and *p53* (the tumor suppressor gene) in human fibroblasts cultured on polymeric

biomaterials. They evaluated the carcinogenic activity of cells, and showed that p53 is a very sensitive marker in the evaluation of the carcinogenic potential of a biomaterial [27].

For practical reasons, typically 1-10 genes can be investigated in qPCR. For this reason, marker genes are pre-defined when performing qPCR. Another limitation of qPCR is the fact that it does not provide gene expression data with single-cell resolution. Therefore, when the marker genes are not known, and gene expression in single-cell resolution is desired, other gene expression methods are used.

Transcriptomics technologies

Although using the aforementioned tools to measure gene expression provides useful data when marker genes are defined, using such methods when marker genes are not defined is more challenging. Transcriptomics has been developed over the last three decades, and is more advanced in that it enables assessment of the global gene expression. An advantage of implementing transcriptomics technologies in biomaterial research is that it enables the discovery of novel genes, and identification of target genes and signaling pathways. This information can then be used to enhance the performance of biomaterials. In our recent work, we investigated the influence of material properties, such as microporosity and ion composition, of a set of synthesized osteoinductive and non-inductive calcium phosphate ceramic materials on the transcriptomics profile of osteogenic cells [28]. Transcriptomics revealed the crucial role of the ECM deposition in osteoinduction, which is controlled by surface topography and calcium phosphate ions.

Microarray and RNA Sequencing

DNA microarray and RNA sequencing (RNA-seq) are the two methods used in transcriptomics-based techniques. They provide mapping and quantification of the whole transcriptome of cells. Microarray relies on the hybridization of fluorescently-labeled complementary DNA (cDNA) obtained from cells to complementary DNA sequences on probes. In RNA-seq, adaptors are added to cDNA fragments in order to allow recognition for each cDNA fragment, and fragments with adapters are amplified. The gene expression is determined based on the fluorescence intensity. Microarray differs from RNA-seq in that it relies on pre-defined DNA sequences, whereas RNA-seq sequences the whole transcriptome of cells. Therefore, RNA-seq provides a complete picture of the cell transcriptome, and increases the likelihood of discovering novel genes. Given these reasons, a microarray is being replaced by RNA-seq in transcriptomics based research.

Both microarray and RNA-seq provide transcriptomics data belonging to a cell population; however, in some cases, it is important to understand the gene expression profile of individual cells. For such cases, single-cell RNA sequencing (scRNA-seq) is used. It works in a manner similar to RNA-seq, but instead provides the whole

transcriptome of each individual cell. This technology has been used in cancer research [29–31] and in developmental biology [32,33]; however, its use has not yet expanded to biomaterials research. scRNA-seq can be extremely useful for understanding the influence of biomaterials that possess heterogeneous structures, such as gradient surfaces or surfaces with various surface chemistry or topographical structures.

Transcriptomics in biomaterial research

As mentioned above, the use of transcriptomics-based technology in research has been growing. In 2000, there was only one publication that included transcriptomics-based methods [34]. In 2019, there are more than 50 publications. We divided the most abundant topics into three categories: 1) 2D-3D culture systems, 2) surface topography, and 3) titanium, which is one of the most frequently used materials in the clinic and biomaterials research.

1) Impact of 2D-3D culture systems on cell differentiation

Herlofsen *et al.* investigated the chondrogenic differentiation of hMSCs cultured on 2D and 3D environments at different time points [35]. They employed the Illumina microarray platform as a transcriptomics tool and identified 1,969 differentially expressed genes between monolayer hMSCs and chondrogenic cells. With further bioinformatics analysis, they highlighted the role of genes involved in the ECM and transcription factors involved in ECM synthesis. Similarly, Kumar *et al.* investigated stem cell response to a library of scaffolds with varied 3D structures [36]. Their transcriptome analysis revealed that each type of scaffold induced a unique gene expression signature. Furthermore, of each structure, only the nanofibrous morphology induced osteogenic differentiation of hBMSC in the absence of osteogenic supplements. Baker *et al.* also adopted transcriptomics-based research to investigate the influence of 2D and 3D culture of hBMSC [37]. They reported that 3D scaffolds induce the activity of TGF-β and cell-adhesion/ECM-receptor pathways that can be used to control hBMSC differentiation. In addition, Zhang *et al.* performed RNA-seq, and reported that gene expression profiles of endothelial cells and pericytes co-cultured in 3D were similar. However, in 2D culture, each cell type displayed different vascular signatures [38].

2) Influence of surface topography on cell fate

This subject has been the focus of many research groups [39–42]; however, only a few studies have made use of transcriptomics to obtain a broader picture of cellular response to a biomaterial. For example, Dalby *et al.* investigated the response of fibroblasts to micro-grooved topographies in order to understand the events taking place at initial cell contact with the scaffold [43]. In their study, they demonstrated that the genes involved in cell signaling, cytoskeleton, ECM remodeling, and DNA transcription are

differentially expressed between microgrooves and flat surfaces. The same group also employed RNA-seq technology to understand the mechanisms through which skeletal stem cells (SSCs) preserve their multipotency or differentiate towards fibroblastic lineage [44]. Their results indicated that activation of mitogen-activated protein kinases (MAPKs) is involved in the control of SSC self-renewal and differentiation. With a similar approach, Abagnale *et al.* showed that different surface topographies induce differentiation of stem cells towards osteogenic and adipogenic differentiation [45]. Furthermore, Darnell *et al.* examined the effect of surface stiffness on the global gene expression of mouse mesenchymal stem cells [46]. They found that stiffer hydrogels induce the expression of genes that are involved in bone remodeling, cell-matrix adhesion, proteolysis, and IL- 1 and androgen receptor signaling.

3) *Effect of titanium on cell phenotype*

Titanium is one of the most frequently used materials in the clinic. Therefore, many researchers have focused on understanding the interaction between cells and titanium surfaces. Ku *et al.* investigated the effect of different titanium surface treatments on the global gene expression of osteoblasts [47]. They reported that the expression of the genes involved in the regulation of FAK and apoptosis depending on the metal ion release from the surface. Similarly, Carinci *et al.* investigated the titanium-cell interaction based on global gene expression profiling by using a custom-made microarray called Human 19.2 K DNA microarray [48]. They reported that the titanium surfaces induced a broad range of functional activities, including apoptosis, vesicular transport, and structural function. Similarly, in our recent work, we made use of microarray technology to explore cell-biomaterial interactions to assess and improve material properties [49]. For this, we tested the response of MG-63 cells to 23 different materials relevant for bone regeneration. Our results showed the role of TGF- β and WNT signalling in the cellular response to osteoinductive materials and activity of FAK signalling in differential cell adhesion kinetics.

Other omics technologies

Alongside transcriptomics, proteomics and metabolomics are the two other omics technologies through which cellular responses to a biomaterial can be investigated. Proteomics allows protein expression profiling, and enables identification of post-translational modification events and subcellular localization, and the relevant functional aspects of the proteome of cells. Metabolomics is another omics technology, which provides chemical fingerprints – metabolites – that specific cellular processes leave behind. Alakpa *et al.* used supramolecular hydrogels to target the range of stem cell phenotypes by measuring the metabolites that they leave behind [50]. Based on their results, they identified the bioactive metabolites that can target bone and cartilage

formation. Proteomics and metabolomics can also be used to generate complementary information to transcriptomics data. Guerette *et al.* showed how the integration of high-throughput RNA-seq with proteomics accelerated biomimetic engineering [51].

The current standing and future of transcriptomics in biomaterials research

Understanding the biology of cells, their healthy and diseased states, and their response to external signals, are the goals in both fundamental and applied biology. Advancements in transcriptomics technology have enabled the collection of the whole transcriptome of all cells in a tissue or organ, which has significantly contributed to our understating of cell biology. Given this, there are attempts to gather transcriptome data in a consortium, and make it useful for public research. One of the consortiums founded with this purpose is The Human Cell Atlas [52]. The Human Cell Atlas is a collection of maps that describes and defines the cellular basis of health and disease. This consortium benefits from the technological power of single-cell profiling. For instance, MacParland *et al.* created a map of cells in the human liver by using scRNA-seq, and provided transcriptional profiles of 8,444 parenchymal and non-parenchymal cells [53]. They further identified 20 discrete cell populations by using gene expression patterns, flow cytometry, and immunohistochemical examinations. A similar approach was taken by Ledergor *et al.* [54], Vento-Tormo *et al.* [55], and Reyfman *et al.* [56], where they revealed the transcriptome of different organs in healthy and diseased donors. The Connectivity Map (CMap) database [57,58] creates a genome-scale library of cellular signatures, and catalogs transcriptional responses to chemical, genetic, and disease perturbation in order to accelerate the discovery of novel therapeutics. Both CMap and The Human Cell Atlas benefit from the collection of large datasets, which in turn informs the research of its users.

Currently, there are several repositories that are used to contain, curate, and maintain metadata, and raw and processed transcriptomics data. The Gene Expression Omnibus (GEO) database [59] and ArrayExpress [60] provide up-to-date raw and processed transcriptomics data of various species. Once downloaded, data is ready for further processing or analysis. The cBiT is an open access online web tool that provides data storage [1]. In fact, it is the only repository that offers biomaterial-based transcriptomics along with metadata of materials, including the biological and technical properties. Therefore, cBiT encourages both material scientists and cell biologists all around the world to submit their transcriptomics data in order to make it publically available. The fact that transcriptome data and metadata of material properties is publically available enables its application in the research of the wider scientific community. Furthermore, comparing and combining the transcriptomics data of different data-sets opens the door for the discovery of new materials. A paradigm shift from traditional experimental

sciences to omics-based sciences can be achieved by combining the information from all the omics data into one repository. When all these data are gathered with the information coming from high content imaging, we will have a better understanding of cellular response to materials, enhance existing materials, and engineer new materials. Therefore, the future of cell-based biomaterials research lies in the collaboration, sharing, and interpretation of existing data. When the biomaterials field follows the slipstream of other transcriptome-based research present in other fields, the discovery of new materials will be inevitable.

References

1. Hebels, D.G.A.J., Carlier, A., Coonen, M.L.J., Theunissen, D.H., and de Boer, J. cBiT: A transcriptomics database for innovative biomaterial engineering. Biomaterials. **149**, 88, 2017.

2. Vinagre, J., Almeida, A., Pópulo, H., Batista, R., Lyra, J., Pinto, V., et al. Frequency of TERT promoter mutations in human cancers. Nat Commun. **4**, 2013.

3. Herranz, D., Muñoz-Martin, M., Cañamero, M., Mulero, F., Martinez-Pastor, B., Fernandez-Capetillo, O., et al. Sirt1 improves healthy ageing and protects from metabolic syndrome-associated cancer. Nat Commun. **1**, 2010.

4. Lu, J., Getz, G., Miska, E.A., Alvarez-Saavedra, E., Lamb, J., Peck, D., et al. MicroRNA expression profiles classify human cancers. Nature. **435**, 834, 2005.

5. Nilsson, J., Skog, J., Nordstrand, A., Baranov, V., Mincheva-Nilsson, L., Breakefield, X.O., et al. Prostate cancer-derived urine exosomes: A novel approach to biomarkers for prostate cancer. Br J Cancer. Nature Publishing Group, **100**, 1603, 2009.

6. Ragazzini, R., Pérez-Palacios, R., Baymaz, I.H., Diop, S., Ancelin, K., Zielinski, D., et al. EZHIP constrains Polycomb Repressive Complex 2 activity in germ cells. Nat Commun. **10**, 1, 2019.

7. Kinsella, C.M., Ruiz-Ruano, F.J., Dion-Côté, A.-M., Charles, A.J., Gossmann, T.I., Cabrero, J., et al. Programmed DNA elimination of germline development genes in songbirds. bioRxiv . Springer US, 444364, 2018.

8. Seishima, R., Leung, C., Yada, S., Bte, K., Murad, A., Tan, L.T., et al. Neonatal Wnt-dependent Lgr5 positive stem cells are essential for uterine gland development. Nat Commun. Springer US, **10**, 1, 2019.

9. Webster, K.A., Schach, U., Ordaz, A., Steinfeld, J.S., Draper, B.W., and Siegfried, K.R. Dmrt1 is necessary for male sexual development in zebrafish. Dev Biol . Elsevier, **422**, 33, 2017.

10. Bratt-Leal, A.M., Carpenedo, R.L., Ungrin, M.D., Zandstra, P.W., and McDevitt, T.C. Incorporation of biomaterials in multicellular aggregates modulates pluripotent stem cell differentiation. Biomaterials . Elsevier Ltd, **32**, 48, 2011. 11. Smith, L.A., Liu, X., Hu, J., and Ma, P.X. The Enhancement of human embryonic stem cell osteogenic differentiation with nano-fibrous scaffolding. Biomaterials. Elsevier Ltd, **31**, 5526, 2010.

12. Wang, W., Itaka, K., Ohba, S., Nishiyama, N., Chung, U. il, Yamasaki, Y., et al. 3D spheroid culture system on micropatterned substrates for improved differentiation efficiency of multipotent mesenchymal stem cells. Biomaterials. Elsevier Ltd, **30**, 2705, 2009.

13. Schuh, E., Kramer, J., Rohwedel, J., Notbohm, H., Müller, R., Gutsmann, T., et al. Effect of matrix elasticity on the maintenance of the chondrogenic phenotype. Tissue Eng - Part A. **16**, 1281, 2010.

14. Prasad, C.K., and Krishnan, L.K. Regulation of endothelial cell phenotype by biomimetic matrix coated on biomaterials for cardiovascular tissue engineering. Acta Biomater. **4**, 182, 2008.

15. Brodkin, K.R., García, A.J., and Levenston, M.E. Chondrocyte phenotypes on different extracellular matrix monolayers. Biomaterials. **25**, 5929, 2004.

16. Yuan, H., Fernandes, H., Habibovic, P., de Boer, J., Barradas, A.M.C., de Ruiter, A., et al. Osteoinductive ceramics as a synthetic alternative to autologous bone grafting. Proc Natl Acad Sci . **107**, 13614, 2010.

17. Zhang, B., Luo, Q., Deng, B., Morita, Y., Ju, Y., and Song, G. Construction of tendon replacement tissue based on collagen sponge and mesenchymal stem cells by coupled mechano-chemical induction and evaluation of its tendon repair abilities. Acta Biomater. Acta Materialia Inc., **74**, 247, 2018.

18. Zhang, J., Li, B., and Wang, J.H.C. The role of engineered tendon matrix in the stemness of tendon stem cells in vitro and the promotion of tendon-like tissue formation in vivo. Biomaterials . Elsevier Ltd, **32**, 6972, 2011.

19. Siddappa, R., Martens, A., Doorn, J., Leusink, A., Olivo, C., Licht, R., et al. cAMP/PKA pathway activation in human mesenchymal stem cells in vitro results in robust bone formation in vivo. Proc Natl Acad Sci. **105**, 7281, 2008.

20. Xu, B., Song, G., Ju, Y., Li, X., Song, Y., and Watanabe, S. RhoA / ROCK , Cytoskeletal Dynamics , and Focal Adhesion Kinase are Required for Mechanical Stretch-Induced Tenogenic Differentiation of Human Mesenchymal Stem Cells. J Cell Physiol. 2722, 2011.

21. Schellenberg, A., Joussen, S., Moser, K., Hampe, N., Hersch, N., Hemeda, H., et al. Matrix elasticity, replicative senescence and DNA methylation patterns of mesenchymal stem cells. Biomaterials. Elsevier Ltd, **35**, 6351, 2014.

22. Downing, T.L., Soto, J., Morez, C., Houssin, T., Fritz, A., Yuan, F., et al. Biophysical regulation of epigenetic state and cell reprogramming. Nat Mater . Nature Publishing Group, **12**, 1154, 2013. Available from: http://dx.doi.org/10.1038/nmat3777

23. Zreiqat, H., and Howlett, C.R. Titanium substrata composition influences osteoblastic phenotype: In vitro study. J Biomed Mater Res. **47**, 360, 1999.

24. Knabe, C., Stiller, M., Berger, G., Reif, D., Gildenhaar, R., Howlett, C.R., et al. The effect of bioactive glass ceramics on the expression of bone-related genes and proteins in vitro. Clin Oral Implants Res. **16**, 119, 2005.

25. Hulshof, F.F.B., Papenburg, B., Vasilevich, A., Hulsman, M., Zhao, Y., Levers, M., et al. Mining for osteogenic surface topographies: In silico design to in vivo osseo-integration. Biomaterials . Elsevier Ltd, **137**, 49, 2017.

26. Kato, S., Akagi, T., Kishida, A., Sugimura, K., and Akashi, M. Evaluation of biological responses to polymeric biomaterials by RT-PCR analysis III: Study of HSP 70, 90 and 47 mRNA expression. J Biomater Sci Polym Ed. **8**, 809, 1997.

27. Kato, S., Akagi, T., Kishida, A., Sugimura, K., and Akashi, M. Evaluation of biological responses to polymeric biomaterials by RT-PCR analysis IV: study of c-myc, c-fos and p53 mRNA expression Shinya. Biomaterials. **21**, 521, 2000.

28. Groen, N., Yuan, H., Hebels, D.G.A.J., Koçer, G., Mbuyi, F., LaPointe, V., et al. Linking the Transcriptional Landscape of Bone Induction to Biomaterial Design Parameters. Adv Mater. **29**, 2017.

29. Chung, W., Eum, H.H., Lee, H.-O., Lee, K.-M., Lee, H.-B., Kim, K.-T., et al. Single-cell RNA-seq enables comprehensive tumour and immune cell profiling in primary breast cancer. Nat Commun. The Author(s), **8**, 15081, 2017.

30. Ramsköld, D., Luo, S., Wang, Y.-C., Li, R., Deng, Q., Faridani, O.R., et al. Full-length mRNA-Seq from single-cell levels of RNA and individual circulating tumor cells. Nat Biotechnol . Nature Publishing Group, a division of Macmillan Publishers Limited. All Rights Reserved., **30**, 777, 2012.

31. Lee, M.-C.W., Lopez-Diaz, F.J., Khan, S.Y., Tariq, M.A., Dayn, Y., Vaske, C.J., et al. Single-cell analyses of transcriptional heterogeneity during drug tolerance transition in cancer cells by RNA sequencing. Proc Natl Acad Sci . **111**, E4726 LP, 2014. A

32. Pollen, A.A., Nowakowski, T.J., Shuga, J., Wang, X., Leyrat, A.A., Lui, J.H., et al. Low-coverage single-cell mRNA sequencing reveals cellular heterogeneity and activated signaling pathways in developing cerebral cortex. Nat Biotechnol . Nature Publishing Group, **32**, 1053, 2014. A33.   Xue, Z., Huang, K., Cai, C., Cai, L., Jiang, C., Feng, Y., et al. Genetic programs in human and mouse early embryos revealed by single-cell RNA sequencing. Nature . Nature Publishing Group, a division of Macmillan Publishers Limited. All Rights Reserved., **500**, 593, 2013.

34. Xynos, I.D., Edgar, A.J., Buttery, L.D.K., Hench, L.L., and Polak, J.M. Ionic products of bioactive glass dissolution increase proliferation of human osteoblasts and induce insulin-like growth factor II mRNA expression and protein synthesis. Biochem Biophys Res Commun. **276**, 461, 2000.

35. Herlofsen, S.R., Küchler, A.M., Melvik, J.E., and Brinchmann, J.E. Chondrogenic Differentiation of Human Bone Marrow-Derived Mesenchymal Stem Cells in Self-Gelling Alginate Discs Reveals Novel Chondrogenic Signature Gene Clusters. Tissue Eng Part A . **17**, 1003, 2011.

36. Kumar, G., Tison, C.K., Chatterjee, K., Pine, P.S., Mcdaniel, H., Salit, M.L., et al. The Determination of Stem Cell Fate by 3D Scaffold Structures through the Control of Cell Shape. Biomaterials. **32**, 9188, 2012.

37. Baker, B.A., Pine, P.S., Chatterjee, K., Kumar, G., Lin, N.J., McDaniel, J.H., et al. Ontology analysis of global gene expression differences of human bone marrow stromal cells cultured on 3D scaffolds or 2D films. Biomaterials . Elsevier Ltd, **35**, 6716, 2014.

38. Zhang, J., Schwartz, M.P., Hou, Z., Bai, Y., Ardalani, H., Swanson, S., et al. A Genome-wide Analysis of Human Pluripotent Stem Cell-Derived Endothelial Cells in 2D or 3D Culture. Stem Cell Reports . ElsevierCompany., **8**, 907, 2017.

39. Pieuchot, L., Marteau, J., Guignandon, A., Dos Santos, T., Brigaud, I., Chauvy, P.F., et al. Curvotaxis directs cell migration through cell-scale curvature landscapes. Nat Commun. **9**, 2018.

40. Costa, D.O., Prowse, P.D.H., Chrones, T., Sims, S.M., Hamilton, D.W., Rizkalla, A.S., et al. The differential regulation of osteoblast and osteoclast activity bysurface topography of hydroxyapatite coatings. Biomaterials . Elsevier Ltd, **34**, 7215, 2013.

41. Khang, D., Choi, J., Im, Y.M., Kim, Y.J., Jang, J.H., Kang, S.S., et al. Role of subnano-, nano- and submicron-surface features on osteoblast differentiation of bone marrow mesenchymal stem cells. Biomaterials . Elsevier Ltd, **33**, 5997, 2012.

42. Viswanathan, P., Ondeck, M.G., Chirasatitsin, S., Ngamkham, K., Reilly, G.C., Engler, A.J., et al. 3D surface topology guides stem cell adhesion and differentiation. Biomaterials . Elsevier Ltd, **52**, 140, 2015.

43. Dalby, M.J., Riehle, M.O., Yarwood, S.J., Wilkinson, C.D.W., and Curtis, A.S.G. Nucleus alignment and cell signaling in fibroblasts: Response to a micro-grooved topography. Exp Cell Res. **284**, 274, 2003.

44. Lee, L.C.Y., Gadegaard, N., de Andrés, M.C., Turner, L.A., Burgess, K. V., Yarwood, S.J., et al. Nanotopography controls cell cycle changes involved with skeletal stem cell self-renewal and multipotency. Biomaterials. 2017.

45. Abagnale, G., Steger, M., Nguyen, V.H., Hersch, N., Sechi, A., Joussen, S., et al. Surface topography enhances differentiation of mesenchymal stem cells towards osteogenic and adipogenic lineages. Biomaterials . Elsevier Ltd, **61**, 316, 2015.

46. Darnell, M., Gu, L., and Mooney, D. RNA-seq reveals diverse effects of substrate stiffness on mesenchymal stem cells. Biomaterials . Elsevier Ltd, **181**, 182, 2018.

47.   Ku, C.H., Browne, M., Gregson, P.J., Corbeil, J., and Pioletti, D.P. Large-scale gene expression analysis of osteoblasts cultured on three different Ti-6Al-4V surface treatments. Biomaterials. **23**, 4193, 2002.

48.   Carinci, F., Volinia, S., Pezzetti, F., Francioso, F., Tosi, L., and Piattelli, A. Titanium-Cell Interaction: Analysis of Gene Expression Profiling. J Biomed Mater Res - Part B Appl Biomater. **66**, 341, 2003.

49.   Groen, N., Tahmasebi, N., Shimizu, F., Sano, Y., Kanda, T., Barbieri, D., et al. Exploring the Material-Induced Transcriptional Landscape of Osteoblasts on Bone Graft Materials. Adv Healthc Mater. **4**, 1691, 2015.

50.   Alakpa, E. V., Jayawarna, V., Lampel, A., Burgess, K. V., West, C.C., Bakker, S.C.J., et al. Tunable Supramolecular Hydrogels for Selection of Lineage-Guiding Metabolites in Stem Cell Cultures. Chem. **1**, 298, 2016.

51.   Guerette, P.A., Hoon, S., Seow, Y., Raida, M., Masic, A., Wong, F.T., et al. Accelerating the design of biomimetic materials by integrating RNA-seq with proteomics and materials science. Nat Biotechnol . Nature Publishing Group, **31**, 908, 2013.

52.   Rozenblatt-Rosen, O., Stubbington, M.J.T., Regev, A., and Teichmann, S.A. The Human Cell Atlas: From vision to reality. Nature. pp. 451–3, 2017.

53.   MacParland, S.A., Liu, J.C., Ma, X.Z., Innes, B.T., Bartczak, A.M., Gage, B.K., et al. Single cell RNA sequencing of human liver reveals distinct intrahepatic macrophage populations. Nat Commun. **9**, 1, 2018.

54.   Ledergor, G., Weiner, A., Zada, M., Wang, S.Y., Cohen, Y.C., Gatt, M.E., et al. Single cell dissection of plasma cell heterogeneity in symptomatic and asymptomatic myeloma . Nat. Med. Springer US, 2018.

55.   Vento-tormo, R., Efremova, M., Botting, R.A., Turco, M.Y., Payne, R.P., Goncalves, A., et al. Reconstructing the human first trimester fetal–maternal interface using single cell transcriptomics. bioRxiv. 2018.

56.   Reyfman, P.A., Walter, J.M., Joshi, N., Anekalla, K.R., McQuattie-Pimentel, A.C., Chiu, S., et al. Single-cell transcriptomic analysis of human lung provides insights into the pathobiology of pulmonary fibrosis. Am J Respir Crit Care Med. **199**, 1517, 2019.

57.   Subramanian, A., Narayan, R., Corsello, S.M., Peck, D.D., Natoli, T.E., Lu, X., et al. A Next Generation Connectivity Map: L1000 Platform and the First 1,000,000 Profiles. Cell. Elsevier, **171**, 1437, 2017.

58.   Molecules, S., Lamb, J., Crawford, E.D., Peck, D., Modell, J.W., Blat, I.C., et al. The Connectivity Map: Using Gene-Expression Signatures to Connect Small Molecules, Genes, and Disease. **313**, 1929, 2006.

59.   Clough, E., and Barrett, T. The Gene Expression Omnibus Database. In: Mathé, E., and Davis, S., eds. Stat Genomics Methods Protoc . New York, NY: Springer New York, pp. 93–110, 2016.

60.   Parkinson, H., Kapushesky, M., Shojatalab, M., Abeygunawardena, N., Coulson, R., Farne, A., et al. ArrayExpress - A public database of microarray experiments and gene expression profiles. Nucleic Acids Res. **35**, 747, 2007.

Chapter IV

Self-agglomerated collagen patterns govern cell behaviour

Reciprocity between cells and their surrounding extracellular matrix is one of the main drivers for cellular function and, in turn, matrix maintenance and remodelling. Unravelling how cells respond to their environment is key in understanding mechanisms of health and disease. In all these examples, matrix anisotropy is an important element, since it can alter the cell shape and fate. In this work, the objective is to develop and exploit easy-to-produce platforms that can be used to study the cellular response to natural proteins assembled into diverse topographical cues. We demonstrate a robust and simple approach to form collagen substrates with different topographies by evaporating droplets of a collagen solution. Upon evaporation of the collagen solution, a stain of collagen is left behind, composed of three regions with a distinct pattern: an isotropic region, a concentric ring pattern, and a radially oriented region. The formation and size of these regions can be controlled by the evaporation rate of the droplet and initial collagen concentration. The patterns form topographical cues inducing a pattern-specific cell (tenocyte) morphology, density, and proliferation. Rapid and cost-effective production of different self-agglomerated collagen topographies and their interfaces enables further study of the cell shape-phenotype relationship *in vitro*. Substrate topography and in analogy tissue architecture remains a cue that can and will be used to steer and understand cell function *in vitro*, which in turn can be applied *in vivo*, e.g. in optimizing tissue engineering applications.

Chapter IV

Introduction

Cell morphology is affected by its physical environment, which was shown to strongly modulate cell fate. For instance, healthy tendon tissue is composed of highly ordered anisotropic collagen fibers and tenocytes adopt a spindle-like cell morphology and ultimately, functionally contribute to tissue homeostasis[1]. In tendinopathy, however, tissue organization is disrupted and, hence, the collagen network becomes more isotropic. Concordantly, tenocyte morphology transforms into a stellate-shape, and they change their proliferation speed and produce matrix proteins that compromise tendon function[2]. Various *in vitro* platforms have been developed to study the relation between matrix structure or substrate topography and cell morphology and the resulting downstream responses. Production of such *in vitro* platforms often requires the use of advanced tools such as micro-contact printing [3], electrospinning [4], or dip-pen nanolithography [5]. Whilst these tools allow the generation of a wide variety of surface patterns that can induce an elongated cell morphology, they are also time-consuming and expensive. Therefore, there is a need for a simple, fast, and cheap method to produce topographies that can induce specific morphologies of tenocytes (spindle-shaped versus stellate-shaped) to study the cell shape-fate relation.

Evaporation of a liquid solution droplet is a simple, yet powerful technique to assemble non-volatile solutes into highly-ordered structures[6]. When a liquid droplet containing colloidal particles or polymers evaporates, it leaves behind a distinct and reproducible pattern, such as the well-known coffee stain[7]. The key behind this remarkably robust pattern formation is an evaporation-driven capillary flow that transports particles towards the contact-line of the droplet[7,8] . The local increase in solute concentration near the contact line subsequently leads to jamming[9] , crystallisation[10], gelation[11] or phase separation[12] depending on the molecular interaction of the various components. By controlling the evaporation rate of the droplet and the motion of its contact line, a sequence of deposits with a rich spectrum of deposition patterns can be formed[7,13]. This evaporative self-assembly of solutes is widely used in the soft-matter, fluid-dynamics, material-science, and chemistry communities to create ordered structures on the nano- and micrometer scale, i.e. where direct manipulation is impossible[7,13–16]. In earlier phenomenological reports[17,18], experiments revealed that remarkable well-ordered deposition patterns form by simply letting droplets consisting of a solution of collagen type I triple helices evaporate on a glass substrate. In a recent study this method has also been applied to radially orient skeletal muscle cells[19]. However, here we show a wider variety of collagen patterns to which tenocytes respond differently. The method has not yet been exploited to generate collagen platforms for the study of the physiological response of cells to different topographies and interfaces.

In this study, we present a robust and simple approach to generate complex collagen topographies consisting of isotropic and two kinds of anisotropic domains of different structures by evaporating collagen type I solution droplets. We demonstrate how the initial collagen concentration and evaporation rate of the droplet can be used to control the pattern morphology. Moreover, we explore the ability of different isotropic and anisotropic collagen patterns to steer cellular functions such as cell alignment, distribution, shape, and proliferation.

Results

Multiscale well-ordered organization of collagen patterns depends on concentration and humidity.

In this study, droplets of a collagen solution with different concentrations were evaporated on glass substrates inside a climate chamber with well-controlled humidity, schematically shown in Fig. 1a. Using Polarized Light Microscopy (PLM), we analysed the deposition patterns formed for different initial collagen concentrations and relative humidity (and hence the evaporation rate of the droplet). Three types of deposition patterns were observed. Fig. 1 shows the different patterns found at the center, middle, and periphery of the dried stain. Due to the structural differences in the collagen deposition pattern in each region, as discussed below, we from now on define the regions as isotropic for the center, concentric for the middle region and radial for the periphery. A complete overview of the collagen patterns obtained at the periphery and middle regions and the influence of the relative humidity and collagen concentration is presented in Fig. 2. PLM images obtained from the center region are not included in Fig. 2 as the center region demonstrates more or less a flat homogenous characteristic. In the peripheral region radially oriented v-shaped collagen patterns appear, which becomes more abundant at high initial collagen concentration (Fig. 2a). Moving radially inwards from the periphery towards the center, different collagen patterns appeared (Fig. 2b). For collagen solutions with initial concentrations of 1 mg/ml and 10 mg/ml, little or no collagen patterning was observed in the middle region. Note that PLM only produces a signal when there is alignment of collagen that results in birefringence, i.e. polarization of the light. By consequence, the absence of a signal does not imply that there is no collagen present on the substrate.
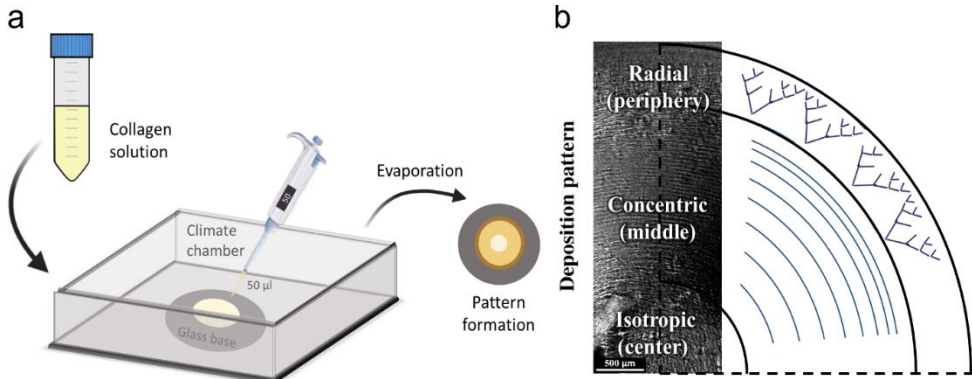
Figure 1. Different topographical patterns formed after collagen droplet evaporation. *(a) Schematic overview of the climate chamber and pipetted collagen droplets on glass samples, which form a collagen stain. (b) Polarized light microscopy (PLM) image accompanied by a sketch of the collagen patterns formed when using a 5 mg/ml collagen solution. Three different regions formed, i.e. an isotropic region in the center, a region with concentric collagen rings patterns in the middle and a radial v-shaped pattern at the periphery. For high magnification images of the patterns, see Fig. 6b1, c1 and d1.*

However, well-ordered concentric-ring shaped collagen patterns were found for collagen solutions with an initial concentration of 5 mg/ml (Fig. 2b, middle row). Irrespective of the concentration or humidity, the central area consisted of a random collagen pattern. In the remainder of the paper, we will refer to the center of the stain as 'isotropic region', the middle of the stain as 'concentric region', and the periphery as 'radial region'.

The most striking pattern formation was thus observed at an initial collagen concentration of 5 mg/ml, regardless of the humidity. A more detailed structural analysis was employed on samples that originated from an initial collagen concentration of 5 mg/ml and 20% humidity (i.e. the fastest evaporation), as shown in Fig. 2. From the periphery towards the center, initially a region of collagen molecules with a radially-oriented v-shaped organization was observed, covering only a narrow area. This peripheral region transitions into a well-ordered concentric ring pattern of collagen molecules. Finally, in the center of the drying stain an isotropic region, which lacks ordered aggregation of collagen, was found. The alternating dark and bright arcs in the concentric zone shown in the PLM image in Fig. 2 indicate a change in orientation of the collagen molecules from one ring to the next.

Peripheral region

a

Collagen concentration

10 mg/ml — 5 mg/ml — 1 mg/ml

Relative Humidity

20%   40%   60%

Middle region

b

Collagen concentration

10 mg/ml — 5 mg/ml — 1 mg/ml

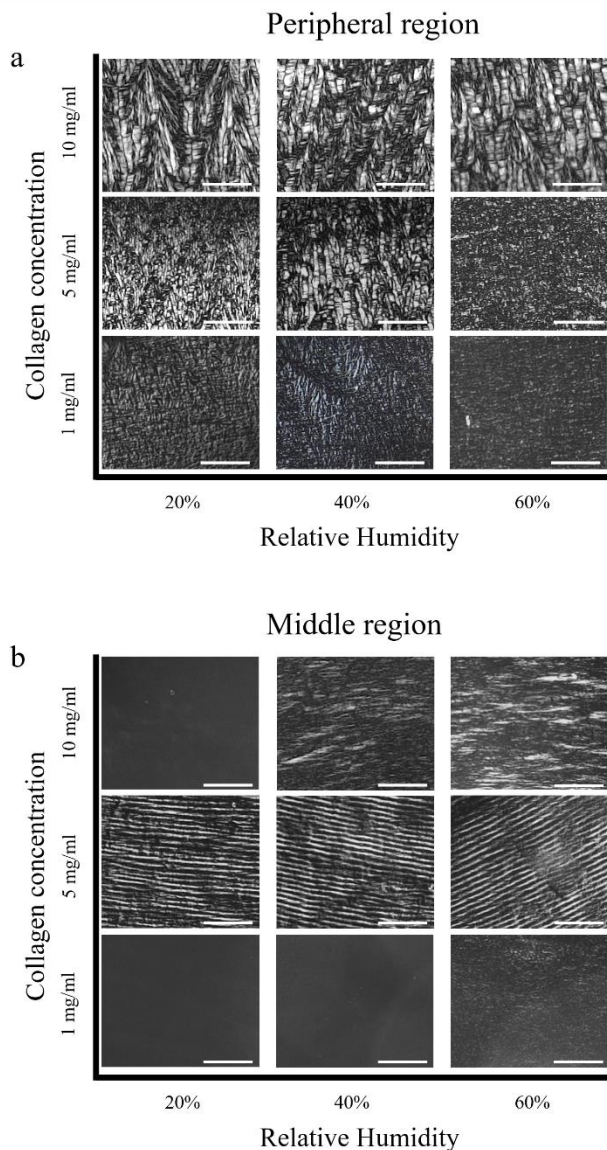Relative Humidity

20%   40%   60%

Figure 2. Collagen concentration and relative humidity affect the final structure of collagen stains. (a) Peripheral region; A radially-oriented v-shaped collagen pattern is observed at collagen concentrations of 5 mg/ml and 10 mg/ml, whereas at 1 mg/ml radial patterns were not observed. (b) Middle region; Concentric-ring patterns were exclusively observed at a concentration of 5 mg/ml, regardless of the relative humidity (middle row). Scale bars are 100 μm. For all experiments, N = 3. Displayed figures are representative images.

Strikingly, the distance between individual concentric collagen patterns in the middle region appeared to widen moving from the periphery towards the center. To evaluate the uniformity of concentric collagen patterns we measure the distance between black and white arcs, i.e. the wavelength of the pattern, as shown in Fig. 3a. Irrespective of the concentric pattern wavelength, the alternating bright and dark collagen pattern on PLM suggests alternating orientations of the collagen fibrils within the pattern. Fig. 3b

and 3c show that the wavelength of collagen patterns indeed becomes wider upon moving radially inwards from the periphery to the center. The wavelength of the collagen patterns close to the periphery of the stain was 5.1 ± 0.9 µm while close to the center it was 26.7 ± 1.4 µm. PLM images acquired at higher magnification confirm this large difference in wavelength of the concentric rings from the periphery to center (Fig. 3d and 3e).

Given the results, in the remainder of the manuscript we have used 5 mg/ml collagen solutions dried at 20% humidity, which resulted in three distinct regions, namely with a radial collagen orientation at the periphery, concentric in the middle region and an isotropic orientation in the center of the stain.
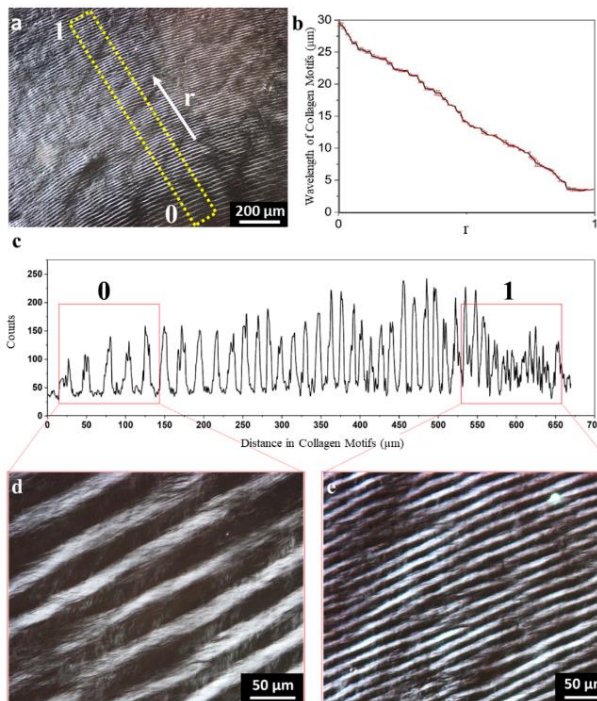

Figure 3. Concentric collagen patterns demonstrate differences in wavelength of collagen motifs (5 mg/ml collagen solution dried at 20% relative humidity). *(a) PLM image of a concentric collagen pattern, the white arrow points radially outward. (b) The mean average of three different measurements that demonstrate the decreasing linear trend of collagen wavelength. (c) Wavelength of collagen patterns from the region that was highlighted with the yellow rectangle in a. (d,e) Close-up PLM images from collagen patterns that correspond to the regions 0 and 1. For all experiments, N = 3. Displayed figures are representative images. Error bars in b indicate the standard deviation of the mean.*

To further elucidate the fine details of the patterns at the nano-scale, the concentric collagen patterns were examined by atomic force microscopy (AFM) and scanning electron microscopy (SEM). From the AFM images, we observe that the alternating

dark and bright regions of the concentric pattern observed under the PLM represent a valley-ridge-like topography (Fig. 4a, 4b, and 4c). The height profile from two adjacent collagen patterns showed a height difference between the valley and ridge of about 180 nm (Fig. 4b and 4c). Moreover, Fig. 4a demonstrates fibrillar structures (marked with white arrows) which were further imaged by SEM. Figure 4d and 4e show that the deposition patterns consist of collagen fibrils, despite the fact that fibrillogenesis was not actively induced in our samples. SEM results confirm the presence of fibrils, which are measured as 37.7 ± 7.9 nm in diameter, by demonstrating the tightly packed collagen fibrils within the concentric pattern. Hence, we conclude that the evaporative aggregation of collagen naturally induced fibril formation within the deposition pattern.
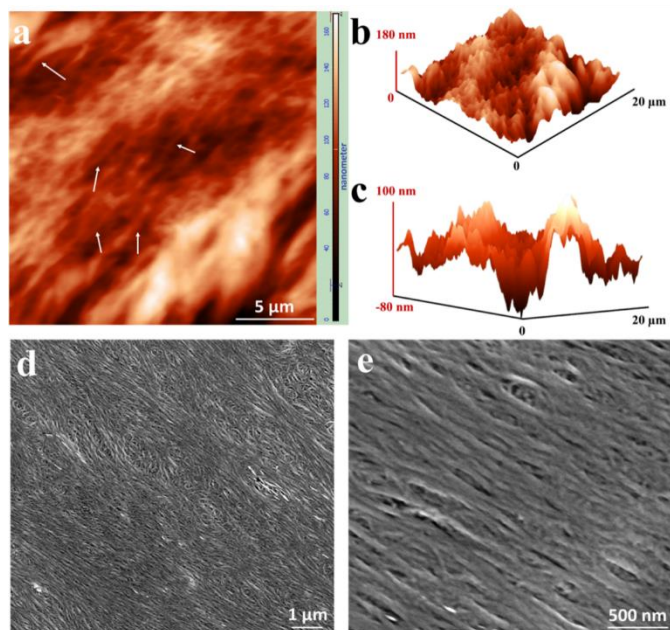

Figure 4. Collagen fibril formation after evaporation of a collagen droplet (5 mg/ml collagen solution at 20% relative humidity). (a) Atomic force microscopy image displaying the height difference of adjacent concentric patterns. Colours correspond to different heights according to the colour bar. The white arrows indicate collagen fibrils formed after drying. (b,c) Three-dimensional views of the same image in (a). (d,e) Scanning electron microscopy images demonstrating tightly packed collagen fibrils. Collagen fibrils of approximately 40 nm in diameter can be seen in the magnified image (e). For all experiments, N = 3. Displayed figures are representative images.

Pattern formation is essential for driving tenocyte alignment

Next, we assess whether different collagen topographies formed by evaporating droplets can promote different cell alignment. To this end, we investigate the cell response to these patterns by visualizing and quantifying cell alignment. Collagen stains were formed by evaporating droplets of 1 mg/ml (no distinct pattern formation) and 5 mg/ml collagen solution at 20% humidity (3 distinct patterns). Rat tenocytes were

seeded at low density (LD, 1000 cells/cm²), fixed after 24 hours, and stained with Phalloidin (green) to visualize the actin cytoskeleton (Fig. 5). In absence of a clear pattern formation at 1mg/ml, cells were randomly distributed and did not display differences in cell morphology between locations (Fig. 5a and supplementary figure 1). For the 5mg/ml samples, where clear collagen patterns were observed, we first identified the regions that cells attach to by using PLM. Subsequently, cellular alignment was assessed: i.e. cells aligned preferentially radially in the radial region, strongly circumferentially with a spindle-shaped morphology in the concentric region and randomly in the central isotropic region (Fig. 5b).

Previous research has shown that cell density influences cell shape, migration and downstream signalling[18], and may possibly override the effect of the substrate topography. Therefore, we investigated whether the observed influence of topography on cell shape in a confluent cell culture is still effective. To this end, rat tenocytes were seeded at high density (HD, 10000 cells/cm²) and visualized as explained earlier (Fig. 5c). Despite confluency, cells exposed to the pattern still displayed a strong alignment and spindle-shaped morphology with the patterns they were exposed to (Fig. 5c). The different wavelengths of the concentric-ring topographies (as displayed in Fig. 3 and supplementary figure 2) in the concentric – middle region did not appear to affect cell alignment, in both LD and HD conditions. Overall, our results indicate that the concentric ring pattern in the 5 mg/ml-stain can promote cellular orientation and morphology, regardless of the cell-seeding density.
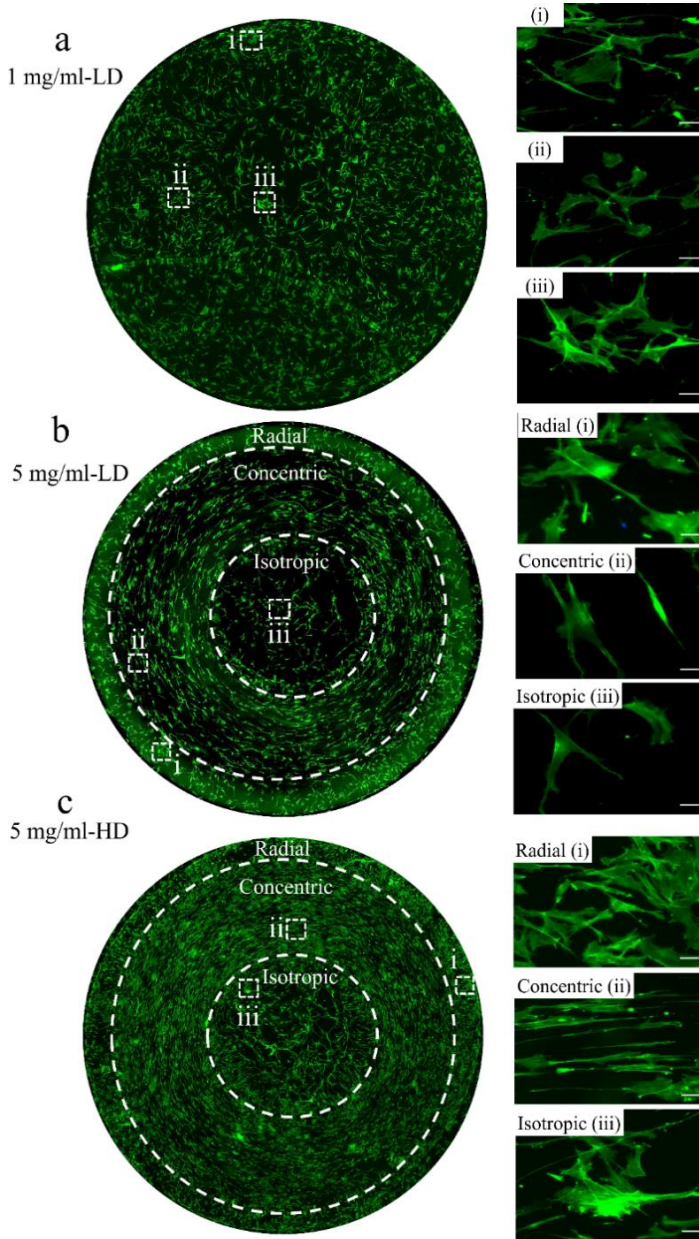
Figure 5. Tenocytes obey topographies created by evaporated collagen droplets. *(a) Rat tenocytes cultured at low seeding density on 1 mg/ml collagen stains for 24 hours and stained with phalloidin (green) to visualize cytoskeleton. Cells neither display any orientation, nor adapt their cell shape. (b) Rat tenocytes cultured at low seeding density on 5 mg/ml collagen stain for 24 hours and stained with phalloidin (green) to visualize cytoskeleton. Cells display an elongated shape and a circumferential orientation aligned with the concentric pattern. (c) Rat tenocytes cultured at high seeding density on 5 mg/ml collagen stain for 24 hours and stained with Phalloidin (green) to visualize cytoskeleton. Similar to (b), cells display an elongated shape and a circumferential orientation aligned with the concentric pattern. The dashed squares indicate the regions where the magnified images were captured. For all experiments, N = 3. Displayed figures are representative images.*

Tenocyte orientation and shape are altered by different topographies

To further assess the strength of the pattern in driving cellular alignment and morphology, cellular F-actin was visualized and quantified (Fig. 6). Results reveal that the F-actin orientation in the concentric region displayed a clear peak at 90° , representative for a strong collagen anisotropy in the concentric direction (Fig 6.b1-b3). In the radial region, collagen displayed a marginal preference for the 0/180° angle, representative for collagen to align to the radial direction (Fig 6.c1-c3). In this region, we did not observe a clear cell alignment based on both visual inspection (Fig. 6b2) and alignment calculations (Fig 6b3), yet only a small preference towards the radial direction was observed. In the isotropic region, no preferred collagen orientation was found, since the bimodal fit (represented by the blue dotted line) only has an R^2 of 0.19 (Fig 6.d1-d3). Therefore, despite that, the collagen topographies strongly differed between the radial and central regions according to the polarized light microscopy images, they failed to induce a striking difference in cellular alignment.

Subsequently, cell shape was quantified in terms of area, eccentricity, compactness, and solidity (Fig. 6) and performed ANOVA to determine the statistical difference. Cells located on the radial region displayed the smallest cell area and cells in the isotropic region the largest cell area. Cellular eccentricity, a measure for cell elongation (the more elongated the cell, the closest the eccentricity value is to 1), was highest for cells in the concentric region. Despite the modest anisotropic orientation of the cells in the radial region, the eccentricity was lower compared to the random region (Fig. 6f). Cell compactness (higher value indicates a more elongated cell) was highest for cells on the concentric region (Fig. 6g). Cell solidity (values are oppositely correlated with cell branching and filopodial protrusions) was highest for cells on the radial region and significantly different compared to cells in the isotropic region (Fig. 6h). Overall, these results indicate that concentric regions induced aligned and more elongated, i.e. spindle-shaped, tenocyte morphology, whereas isotropic and radial regions only induced differences in cellular morphology.
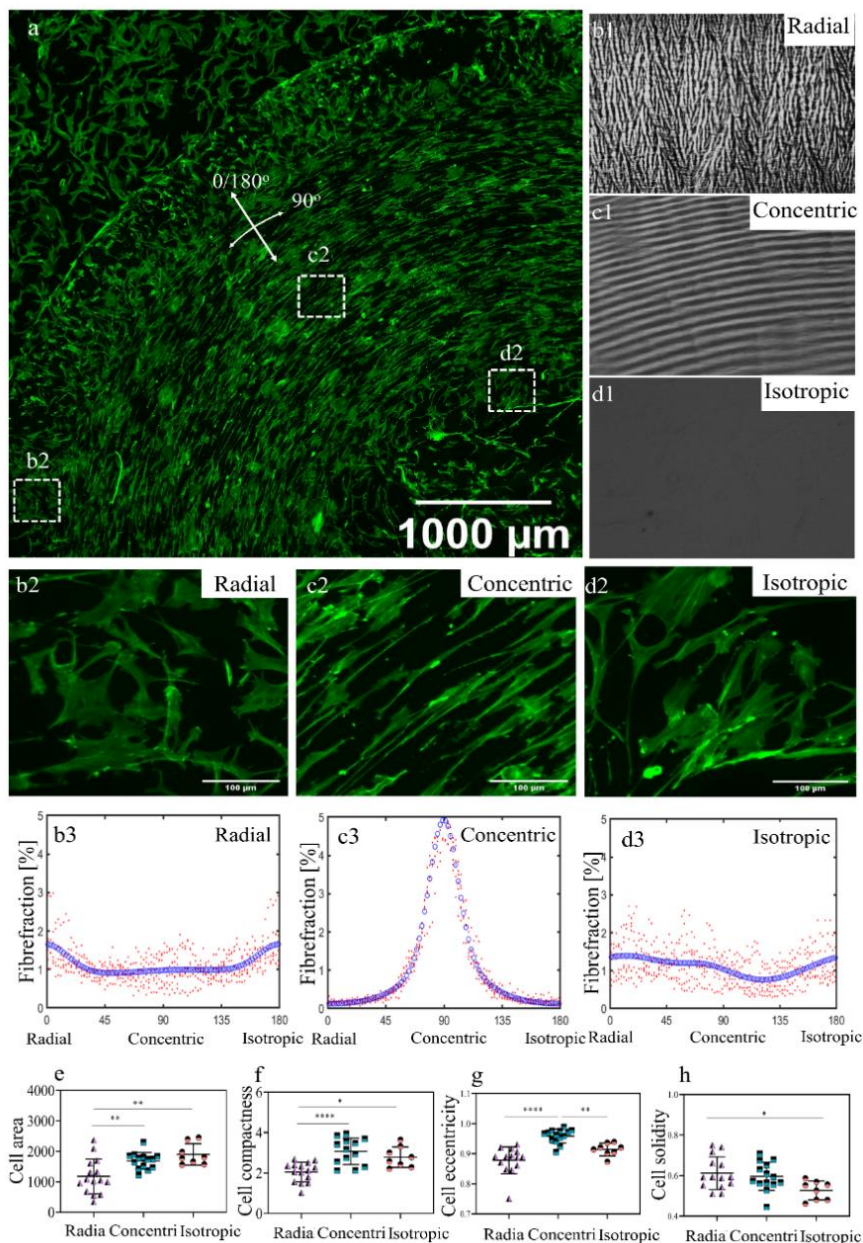
Figure 6. Topographies created after evaporation of collagen droplets influence tenocyte orientation and shape. *(a) Quarter of a collagen stain that is seeded with Phalloidin-stained rat tenocytes (5 mg/ml collagen concentration, cells seeded at high density). (b1, c1 and d1) Representative image of the radial, concentric and random region, respectively. (b2, c2 and d2) Representative higher magnification phalloidin images. (b3, c3 and d3) F-actin fiber distributions*

showing a radial, concentric and random fiber distribution for the three respective regions. Red dots represent individual fiber fractions of the images analysed, where the blue line represents a bimodal fit. R^2 values of b3, c3 and d3 are 0.31, 0.97 and 0.19, respectively. (e) Quantification of cell area, (f) eccentricity, (g) compactness and (h) solidity for cells on radial, concentric and isotropic regions. Scale bars in b2-d2 represent 100 μm. In e-h, each symbol represents a single image. Area, eccentricity, solidity and compactness values are represented in arbitrary units. Error bars represent 95% confidence intervals. Each asterisk represents statistical significance of the differences of cell area, compactness, eccentricity and solidity in redial, concentric and isotropic regions. *P < 0.05, **P < 0.01. For all experiments, N = 5. The dashed squares indicate the regions where the magnified images were captured.

Topographical architectures on collagen stains affect cell density

Surface topography is known to affect not only cell shape, but also proliferation and differentiation[18,20]. Therefore, as a next step we investigated how the different topographies of the collagen stains affected the cell density as illustrated in Fig. 7. The different colours of the cells indicate the three regions. To obtain the average cell densities we calculated the total number of cells per region and the corresponding area of that region (Fig. 7a&b). After performing ANOVA test, our results show that on average the cell density is 180 ± 24 cells/mm² in the radial region, 184 ± 21 in the concentric region and 123.3 ± 59 cells/mm² in the isotropic region (Fig. 7c). This results suggest that there is no significant difference in cell density between radial, concentric and isotropic region.
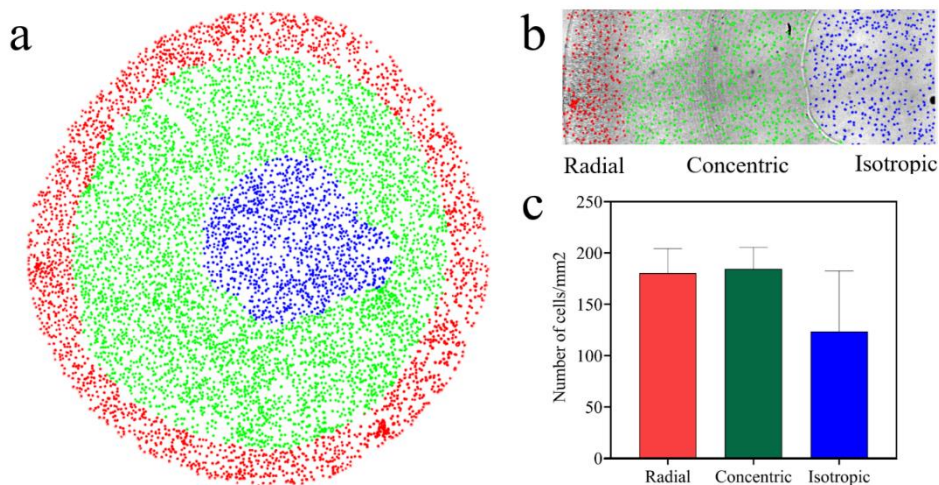
Figure 7. Cell density varies between patterns and is lowest for the isotropic region. *(a) The cells are labelled red, green and blue for radial, concentric and isotropic regions. (b) Detailed view of the cells (with the same colour coding as in a) together with the corresponding stain, shown in the background. (c) The average densities in the radial (180 ± 24), concentric (184 ± 21) and isotropic region 123.3 ± 59 cells/mm² are displayed. Error bars represent 95% confidence intervals. For all experiments, N = 3.*

Surface topography does not alter cell proliferation

Cell proliferation is a feature, known to be affected by environmental factors, including surface topography[21]. Concordantly, we assessed whether the topography-induced cell shape results in different proliferation rates after 24 hours of seeding (Fig. 8). Image analysis showed that in isotropic region 70±25%, in radial region 89±9% and in concentric region 85±7% of the cells were EdU positive, hence proliferating, and no statistical difference detected. (Fig. 8b). As shown in our previous work[22], a surface topography that alters cellular morphology (as found in the radial and concentric zones, see Fig. 6a) can result in a decrease in nuclear size, and hence a decrease in cell proliferation[22]. Therefore, we further evaluated whether topographies on the radial, concentric and isotropic region induce changes in the nucleus shape in all cells and also specifically (Fig. 8c) EdU positive cells (proliferating cells) (Fig. 8d). The nucleus area, compactness, elongation, and solidity were similar for all regions, and did not differ between EdU positive cells (Fig. 8 c&d). These results indicate that proliferation and nucleus shape remained unaffected by the surface topographies.
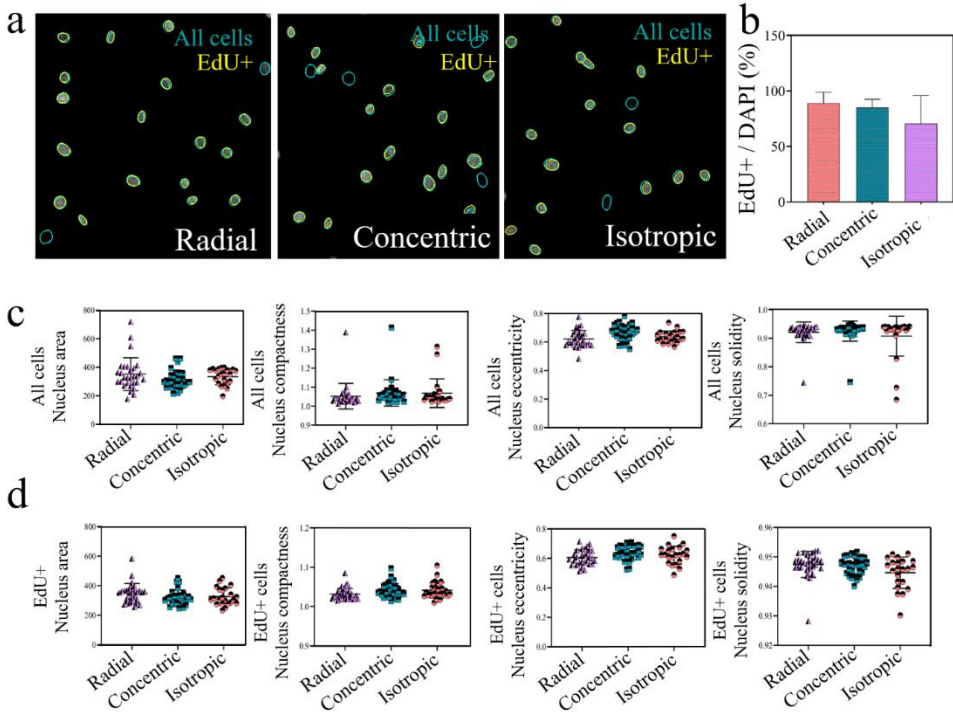
Figure 8. Tenocyte proliferation and nucleus shape was not affected by topographies. *(a) Representative image of all cells (DAPI, Green-Blue) and EdU positive cells (yellow) on radial, concentric and isotropic regions. (b) Quantification of EdU positive cells with a trend towards lower proliferation in the isotropic region. (c) Quantification of nuclear shape parameters on the different regions for all cells (area, compactness, eccentricity, solidity) and (c) for EdU⁺ cells. Each symbol represents the average of a single image. Error bars represent 95% confidence intervals. For all experiments, N = 3.*

Discussion and Conclusion

In the present work, we demonstrated a simple method to create multiscale well-ordered collagen patterns by evaporating a droplet containing collagen molecules in a well-controlled environment and investigated how cells are affected upon being cultured on this material.

The final deposition pattern that forms is the result of a complex interplay between the evaporation-driven capillary flow inside the droplet[23,24] that transports the collagen fibers towards the contact line, the motion and/or pinning of the contact line[13,25], the interaction between the collagen and the substrate[26] and the solution rheology[27]. At the

periphery of the stain, a pattern of radially-oriented v-shaped stripes was observed. These structures are the first that form as the droplet evaporates. Similar deposits for colloidal-particle laden droplets have been reported[28]. Possible explanations for these structures range from buckling caused by the build-up of internal stress during desiccation, shear banding due to internal flow[29], and contact line instabilities[30], but the precise mechanism remains to be explored. Further experiments are necessary to reveal whether the radial deposit forms during the pinning phase of the contact line, and hence result from the self-assembly of the collagen fibers upon accumulation at the contact line by the capillary flow[23], or during the first stages of contact line recession. In later stages of the droplet life, when the contact line recedes while the contact angle remains constant, regular concentric ring patterns were formed consisting of ridges and valleys. In literature, such robust periodic patterns have been reported for evaporating polymer solutions[13] and are attributed to a stick-slip motion of the contact line that is caused by pinning/depinning events[31]. In polymer solutions, the regularity of the pattern is caused by a self-organized pinning-depinning cycle that results from local changes in the solution viscosity due to the convective transport of material to the contact line[31]. A detailed analysis of the collagen aggregation in the radial and concentric regions in presence of evaporation-driven capillary flow and contact-line motion is left for future work. Clearly, there is a need for a full exploration of the parameter space and the development of adequate models to predict the patterns that will form and when pattern-to-pattern transitions will occur, depending on e.g. the droplet volume, evaporation rate and collagen concentration. Such modelling will help to delineate the differences between the results of Nerger *et. al.*[19], where only radial patterns are found, and the present work where both radial and concentric ring patterns reproducibly formed. Furthermore, it is not so clear why a concentration of 5 mg/ml yields a much more pounced topography than either 1 mg/ml or 10 mg/ml. The useful concentration window seems to be rather narrow, but the process probably can be optimised. Additionally, the transition from concentric to isotropic collagen organisation that occurs during the final stage of the droplet life needs to be further investigated to determine the influence of e.g. gelation[11], rapid solute accumulation causing order-to-disorder transitions[23] and collagen adhesion on the absence of a well-defined pattern anisotropy in the center of the stain.

Studying the interactions between cells and their surrounding extracellular matrix is one of the main steps on the path to understanding mechanisms of health and disease; hence, here we investigated how the nano-topographies created upon self-assembly of collagen molecules affect tenocytes with respect to their cytoskeletal organization, orientation and proliferation. We first evaluated the impact on topography on cell shape as upon cell attachment, initial changes are observed in the cell cytoskeleton. Different cell types (e.g. mesenchymal stem cells, tenocytes, epithelial cells) have been shown to

adopt their cytoskeleton based on the micro-topographies [22,32–34] and nano-topographies[35],[36] that they exposed to. The topographies on the collagen stains are at nano-level and forced tenocytes to form an elongated shape. This result is also supported by Yang *et. al.* where they show that nano topographies as small as 50 nm led elongation and orientation of human dermal fibroblasts[37], and human bone marrow-derived mesenchymal stem cells[38]. However, characteristics (pitch, ridge, and groove dimensions) of the nano-groove surface topography matter and can either result in elongated cell shape or lead to the formation of spherical aggregates of human tenocytes[39].

In the current study, we used rat tenocytes as a cell type to investigate the role of surface topography on cell behaviour for the following reasons: 1) Tendon tissue naturally possesses a hierarchical order of strongly anisotropic collagen fibers. 2) Tenocytes naturally possess an elongated shape in the native tissue. However, upon culturing tenocytes on a flat surface, or upon disruption of the native tissue architecture, they dedifferentiate, change their morphology to become more spread, alter their phenotypical marker expression, and proliferation characteristics. 3) In the native tendon, tenocytes experience biomechanical cues originating from collagen fibrils at the nanometer scale (20-150 nm) and fibers are at micrometer-scale (10-50 μm)[40], suggesting that they can respond to very small topographies, such as the concentric rings. Concentric rings in the collagen stain, which have 180 nm depth valleys in between, pushed tenocytes to an elongated morphology, which is characterized by an eccentricity value close to 1. Additionally, in the native tendon, tenocytes are oriented in the direction of collagen fibers, which was also accomplished by concentric rings. Furthermore, since formation of hierarchical aggregation of collagen is challenging in an *in vitro* system, our system allows tenocytes to experience more "*natural*" environment, particularly in the concentric ring with respect to topographical architecture and substrate itself and hence tenocytes are exposed to a rather natural ECM that is closed to a native healthy tendon. Therefore, collagen stains containing these concentric rings are excellent tools to give the sense of a natural ECM to tenocytes and further investigate cell-biomaterial interactions with respect to tenocyte biology.

Proliferation is one of the highly investigated read-outs on cell-biomaterial interaction studies as *in vivo* cells do respond to changes in tissue architecture. For instance, in the heathy tendon, tenocytes are relatively quiescent and start proliferating during tissue remodelling in case the tissue anisotropy is lost[41],[42]. This *in vivo* phenomenon was recently replicated in *vitro* by showing that, upon culturing tenocytes[32] and human mesenchymal stem cells[43] on a tendon-biomimetic topography which possess anisotropic topographical features, tenocytes displayed a quiescent phenotype

compared to cells cultured on a flat surface. Therefore, we investigated cell-biomaterial interactions with respect to cell density and proliferation in order to elaborate on the influence of isotropy or anisotropy in analogy to healthy and damaged tissue. To our surprise, we did not observe striking differences in cell proliferation between radial, concentric and isotropic regions, similar to the cell density after 24 hours. It is hypothesized that the nuclear deformation can lead to changes in chromatin structure and therefore led to a decrease in cell proliferation[22,44]. For this reason, we calculated the deformation in the nucleus with respect to its shape but did not observe differences between regions or between EdU negative and positive cells. In a future study, we will focus on how to control the wavelength, width, and height of the concentric ring pattern, to investigate the possibility to optimize the pattern for inducing nuclear shape changes/cell proliferation. It was also suggested by the work of Milner and Siedlecki *et. al.*[45] and Christopherson *et. al.*[46] that a reduction in feature sizes on the material eradicated the discrepancy between nano-topographies and flat substrates in terms of cell proliferation. Similar to our proliferation results, we did not observe any significant differences in cell density after 24 hours between the different regions. However, our experiments suggest a decrease in cell density in the isotropic region compared to the concentric and radial regions. Future experiments are required to investigate this trend, and delineate whether its origin lies in differences in cell migration, proliferation or apoptosis between the different zones.

Nevertheless, other mechanisms such as integrin signalling and focal adhesion dynamics also influence cell proliferation and cell adhesion. Integrin signalling is one of the first steps upon cell attachment and initiates downstream signalling cascades for cellular responses such as cell adhesion, growth, motility, shape, and differentiation[47]. Integrins are transmembrane proteins that modulate cell-biomaterial crosstalk by interacting their extracellular domain with the ECM and the intracellular domain with signalling molecules and can be activated by both surface topography [48–50] and surface chemistry [51–53]. However, it is still under debate whether cells react initially to surface chemistry [54,55] or surface topograpy[55,56]. In evaporated collagen, all the regions are formed by collagen, and therefore the ligand possibly suppresses the effect of topographical differences. As a result, cell proliferation was not significantly different between regions and between cells. To support this, proliferation of human osteoblasts on nano rough titanium films was similar to that on smooth surfaces[57]. Furthermore, proliferation of human mesenchymal stem cells on nano topographic poly(methyl methacrylate) (PMMA) was shown to be increased after 14 days of culture compared to their smooth counterparts[58]. Accordingly, we suggest two possible explanations for our proliferation results: 1) The height difference between the valley and ridge, providing the topographical cue, is too low to cause a nuclear deformation, and thus do not strongly affect proliferation rate. This is supported by the lack of any topography on the isotropic

region, which even displayed a decreasing trend in the proliferation. 2) Collagen as a substrate that cells bind to create a stronger signal compared to the topography of that collagen, and therefore the nuclear response towards proliferation was fairly similar. Nonetheless, considering that surface topography and chemistry act together to produce a biological response, these results should be further explored. For instance, focal adhesion kinase (FAK), Src, and Rho GTPases are among the downstream effectors of the integrin signalling that are known to affect cell proliferation as well as cytoskeletal changes[50], hence, further investigation on the activation of these pathways can aid us to understand the effect of integrin signalling on the proliferation.

The topographies created by the evaporation of collagen droplets enables studying cell-biomaterial interactions. Firstly, the stains consist of three different topographical regions and with sharp interfaces in between, which enables a direct comparison of read-outs in the same sample. Firstly, how cells migrate on different topographies, a cell's preference to migrate towards certain topography and cell behaviour at the interface between different topographies can be investigated within a single sample. Secondly, topographies are made up of collagen type I, which is one of the most abundant types of collagen in the connective tissues such as bone and tendon. Therefore, together with biomechanical cues created by topographies, the effect of the biochemical cues can be investigated.

Overall, our robust and simple approach to generate complex topographical collagen patterns by droplet evaporation can be used to unravel cell-matrix interactions and better understand and control cellular function. The collagen stains formed bear three distinct patterns and their interfaces, which can mimic physiological conditions. For example, the concentric pattern can be used to mimic a healthy tendon and the isotropic region to feature a tendinopathic condition. Thereby, our material can be used to reveal how cells respond to the different patterns and their interfaces in terms of cellular capacity for functional remodeling and to explore strategies to push cells on the e.g. isotropic patterns to display improved functional remodeling capacity. In addition, the underlying molecular mechanisms that affect this remodeling capacity, associated with topography-induced cell shape, can be studied. Hereby, optimal control over the pattern formed by evaporation is essential. In future work, we will therefore focus on mapping out the parameter space for collagen pattern formation inside evaporating drops and identifying the key physical mechanisms that control the pattern.

Materials and method

Preparation of collagen solutions

Lyophilized collagen I from calfskin (Elastin products, C857) was dissolved in 0.5 M acetic acid at 1 mg/ml, 5 mg/ ml and 10 mg/ml collagen concentrations and vortexed vigorously to ensure collagen was dissolved in the solution. Next, solutions were centrifuged 5 minutes at 300 RCF. For each experiment, fresh solutions were prepared.

Climate chamber and sample preparation

The collagen stains are made by evaporating 50 μL droplets of the fresh collagen solution. Five droplets are pipetted on different glasses and placed inside the climate chamber. The chamber is a transparent plexiglas box in which the temperature is monitored and is 23±1 °C for all the experiments. The relative humidity in the chamber is controlled via a N_2-gas inflow to lower the humidity to a specified level. After an initial transient of about 15 minutes, a stable humidity is obtained within ±1% of the target value (a typical experiment lasts 2.5 hours). Droplet evaporation is recorded in side- and bottom-view. In the bottom-view, the formation of the stain and the contact line motion are recorded via Bright Light Microscopy (BLM). A side-view camera is used to measure the size of the droplet and the contact angle with the glass substrate over time. Once all the liquid has evaporated, the collagen stains are stored at 4 °C until use.

Isolation of rat tenocytes

Rats were collected after euthanization considering their surplus status from the breeding program. Tenocytes were isolated from the hind limbs of 23 weeks old Cyp1a2ren strain rats by using a previously published protocol[32]. Briefly, tendons from the hind limbs were digested in a solution containing collagenase type II (3mg/ml) (Worthington Biochemical), dispase II (Sigma-Aldrich) (4mg/ml) and 100 U/ml Penicillin/Streptomycin (Thermo Fisher Scientific) for 4 hours at 37 °C. Next, the solution was passed through a 70 mm cell strainer (Life sciences) and further spinned at 300 G for 5 minutes. Then, pellet was re-suspended in Dulbecco's modified Eagle's medium (DMEM, Sigma-Aldrich) supplemented with 10% fetal bovine serum (FBS), 100 U/ml penicillin/streptomycin, tenocytes were cultivated in T-25 flasks until 70% confluency.

Sterilization of tendon imprints and cell culture

Collagen stains was sterilized by incubating the materials in 70% ethanol for 30 minutes. Next, ethanol was aspirated, and remaining ethanol let to air-dry under sterile conditions. Subsequently, samples were washed in sterile phosphate-buffered saline (PBS, Sigma-Aldrich) at 37 °C three times and washed with culture medium twice before use. Passage 4 tenocytes were seeded at 1000 cells/cm^2 (for low-density culture) and

10000 cells/cm² (for high density culture) for subsequent orientation, cell density and proliferation analyses.

Phalloidin and EdU staining

Upon 24 hours after seeding, cells were fixed with 4% paraformaldehyde (PFA, ThermoFisher Scientific) at room temperature for 20 minutes and subsequently washed with PBS. Afterwards, samples were incubated in were incubated in Phalloidin–Tetramethylrhodamine B isothiocyanate (Phalloidin-TRITC, 1:200; ThermoFisher) in PBS for 1 hour and washed 3 times with PBS to stain F-actin. Next, 4',6-diamidino-2-phenylindole (DAPI, 1:500; Sigma-Aldrich) in PBS was used to stain nuclei for 1 hour and further washed 3 times with PBS. Finally, samples were mounted on glass cover slides with mounting medium (Dako, Agilent). Samples were stored at 4 ºC at dark.

Click-iT EdU Cell Proliferation Kit (Invitrogen, C10340) for Imaging (Thermo Fisher) was used to detect proliferating cells as described on the manufacturer's instructions. Briefly, cells were serum-starved for 24 hours before to EdU labelling to synchronize their biological clock. Next, cells were fixed with 4% paraformaldehyde (PFA, ThermoFisher Scientific) at room temperature for 20 minutes and permeabilized with 0.5% (v/v) Triton X-100 in PBS for 20 minutes after 24 hours of incubation in 10 μM EdU solution. Afterwards, cells were treated with EdU reaction cocktail for 30 minutes in the dark and incubated in Hoechst for another 30 minutes to stain the nucleus. Next, samples were mounted on glass cover slides and stored at 4 ºC at dark.

Imaging

Borosilicate Glass substrates that were employed to dry collagen solutions, were used without any further sample preparation step. Regions of interest were imaged between two polarizers with a Zeiss Axioplan 2 light microscope using transmission mode at magnifications 10×, 20×, and 50×. The scanning electron microscopy (SEM) imaging of the glass substrates was performed by using a FEI Quanta FEG 600 (Thermo Fisher Scientific). Glass substrates were sputter-coated prior to SEM imaging in order to avoid a possible charging effect and to improve the imaging quality. Atomic force microscopy (AFM) measurements were conducted by using a NTegra Agura (NT-MDT) machine in tapping mode and Si microcantilever probes with a spring constant of 5 N/m. Fluorescent images were taken with a Leica DMi8 with TIRF Multi Color microscope (Leica Microsystems CMS) at 10× magnification. Lasers at excitation wavelengths of 532 nm and 647 nm were used for phalloidin and EdU respectively. Tile images were stitched together with LAS-AF Lite version 2.6 (Leica Microsystems CMS).

Quantification of F-actin orientation by fiber tracking and bimodal fitting

F-actin stress-fiber orientation was measured by using actin stained samples based on previously developed fiber-tracking algorithm[54]. Briefly, via employing a multi-scale approach the principle curvature directions from the eigenvalues and the eigenvectors of the Hessian matrix of the image were calculated. For each image, a histogram that contains fiber fraction per angle (ranging from 0° to 180° and 0° to 90° degrees with a 2° interval) was obtained. For bimodal fitting, average fiber fractions for all images from the same protocol were used. To quantify the fiber distribution, the experimentally observed fractions were approximated by a bi-modal periodic normal probability distribution function using a nonlinear least-squares approximation algorithm:

$$\varphi_f(\gamma) = A_1 \exp\left[\frac{\cos(2(\gamma - \alpha_1) + 1)}{\beta_1}\right]$$
$$+ A_2 \exp\left[\frac{\cos(2(\gamma - \alpha_2) + 1)}{\beta_2}\right]$$

Hereby, $\varphi_f(\gamma)$ is the fiber fraction as a function of the fiber angle γ. Variables α_1 and α_2 are the two main fiber angles and β_1 and β_2 represent the dispersities of the two fiber distributions. An angle of 90° is parallel to the radial direction and aligned with the concentric direction. The parameters A_1 and A_2 are scaling factors for the total fiber fractions of the distributions.

Image analysis

Analysis of acquired PLM and SEM images was done by using the software packages provided by Digital Gatan Micrograph and Image J such as Plot Profile tool to quantitively measure the wavelength of the collagen patterns and diameter of collagen fibrils. Approximately 60 images were used to calculate the wavelength of the collagen patterns and more than 100 collagen fibrils were picked to measure the diameter of collagen fibrils and results are reported as mean ± standard deviation of the mean. Cell and nucleus shape parameters were extracted from CellProfiler[55] by using customized pipelines for Phalloidin and EdU analysis. Each pipeline included background correction, nucleus and cell segmentations for further cell and nucleus shape analysis. Cell shape parameters were calculated by CellProfiler: Eccentricity is calculated by taking the ratio of the distance between the foci of the ellipse and its major axis length. Compactness calculated by the mean squared distance of the object's pixels from the centroid divided by the area. Solidity calculated by taking the proportion of the pixels in the convex hull that are also in the object[32,59]. The analysis on the regional cell densities are done with MATLAB. First, PLM images are used to define masks for the

radial, concentric and isotropic region. The area and number of cells per region are calculated after placing the corresponding masks on the DAPI images. The cells in the image (white) are easily distinguished from the surrounding background (black) with a threshold in the grayscale values. Graphs are drown in GraphPad Prism version 8.0 (GraphPad Software, Inc., San Diego, CA) and images are prepared in Fiji[60].

Statistics

Statistical analyses for cell and nucleus shape analysis and proliferation were performed by using GraphPad Prism version 8.0 (GraphPad Software, Inc., San Diego, CA). One-way analysis of variance (ANOVA) was carried out to calculate the statistical difference in three different regions. For all statistical analysis, significance is set at $p < 0.05$ and significance was determined by Tukey's post-hoc test.

References

1.   Nourissat, G., Berenbaum, F., and Duprez, D. Tendon injury: From biology to tendon repair. Nat Rev Rheumatol. Nature Publishing Group, **11**, 223, 2015.

2.   Xu, Y., and Murrell, G.A.C. The basic science of tendinopathy. Clin Orthop Relat Res. **466**, 1528, 2008.

3.   Jackman, R.J., Wilbur, J.L., and Whitesides, G.M. Fabrication of submicrometer features on curved substrates by microcontact printing. Science (80-) . **269**, 664 LP, 1995.

4.   Sundaramurthi, D., Krishnan, U.M., and Sethuraman, S. Electrospun nanofibers as scaffolds for skin tissue engineering. Polym Rev. **54**, 348, 2014.

5.   Wilson, D.L., Martin, R., Cronin-Golomb, M., Mirkin, C.A., and Kaplan, D.L. Surface organization and nanopatterning of collagen by dip pen nanolithography. Microsc Microanal. **8**, 1020, 2002.

6.   Han, W., and Lin, Z. Learning from "coffee rings": Ordered structures enabled by controlled evaporative self-assembly. Angew Chemie - Int Ed. **51**, 1534, 2012.

7.   Deegan, R.D. Pattern formation in drying drops. Phys Rev E . American Physical Society, **61**, 475, 2000. Available from: https://link.aps.org/doi/10.1103/PhysRevE.61.475

8.   Hu, H., and Larson, R.G. Analysis of the microfluid flow in an evaporating sessile droplet. Langmuir. **21**, 3963, 2005.

9.   Trappe, V., Prasad, V., Cipelletti, L., Segre, P.N., and Weitz, D.A. Jamming phase diagram for attractive particles. Nature . **411**, 772, 2001.

10.   Yabu, H., Akagi, K., and Shimomura, M. Micropatterning of liquid crystalline polyacetylene derivative by using self-organization processes. Synth Met . **159**, 762, 2009.

11.   Zaccarelli, E. Colloidal gels: equilibrium and non-equilibrium routes. J Phys Condens Matter. IOP Publishing, **19**, 323101, 2007.

12.   Náraigh, L.Ó., and Thiffeault, J.-L. Nonlinear dynamics of phase separation in thin films. Nonlinearity . IOP Publishing, **23**, 1559, 2010.

13.   Thiele, U. Patterned deposition at moving contact lines. Adv Colloid Interface Sci . **206**, 399, 2014. A

14.   Mar\'\in, Á.G., Gelderblom, H., Lohse, D., and Snoeijer, J.H. Order-to-Disorder Transition in Ring-Shaped Colloidal Stains. Phys Rev Lett . American Physical Society, **107**, 85502, 2011.

15.   Pauchard, L., Parisse, F., and Allain, C. Influence of salt content on crack patterns formed through colloidal suspension desiccation. Phys Rev E . American Physical Society, **59**, 3737, 1999.

16. Weon, B.M., and Je, J.H. Fingering inside the coffee ring. Phys Rev E . American Physical Society, **87**, 13003, 2013.

17. Maeda, H. An Atomic Force Microscopy Study of Ordered Molecular Assemblies and Concentric Ring Patterns from Evaporating Droplets of Collagen Solutions. Langmuir . American Chemical Society, **15**, 8505, 1999.

18. Maeda, H. Observation of Spatially Rhythmic Patterns from Evaporating Collagen Solution Droplets. Langmuir . American Chemical Society, **16**, 9977, 2000.

19. Nerger, B.A., Brun, P.T., and Nelson, C.M. Marangoni flows drive the alignment of fibrillar cell-laden hydrogels. Sci Adv. **6**, 2020.

20. Macgregor, M., Williams, R., Downes, J., Bachhuka, A., and Vasilev, K. The role of controlled surface topography and chemistry on mouse embryonic stem cell attachment, growth and self-renewal. Materials (Basel). **10**, 2017.

21. Jeon, H.J., Simon, C.G., and Kim, G.H. A mini-review: Cell response to microscale, nanoscale, and hierarchical patterning of surface structure. J Biomed Mater Res - Part B Appl Biomater. **102**, 1580, 2014.

22. Beijer, N.R.M., Nauryzgaliyeva, Z.M., Arteaga, E.M., Pieuchot, L., Anselme, K., van de Peppel, J., et al. Dynamic adaptation of mesenchymal stem cell physiology upon exposure to surface micropatterns. Sci Rep . Springer US, **9**, 1, 2019.

23. Marín, Á.G., Gelderblom, H., Lohse, D., and Snoeijer, J.H. Rush-hour in evaporating coffee drops. Phys Fluids . American Institute of Physics, **23**, 91111, 2011.

24. Hu, H., and Larson, R.G. Evaporation of a Sessile Droplet on a Substrate. J Phys Chem B . American Chemical Society, **106**, 1334, 2002.

25. Fraštia, Ľ., Archer, A.J., and Thiele, U. Modelling the formation of structured deposits at receding contact lines of evaporating solutions and suspensions. Soft Matter . The Royal Society of Chemistry, **8**, 11363, 2012.

26. Geoghegan, M., and Krausch, G. Wetting at polymer surfaces and interfaces. Prog Polym Sci . **28**, 261, 2003.

27. Malkin, A.Y., and Isayev, A.I. Rheology: Concepts, Methods, and Applications. In: Malkin, A.Y., and Isayev Methods, and Applications (Second Edition), A.I.B.T.-R.C., eds. Oxford: Elsevier, pp. 127–221, 2012.

28. Kaya, D., Belyi, V.A., and Muthukumar, M. Pattern formation in drying droplets of polyelectrolyte and salt. J Chem Phys . American Institute of Physics, **133**, 114905, 2010.

29. Berteloot, G., Hoang, A., Daerr, A., Kavehpour, H.P., Lequeux, F., and Limat,

L. Evaporation of a sessile droplet: Inside the coffee stain. J Colloid Interface Sci . **370**, 155, 2012.

30. Wilczek, M., Tewes, W.B.H., Gurevich, S. V, Köpf, M.H., Chi, L.F., and Thiele, U. Modelling Pattern Formation in Dip-Coating Experiments. Math Model Nat Phenom . **10**, 44, 2015.

31. Fraštia, Ľ., Archer, A.J., and Thiele, U. Modelling the formation of structured deposits at receding contact lines of evaporating solutions and suspensions. Soft Matter. **8**, 11363, 2012.

32. Dede Eren, A., Vasilevich, A., Eren, E.D., Sudarsanam, P., Tuvshindorj, U., de Boer, J., et al. Tendon-derived biomimetic surface topographies induce phenotypic maintenance of tenocytes in vitro. Tissue Eng Part A . 2020.

33. Vermeulen, S., Vasilevich, A., Tsiapalis, D., Roumans, N., Vroemen, P., Beijer, N.R.M., et al. Identification of topographical architectures supporting the phenotype of rat tenocytes. Acta Biomater. **83**, 2019.

34. Vermeulen, S., Roumans, N., Honig, F., Carlier, A., Hebels, D., Dede Eren, A., et al. Mechanotransduction is a context-dependent activator of TGF-β signaling in mesenchymal stem cells. Biomaterials. **259**, 2020.

35. Teixeira, A.I., Abrams, G.A., Bertics, P.J., Murphy, C.J., and Nealey, P.F. Epithelial contact guidance on well-defined micro- and nanostructured substrates. J Cell Sci . **116**, 1881 LP, 2003.

36. Dalby, M.J., Riehle, M.O., Sutherland, D.S., Agheli, H., and Curtis, A.S.G. Morphological and microarray analysis of human fibroblasts cultured on nanocolumns produced by colloidal lithography. Eur Cells Mater. **9**, 1, 2005.

37. Yang, L., Ge, L., and van Rijn, P. Synergistic Effect of Cell-Derived Extracellular Matrices and Topography on Osteogenesis of Mesenchymal Stem Cells. ACS Appl Mater Interfaces . American Chemical Society, **12**, 25591, 2020.

38. Yang, L., Gao, Q., Ge, L., Zhou, Q., Warszawik, E.M., Bron, R., et al. Topography induced stiffness alteration of stem cells influences osteogenic differentiation. Biomater Sci . The Royal Society of Chemistry, **8**, 2638, 2020.

39. Iannone, M., Ventre, M., Formisano, L., Casalino, L., Patriarca, E.J., and Netti, P.A. Nanoengineered surfaces for focal adhesion guidance trigger mesenchymal stem cell self-organization and tenogenesis. Nano Lett. **15**, 1517, 2015.

40. Benjamin, M., and Ralphs, J.R. Tendons and ligaments - An overview. Histol Histopathol. **12**, 1135, 1997.

41. Riley, G. Tendinopathy - From basic science to treatment. Nat Clin Pract Rheumatol. **4**, 82, 2008.

42. Andarawis-Puri, N., Flatow, E.L., and Soslowsky, L.J. Tendon basic science: Development, repair, regeneration, and healing. J Orthop Res. **33**, 780, 2015.

43. Tong, W.Y., Shen, W., Yeung, C.W.F., Zhao, Y., Cheng, S.H., Chu, P.K., et al. Functional replication of the tendon tissue microenvironment by a bioimprinted substrate and the support of tenocytic differentiation of mesenchymal stem cells. Biomaterials . Elsevier Ltd, **33**, 7686, 2012.

44. Versaevel, M., Riaz, M., Grevesse, T., and Gabriele, S. Cell confinement: Putting the squeeze on the nucleus. Soft Matter. **9**, 6665, 2013.

45. Milner, K.R., and Siedlecki, C.A. Fibroblast response is enhanced by poly(L-lactic acid) nanotopography edge density and proximity. Int J Nanomedicine. **2**, 201, 2007.

46. Christopherson, G.T., Song, H., and Mao, H.-Q. The influence of fiber diameter of electrospun substrates on neural stem cell differentiation and proliferation. Biomaterials . **30**, 556, 2009.

47. Harburger, D.S., and Calderwood, D.A. Integrin signalling at a glance. J Cell Sci. **122**, 1472, 2009.

48. Zheng, H., Tian, Y., Gao, Q., Yu, Y., Xia, X., Feng, Z., et al. Hierarchical Micro-Nano Topography Promotes Cell Adhesion and Osteogenic Differentiation via Integrin α2-PI3K-AKT Signaling Axis. Front Bioeng Biotechnol. **8**, 1, 2020.

49. Chaudhuri, P.K., Pan, C.Q., Low, B.C., and Lim, C.T. Topography induces differential sensitivity on cancer cell proliferation via Rho-ROCK-Myosin contractility. Nat Publ Gr . Nature Publishing Group, 1, 2016.

50. Dalby, M.J., Gadegaard, N., and Oreffo, R.O.C. Harnessing nanotopography and integrin-matrix interactions to influence stem cell fate. Nat Mater. Nature Publishing Group, **13**, 558, 2014.

51. Keselowsky, B.G., Collard, D.M., and García, A.J. Integrin binding specificity regulates biomaterial surface chemistry effects on cell differentiation. Proc Natl Acad Sci U S A. **102**, 5953, 2005.

52. Keselowsky, B.G., and García, A.J. Surface chemistry modulates integrin binding to direct cell adhesion and function. Trans - 7th World Biomater Congr. 369, 2004.

53. Shie, M.Y., and Ding, S.J. Integrin binding and MAPK signal pathways in primary cell responses to surface chemistry of calcium silicate cements. Biomaterials . Elsevier Ltd, **34**, 6589, 2013.

54. Hallab, N.J., Bundy, K.J., O'Connor, K., Moses, R.L., and Jacobs, J.J. Evaluation of metallic and polymeric biomaterial surface energy and surface roughness characteristics for directed cell adhesion. Tissue Eng. United States, **7**, 55, 2001.

55. Anselme, K., Ploux, L., and Ponche, A. Cell/material interfaces: Influence of surface chemistry and surface topography on cell adhesion. J Adhes Sci Technol. **24**, 831, 2010.

56. Dos Santos, E.A., Farina, M., Soares, G.A., and Anselme, K. Chemical and topographical influence of hydroxyapatite and β-tricalcium phosphate surfaces on human osteoblastic cell behavior. J Biomed Mater Res - Part A. **89**, 510, 2009.

57. Puckett, S., Pareta, R., and Webster, T.J. Nano rough micron patterned titanium for directing osteoblast morphology and adhesion. Int J Nanomedicine. **3**, 229, 2008.

58. Janson, I.A., Kong, Y.P., and Putnam, A.J. Nanotopographic Substrates of Poly (Methyl Methacrylate) Do Not Strongly Influence the Osteogenic Phenotype of Mesenchymal Stem Cells In Vitro. **9**, 2014.

59. Carpenter, A.E., Jones, T.R., Lamprecht, M.R., Clarke, C., Kang, I.H., Friman, O., et al. CellProfiler: image analysis software for identifying and quantifying cell phenotypes. Genome Biol . **7**, R100, 2006.

60. Schindelin, J., Arganda-Carreras, I., Frise, E., Kaynig, V., Longair, M., Pietzsch, T., et al. Fiji: An open-source platform for biological-image analysis. Nat Methods. **9**, 676, 2012.

Supplementary figures
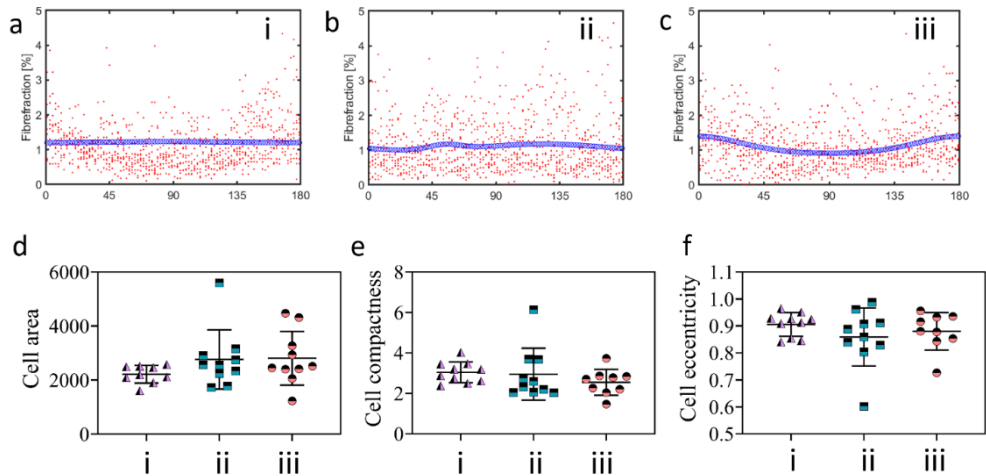
Supplementary Figure 1. *Random cellular alignment on a collagen stain, derived from evaporating a 1mg ml⁻¹ collagen droplet. Images are obtained from randomly selected regions close to the stain in (i) the peripheral region, (ii) the middle region, and (iii) the central region were quantified for orientation and cell morphological parameters. Tenocytes neither displayed preferred orientations (a-c), nor differences in cell shape, between locations (d-f).*
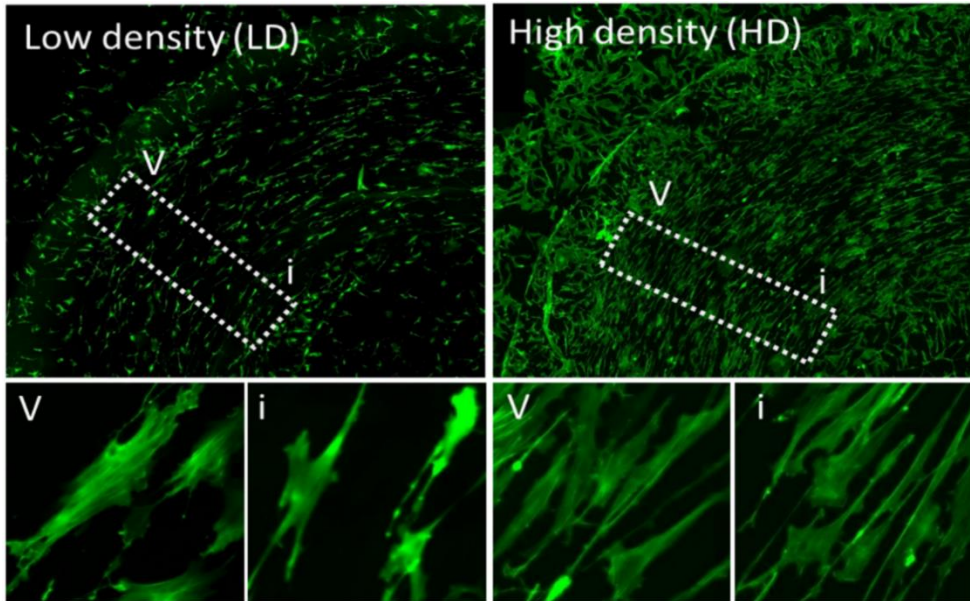
Supplementary Figure 2. *The differences in collagen wavelength motifs in the concentric area did not affect cell shape, irrespective of the cell seeding density (low density in the left panel; high density in the right panel).*

Chapter V

Tendon-derived biomimetic surface topographies induce phenotypic maintenance of tenocytes *in vitro*

T‌he tenocyte niche contains biochemical and biophysical signals that are needed for tendon homeostasis. The tenocyte phenotype is correlated with cell shape *in vivo* and *in vitro*, and shape-modifying cues are needed for tenocyte phenotypical maintenance. Indeed, cell shape changes from elongated to spread when cultured on a flat surface, and rat tenocytes lose the expression of phenotypical markers throughout five passages. We hypothesized that tendon gene expression can be preserved by culturing cells in the native tendon shape. To this end, we reproduced the tendon topographical landscape into tissue culture polystyrene, using imprinting technology. We confirmed that the imprints forced the cells into a more elongated shape, which correlated with the level of Scleraxis expression. When we cultured the tenocytes for seven days on flat surfaces and tendon imprints, we observed a decline in tenogenic marker expression on flat but not on imprints. This research demonstrates that native tendon topography is an important factor contributing to the tenocyte phenotype. Tendon imprints therefore provide a powerful platform to explore the effect of instructive cues originating from native tendon topography on guiding cell shape, phenotype and function of tendon-related cells.

Chapter V

Introduction

Tendon is a unique type of connective tissue that transmits muscle contraction forces to bones to produce motion and maintain body posture. [1] In healthy tendon, a typical hierarchical arrangement of parallel collagen fibrils and fibers forms a tendon unit, which in an unloaded state adopts a crimp-type/wavy configuration.[2] Tendon fibroblasts, i.e. tenocytes, contribute to tissue homeostasis when exposed to this highly ordered collagen extracellular matrix (ECM) by producing ECM proteins and thus collagen assembly and turnover. [3,4] However, due to its low cellularity and hypovascularity, tendons possess a low regenerative capacity that results in poor and slow healing. [5–7] Injury or tissue damage often results in an increased ratio of type III collagen to type I collagen and additional deposition of glycosaminoglycans (GAG). [1] From a structural point of view, the organization of collagen fibers change from highly anisotropic to more isotropic and at the micro-level, they become more angulated and the number of small-diameter collagen fibers is increased. [8] At the cellular level, tenocytes become more stellate-shaped [1,8–10] and the expression of chondrogenic genes such as *Col2a1 and Aggrecan* increases [9,11] while expression of tendon-related markers, i.e. *Tenomodulin (Tnmd)* [12] and *Scleraxis (Scx)* decreases [13].

Similar to *in vivo,* changes in tenocyte phenotype, shape and function are observed during *in vitro* culture of tendon-derived cells on flat tissue culture plastic, which thus lacks the tendon ECM niche. On flat tissue culture polystyrene, tenocytes quickly lose their elongated shape and decrease the expression levels of *Scx* [14]. Yao *et al.*, reported that the amount of collagen type I (COL1) and decorin (DCN) protein expression levels decreased significantly from passage 0 to passage 8 during *in vitro* culture [15]. Mazzocca *et al.*, showed that in addition to *Scx, Dcn* and *Col1*, gene expression levels of other tenocyte markers, i.e. Tenascin-C (*Tn-C*) and *Tnmd*, decline from passage 0 to passage 6 [16]. This phenomenon is referred to as dedifferentiation, and is also a well-known phenomenon observed in chondrocytes [17]. These results point towards the lack of a healthy tendon niche, i.e. biochemical and topographical changes, driving this loss of tenocyte phenotype, in analogy to changes in tissue organization *in vivo* that similarly affect tenogenicity.

Various strategies were used to re-differentiate the dedifferentiated tenocytes to rescue their tenocyte phenotype *in vitro*. Supplementing culture medium with various growth factors such as VEGF [18], IGF [19] and GDF5 [20] increases expression of tenocyte marker genes including *Scx* and *Tnmd*. Additionally, serum-deprivation, i.e. depletion of medium-associated growth factors rescued the lost tenocyte phenotype [21]. In addition, the small molecule tazaratone, which targets the retinoic acid receptor, preserves tenocyte phenotype via scleraxis [22]. Manipulating tenocyte shape has also been used as

an approach to re-differentiate dedifferentiated tenocytes as well as induce tenogenic differentiation of stem cells, and one such approach that pushes cells into an elongated shape is by exposing cells to a topographical cue, i.e. a substrate composed of anisotropic fibers [23–32] or microgrooves[26,33]. For instance, Kishore *et al.*, used aligned collagen threads to mimic the packing density, alignment and strength of native tendon, and observed an increase in gene expression of *SCX, TNMD* and *TN-C* compared to the randomly organized fibers in human mesenchymal stem cells [27]. Similarly, Younesi *et al.*, fabricated 3D-bio textiles from collagen and observed that compared to random fibers, expression of *Col1a1* and *Tnmd* increased more than 6- and 11-fold, respectively, in human mesenchymal stem cells [34]. Tu *et al.*, promoted tenogenic differentiation of mouse mesenchymal stem cells *in vitro* and tendon regeneration *in vivo* by aligned electrospun fibers derived from tendon ECM [29]. An increase in the expression of tenogenic marker genes, including *Scx, Dcn* and Biglycan (*Bgn*), was observed both *in vivo* and *in vitro* [29]. Similarly, Zhu *et al.,* reported that morphology of pig tenocytes become elongated upon culturing on anisotropic microgrooves, compared to flat surface, and expression of TNMD elevated[26]. We previously reported that tendon-derived cells populating a reconstituted collagen tissue, ranging from uniaxially constrained with spindle-shaped cells to biaxially constrained with stellate-shaped cells, display the strongest functional remodelling capacity and tenocyte phenotype when adopting a spindle-shaped morphology [35]. In another approach, we took the cell shape concept one step further by using a micro-topographical screening platform with a large amount of unique micro-topographies for identifying feature-characteristics associated with Scleraxis levels, and revealed a strong correlation of specific cell shapes, i.e. cell and nuclear area with Scleraxis intensity in rat tenocytes [14]. These studies underline the impact of stimulating the tenocyte phenotype by manipulating the cell shape.

Based on the above, we hypothesized that the topographical cues present in the tenocyte niche contribute to phenotypic maintenance of tenocytes. We tested this by exploiting an imprinting method to replicate the native tendon topography to polystyrene. Results of this study showed the importance of the tendon topography, pushing cells in a spindle-shaped morphology, in the maintenance of the tenocyte phenotype *in vitro*, which can shed a light on further understanding of tendinopathy.

Results

Tendon-derived cells rapidly change morphology and phenotype on a flat substrate

Flat polystyrene surfaces were used to assess the influence of passage number on tenocyte shape and tenocyte phenotype. Therefore, passage one (P1) rat tenocytes were cultured and subsequently passaged four times (Fig. 1). We first investigated the changes in cell and nuclear shape parameters including area, compactness, solidity and aspect

ratio and changes in gene expression levels of tendon-related genes. Aspect ratio is calculated by calculated by dividing the length of the major axis by the length of the minor axis; so, the higher the value, the more elongated the cells. Compactness is correlated with elongation; high compactness values indicate more elongated cells. Solidity is related with cell branching and the closer its value to 1, the more solid the cells. Results showed a slight increase in cell area, i.e. cell size, with passage number (Fig. 1B). Cell aspect ratio and compactness significantly decreased after P1, yet solidity remained the same in all groups (Fig. 1B). The increase in the nucleus area was statistically significant between P1 and P3, P4 but remained at similar values at P2 and P5 (Fig. 1B). Nucleus aspect ratio significantly reduced after P2, yet compactness and solidity remained unchanged between passages (Fig. 1B, supplementary file 1 containing raw data). Overall, our data indicates that with passaging of tenocytes to P4 on flat tissue culture plastic, they undergo shape-related changes; cells and their nucleus steadily increase in size and transform from the original spindle-shaped/elongated morphology to a stellate-shaped/round morphology.

To further evaluate the loss in tenocyte phenotype, gene expression levels of *Scx*, *Col1a1*, *Col3*, *Dcn* , *Mkx* and *Bgn* were measured (Fig. 1D)). *Scx,* which is a tenogenic transcription factor [36], showed a significant decrease after passage one. A similar reduction was observed for the expression of *Col1a1*, which is the most abundant protein in the tendon extracellular matrix (ECM), *Mkx,* which is a homeobox gene is and involved in the regulation of tendon differentiation[37] and *Col3* [38]. Furthermore, we measured the expression of genes coding for non-collagenous matrix proteins *Dcn* and *Bgn* that bind to collagen, which displayed a decreasing trend from P1 to P5 [39]. With these results, we confirmed that tenocytes dedifferentiate by rapidly losing their morphological characteristics and expression of tenocyte marker genes on a flat surface during *in vitro* sub-culture.
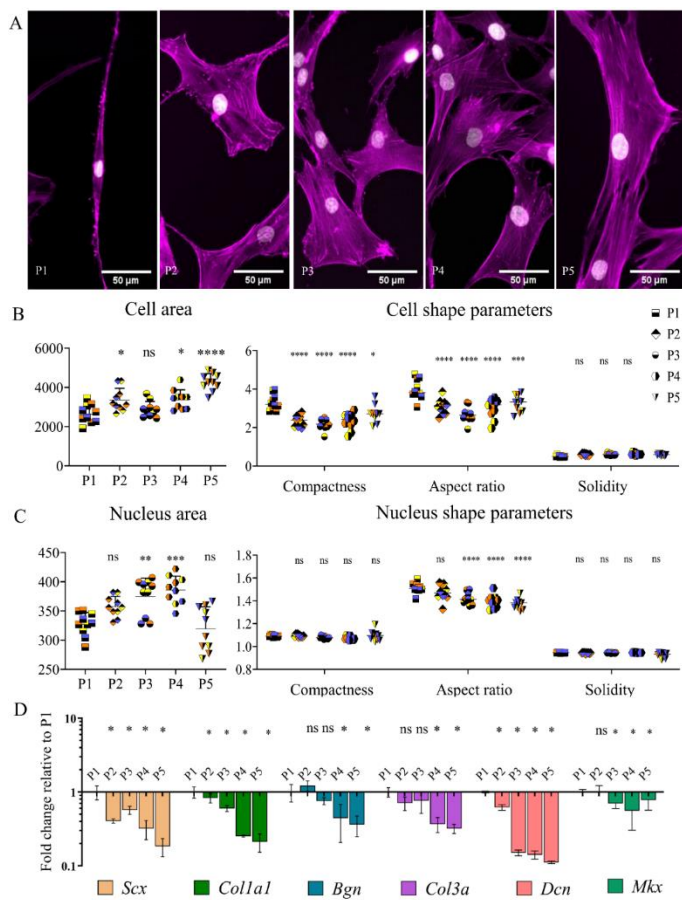
Figure 1. Tendon-derived cells rapidly lose their morphology and phenotype on a flat substrate. *(A) Representative images of rat tenocytes stained with Phalloidin-568 to visualize F-actin filaments (Magenta-artificial color) and counterstained with DAPI to visualize the nucleus (Cyan-artificial color) cultured on flat surfaces from passage 1 (P1) until passage 5 (P5). (B) Changes in cell area, aspect ratio, compactness and solidity from P1 to P5 (*P < 0.05, **P < 0.01,***P < 0.005, ****P < 0.0001). (C) Changes in nucleus area, aspect ratio and solidity from P1 to P5 (**P < 0.01,***P < 0.005, ****P < 0.0001). (D) Expression of tenogenic marker genes Scleraxis (Scx), Collagen type 1 (Col1a1), Collagen type three (Col3), Decorin (Dcn), Mohawk (Mkx) and Biglycan (Bgn) from P1 towards P5 all decreased with passage number. A $\log_{10}$ transformation of expression fold changes is used to visualize the differences in gene expression. Scale bars represent 100 μm. (Error bars represent 95% confidence intervals, *P < 0.05,**P < 0.01). For all experiments, N = 3. Different colors in the graphs illustrate the data obtained from biological replicates.*

The native tendon imprint as cellular niche on polystyrene

After establishing that with passaging, tenocytes lose their phenotype on flat polystyrene, the effect of the tendon surface topography, as an isolated effect, was assessed. To this end, we used the soft embossing method to imprint a native tendon topography onto polystyrene (Fig. 2). The imprinting protocol involved polymerization of PDMS using a 10:1 ratio of monomers and curing agent on a native tendon (Fig.2A, 3), and embossing the PMDS negative imprint on polystyrene (Fig.2A,6). The imprinted

material was imaged using scanning electron microscopy (SEM) (Fig.2B and supplementary video 1), atomic force microscopy (Fig.2C) and profilometry (Fig.2D and supplementary video 2). SEM and profilometer images reveal that native tendon can indeed be imprinted onto polystyrene, and the polystyrene imprint possesses a tendon-like topography. AFM analysis shows that surface topographies on tendon imprints can reach a depth of 5μm.
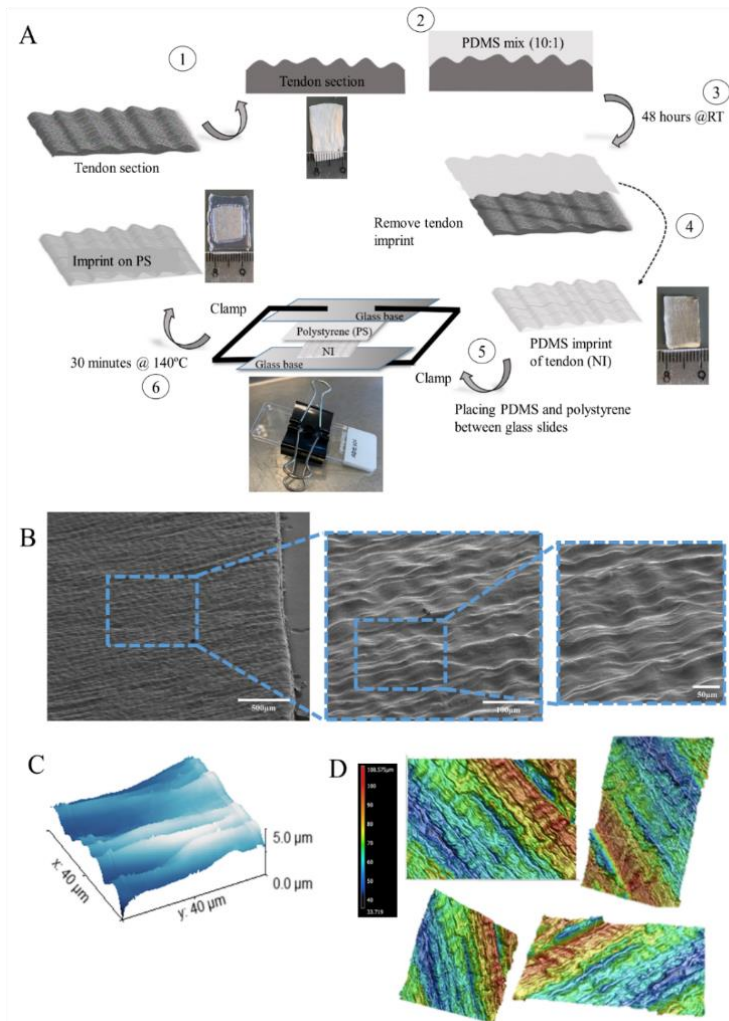

Figure 2. The native tendon imprinted as a cellular niche on polystyrene. *(A) Procedure to develop a native tendon imprint, using an embossing technique of a native tendon tissue into polystyrene. (B) SEM image of tendon imprint with lower (left) and higher (right) magnification. The red dotted box represents a randomly selected region on the imprint. (C) Representative AFM image of tendon imprint showing that the imprint can reach a depth of 5μm height. (D) Representative image of profilometer images of tendon imprint, depicted from different angles.*

Late passage tenocytes adapt early passage tenocyte morphology on tendon imprints

Next, the morphological response of tenocytes to the tendon imprint was assessed (Fig.3). Flat control surfaces were prepared by imprinting a flat PDMS mold to the polystyrene sheets. Rat tenocytes (P4) were seeded on flat and imprint surfaces and stained with phalloidin to visualize F-actin (grey) and DAPI to visualize nuclei (blue). On the flat surface, (Fig.3A&B, top panel) a spread morphology was observed, contrary to tendon imprints, where cells on each replicate displayed an elongated shape (Fig.3A&B, bottom panel).

We further investigated the effect of tendon topography on cell and nuclear shape parameters including aspect ratio, area, solidity and compactness (Fig.3D&E). We first visualized the difference in cell shape. Rat tenocytes were exposed to either a flat surface or tendon imprint topography and subsequently SEM imaging was performed (Fig.3A). On the flat surface, we observed that tenocytes are more spread and stress fibers were observed (yellow arrows) (Fig.3A-top panel). On tendon imprints, rat tenocytes were highly elongated (red arrow) (Fig.3A-bottom panel). We observed similar results when we stained tenocytes with phalloidin to visualize the actin cytoskeleton (Fig.3B) and DAPI to visualize nuclei (Fig.3C). Cell and nuclear area were significantly smaller on tendon imprints compared to flat (Fig.3E&F). Additionally, cellular and nuclear aspect ratio and compactness were significantly higher on tendon imprints, compared to flat (Fig.3E). Cell solidity on imprints (0.61 ± 0.05) was significantly higher and closer to 1, compared to the flat surface (0.51 ± 0.04); indicating that cell branching was less pronounced on tendon imprint. Nuclear solidity was not significantly different for both topographies. Therefore, results indicate that tendon imprints induce an elongated shape and reduces cytoskeletal branching, resembling the early passage tenocytes on flat polystyrene.
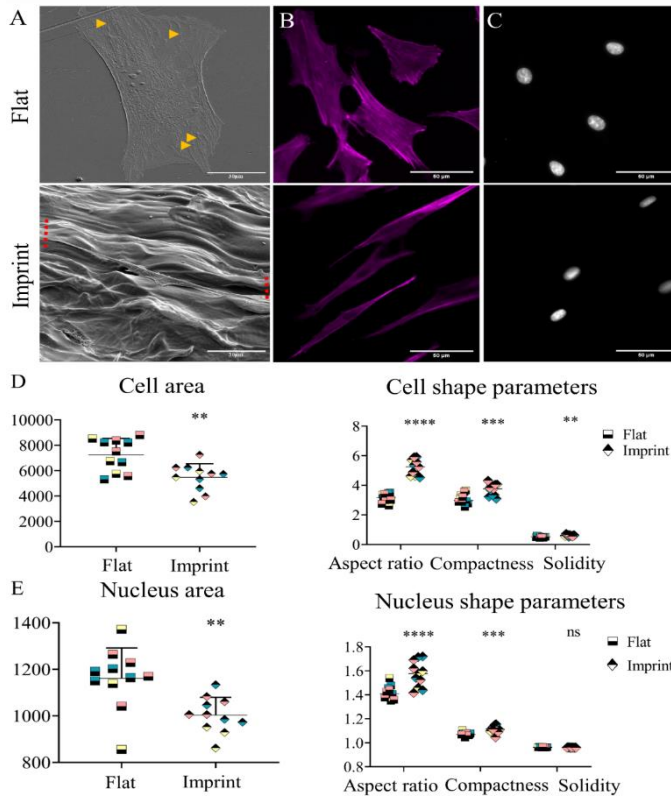
Figure 3. Tendon imprint topography manipulates tenocytes to their natural morphology. *Tendon imprint topography pushes tenocytes to their natural morphology (A) Representative images of tenocytes cultured on the flat surface (left) and four replicates of the tendon of tendon imprints (right). Top images belong to SEM imaging, bottom images belong to fluorescent staining (Phalloidin in Gray, artificial color. DAPI in blue). Scale bars represent 100 μm. (B) SEM images of tenocytes cultured on a flat surface (top) and tendon imprint (bottom).*

Yellow arrows represent stress fibers on the tenocytes on the flat surface. Red dotted lines represent the major axis boundaries of tenocytes. Scale bars represent 30 μm. (C) Representative images of cell shape (magenta, artificial color) of rat tenocytes cultured on flat (top) and tendon imprint (bottom). Scale bars represent 10 μm. (D) Representative images of nucleus shape (grey, artificial color) of rat tenocytes cultured on flat (top) and tendon imprint (bottom). Scale bars represent 10 μm. (E) Cell shape parameters are significantly different between both flat and imprint topographies, except for nuclear solidity (* $p<0.05$). For all experiments, $N = 3$. Different colors in the graphs illustrate the data obtained from biological replicates.

Tendon imprint topography decreases tenocyte proliferation

Surface topography has been identified as a regulator of cell proliferation [40] [41]. Therefore, the effect of tendon imprint topography on tenocyte proliferation compared to the flat surface was assessed. Rat tenocytes were thus cultured on a flat surface and tendon imprint, and after 24 hours the proportion of cells in the S-phase of the cell cycle (pink-purple) to all cells (blue) was measured by EdU labelling (Fig.4A&B). On tendon imprints, 37% of the tenocytes were EdU positive whereas on a flat surface,

63% of the cells were EdU positive. This indicates that tendon topography relates to a less proliferative tenocyte state.
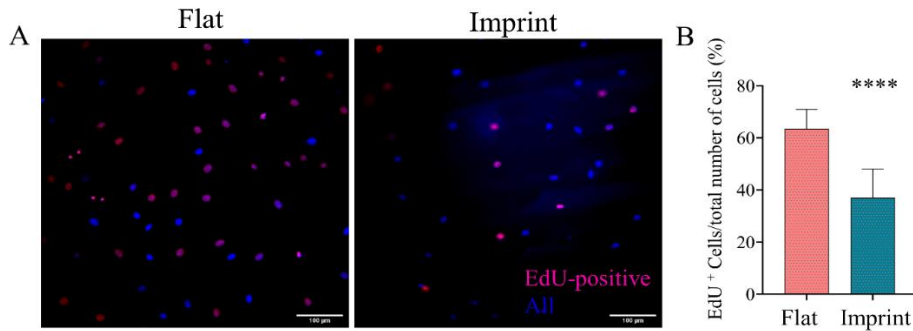

Figure 4. Tendon imprint topography lower cell proliferation capacity. *(A) Representative images of EdU staining in which proliferating cells are labelled in pink-purple color and Hoechst is used as a counterstain (in blue color). (B) Quantification of EdU positive tenocytes on the flat surface and tendon imprints. On the flat surface, 63% of the cells was EdU positive, whereas on tendon imprints it was only 37%. Scale bars represent 100 µm. (Error bars represent 95% confidence intervals, * p<0.05). For all experiments, N = 3.*

SCX intensity correlates with cellular and nuclear features

Tendon imprints significantly affect tenocyte cell and nucleus shape. Next, the influence of tendon imprint topography on tenocyte marker gene expression was assessed (Fig.5). Therefore, rat tenocytes at P4 were cultured on tendon imprints and flat surfaces for 24 hours and the amount of SCX was measured by immunocytochemistry and subsequent quantification (Fig.5A). SCX intensity were significantly higher on tendon imprint after 24 hours (Fig.5B), which was subsequently correlated with cell shape, using a Spearmen correlation calculation. A positive and significant correlation was detected of SCX intensity level with cell compactness (r_s= 0.71), nucleus compactness (r_s= 0.71), cell eccentricity (r_s= 0.82) and nucleus eccentricity (r_s= 0.78) (Fig. 5C&D, supplementary file 2 containing raw data). In addition, a negative and significant correlation was detected of SCX intensity with cell area (r_s= -0.58) and nucleus area (r_s= -0.70) (Fig. 5C&D). SCX level thus correlates with elongated cell and nucleus shape, driven by tendon surface topography.
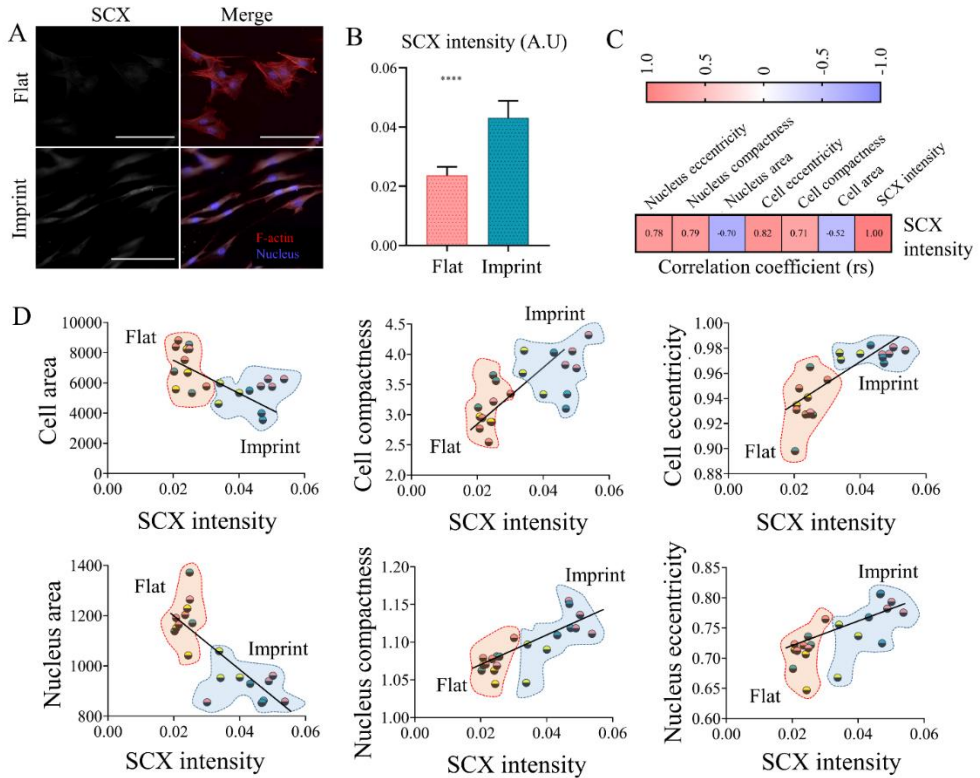
Figure 5. SCX intensity correlates with cellular and nuclear features. *Tenocyte phenotype is maintained by tendon imprints (A) Representative images of rat tenocytes cultured for 24 hours on a flat surface and a tendon imprint and stained for SCX. (B) Quantification of SCX intensity levels in tenocytes on flat surface and tendon imprint. (C) Levels of SCX intensity correlates with cellular and nuclear features Spearmen correlation values (rs) between SCX intensity levels and eccentricity, compactness and area of cell and nucleus. (D) X-Y graphs of cell and nuclear area, compactness and eccentricity correlated with SCX intensity levels. Each data point represents the median value of images contain individual intensities of all cells measured in a single image. Area indicated in red and blue belong to cells on flat and imprint surfaces, respectively. For visual purposes, a trend line was added derived from a simple linear regression calculation. For all experiments, N = 3. Different colors in the graphs illustrate the data obtained from biological replicates.*

Tenogenic gene expression is maintained on tendon imprints

After showing that native tendon topography can increase SCX at protein level on the short term, we investigated whether tenocyte phenotype can be maintained for 7 days of culture. (Fig. 6). Therefore, P4 tenocytes were cultured on flat surfaces and imprints

for 7 days and gene expression levels of *Scx*, *Col1a1*, *Sox9*, *Dcn*, and *Runx2* were measured on day 1 (D1), day 3 (D3) and day 7 (D7). On the flat surface, expression of tendon-related genes *Scx, Dcn* and *Col1a1* decreased over 7 days of culturing, indicating ongoing dedifferentiation (Fig. 6A-C). Expression of *Sox9,* a chondrogenic transcription factor that is also expressed at the tendon-bone junction, also decreases on the flat surface (Fig. 6E). Lastly, *Runx2* gene expression, an osteogenic-associated transcription factor, significantly increased on the flat surface. Contrary, on tendon imprints, gene expression levels of *Scx, Dcn, Col1a1* and *Sox9* increased at D1 and subsequently remained stable over the 7 days, indicating that tendon imprints can both induce a slight increase in tenogenic gene expression and prevent the dedifferentiation that occurs on the flat surface (Fig. 6A-C, E). Lastly, gene expression of *Runx2* did not increase on the tendon imprints.
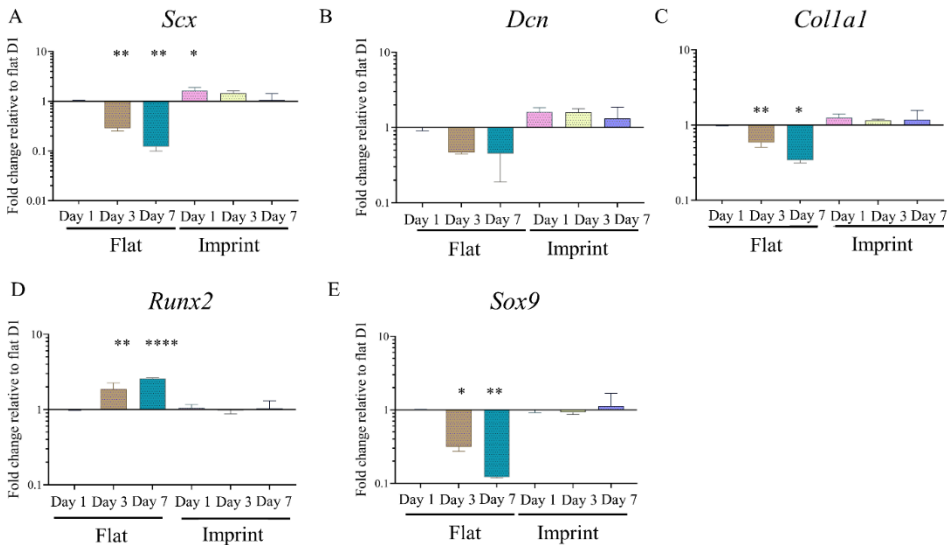

Figure 6. Tenocyte phenotype is maintained on tendon imprint topography. *Gene expression levels of (A) Scx, (B) Dcn, (C) Col1a1, (D) Runx2 and (E) Sox9 of tenocytes cultured on flat surfaces and tendon imprints over 7 days of culture. On a flat surface, expression of Scx, Dcn, Col1a1, Sox9 decrease whereas Runx2 increases. Contrary, tendon imprints preserved tenocyte phenotype. A log10 transformation of the expression fold changes is used to visualize the differences in gene expression. (Error bars represent 95% confidence intervals, *P < 0.05,**P < 0.01). For all experiments, N = 3.*

Discussion

Surface topography of various organs and tissues in nature give a series of evolutionary advantages and provide specialized functions. They provide cells with signals to differentiate, migrate, proliferate or maintain their phenotype. The surface topography of tendon tissue is also considered to provide such strong cues. However, whether the tendon topography alone, devoid of other cues (e.g. ligand type and density, changing mechanical properties, etc), provides a strong cellular cue remained to be explored. Therefore, the soft embossing method was exploited to imprint native tendon on a polystyrene surface to study the effect of tendon surface topography on cell shape, proliferation and phenotype, when compared to flat polystyrene surfaces. Results of this study confirm that flat polystyrene surfaces drastically alter tenogenic cell shape and phenotype, and highlight that: 1) native tendon topography can be imprinted onto a polystyrene surface to conduct tendon-related studies *in vitro* 2) cellular proliferation is decreased on imprint topographies, compared to flat surfaces, 3) tenocyte phenotype is maintained on tendon imprint topographies and 4) remarkably, Intensity levels of Scleraxis, a key tenocyte marker, beautifully correlates with specific cell and nuclear shape parameters. Concordantly, results of this study imply that imprinting the natural tendon surface on materials, such as polystyrene, provides a tool to control tenocyte cell shape and maintenance of the tenocyte phenotype, as summarized in Fig. 7.
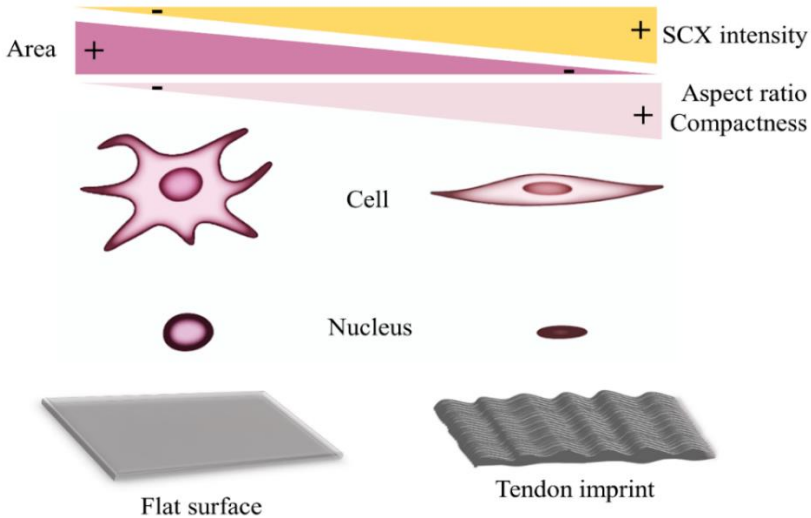

Figure 7. Summary of the results. *Tenocytes on imprint surfaces display a lower cell area and higher aspect ratio, compactness and solidity, which results in increased SCX intensity.*

Drastic changes in cell shape of freshly isolated or early passage cells upon culturing on tissue culture plastic were shown for a wide variety of cell types, including tenocytes [15], [14], [42–47]. Vermeulen *et al.* and Yao *et al.* showed that the elongated shape of tenocytes at P0 transforms to stellate-shaped at P1 [15], [14], which is in agreement with the changes observed in cell and nucleus shape of the current study. Similarly, our observation on the decrease in tenogenic marker genes corroborate with previously published reports [14,15], [16], indicative for a dedifferentiation process. Due to the rather limited availability of the early passage cells (P0 or P1), dedifferentiation has become an obstacle for *in vitro* research and associated interpretation of acquired data of many cell types. This gives rise to the interesting concept of re-differentiation in order to promote/restore the native phenotype.

The interplay between cell shape and cell fate (e.g. differentiation, proliferation, apoptosis etc.) is an established concept [48] [17]. Following that concept, because healthy tenocytes *in vivo* adopt an elongated morphology, i.e. the nucleus and cell body, which are aligned between collagen fibers, re-differentiation research has focused on pushing cells towards similar morphologies. Among these approaches, cells have been exposed to anisotropic fibers [24,27,31,32,49–56] or nano/micro-grooves [14,26,57]. For instance, Zhu *et al.,* reported that dedifferentiated tenocytes become elongated upon culturing on microgrooves, which partially reversed the dedifferentiation process [26]. A similar study by Schoenenberger *et al.*, showed that tendon fibroblasts displayed a higher expression of the tendon-related marker *Mohawk* (MKX), COL, BGN and DCN on aligned PCL fibers, compared to random fibers [58]. Despite their impact on tenocyte phenotype, microgrooves or anisotropic fibers may not reflect topographical cues that tenocytes or mesenchymal stem cells experience when exposed to imprint substrates as the delicate variations in roughness, ridges and valley that create specific spatial cellular attachment sites are absent. For this, replication of native tendon topography on PDMS[40] and silica[59] have silica have previously been performed to differentiate mesenchymal stem cells towards the tenogenic lineage, and both increased to an elevation in the expression of TNMD, compared to flat surfaces. This also suggest that tendon imprints can promote tenogenic differentiation. Results of the current study supports the concept that enforcing a spindle-shaped tenocyte morphology is beneficial for maintaining/restoring their native phenotype. Specifically, our results showed that elongated cell shape, i.e. high cell aspect ratio, eccentricity and compactness, is correlated with SCX levels. However, a degree of heterogeneity in cell phenotype, i.e. shape parameters and SCX levels, was observed especially for tendon imprints. Explanations for this may relate to the imprinting technique that potentially disturbs native architecture locally, or the fact that cells on imprints are exposed to a 2D surface with more freedom to adopt a preferential shape, rather than the strongly confined 3D *in vivo* environment. Despite that, the expression of tenocyte marker genes *Scx, Dcn* and

Col1a1 was still shown to be stabilized on tendon imprints, contrary to a decay observed on flat surfaces.

The observation in the current study that osteogenesis (*Runx2*) increased on flat surfaces, compared to imprints, was also observed in another study, using osteocalcin and alkaline phosphatase as osteogenic marker genes [31]. Possibly, this relates to the increased proliferation rate on flat surfaces resulting in cell confluency, a phenomenon that was previously linked to increased *Runx2* gene expression [14,24,60]. Although tenocytes are the most abundant cell type in tendon tissue, depending on the location of the cells within the tendon, a *Sox9* positive subpopulation of tenocytes exists that is located at the junction between bone and tendon/ligament [61,62]. The expression of *Sox9* was previously shown to remain stable when tenocytes were cultured, either cyclically stretched or left unstretched, on microgrooved substrates, which induces an elongated morphology [33]. Therefore, the naturally present *Sox9* gene expression level in elongated tenocytes, which is stabilized on imprint surfaces, is lost on flat surfaces since the differentiation process is initiated. Suggestively, different topographical cues present *in vivo* in the tendon towards the enthesis, contribute to differences in phenotype of locally present cells.

Healthy tendon comprises of relatively quiescent tenocytes, whereas proliferation increases during the remodelling phase of tendon during healing, during which the strong tissue anisotropy is absent [63]. In analogy, tendon imprints resulted in suppression of proliferation, when compared to flat surfaces. Similarly, proliferation capacity of human mesenchymal stem cells is also lower on aligned collagen fibers or anisotropic topographies, compared to randomly oriented substrates [64]. One explanation for different proliferation rates on different topographies is a difference in cell shape and alignment of stress fibers, as previously shown [65]. In elongated smooth muscle cells (SMCs), DNA synthesis was decreased, indicating that the directed cell spreading can be positively linked with DNA synthesis and thus cell proliferation [66]. A possible underlying mechanism for this could relate to *NOR-1*, a gene involved in SMCs proliferation. *NOR-1* expression is among others modulated by protein kinase C (PKC). In elongated cells, the activity of protein kinase C was shown to be decreased, which was associated with a decreased *NOR-1* expression and thus ultimately decreased cell proliferation [65]. Considering the similarities in shape influences between SMCs and tenocytes, this could be a possible explanation. Another, or additional, explanation is that changes in cell proliferation are linked to surface-topography-induced mechanotransduction. Surface topography was shown to alter integrin activation and focal adhesion dynamics, which affects cell proliferation [67,68]. Flat surfaces results in specific cell spreading and integrin binding, resulting in focal adhesion kinase phosphorylation and activation, which in turn activates the ERK pathway, cyclin D1,

and finally the G_1-S cell cycle transition [69]. However, activation of integrins α5 and α6 have been shown to create the opposite effect [70]. This indicates that the exact mechanism by which tenocyte proliferation is coupled to cell shape, surface topography, mechanotransduction pathways and specific integrin recruitment on tendon imprints should further be explored.

The use of tendon imprints in research has several advantages. Firstly, the production of tendon imprints requires only PDMS, polystyrene and tools to perform soft embossing; therefore, upscaling the production can be cheap and fast. Secondly, they bear the potential to be used as a model system to study the molecular mechanism behind the dedifferentiation and re-differentiation process, including the role of surface topographies on the activation of mechanotransduction pathways. Thirdly, the imprinting technology is facile enough that it can be applied to any polymer that does not degrade above 140ºC. Therefore, in addition to the influence of healthy tendon surface topography, the effect of other polymers on tenocyte phenotype can be investigated. Finally, the technique also allows imprinting the pathogenic or damaged tendon topography on polystyrene; therefore, the role of altered surface topography on tenocyte phenotype can be further explored *in vitro*.

Conclusion

This study shows that tenocyte cell shape and expression of tenogenic marker genes drastically change during *in vitro* subculture, which leads to decreased tenogenic characteristics. Furthermore, we demonstrated that tendon imprints, which carry the topological cues from the native tendon, led to an elongated cell shape and resulted maintenance in the expression of tenogenic-associated markers genes, which is positively correlated with elongated cell and nuclear shape parameters, i.e. aspect ratio, compactness and eccentricity. Overall, results of this study support the concept of cell shape-to-phenotype in tenocytes and stresses the role of surface topography on tenocyte phenotype.

Materials and Method

Tendon tissue imprinting

Fresh porcine Achilles tendons were obtained from crossbreeds of Great Yorkshire and Dutch land pigs aged between 6-8 months old and between 85-95 kg of weight, supplied by a local slaughterhouse (Compaxo Meat B.V, the Netherlands). Muscle, fat, bone-like tissues, synovial sheath, and paratenon were aseptically dissected and the remaining tendon was cut into 1cm³ blocks and stored at -80 °C. Frozen tendons were embedded in a mixture of polyvinyl alcohol and polyethene glycol (OCT, Sakura) and fixed to the cutting base plate of a cryotome (Leica CM1950) after which longitudinal sections were

cut with a thickness of 300 μm. Sections were washed with PBS and stored at -80 °C until use.

Tendon sections were thawed at room temperature for 30 minutes and placed in a 6-Well plate. Polydimethylsiloxane (PDMS, Dow Corning Sylgard 184, 4019862) was mixed with curing agent at a ratio of 10:1 (w/w) and mixed vigorously. In order to remove the air bubbles, the mixture was centrifuged at 3000 G for 10 minutes and poured on tendon sections. They were allowed to cure for 48 hours at room temperature on a stable flat surface. Then, the tendon section was peeled off from the PDMS resulting in a negative imprint of a tendon on PDMS. In between two glass slides, a negative imprint of PDMS was placed onto a polystyrene film (PS,GoodFellow) and pressed together with clamps and incubated at 140°C for 30 minutes. Flat surfaces were prepared by performing the same embossing method but using a flat PDMD mold. In order to allow cell attachment, polystyrene surfaces were oxygen plasma treated for 45 s at 75 mTor, 50 sccm O2, and 50 W.

Isolation of rat tenocytes
Rat tenocytes were isolated from the Achilles tendon of 23 weeks old Cyp1a2ren strain rats, after euthanization due their surplus status from the breeding program. Briefly, tendons were cut into small pieces and digested in a buffer containing 3mg/ml collagenase type II (Worthington Biochemical), 4mg/ml dispase II (Sigma-Aldrich) and 100 U/ml Penicillin/Streptomycin (Thermo Fisher Scientific) for 4 hours at 37°C in a humidified tissue culture chamber with 5% CO2. Then, the suspension was passed through a 70 mm cell strainer (Life sciences) to obtain a cell-only suspension. The cell suspension was centrifuged at 300 G for 5 minutes and re-suspended in Dulbecco's modified Eagle's medium (DMEM, Sigma-Aldrich) supplemented with 10% fetal bovine serum (FBS), 100 U/ml penicillin/streptomycin. Cells were cultured in T-25 flasks until 70% confluency.

Sterilization of tendon imprints and cell culture
Sterilization of flat and tendon imprints was performed by incubating the materials in 70% ethanol for 1 hour, and remaining ethanol was air-dried under sterile conditions. Next, samples were incubated with sterile PBS for 30 minutes at 37°C and subsequently with culture medium for 30 minutes at 37°C before use. Rat tenocytes were seeded on the surfaces at a density of 5000 cells/cm² in Dulbecco's modified Eagle's medium (DMEM, Sigma-Aldrich) supplemented with 10% fetal bovine serum (FBS) (Sigma-Aldrich) and 100 U/ml penicillin/streptomycin (Thermo Fisher Scientific). Cells were trypsinized once they reached 70% confluency. Tenocytes at passage 4 were used, unless stated otherwise.

RNA isolation and quantitative PCR (RT-qPCR)

Total RNA from each sample was isolated based on the protocol described in the RNeasy Mini Kit (QIAGEN). The yield and the quality of the RNAs obtained after RNA isolation is demonstrated in supplementary table 1. Reverse transcription was carried out based on the protocol provided by iScript™ Select cDNA Synthesis Kit (Bio-Rad). Quantitative PCR was performed by using iQ™SYBR® Green Supermix (Bio-Rad) by using the Bio-Rad CFX manager. Ribosomal Protein L13a (*Rpl13a*) was used as a housekeeping gene and relative expression was determined using the ΔΔCt method. Primer sequences are listed in table 1.

Immunofluorescence staining of Scleraxis

Cells attached to flat or tendon imprint surfaces were fixed at day 1, day 3 or day 7 after the start of culturing with 4% paraformaldehyde (PFA, ThermoFisher Scientific) at room temperature for 20 minutes and then washed with phosphate-buffered saline (PBS, Sigma-Aldrich), twice. Next, samples were permeabilized with 0.5 % (v/v) Triton X-100 in PBS for 10 minutes at room temperature. After permeabilization, cells were blocked with 1:100 horse serum in PBS for one hour at room temperature. Afterwards, samples were incubated in primary antibody for Scx (1:200; Abcam; ab58655) dissolved in 0.01% (v/v) Triton X-100 and 0.5% BSA in PBS overnight at 4°C. Next, cells were washed with 0.01% (v/v) Triton X-100 and 0.5% BSA in PBS three times and incubated with anti-rabbit secondary antibody conjugated to Alexa Fluor 647 (1:200; ThermoFisher A27040), together with Phalloidin–Tetramethylrhodamine B isothiocyanate (Phalloidin-TRITC, 1:200; ThermoFisher) in PBS with 0.01% (v/v) Triton X-100 and 0.5% BSA in PBS for 1 hour. Nuclei were stained with 4',6-diamidino-2-phenylindole (DAPI, 1:500; Sigma-Aldrich) for 1 hour after washing. Finally, samples were mounted on glass cover slides with mounting medium (Dako, Agilent). Imaging was performed by using Leica DMi8 with a TIRF Multi Color microscope (Leica Microsystems CMS) with lasers at excitation wavelengths of 532 nm and 647 nm, for phalloidin and scleraxis respectively.

EdU labelling

In order to identify the proliferating cells, Click-iT™ EdU Cell Proliferation Kit (Invitrogen, C10340) for Imaging (Thermo Fisher) was used based on the manufacturer's instructions. Briefly, tenocytes were serum-starved for 24 hours prior to EdU labelling in order to set the biological clock of the cells equally. Samples were fixed with 4% paraformaldehyde (PFA, ThermoFisher Scientific) at room temperature for 20 minutes and permeabilized with with 0.5 % (v/v) Triton X-100 in PBS for 20 minutes after 24 hours of incubation in 10 μM EdU solution. Afterwards, cells were treated with EdU reaction cocktail for 30 minutes in the dark and incubated in Hoechst for another 30 minutes. Images were taken with a Leica DMi8 with TIRF Multi Color microscope

(Leica Microsystems CMS) at 20x magnification. The reported number of proliferating cells was reported as the number of EdU labelled cells/total number of cells.

Atomic force microscopy (AFM) and Profilometer

Tendon imprints were imaged for surface architecture by using a tapping mode atomic force microscopy (AFM; XE-100, Park Systems) by using non-contact cantilevers (PPP-NCHR, Park Systems). Data were recorded with XEP software and GWYDDION software was used to image the data. A Keyence VK-H1XM-131 at 20x magnification was used for profilometer images.

Scanning electron microscopy (SEM)

Samples were fixed with 2.5 % glutaraldehyde (Fisher Scientific) at room temperature for one hour. Then, they were washed with distilled water 3 times for 10 minutes, dehydrated in 25%, 50%, 75%, 90%, and 100% ethanol for 15 minutes each, and incubated in 100% ethanol for an additional 15 minutes. Next, samples were dried in Hexamethyldisilazane (HMDS) (Sigma-Aldrich) for 1 hour. Prior to imaging, samples were coated with 5 nm gold-palladium and imaged using a scanning electron microscope (SEM) (FEI Quanta 3D FEG Dual Beam).

Image analysis

An image analysis pipeline was created in CellProfiler version 3.19. To calculate expression levels of SCX and other shape parameters, 3-4 random images from three biological replicates was selected. Median values of all cells were per image calculated by CellProfiler and used to calculate the Spearmen correlation between median SCX intensity and cell shape parameters. Shape parameters were calculated by taking the median value of all the cells in each single image, and subsequently depicted as a single data point in the figures. This median was derived from ~70 cells per image in Fig. 1, ~40 cells per image in Fig. 3 & 5.

Statistical analysis

All statistical analyses were performed by using GraphPad Prism version 8.0 (GraphPad Software, Inc., San Diego, CA). Student's t-test was performed to calculate statistical difference between cell and nuclear areas. One-way analysis of variance (ANOVA) were carried out to calculate the statistical difference in RT-qPCR experiments and calculate cell/nuclear shape parameters between different passages and imprint vs flat surface. Spearman correlation coefficient was calculated by GraphPad correlation calculation option. For all statistical analysis, significance set at $p < 0.05$ to determine the significance between means. All quantitative data represented in this study are based on triplicated experiments.

Chapter V

References

1. Millar, N.L., Murrell, G.A.C., and Mcinnes, I.B. Inflammatory mechanisms in tendinopathy - towards translation. Nat Rev Rheumatol . Nature Publishing Group, **13**, 110, 2017.

2. Franchi, M., Trirè, A., Quaranta, M., Orsini, E., and Ottani, V. Collagen structure of tendon relates to function. ScientificWorldJournal. **7**, 404, 2007.

3. Benjamin, M., Kaiser, E., and Milz, S. Structure-function relationships in tendons: A review. J Anat. **212**, 211, 2008.

4. Snedeker, J.G., and Foolen, J. Tendon injury and repair – A perspective on the basic mechanisms of tendon disease and future clinical therapy. Acta Biomater . Acta Materialia Inc., **63**, 18, 2017. A

5. Fenwick, S.A., Hazleman, B.L., and Riley, G.P. The vasculature and its role in the damaged and healing tendon. Arthritis Res. **4**, 252, 2002.

6. Fan, W., Michael, N., and Denitsa, D. Tendon injuries: basic science and new repair proposals. Gen Orthop. **2**, 211, 2017.

7. Docheva, D., Müller, S.A., Majewski, M., and Evans, C.H. Biologics for tendon repair. Adv Drug Deliv Rev . Elsevier B.V., **84**, 222, 2015.

8. Pingel, J., Lu, Y., Starborg, T., Fredberg, U., Langberg, H., Nedergaard, A., et al. 3-D ultrastructure and collagen composition of healthy and overloaded human tendon: Evidence of tenocyte and matrix buckling. J Anat. **224**, 548, 2014.

9. Clegg, P.D., Strassburg, S., and Smith, R.K. Cell phenotypic variation in normal and damaged tendons. Int J Exp Pathol. **88**, 227, 2007.

10. Jelinsky, S.A., Rodeo, S.A., Li, J., Gulotta, L. V, Archambault, J.M., and Seeherman, H.J. Regulation of gene expression in human tendinopathy. BMC Musculoskelet Disord. **12**, 86, 2011.

11. Archambault, J.M., Jelinsky, S.A., S.P., L., Hill, A.., Glaser, D.., and Soslowsky, L.J. Rat Supraspinatus Tendon Expresses Cartilage Markers with Overuse. J Orthop Res. **25**, 1121, 2007.

12. Qi, J., Dmochowski, J.M., Banes, A.N., Tsuzaki, M., Bynum, D., Patterson, M., et al. Differential expression and cellular localization of novel isoforms of the tendon biomarker tenomodulin. J Appl Physiol. **113**, 861, 2012.

13. Dyment, N.A., Liu, C.F., Kazemi, N., Aschbacher-Smith, L.E., Kenter, K., Breidenbach, A.P., et al. The Paratenon Contributes to Scleraxis-Expressing Cells during Patellar Tendon Healing. PLoS One. **8**, 2013.

14. Vermeulen, S., Vasilevich, A., Tsiapalis, D., Roumans, N., Vroemen, P., Beijer, N.R.M., et al. Identification of topographical architectures supporting the

phenotype of rat tenocytes. Acta Biomater. **83**, 2019.

15. Yao, L., Bestwick, C.S., Bestwick, L.A., Maffulli, N., and Aspden, R.M. Phenotypic drift in human tenocyte culture. Tissue Eng. **12**, 1843, 2006.

16. Mazzocca, A.D., Chowaniec, D., McCarthy, M.B., Beitzel, K., Cote, M.P., McKinnon, W., et al. In vitro changes in human tenocyte cultures obtained from proximal biceps tendon: Multiple passages result in changes in routine cell markers. Knee Surgery, Sport Traumatol Arthrosc. **20**, 1666, 2012.

17. Von Der Mark, K., Gauss, V., Von Der Mark, H., and Müller, P. Relationship between cell shape and type of collagen synthesised as chondrocytes lose their cartilage phenotype in culture [26]. Nature. **267**, 531, 1977.

18. Kraus, A., Sattler, D., Wehland, M., Luetzenberg, R., Abuagela, N., and Infanger, M. Vascular endothelial growth factor enhances proliferation of human tenocytes and promotes tenogenic gene expression. Plast Reconstr Surg. **142**, 1240, 2018.

19. Caliari, S.R., and Harley, B.A.C. Composite growth factor supplementation strategies to enhance tenocyte bioactivity in aligned collagen-GAG scaffolds. Tissue Eng - Part A. **19**, 1100, 2013.

20. Xia, D., Sumita, Y., Liu, Y., Tai, Y., Wang, J., Uehara, M., et al. GDFs promote tenogenic characteristics on human periodontal ligament-derived cells in culture at late passages. Growth Factors. **31**, 165, 2013.

21. Vijven, M., Wunderli, S.L., Ito, K., Snedeker, J.G., and Foolen, J. Serum deprivation limits loss and promotes recovery of tenogenic phenotype in tendon cell culture systems. J Orthop Res. 2020.

22. Webb, S., Gabrelow, C., Pierce, J., Gibb, E., and Elliott, J. Retinoic acid receptor signaling preserves tendon stem cell characteristics and prevents spontaneous differentiation in vitro. Stem Cell Res Ther . Stem Cell Research & Therapy, 1, 2016.

23. Metavarayuth, K., Sitasuwan, P., Zhao, X., Lin, Y., and Wang, Q. Influence of Surface Topographical Cues on the Differentiation of Mesenchymal Stem Cells in Vitro. ACS Biomater Sci Eng. **2**, 142, 2016.

24. Younesi, M., Islam, A., Kishore, V., Anderson, J.M., and Akkus, O. Tenogenic Induction of Human MSCs by Anisotropically Aligned Collagen Biotextiles. Adv Funct Mater. 5762, 2014.

25. Peng, R., Yao, X., and Ding, J. Effect of cell anisotropy on differentiation of stem cells on micropatterned surfaces through the controlled single cell adhesion. Biomaterials . Elsevier Ltd, **32**, 8048, 2011.

26. Zhu, J., Li, J., Wang, B., Zhang, W.J., Zhou, G., Cao, Y., et al. The regulation of phenotype of cultured tenocytes by microgrooved surface structure.

Biomaterials . Elsevier Ltd, **31**, 6952, 2010.

27. Kishore, V., Bullock, W., Sun, X., Scott, W., Dyke, V., and Akkus, O. Tenogenic differentiation of human MSCs induced by the topography of electrochemically aligned collagen threads. Biomaterials . Elsevier Ltd, **33**, 2137, 2012.

28. Popielarczyk, T.L., Nain, A.S., and Barrett, J.G. Aligned nanofiber topography directs the tenogenic differentiation of mesenchymal stem cells. Appl Sci. **7**, 2017.

29. Tu, T., Shen, Y., Wang, X., Zhang, W., Zhou, G., Zhang, Y., et al. Tendon ECM modified bioactive electrospun fibers promote MSC tenogenic differentiation and tendon regeneration. Appl Mater Today . Elsevier Ltd, **18**, 100495, 2020. A

30. Caliari, S.R., Weisgerber, D.W., Ramirez, M.A., Kelkhoff, D.O., and Harley, B.A.C. The influence of collagen-glycosaminoglycan scaffold relative density and microstructural anisotropy on tenocyte bioactivity and transcriptomic stability. J Mech Behav Biomed Mater . Elsevier Ltd, **11**, 27, 2012.

31. Yin, Z., Chen, X., Chen, J.L., Shen, W.L., Hieu Nguyen, T.M., Gao, L., et al. The regulation of tendon stem cell differentiation by the alignment of nanofibers. Biomaterials . Elsevier Ltd, **31**, 2163, 2010.

32. Wang, W., He, J., Feng, B., Zhang, Z., Zhang, W., Zhou, G., et al. Aligned nanofibers direct human dermal fibroblasts to tenogenic phenotype in vitro and enhance tendon regeneration in vivo. Nanomedicine. **11**, 1055, 2016.

33. Zhang, J., and Wang, J.H.C. Mechanobiological response of tendon stem cells: Implications of tendon homeostasis and pathogenesis of tendinopathy. J Orthop Res. **28**, 639, 2010.

34. Younesi, M., Islam, A., Kishore, V., Anderson, J.M., and Akkus, O. Tenogenic Induction of Human MSCs by Anisotropically Aligned Collagen Biotextiles. Adv Funct Mater. 5762, 2014.

35. Foolen, J., Wunderli, S.L., Loerakker, S., and Snedeker, J.G. Tissue alignment enhances remodeling potential of tendon-derived cells - Lessons from a novel microtissue model of tendon scarring. Matrix Biol . The Authors, **65**, 14, 2018.

36. Schweitzer, R., Chyung, J.H., Murtaugh, L.C., Brent, A.E., Rosen, V., Olson, E.N., et al. Analysis of the tendon cell fate using Scleraxis, a specific marker for tendons and ligaments. Development. **128**, 3855, 2001.

37. Ito, Y., Toriuchi, N., Yoshitaka, T., Ueno-Kudoh, H., Sato, T., Yokoyama, S., et al. The Mohawk homeobox gene is a critical regulator of tendon differentiation. Proc Natl Acad Sci U S A. **107**, 10538, 2010.

38. Screen, H.R.C., Berk, D.E., Kadler, K.E., Ramirez, F., and Young, M.F. Tendon functional extracellular matrix. J Orthop Res. **33**, 793, 2015.

39. J.H., Y., and J., H. Tendon proteoglycans: Biochemistry and function. J Musculoskelet Neuronal Interact . **5**, 22, 2005.

40. Tong, W.Y., Shen, W., Yeung, C.W.F., Zhao, Y., Cheng, S.H., Chu, P.K., et al. Functional replication of the tendon tissue microenvironment by a bioimprinted substrate and the support of tenocytic differentiation of mesenchymal stem cells. Biomaterials . Elsevier Ltd, **33**, 7686, 2012.

41. Beijer, N.R.M., Nauryzgaliyeva, Z.M., Arteaga, E.M., Pieuchot, L., Anselme, K., van de Peppel, J., et al. Dynamic adaptation of mesenchymal stem cell physiology upon exposure to surface micropatterns. Sci Rep . Springer US, **9**, 1, 2019. Available from: http://dx.doi.org/10.1038/s41598-019-45284-y

42. Schulze-Tanzil, G., De Souza, P., Villegas Castrejon, H., John, T., Merker, H.J., Scheid, A., et al. Redifferentiation of dedifferentiated human chondrocytes in high-density cultures. Cell Tissue Res. **308**, 371, 2002.

43. Caron, M.M.J., Emans, P.J., Coolsen, M.M.E., Voss, L., Surtel, D.A.M., Cremers, A., et al. Redifferentiation of dedifferentiated human articular chondrocytes: Comparison of 2D and 3D cultures. Osteoarthr Cartil . Elsevier Ltd, **20**, 1170, 2012.

44. Mueller, A.J., Tew, S.R., Vasieva, O., and Clegg, P.D. A systems biology approach to defining regulatory mechanisms for cartilage and tendon cell phenotypes. Nature Publishing Group, 1, 2016.

45. Holtzer, H., Abbott, J., Lash, J., and Holtzer, S. the Loss of Phenotypic Traits By Differentiated Cells in Vitro, I. Dedifferentiation of Cartilage Cells. Proc Natl Acad Sci. **46**, 1533, 1960.

46. Tata, P.R., Mou, H., Pardo-Saganta, A., Zhao, R., Prabhu, M., Law, B.M., et al. Dedifferentiation of committed epithelial cells into stem cells in vivo. Nature . Nature Publishing Group, **503**, 218, 2013.

47. Pennock, R., Bray, E., Pryor, P., James, S., McKeegan, P., Sturmey, R., et al. Human cell dedifferentiation in mesenchymal condensates through controlled autophagy. Sci Rep . Nature Publishing Group, **5**, 1, 2015.

48. Luxenburg, C., and Zaidel-Bar, R. From cell shape to cell fate via the cytoskeleton — Insights from the epidermis. Exp Cell Res . Elsevier Inc., **378**, 232, 2019.

49. Fang, Q., Chen, D., Yang, Z., and Li, M. In vitro and in vivo research on using Antheraea pernyi silk fibroin as tissue engineering tendon scaffolds. Mater Sci Eng C . Elsevier B.V., **29**, 1527, 2009.

50. Dede Eren, A., Sinha, R., Deniz, E., Huipin, Y., Gulce-iz, S., Valster, H., et al. Decellularized Porcine Achilles Tendon Induces Anti-inflammatory Macrophage Phenotype In Vitro and Tendon Repair In Vivo. J Immunol Regen Med . Elsevier, **8**, 100027, 2020.

51.   Zhang, C., Yuan, H., Liu, H., Chen, X., Lu, P., Zhu, T., et al. Well-aligned chitosan-based ultrafine fibers committed teno-lineage differentiation of human induced pluripotent stem cells for Achilles tendon regeneration. Biomaterials . Elsevier Ltd, **53**, 716, 2015.

52.   Yin, Z., Chen, X., Song, H. xin, Hu, J. jie, Tang, Q. mei, Zhu, T., et al. Electrospun scaffolds for multiple tissues regeneration invivo through topography dependent induction of lineage specific differentiation. Biomaterials . Elsevier Ltd, **44**, 173, 2015.

53.   Chen, E., Yang, L., Ye, C., Zhang, W., Ran, J., Xue, D., et al. An asymmetric chitosan scaffold for tendon tissue engineering: In vitro and in vivo evaluation with rat tendon stem/progenitor cells. Acta Biomater . Acta Materialia Inc., **73**, 377, 2018.

54.   Cardwell, R.D., Dahlgren, L.A., and Goldstein, A.S. Electrospun fibre diameter, not alignment, affects mesenchymal stem cell differentiation into the tendon/ligament lineage. J Tissue Eng Regen Med . **8**, 937, 2012.

55.   Zheng, Z., Ran, J., Chen, W., Hu, Y., Zhu, T., Chen, X., et al. Alignment of collagen fiber in knitted silk scaffold for functional massive rotator cuff repair. Acta Biomater . Acta Materialia Inc., **51**, 317, 2017.

56.   Czaplewski, S.K., Tsai, T.L., Duenwald-Kuehl, S.E., Vanderby, R., and Li, W.J. Tenogenic differentiation of human induced pluripotent stem cell-derived mesenchymal stem cells dictated by properties of braided submicron fibrous scaffolds. Biomaterials . Elsevier Ltd, **35**, 6907, 2014.

57.   Zhou, K., Feng, B., Wang, W., Jiang, Y., Zhang, W., Zhou, G., et al. Nanoscaled and microscaled parallel topography promotes tenogenic differentiation of asc and neotendon formation in vitro. Int J Nanomedicine. **13**, 3867, 2018.

58.   Schoenenberger, A.D., Foolen, J., Moor, P., Silvan, U., and Snedeker, J.G. Substrate fiber alignment mediates tendon cell response to inflammatory signaling. Acta Biomater . Acta Materialia Inc., **71**, 306, 2018.

59.   Tang, S.W., Yuen, W., Kaur, I., Pang, S.W., Voelcker, N.H., and Lam, Y.W. Capturing instructive cues of tissue microenvironment by silica bioreplication. Acta Biomater . Elsevier Ltd, **102**, 114, 2020.

60.   English, A., Azeem, A., Spanoudes, K., Jones, E., Tripathi, B., Basu, N., et al. Substrate topography: A valuable in vitro tool, but a clinical red herring for in vivo tenogenesis. Acta Biomater . Acta Materialia Inc., **27**, 3, 2015.

61.   Sugimoto, Y., Takimoto, A., Akiyama, H., Kist, R., Scherer, G., Nakamura, T., et al. Scx+/Scx9+ progenitors contribute to the establishment of the junction between cartilage and tendon/ligament. Dev. **140**, 2280, 2012.

62.   Buckley, M.R., Evans, E.B., Matuszewski, P.E., Chen, Y.L., Satchel, L.N.,

Elliott, D.M., et al. Distributions of types I, II and III collagen by region in the human supraspinatus tendon. Connect Tissue Res. **54**, 374, 2013.

63. Nourissat, G., Berenbaum, F., and Duprez, D. Tendon injury: From biology to tendon repair. Nat Rev Rheumatol . Nature Publishing Group, **11**, 223, 2015.

64. Kishore, V., Bullock, W., Sun, X., Van Dyke, W.S., and Akkus, O. Tenogenic differentiation of human MSCs induced by the topography of electrochemically aligned collagen threads. Biomaterials . Elsevier Ltd, **33**, 2137, 2012.

65. Thakar, R.G., Cheng, Q., Patel, S., Chu, J., Nasir, M., Liepmann, D., et al. Cell-shape regulation of smooth muscle cell proliferation. Biophys J . Biophysical Society, **96**, 3423, 2009.

66. Liliensiek, S.J., Campbell, S., Nealey, P.F., and Murphy, C.J. The scale of substratum topographic features modulates proliferation of corneal epithelial cells and corneal fibroblast. J Biomed Mater Res Part A . **79**, 963, 2006.

67. McMurray, R.J., Gadegaard, N., Tsimbouri, P.M., Burgess, K. V., McNamara, L.E., Tare, R., et al. Nanoscale surfaces for the long-term maintenance of mesenchymal stem cell phenotype and multipotency. Nat Mater. Nature Publishing Group, **10**, 637, 2011.

68. Gronthos, S., Simmons, P.J., Graves, S.E., and G. Robey, P. Integrin-mediated interactions between human bone marrow stromal precursor cells and the extracellular matrix. Bone. **28**, 174, 2001.

69. McMurray, R.J., Dalby, M.J., and Tsimbouri, P.M. Using biomaterials to study stem cell mechanotransduction, growth and differentiation. J Tissue Eng Regen Med . **9**, 528, 2014.

70. Wang, Y., Shenouda, S., Baranwal, S., Rathinam, R., Jain, P., Bao, L., et al. Integrin subunits alpha5 and alpha6 regulate cell cycle by modulating the chk1 and Rb/E2F pathways to affect breast cancer metastasis. Mol Cancer . BioMed Central Ltd, **10**, 84, 2011.

Supplementary figures
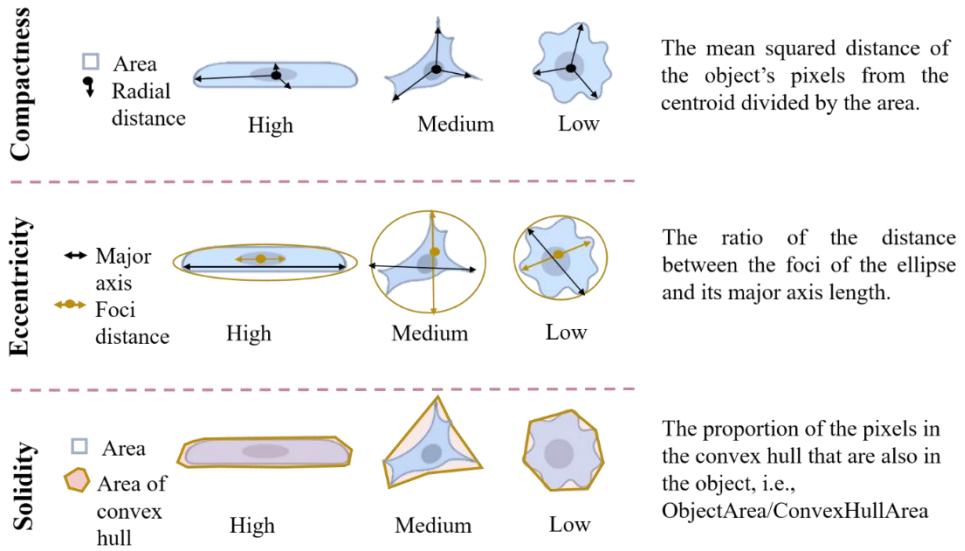
Supplementary figure 1. *Explanation of shape parameters*

Chapter VI

Cells dynamically adapt to surface geometry by remodelling their focal adhesions and actin cytoskeleton

Cells probe their environment and adapt their shape accordingly via organization of focal adhesions and actin cytoskeleton. In an earlier publication, we described the relation between cell shape and physiology e.g. shape-induced differentiation, metabolism and proliferation in mesenchymal stem cells and tenocytes. In this study, we investigated how these cells organize their adhesive machinery over time when exposed to microfabricated surfaces of different topographies and adhesive island geometries. We further examined the reciprocal interaction between stress fiber and focal adhesion formation by pharmacological perturbation. Our results suggest that the spatial organisation of adhesive sites determines the ability to form focal adhesions and stress fibers. Therefore, cells on roughened surfaces have smaller focal adhesion and less stress fibers. Transcriptomics analysis demonstrates how the cells further adapt to a new surface by changing the expression of integrins. Our results further highlight the importance of integrin-mediated adhesion in the adaptive properties of cells and provides clear links to the development of bioactive materials.

Chapter VI

Introduction

"Contact guidance" is a term coined by Paul Weiss in 1945 to describe that nerve cells adapt their shape to geometrical patterns of the substrate on which they grow[1], be it epithelial hydra *in vivo*[2] or microfabricated topographical surfaces *in vitro*[3]. It illustrates that cells constantly probe their surrounding and adapt their interaction accordingly. Cell shape, adhesion and actin organization are intricately linked in their relation to 'the topographical design of the substrate[4,5]. This is very clear when comparing cells on flat versus topographical surfaces. Flat surfaces lead to cells with very large focal adhesions and abundant stress fiber formation and cells have a very high area and are flat[5]. On topographies, cell area is typically smaller, cells are higher, have smaller focal adhesion and have less stress fibers[6]. For instance, Cassidy *et al.* reported that mesenchymal stem cells and osteoprogenitors have a spread morphology, higher surface tension and large focal adhesions (bigger than 8 μm in length) on flat surfaces whilst on grooved substrates, cells were elongated and possessed smaller focal adhesions (1-5 μm in length)[7]. Similarly, Baharloo *et al.* demonstrated that epithelial cell area was larger on smooth surfaces and had more and larger focal adhesions compared to roughened surfaces[8].

This phenomenon can be explained with the cellular tensegrity model that proposes that cells are normally in a pre-stressed state which is actively created by the actomyosin-based contractile apparatus of cells and coordinated with the cell's adhesion to the extracellular matrix (ECM)[9,10]. Tension can only be created when the surface on which the cells grow permits it. For instance, cells on surfaces with high stiffness allow the creation of high tension and force on focal adhesions without distortion of the matrix, and thus allows larger focal adhesions and more tension in their cytoskeleton[11]. Cells on surfaces with low stiffness have smaller focal adhesions[11]. On rigid substrates, cells display high spreading and large and uniformly distributed focal adhesions compared to softer substrates on which cells possess radially oriented focal adhesions with smaller cell size[11–14]. Similarly, cells have fewer adhesion points on roughened surfaces, and can therefore create less tension via smaller focal adhesions[15–17]. In its turn, cell shape follows the ability of the cells to form focal adhesions. The formation of focal adhesions, actin cytoskeleton and the forces placed on it is well regulated and determined by the geometry of the substrate.

The cells' adaptation to substrate geometry has consequences for cell physiology[18]. The material properties of ECM influence mechanosensitive signaling pathways, which control the expression of genes involved in differentiation, proliferation and metabolism[4,19,20]. We and others have previously investigated the relationship between surface topography and cell physiology in tenocytes[21] and mesenchymal stem cells[22]. Tenocytes possess a spindle-shaped morphology in their native tendon ECM but upon

in vitro culture become spread with a bigger cell area and lower aspect ratio, as well as an increased number of stress fibers and they lose the expression of typical tendon marker genes, such as tenomodulin, scleraxis and mohawk[23]. Rat tenocytes cultured on tendon imprint and microtopographies led to elongated cell morphology, reduced cell area, fewer stress fibers, and higher expression of scleraxis[24,25]. The same was observed in human mesenchymal stem cells, another frequently used cell type in tenogenic differentiation studies[26–30]. The Rho/ROCK signalling pathway is one of the pathways engaged in the link between adhesion and phenotype. Rho proteins are involved in various biological processes including cell shape and actin cytoskeleton organization[31] and non-muscle myosin-II is involved in actin-myosin interactions[32]. In several studies, the involvement of Rho/ROCK/SRF signaling in tenocyte phenotype was demonstrated by targeting this pathway with small molecules [29, 33–35].

In our previous reports, we focused particularly on the downstream phenotypic consequences of different topographies on tenocytes[25,29,36] and mesenchymal stem cells[29]. We demonstrated that tenocyte marker gene expression is induced on topographic imprints of the tendons' collagen bundles[25] and that their expression depends on Rho/ROCK signaling. Using our TopoChip platform, we recently reported that human mesenchymal stem cells (hMSCs) gene expression and phenotypical responses, such as differentiation, proliferation and apoptosis, strongly correlate to cell shape[37] and also found evidence that actin mediated signaling processes play a role based on cell shape. Therefore, we hypothesize that tendon imprints and microfabricated topographies influence focal adhesion formation and stress fibers in tenocytes and mesenchymal stem cells.

Results

Tenocytes display more punctate attachment on tendon imprint surfaces

To investigate the effect of the topographical environment on attachment, we cultured primary rat tenocytes on polystyrene (PS) tendon imprints and flat control surfaces for 24 hours (Fig.1A). Tendon imprints reproduce the natural crimped architecture of collagenous tendons, resulting in hills and valleys. Due to its heterogeneous nature, the depth of the valleys varies between 5 μm to 20 μm and the frequency of the valleys and hills varies. The heterogenic nature of the tendon imprint landscape is reflected in the cell morphologies that we observe. Yet, we do see clearly that tenocytes on imprints displayed a morphology similar to *in vivo* tenocytes with an increased aspect ratio (Fig.1C), i.e. they are less wide than a typical flat surface cultured tenocyte. Also, tenocytes appeared to be flatter on the flat surface (Fig.1B) whilst cells on the tendon imprint were higher. The length of the cells appeared to be the same. On the flat surface, we observed filamentous (F)-actin stress fibers reaching from one end of the cells to the other, as pointed in Fig.1A&B with red arrows, we did not observe such on the imprints. Interestingly, cells on the imprint were not in continuous contact with the surface. Rather, the cells were associated with the surface on an estimated dozen sites, whereas large parts of the cell body were not in direct contact with the surface. In contrast, cells on the flat surfaces seemed to be in contact over their full length. Furthermore, both cells exhibit filopodia yet lamellipodia were more predominant in tenocytes on the flat surface. Finally, we observed that cells on tendon imprint have membrane invaginations sticking from the plasma membrane, similar to the observations by Erlach *et.al.*[18] as illustrated with yellow arrows in Fig.1D. Overall, tendon imprint results in a 3D cell shape with fewer adhesion sites, suggesting changes in focal adhesion and actin cytoskeleton organization.
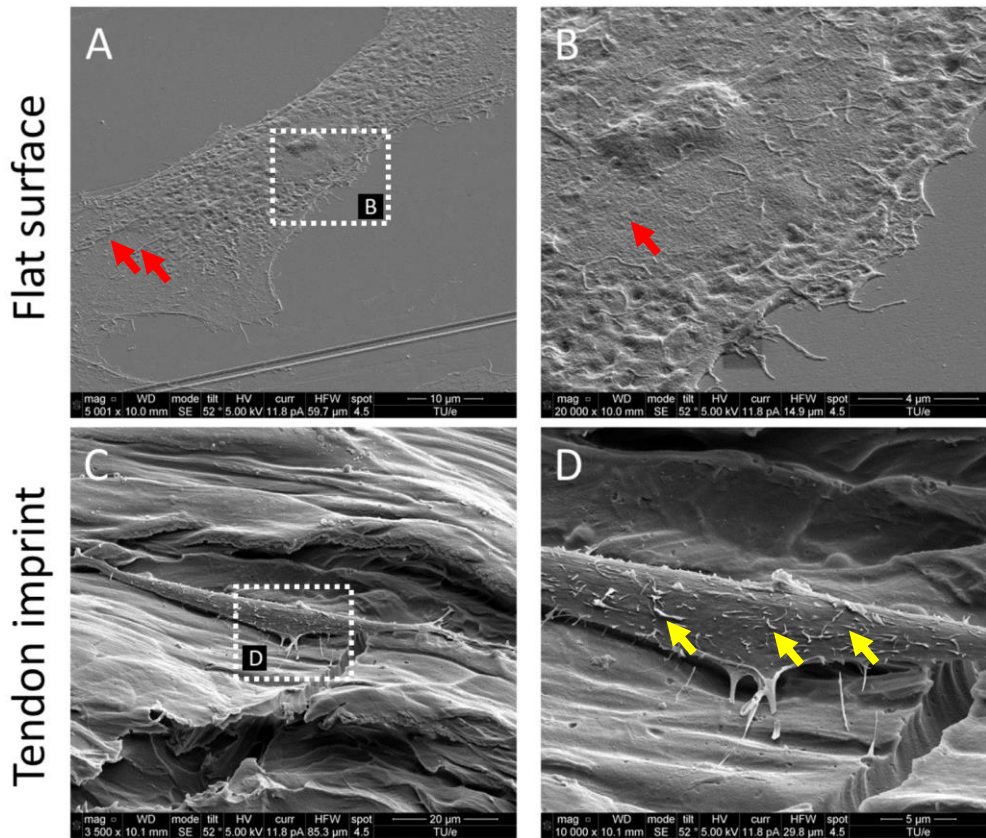
Figure 1. Tendon imprints induce cell shape changes. *(A) Tenocyte on flat surface. (B) Higher magnification image of tenocyte on flat surface that illustrates cell adhesion points in higher resolution. Red arrows indicate stress fibers. (C) Tenocyte on tendon imprint. (D) Higher magnification image of tenocytes on tendon imprint. Filopodia are observed on both substrates.*

Tenocyte shape and actin response are different on cells on the flat surface and tendon imprint

To verify that tendon imprints affect actin organization, we monitored the dynamics of actin organization and adaptation of cytoskeleton and cell shape on the flat surface and the tendon imprint. We stained tenocytes with SiR-Actin and imaged them for 40 hours (Supplementary video 1-2, Fig.2A&B). In cells on the flat surface at 2 hours, we observed dorsal stress fibers, non-contracting actin fibers at the periphery of cell[38], and ventral stress fibers, which are contracting actomyosin fibers located at the posterior parts of the cells and have direct attachments to focal adhesions[38]. In recently divided cells, stress fibers organized as cortical and transverse arcs, which are curved actin

bundles that transmit contractile forces and through dorsal stress fibers[38]. As the cell size increased, stress fibers became thicker and appeared more ventral and peripheral (Fig. 2A, Supplementary video 1). Cells displayed a variety of shapes, migrated freely in all directions, and constantly formed lamellipodia. Tenocytes on tendon imprint cells migrated preferentially in the direction of the valleys (Fig. 2B, Supplementary video 2). Furthermore, cells acquired the shape of the topography underneath approximately within 40 minutes after cell division. Stress fibers were observed to be only in the long axis of the cells (Fig. 2B, Supplementary video 2).

To quantify cell area and elongation tenocytes were fixed after 2, 4, 12 and 24 hours and stained for F-actin (Fig. 2C&D). On the flat surface, we confirmed stress fiber formation from 2 hours on, becoming thicker as the cells became larger (Fig.2C, top panel). On tendon imprints, elongated cell morphology peaked after 24 hours (Fig.2C, bottom panel) and cell area remained significantly less compared to the flat surface (Fig.2D). Nonetheless, we observed more stress fiber formation in the cells on flat surface than on tendon imprint. Therefore, we conclude that there is a dynamic change in cell area and elongation in tenocytes upon culturing them on tendon imprint and flat surface. Changes in cell shape seem to occur once a small number of stress fibers form in the direction of contact guidance.
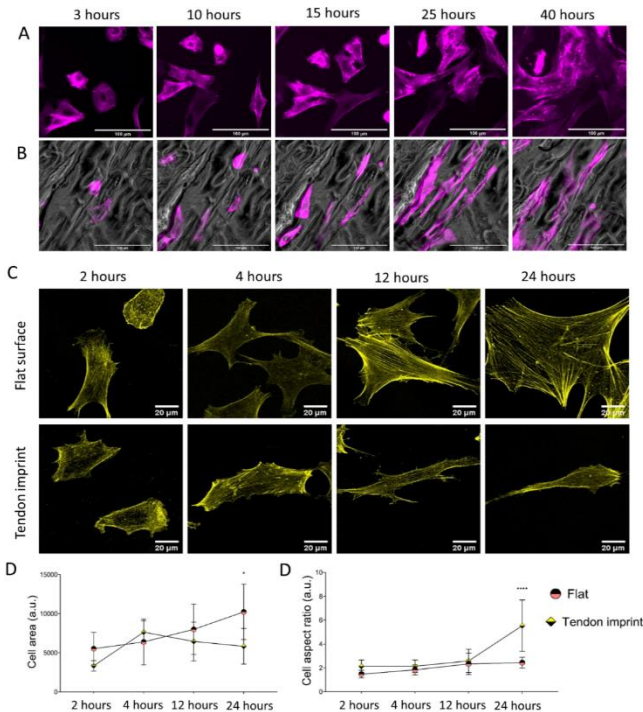

Figure 2. Dynamic cytoskeletal organization, cell area and aspect ratio of tenocytes. (A) Snap-shots of tenocytes cultured on flat surface, stained with SiR-Actin (purple) to illustrate actin cytoskeleton and stress fibers. Scale bars represent 100 μm. (B) Snap-shots of tenocytes cultured on tendon imprint, stained with SiR-Actin (purple) to illustrate actin cytoskeleton and stress fibers. Scale bars represent 100 μm. (C) Tenocytes seeded on flat surface (top panel) and tendon imprint (bottom panel), fixed after 2 hours, 4 hours, 12 hours and 24 hours, and stained with Phalloidin (yellow). (D) Quantification of cell area (left) and

cell aspect ratio (right) at different time points. The area of tenocytes on flat surface increased over time, displaying dynamic enlargement overtime, whereas on tenocytes this remained at statistically similar levels after 4 hours. The cell aspect ratio on tendon imprint makes a peak after 24 hours yet remained in similar values between 2 hours and 24 hours on flat surface. Scale bars represent 20 μm. (Error bars represent 95% confidence intervals, *p < 0.05, ****p<0.001). For all experiments, N = 3.

Surface topography guides stress fiber formation and cell shape in human mesenchymal stem cells.

We previously noticed that human bone-derived mesenchymal stem cells (hMSCs) dynamically adapt shape and physiology upon interaction with Topo1018[29], which is a platform composed of uniquely designed micro-topographies. To see if changes in actin organization run in parallel to those in cell shape, as it did in tenocytes, we seeded hMSCs on a flat surface and Topo1018 and stained the actin cytoskeleton after 30 minutes, 2 hours, 4 hours, 12 hours and 24 hours (Fig. 3A). Cell area was similar 30 minutes after seeding but was significantly different between the flat surface and Topo1018 surface already after 4 hours. On the flat surface, cell area kept increasing as the cells were spreading, whereas on Topo1018 cell area stabilized after 2 hours (Fig.3B). The aspect ratio remained similar from 4 hours onwards in hMSCs on the flat surface, but on Topo1018 surface, there was a steady increase (Fig.3C), i.e. cells became thin and elongated. Interestingly, cells on Topo1018 were mainly observed on top of the pillars at 30 minutes, 2 hours and 4 hours, but after 12 and 24 hours they were mostly confined between the pillars. On the flat surface, hMSCs possess transverse arcs and dorsal stress fibers as we observed previously in tenocytes. From 4 hours on, we observed that the thickness of stress fibers increased, and the actin cytoskeleton was mainly formed by ventral stress fibers, reaching from one end of the cell to the other (Fig. 3A-top panel). On Topo1018, the switch in the location from pillar top to the valleys coincided with the appearance of stress fibers in the main axis of the cells (see 4 hours versus 12 hours in Figure 3A). After 24 hours, the number of stress fiber was smaller in hMSCs on Topo1018 surfaces than on flat surfaces.
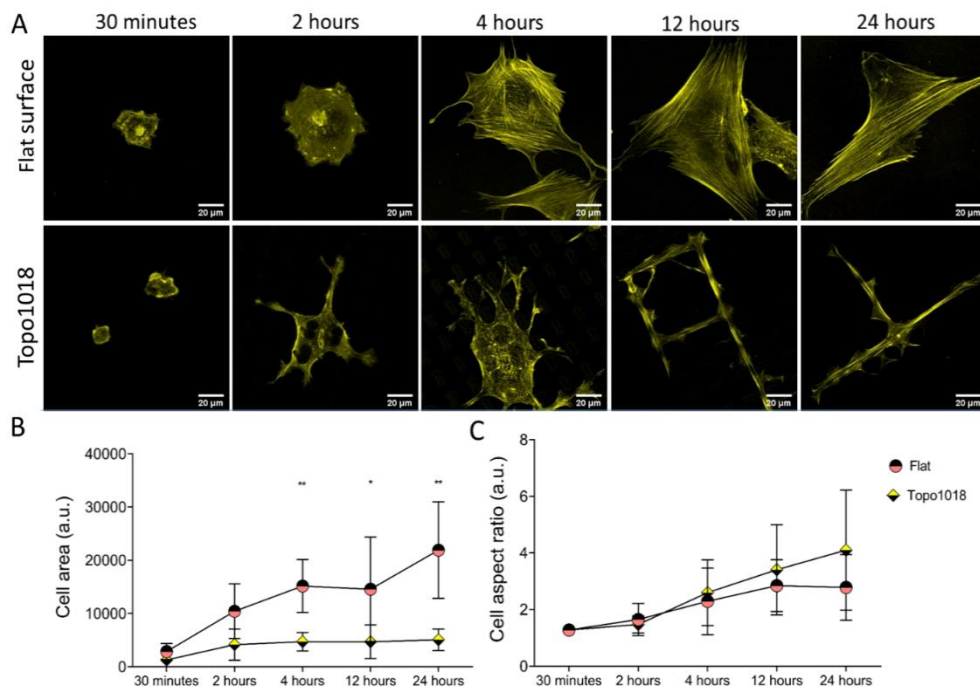
Figure 3. hMSC shape and cytoskeletal organization on topography 1018 and flat surfaces. *(A) hMSCs cultured on flat surface and Topo1018 surface and stained with Phalloidin to visualize F-actin (yellow) at 30 minutes, 2 hours, 4 hours, 12 hours and 24 hour time points. On flat surface (top panel), transverse arcs and dorsal stress fibers are observed at 2 hours. This replaces itself with thick ventral stress fibers after 4 hours. On Topo1018 surface (bottom panel), hMSCs are on top of the pillars and stress fibers are observed on the lamellipodia on the bottom of the topography at 4 hours. After 12 hours, cells settled between the pillars and sit between the topographies and display long and think stress fibers along their long axis. Scale bars represent 20 μm. (B) Quantification of cell area overtime showed that after 4 hours, the difference between cell area between hMSCs on flat surface and Topo1018 surface becomes significant. (C) Quantification of cell aspect ratio suggests that on Topo1018 surface there is a steady increase in cell elongation whilst on flat surface it stabilized after 12 hours. (Error bars represent 95% confidence intervals, *p < 0.05, **p<0.01, ****p<0.001). For all experiments, N = 3.*

Maturation of focal adhesion differs between cells on flat surface and topographies

The effect of topography on actin organization suggests that the contact of cells with the surface is different. To investigate this, we seeded rat tenocytes on tendon imprint and flat surface and stained them for vinculin to measure focal adhesions length

(Fig.4A&B). We observed a steady increase in focal adhesions length in tenocytes on flat surfaces, consistent with the maturity of the stress fibers and an increase in cell area (Fig.1C&D). On tendon imprints, we see only very few focal adhesions at early time points but more after 24 hours. However, focal adhesions length does not seem to increase, which is in line with stress fiber formation and cell area. We observed a similar, even more, pronounced response on Topo1018. 30 minutes and 2 hours after seeding, we did not observe focal adhesions and those that appeared later are at the end of stress fibers at the bottom, confined between the pillars, but not on the pillars. The focal adhesion length is consistently lower in hMSCs on Topo1018 than on flat surface. These data show that the maturation of stress fibers and focal adhesions is in sync with the topographical information provided by the surface on which they grow.
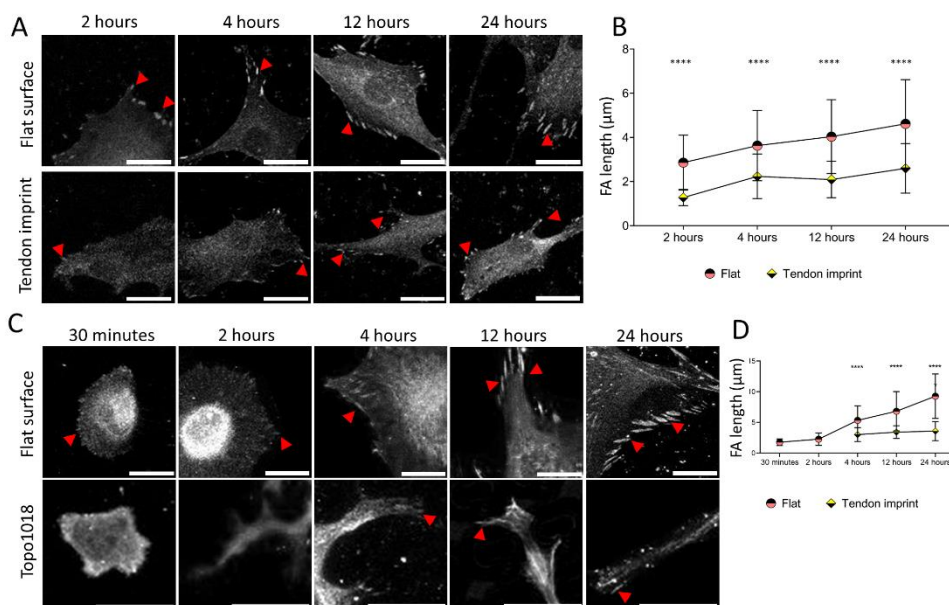

Figure 4. Surface topography modulates maturity and position of focal adhesions. *(A) Rat tenocytes cultured on flat surface and tendon imprint for 2 hours, 4 hours, 12 hours and 24 hours, and stained for Vinculin (fair grey color) and pointed with red arrows. Scale bars represent 20 μm. (B) Quantification of focal adhesion length indicates that on flat surface, as the cells become larger, focal adhesions become longer indicating their maturation. On tenocytes on tendon imprint, focal adhesion length is significantly smaller compared to flat surface in all-time point. (C) hMSCs cultured on flat surface and Topo1018 surface for 30 minutes, 2 hours, 4 hours, 12 hours and 24 hours, and stained with Vinculin (fair grey color) and pointed with red arrows. Scale bars represent 20 μm. (D) Focal adhesion length increases steadily in cells cultured on flat surface. On*

Topo1018 surface, we did not observe focal adhesions after 30 minutes and 2 hours, and from 4 hours on, their length remained at similar levels and significantly shorter compared to their flat surface counterparts. (Error bars represent 95% confidence intervals, ****p<0.001). For all experiments, N = 3. (FA= focal adhesion)

Spatial organization of adhesive islands steers focal adhesion formation, actin cytoskeleton and cell shape

We next wondered whether contact guidance is necessary for guiding cell shape, i.e. if the confinement imposed by the third dimension of the topography is required for the spatial organization of focal adhesions and F-actin that we observe on topographies. To this end, we used the Galapagos library of binary adhesive micropatterns, in which 2074 different islands of RGD peptides are produced on a glass substrate based on the pillar design of the TopoChip (manuscript in preparation). hMSCs were cultured for 4 hours on the Galapagos chip and stained for F-actin and paxillin (Fig.5). On the control surface, covered with a continious lawn of RGD peptides, lamellipodia were observed randomly and ventral stress fibers are associated with long focal adhesions, indicating high cell tension (Fig.5A). When cells are seeded on small islands which are close to each other, we observed that cells tend to generate more adhesive sites and display a spread morphology and high numbers of lamellipodia (Fig.5B). We observed thick ventral stress fibers with long focal adhesions at each end, indicating high tension in the cells. On small islands separated by 10-15 µm of non-adhesive surface, the cells anchored themselves on a limited number of islands, with focal adhesions having firm ground on the islands and stress fibers attached to them. We also searched the Galapagos chip for cells with a high aspect ratio resembling tenocytes. We found them on surfaces in which islands were relatively close together in one direction but separated in the other direction (Fig.5C&D). On these islands, not only the shape was like tenocytes on tendon imprint, we also observed that focal adhesions were located at the extremities of the cells, with a smaller number of stress fibers than on the fully RGD covered surface. This demonstrates that cell shape is also guided by the availability of adhesive sites and the possibility to build stress fibers.
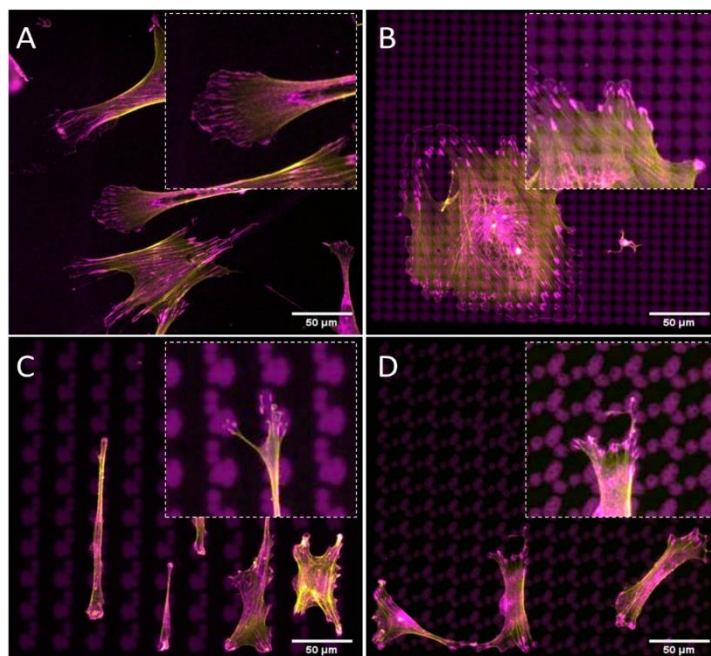
Figure 5. Cell shape can be controlled by the spatial organization of adhesive islands. *(A) hMSCs are cultured surfaces fully covered with RGD or 2D micropatterns for 4 hours and stained with Phalloidin to visualize F-actin (yellow) and Paxillin (magenta). Adhesive islands are presented in magenta. Scale bars represent 50 μm.*

Interfering with integrin-mediated cell adhesion alters cell shape and focal adhesion length

The results so far show that cell shape depends on the spatial organization of the surface on which the cells grow. Next, we wanted to investigate how cell shape depends on the organization of the cell's adhesive machinery, by blocking the interaction between integrins and the extracellular matrix. We grew hMSCs on surface Topo1018 and a flat control for 4 hours, the earliest time point at which we detect focal adhesions on Topo1018 surface and cell size are significantly different. Culture medium was supplemented with peptide Gly-Arg-Gly-Asp-Ser-Pro-Lys (GRGDSPK) or Gly-Arg-Gly-Asp-Ser-Pro (GRGDSP), which bind to integrins and thus block integrin-ECM interaction. Peptide Gly-Arg-Ala-Asp-Ser-Pro (GRADSP) was used as a negative control (Fig.6A). On the flat surface, stress fibers appeared of similar thickness and pattern in control (no RGD peptide supplemented) and GRADSP condition and cell area and F-actin intensity were the same. Similarly, on Topo1018 surface, cell area and F-actin intensity remain similar between control and GRADSP groups. In the presence of the integrin-binding peptides GRGDSPK and GRGDSP however, hMSCs on flat had more dorsal stress fibers, lost their lamellipodia and became more rounded. Peptide GRGDSP also resulted in cells with a smaller area (Fig.6B, top panel) and cells treated with GRGDSPK had smaller focal adhesions, demonstrating the biological activity of the peptides. Remarkably, treatment with either peptide leads to complete loss of focal

adhesions in 1018. Increased F-actin intensity was observed (Fig.6C&D) although the ventral stress fibers reaching from one end to the other end appeared to be lost upon RGD peptide supplementation (Fig.6B, bottom panel). Ironically, this did not affect cell size. Overall, these results indicate integrin-blocking RGD peptides has a drastic effect on focal adhesions organization on topographical surfaces. Furthermore, interfering with cell adhesion indeed changed the organization of the F-actin.
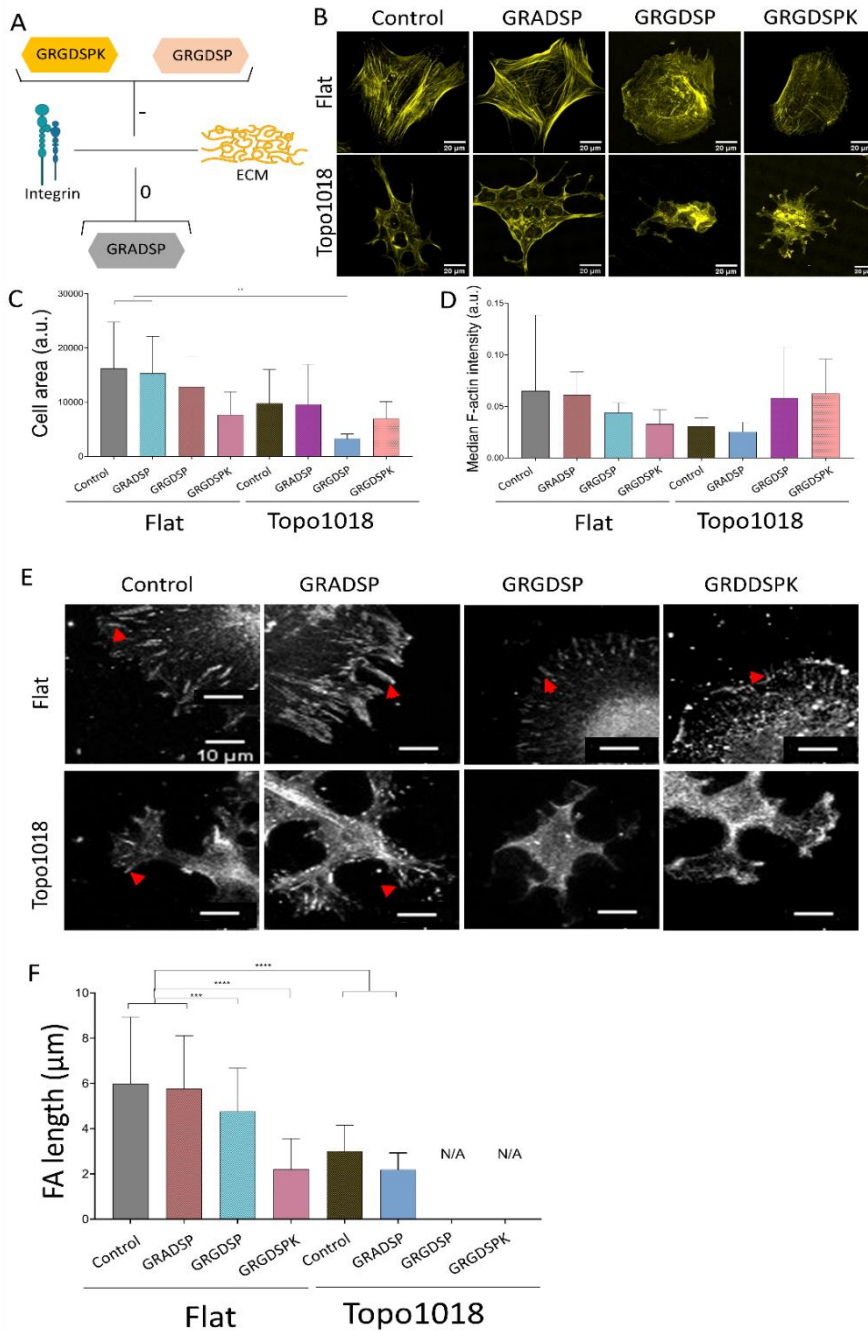
Figure 6. Interfering with integrin-mediated cell adhesion via RGD peptides leads to changes in stress fibers and focal adhesion length. *(A) An illustration of the action mechanism of the peptides used in this study: Gly-Arg-Gly-Asp-Ser-Pro-Lys (GRGDSPK)*

and Gly-Arg-Gly-Asp-Ser-Pro (GRGDSP) to inhibit integrin-mediated cell adhesion and used Gly-Arg-Ala-Asp-Ser-Pro (GRADSP) as a negative control. (B-Top panel) On flat surface, control and GRADSP treatment resulted in similar cell shape and stress fiber appearance. GRGDSPK and GRGDSP treatment altered the stress fiber pattern to a more dorsal stress fiber appearance. Scale bars represent 20 μm. (B-Bottom panel) On Topo1018 surface, we observed changes in cell shape and stress fiber structure. Scale bars represent 20 μm. (C) Quantification of cell area of cells cultured on flat and Topo1018 surfaces and treated with peptides. (D) Quantification of F-actin intensity of cells cultured on flat and Topo1018 surfaces and treated with peptides. (E-Top panel) Focal adhesions of hMSCs cultured on flat surface (grey) are pointed with a red arrow. In control groups, the length of focal adhesions remains similar yet GRGDSPK and GRGDSP treatment resulted in smaller focal adhesions. Scale bars represent 10 μm. (E-Bottom panel) Focal adhesions of hMSCs cultured on Topo1018 surface (grey) are pointed with a red arrow. In control groups, the length of focal adhesions remains similar, however, we did not observe focal adhesions on GRGDSPK and GRGDSP treated groups. Scale bars represent 10 μm. (D) Quantification of focal adhesion length of cells cultured on flat and Topo1018 surfaces and treated with peptides. (Error bars represent 95% confidence intervals, **p<0.01). For all experiments, N = 3. (FA=focal adhesion)

Next, we did the opposite experiment, i.e. increase integrin affinity to ECM, by adding Mn^{2+} to the culture medium in which hMSCs grew on flat and 1018 surfaces. (Fig.7). On flat, we observed a strong increase in cell area and a profound increase in F-actin intensity. Mn^{2+} treated cells have very thick stress fibers, indicating that they induce integrin/ECM interaction and thus affect focal adhesion organization and cell shape. (Fig.7B, left panel, Fig.7C&D). On 1018 surfaces too, Mn^{2+} treatment led to the formation of larger cells with thicker stress fibers (Fig.7B, right panel, Fig.7C&D), demonstrating a correlation between cell area and strength of adhesion of the cells to the surface. However, despite the visible change in cell area and F-actin organization, focal adhesion size did not noticeably change upon addition of Mn^{2+} on either flat or 1018 surface (Fig.8).
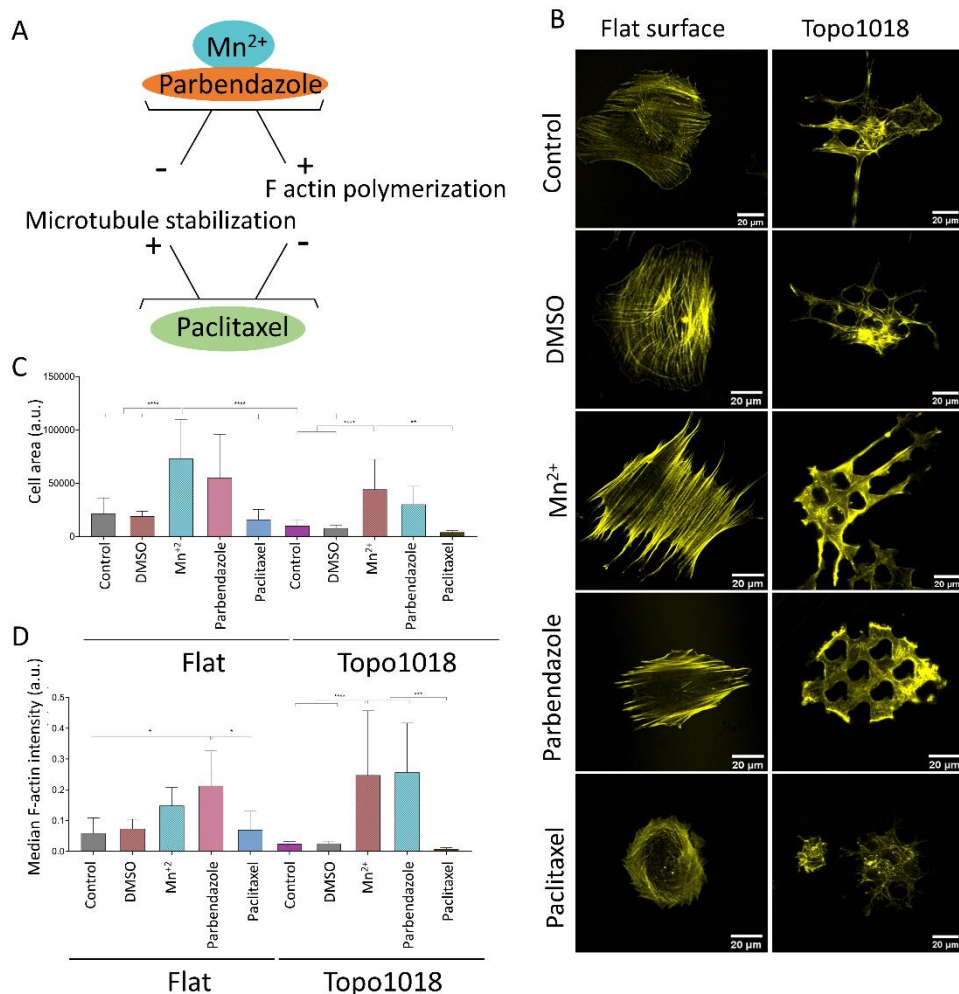
Figure 7. Small molecules that influence integrin signaling, actin polymerization and microtubule stability affected the actin cytoskeleton. *(A) An illustration of the action mechanism of the small molecules used in this study: Mn^{2+} to activate integrin signaling and induce F-actin polymerization, parbendazole to induce F-actin polymerization and degradation of microtubules, paclitaxel to compromise F-actin polymerization and stabilize microtubule assembly (B-Left panel) Treatment with Mn^{2+} and parbendazole increased the thickness of the ventral stress fibers whilst paclitaxel treatment lead to the formation of thinner stress fibers compared to control groups. Scale bars represent 20 μm. (B-Right panel) On Topo1018 surface, similar to flat surface, we observed that stress fibers become thicker and cells attached to the bottom of the surface upon Mn^{2+} and parbendazole treatment. Scale bars represent 20 μm. (C) Quantification of cell area of cells cultured on flat and Topo1018 surfaces and treated with small molecules. (D) Quantification of F-actin intensity*

of cells cultured on flat and Topo1018 surfaces and treated with small molecules. (Error bars represent 95% confidence intervals, *p<0.05, ***p<0.005). For all experiments, N = 3.

Actin organization is essential for cell shape

We next questioned how increasing or reducing actin polymerization affects focal adhesion formation, stress fiber formation and cell shape (Fig.7). As expected, treatment of hMSCs grown on flat surfaces with the microtubule inhibitor parbendazole led to increased actin polymerization with very pronounced stress fibers (Fig.7B), as reported previously[39]. Furthermore, parbendazole treatment resulted in significantly larger cells and increased F-actin intensity compared to untreated controls (Fig.7C&D). The compound paclitaxel compromises F-actin polymerization and has the opposite effect: cells have fewer stress fibers and cell area is reduced 1.5-fold compared to untreated control and 4-fold compared to parbendazole treated cells on the flat surface (Fig.7C). On topography 1018, parbendazole treatment resulted in a significant increase in the cell area, as well as the intensity in the filamentous actin intensity (Fig.7C&D). Similar to our observations on the flat surface, paclitaxel treatment of the cells on Topo1018 surface resulted in a 7.5-fold decrease in cell area compared to parbendazole treated counterparts and a 3-fold decrease compared to untreated controls (Fig.7C&D). Furthermore, paclitaxel treatment in both flat and Topo1018 surfaces resulted in the change of the organization and phenotype of stress fibers. Contrary to parbendazole treatment, which leads to the formation of thick ventral stress fibers, paclitaxel treatment results in the formation of mainly thin dorsal stress fibers and transverse arcs. Finally, we did not notice a change in focal adhesion length upon parbendazole or paclitaxel treatment (Fig.8). These results suggest that manipulation of actin organization can be independent of the maturation of the focal adhesions.
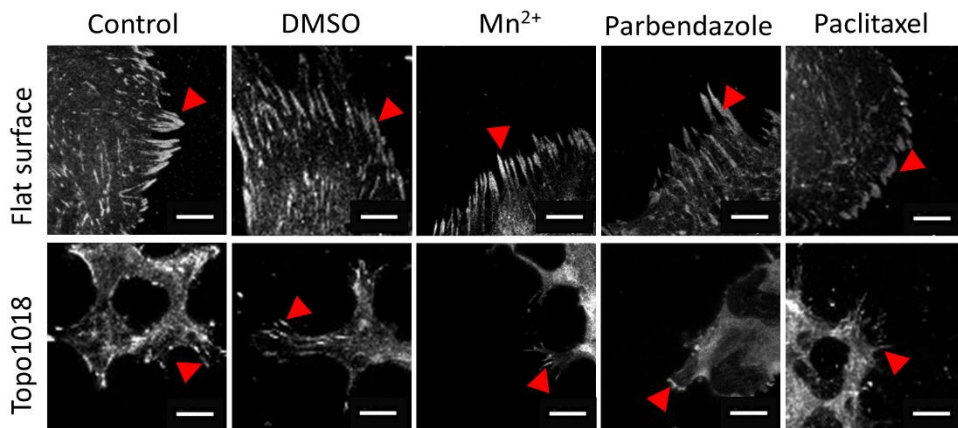
Figure 8. Small molecule targeting microtubule stabilization resulted in shorter focal adhesions. *(A) We cultured hMSCs on flat and Topo1018 surfaces and treated them with small molecules targeting integrins (Mn²⁺), F-actin and microtubules (Paclitaxel and parbendazole) and we stained them with vinculin to visualize focal adhesions and pointed them with red arrows. Scale bars represent 10 μm. For all experiments, N = 3.*

Cells with different stiffness display similar responses to tendon imprints

So far, we manipulated cell adhesive properties by changing the surface or by biochemically interfering with the adhesion and actin cytoskeleton. An alternative approach to investigate the effect of topography on cell shape is to culture cells with reported different stiffnesses and adhesive properties[40,41] and observe their response. For this, we seeded different cell types whose origin tissues have different stiffness, namely monocytes from blood, human umbilical vein endothelial cells (HUVEC), hMSCs from human bone marrow, chondrocytes from cartilage and HeLa cells from cervical cancer tissue (Fig. 9A). All cells adhered well to the surfaces, with the clear formation of stress fibers, except for monocytes that did adhere to the surface but did not spread. Monocytes are the smallest cell type that we selected with the least adhesive properties and upon culturing on tendon imprint, cell shape did not change as cell size is too small to detect the topographical cues on tendon imprint (Fig. 9B,C&H). HUVEC and chondrocytes have similar cell area (Fig.9D&F) and the contact guidance was clearly observed. However, HUVEC display an increase in the cell aspect ratio and cell area remain unchanged in both conditions (Fig. 9B, D & I). hMSCs and HeLa cells are the largest cells and again orient themselves based on the topographical cues underneath (Fig. 9B). Furthermore, in both cell types, cell area and aspect ratio changed, indicating that cell area is an important parameter for cells to organize their actin cytoskeleton.
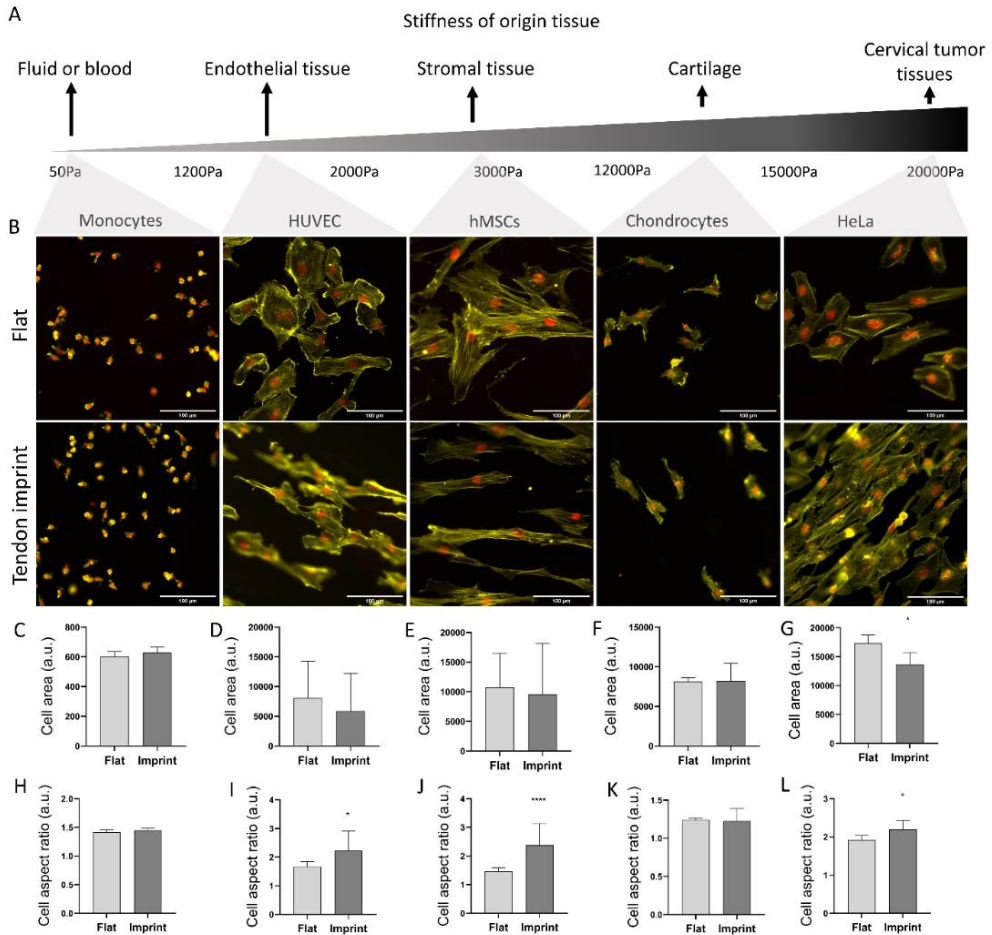
Figure 9. Different cells on tendon imprint undergo similar changes in cell area and aspect ratio. *(A) Panel illustrating the stiffness of tissues in which the monocytes, HUVEC, hMSCs, chondrocytes and HeLa cells originate from. From left to right, tissue stiffness increase. (B) Phalloidin (yellow) and DAPI (red) staining of monocytes, HUVEC, HMSCs, chondrocytes and HeLa cells cultured after 24 hours of culture on flat surface and tendon imprint. Scale bars represent 100 μm. (C-G) Quantification of cell area remained in similar values in all cells except for HeLa cells on tendon imprint. (F-G) Quantification of cell aspect ratio shows that tendon imprint leads to a significant increase in the cell aspect ratio of hMSCs and HeLa cells (Error bars represent 95% confidence intervals, *p<0.05, ****p<0.001). For all experiments, N = 1.*

Small molecules interfering with actin polymerization lead to a decrease in tenocyte phenotype

So far, we demonstrated that cells dynamically adapt their cytoskeletal organization to the surfaces that they attach to, and previous studies emphasized the role of cell shape on their phenotype. In addition, we previously demonstrated that the decrease in the actin stress formation and myosin contraction leads to a decrease in the expression of tenocyte marker genes declines in hMSCs cultured on Topo1018 surfaces[29]. In order to validate this phenomenon in tenocytes on tendon imprint, we cultured rat tenocytes on tendon imprints and exposed them to Y-27632 to inhibit Rho-associated protein kinase (ROCK), CCG-203971 to target Rho/MRTF/SRF and blebbistatin to block non-muscle myosin-II for 24 hours. (Fig.10).

As shown above, tenocytes possess thick ventral stress fibers and spread out cell morphology on flat surface, whilst tendon imprints induce an elongated shape with reduced number of stress fibers. When treated with the small molecules, actin organization was compromised, and tenocytes lost their intact cytoskeleton (Fig.10A). The expression of tenomodulin (TNMD) was measured as a marker for tenogenic differentiation. The tendon imprint induced TNMD expression relative to flat, confirming that stress fibers and large focal adhesions negatively correlate with tenogenesis. It was therefore surprising to see that TNMD expression declined when the actin inhibitors were added to tenocytes on imprint surfaces. Although our results are in line with the current literature on the regulation of Rho/ROCK signaling on tenogenic differentiation or tenocyte phenotype maintenance[34,35], this could also indicate the presence of other regulatory systems and there are more to discover the crosstalk between tenocyte phenotype and Rho/ROCK signaling.
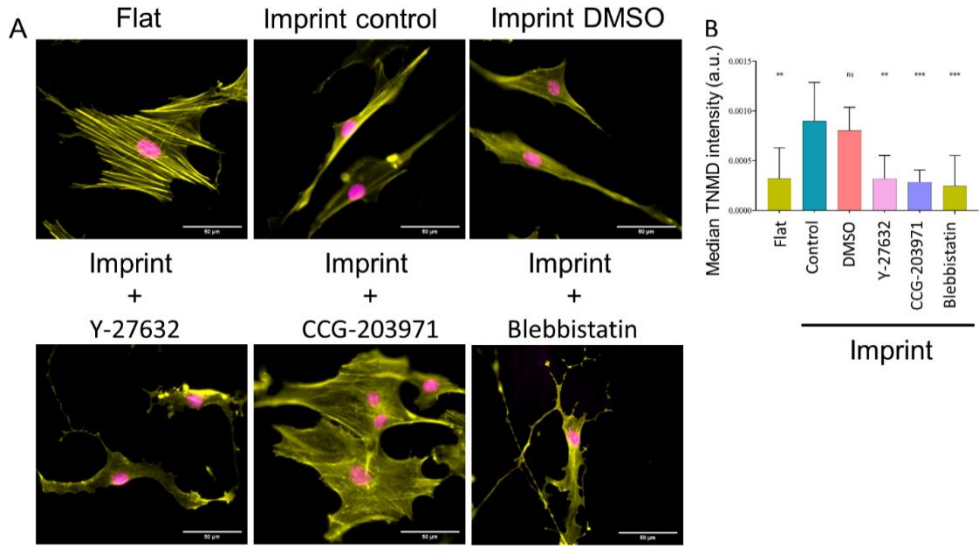
Figure 10. Actin modifiers affect tenocyte phenotype on tendon imprint. *(A) Rat tenocytes cultured on flat surface and tendon imprint with additional inhibitors (Y-27632 to target ROCK, CCG-203971 to target Rho/MRTF/SRF and Blebbistatin to target Myosin II) targeting the actin cytoskeleton formation. Cells on the flat surface possess thick ventral stress fibers whereas this was not visible in tendon imprint control and tendon imprint with DMSO supplementation. When treated with small molecules, intact cell shape was lost. Scale bars represent 50 µm. (B) Quantification of TNMD shows that on tendon imprint, without any inhibitors targeting actin machinery, its level is increased compared to flat surface. Upon treatment with small molecules, TNMD levels significantly decline. (Error bars represent 95% confidence intervals, **p<0.01, ****p<0.001). For all experiments, N = 2.*

Cells modulate the expression of integrin genes based the topographical context

Based on what we presented so far, tenocytes dynamically respond to topographies by organizing their actin cytoskeleton and focal adhesions to fit the topographical reality and they change the expression of tenomodulin. We were interested to learn if tenocytes modulate the expression of integrins based on the topographical context. Therefore, we analyzed the transcriptome profile of dedifferentiated tenocytes growing on flat polystyrene *in vitro* versus those of native *in vivo* rat tenocytes from a previously published study[42]. Figure 11 shows a Volcano plot with differentially expressed genes and with the names of the integrin related genes depicted, with negative fold change being higher expressed in vitro and vice versa. Obviously, tenocytes do change the

expression of integrin related genes. Tenocytes express more *Itga11*, which encodes for the protein α11 integrin monomer (12-fold change compared to *in vivo* tenocytes). The subunit α11 forms the integrin α11β1 dimer and *Itgb1* is also among the differentially expressed genes for dedifferentiated tenocytes. Another integrin encoding gene, *Itgav,* which encodes subunit αv, is highly expressed in *in vitro* tenocytes.
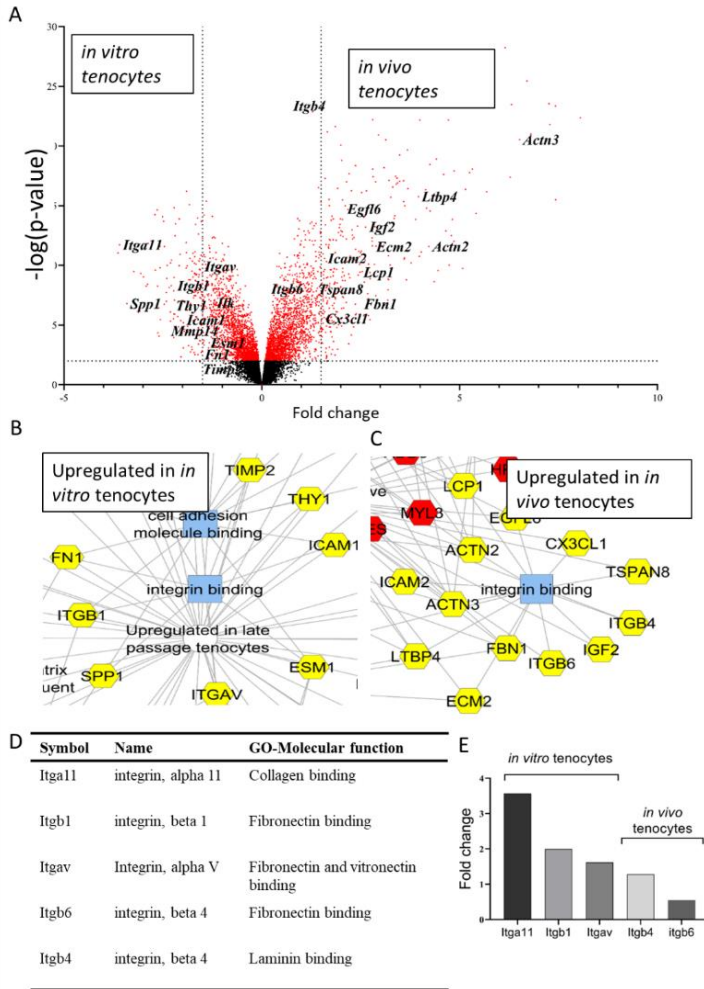
Figure 11. Microarray data analysis results of *in vitro* and *in vivo* rat tenocytes. (*A*) *Volcano plot demonstrating DEGs cut-off is determined at a 1.5-fold change and an adjusted P value of 0.05. The genes involved in the integrin-mediated signaling pathway are illustrated in bold. (B-C) Cluster analysis of genes that are upregulated in in vitro (B) and in vivo (C) tenocytes. (D) Table containing all integrin genes and their gene ontology (GO) molecular function. (E) Fold changes of in vitro integrin genes relative to in vivo (Itga11, Itgb1, Itgav) and fold changes of in vivo integrin genes relative to in vitro (Itgb4, Itgb6).*

Discussion

Previously, we demonstrated that mesenchymal stem cells[29,37,43], tenocytes[4,24,25,36] and pre-hypertrophic chondrocytes[44] actively organize their cytoskeleton upon exposure to topography, and described its phenotypic consequence on differentiation, phenotype maintenance, proliferation and metabolism. In this manuscript, we zoom into the cell-biomaterial interface. We describe how rat tenocytes and human mesenchymal stem cells adopt their focal adhesions on surfaces with different material properties, and how this reflects on the cytoskeletal organization of the cells. We demonstrate that the dynamic organization of the actin cytoskeleton starts very early upon cell attachment and the difference in cell shape becomes more pronounced over time. We provide further evidence on the link between focal adhesion maturation and changes in the actin-stress fiber profile and emphasize this link by interfering with cell adhesive properties. Finally, our results confirm the theory on the influence of cell shape on phenotype and the involvement of Rho/ROCK signalling in it. Overall, the results reported in this manuscript support our hypothesis regarding the involvement of adhesion molecules in cell morphology and further expands the knowledge on the dynamic adaptation and organization of the cell-biomaterial interface.

Dynamic organization of the actin cytoskeleton to adapt to the surrounding extracellular matrix occurs immediately after cell attachment. Curtis *et al.* used interference reflection microscopy to visualise changes in the shape of embryonic chick heart fibroblasts early upon cell attachment[45]. Pierres *et al.* illustrate that initial cell attachment occurs via the formation of small protrusions in a "tiptoe-like" manner to probe the surrounding space and full attachment occurs after tens of seconds[46]. Similarly, fibroblasts organize their shape on fibronectin patterns via contact guidance within 30 minutes[47] but significant topography-guided differences in cell morphology take up to hours in endothelial cells[48] and human osteosarcoma-derived cells[49]. These results are in line with our findings that rat tenocytes adapt to the tendon topography early upon attachment yet differences in cell elongation and area become only outspoken after 24 hours, which coincides with the moment that prominent actin stress fibers become visible. Interestingly, it took hMSCs only 4 hours to acquire a significant difference in cell area on micro-topographies. This suggests that adaptation of cell shape is highly dependent on cell type and topographical properties. Monocytes, for instance, maybe too small to perceive contact guidance provided by the tendon imprint in this manuscript, whereas we saw clear changes in cell shape previously on some TopoChip-derived topographies[50]. Tong *et al.* reported that fibroblast-like cells adapt their cytoskeleton and become more elongated in response to a tendon biomimetic surface topography compared to epithelial-like cells[51]. In their paper, in contrast to our results, Hela cells did not show contact guidance. It is unclear what causes this difference.

As the cues from the surrounding microenvironment to the actin cytoskeleton is mediated through focal adhesions, we hypothesized that the dynamic alterations in cell shape and stress fiber phenotype is associated with focal adhesion maturation. It is known that larger focal adhesions indicate higher cellular tension and come with thick ventral stress fibers[52]. For instance, epithelial-like cells spread more on smooth surfaces and created longer focal adhesions compared to those on rough surfaces[8] indicating stronger adhesion and cellular tension on smooth surfaces. Abagnale *et al.* demonstrated that pluripotent stem cells[14] and hMSCs[53] on aligned topographies have a higher aspect ratio, smaller cell size and smaller focal adhesions whilst cells on flat surfaces have the larger surface area and focal adhesions. An interesting study by Yang *et al.* showed that focal adhesions are not necessarily biggest on flat surfaces. They showed that in hMSCs, the size of focal adhesions per cell become 275 μm^2 and 260 μm^2 when the distance between the microgrooves are 0.5 μm and 3 μm, respectively[54]. The area of focal adhesions was measured around 150 μm^2 on flat surface, and microgrooves with distances of 10 μm and 30 μm and focal adhesion size correlated with higher cell stiffness[54]. We observe this link between cell area and focal adhesion maturation in both rat tenocytes and hMSCs. Over time, parallel to the increase in the cell size, focal adhesion length increases. Furthermore, we provide further evidence on the link between stress fiber and focal adhesion maturation. As the cells grow and spread on the flat surface, the tension in the cells increases and this is balanced with the maturation of the focal adhesions, therefore, supporting the cellular tensegrity model[9]. On topographies, considering that cell spreading is already limited by the surrounding topography, apparent ventral stress fibers and the length of focal adhesions decrease, cells have less tension in their cytoplasm.

Cellular tension also results in the recruitment of more or different integrin receptors to the focal adhesion. In cell suspension, gene expression of *Igta2* and *Igta4* in MG-63 osteosarcoma cells was upregulated after 4 hours, however, upon culturing on a substrate allowing cell attachment, same integrins were not expressed[55]. Similarly, integrins α5β1 and αvβ3 modulate the organization of the actin cytoskeleton in response to changes in surface stiffness or cyclic stretching[56]. The same study demonstrated that αvβ3 expression is enhanced when cells are cultured on lower stiffness ranges[56]. Furthermore, Elosegui-Artola *et al.* demonstrated that sensing and adaptation to matrix rigidity are determined by different integrins[57]. Constitutively expressed α5β1 integrins in healthy tissue or selectively expressed αvβ6 integrins in malignant tissue allows cell attachment, force regeneration and further integrin recruitment[57]. Furthermore, changes in the expression of integrins reflect on the focal adhesion points. For instance, when human fibrosarcoma cells were cultured on fibronectin-coated polyacrylamide gels, focal adhesion kinase (FAK) activation occurred through integrin α5β1, and its activity increased proportionally to substrate rigidity[58]. However, on collagen-coated

polyacrylamides, FAK is activated by integrin α2β1 and its activity was similar in soft and rigid substrates[58]. Similarly, expression of *a5β1* and avβ3 in smooth muscle cultured on fibronectin-coated coverslips was higher than cells on laminin-coated surfaces[59]. Further evidence was put forward by Cassidy *et.al.* who show osteoprogenitors and MG63 human osteoblast-like cells follow the contact guidance on 240 and 540 nm deep grooved surfaces and develop a smaller number of super mature focal adhesions (more than 5 μm in length) yet more focal complexes (less than 1 μm in length) compared to flat controls which allowed cell spreading[7]. The same study also reports that the expression of *ITGA1* is declined in hMSCs cultured on microgrooves compared to those cultured on flat surface[7]. In agreement with the current literature, we report differential expression of integrins in both tenocytes and hMSCs. Expression of *av* integrins induced formation of large focal adhesions in mouse fibroblasts[60], which is in line with our findings on increased expression of *Itgav* in *in vitro* tenocytes, compared to *in vivo* tenocytes. Similarly, in our recent studies[4,29], we report an increase in the expression of *ITGA11, ITGA10* and *ITGB2* in hMSCs cultured on microtopographies compared to flat surface, and with this study we demonstrate that this difference is also observed in the level of focal adhesion maturation and cytoskeletal organization.

The strength of the adhesion between ECM and integrins determines cell shape and stress fiber formation, and here we provide further evidence by treating hMSCs with RGD peptides. Essentially, RGD is a peptide sequence found in cell-adhesive proteins (e.g. fibronectin and vitronectin) and binds to specific integrins, such as integrin β1, β3 and β5 subunits and ultimately influence the actin cytoskeleton *via* focal adhesion complexes[61]. The influence of RGD peptides on the strength of cell adhesion can be measured by using atomic force microscopy (AFM). For instance, AFM was employed to measure the adhesion strength of zebrafish primary mesendodermal progenitors to fibronectin substrates and it was reported that when cells were treated with soluble RGD, less force was needed to detach them from the surface[62]. However, neither on flat surface nor on topographies cell adhesion cannot be fully abolished with RGD peptide treatments[61,62], and in fact, Sawyer *et al.* reported that RGD, alone, is not sufficient to induce a full cell attachment and spreading[63]. This can explain why we observe cell attachment and formation of stress fibers on hMSCs, despite the RGD treatment in hMSCs on both flat surface and microtopographies. However, the spatial organization and phenotype of stress fibers drastically change on both flat surface and microtopographies. Especially on microtopographies, cells appeared to be more rounded and actin fibers are more clustered. Therefore, we speculate that these are accumulations of cortical actin, which could also explain the lack of the focal adhesions on microtopographies as cortical actin is often linked with cadherin-based cell-cell adhesion, rather than cell-surface adhesion[64,65]. However, considering the current literature on the adhesion strength of cells on topographies[54] and RGD treatment[62], our

RGD data suggest that topographies can mimic the RGD effect and leads to the formation of smaller focal adhesions, and thus we can confirm that cells on topographies are less strongly attached to the surface.

Conclusion

In this article we show that cell attachment adapts to the properties of the surface on which the cells grow. The spatial distribution of topographic features is translated into an adjusted distribution of focal adhesions, degree of maturation and the formation of stress fibers. Our data are in accordance with the tensegrity model, which teaches that cells coordinate their internal stress on the actin cytoskeleton with the mechanical properties of their environment. Our data show that cells on topographic surfaces have lower tension than cells on flat surface, and are consistent with the role of actin-related signal transduction pathways in the differentiation of MSCs and tenocytes under the influence of topographies and the relationship we found between cell shape and function. Integrin-mediated bonding is a design feature that can be used in many ways in the functionalization of biomaterials.

Materials and methods

Surface fabrication

A detailed description of the fabrication of the micro-topographies can be found elsewhere [66]. In brief, the inverse pattern of the topographies in PS was etched into a silicon wafer, by deep reactive ion etching, generating a silicon master mould. The master was coated with a layer of perfluorodecyltrichlorosilane (FDTS, Sigma-Aldrich) and copied into polydimethylsiloxane (PDMS). The PDMS intermediate (mould) was subsequently copied into OrmoStamp hybrid polymer (micro resist technology GmbH), which served as the working mould for hot embossing the topographies into PS films (Goodfellow). The conditions for the hot embossing were 140 °C for 5 minutes at a pressure of 10 bar, and a demolding temperature of 90 °C. Before cell culture, PS films were oxygen plasma-treated for 30 seconds at 0.8 mbar, 50 sccm O2, and 100 W to enhance cell attachment.

Production of tendon imprint is described elsewhere [25]. Briefly, porcine tendons were sectioned at 300 μm thickness with a Cryotome (Leica CM1950). Next, a PDMS solution (SYLGARD 184 Silicone Elastomer Base and Elastomer Curing agent) was prepared in 10:1 ratio and subsequently poured onto the tendon slices and vacuum degassed for 30 minutes. Next, PDMS was allowed to polymerize for 48 hours. Next, tendon section was peeled off from PDMS, creating a native tendon topography. For the production of the PS tendon imprint, the following construction was clamped: glass slide – PDMS mould – PS sheet – glass slide, and put in the oven at 140°C for 30 minutes. After cooling down, the PS was removed from the mould and underwent

plasma oxygen treatment (30 sec, O_2). All surfaces were and sterilized with ethanol for at least 30 minutes and washed with PBS prior to cell culture.

To produce the platform with binary micropatterns, a two-step thiol-ene reaction was performed. Before thiol-ene coupling on the surface of a microscopy glass slide, the glass was activated with oxygen plasma and piranha solution. Then, the vinyl silane was vapour-deposited overnight at 80 °C. Next, a two-step thiol-ene reaction was performed on the vinyl-coupled surface. First, 10mM CGGGRGDS (Chinapeptides) peptide solution containing 5mg/ml LAP (Lithium phenyl-2,4,6-trimethylbenzoylphosphinate (TCI chemicals))solution was prepared. On the vinyl-modified glass substrate (25×25×1 mm, width×length×thickness), 3 uL of the RGD thiol solution was dropped, covered with the photomask and irradiated with UV light for 10 min. The volume of the thiol solution for the first thiol-ene reaction is critical to transfer the patterns as a (proximity) gap between mask and glass substrate reduces the resolution of the patterns. After removing the photomask, samples were washed in ethanol, in water in an ultrasonication bath for 10 min, and dried with a nitrogen gun. Then, the second thiol to graft (10 mM of either PEG thiol or HAVDI peptide solution containing 5mg/ml photoinitiator) was dropped onto the pre-patterned surface, covered with a fluorinated quartz slide and UV-irradiated for another 10 min. Finally, the plate was washed with THF, ethanol and water in an ultrasonication bath and dried with a nitrogen gun. The samples were stored in 70% ethanol for further use at 4 °C.

Cell culture

Human mesenchymal stem cells (hMSCs) isolation was conducted from the bone marrow of 74-years old female donor after obtaining written informed consent from the patient. Ethical approval for using the samples was obtained from the ethical advisory board of the Medisch Spectrum Twente, Enschede. All methods were carried out following local and relevant guidelines and regulations. hMSCs were cultured in basic medium (α-MEM, (Gibco)) supplemented with 10 % Fetal Bovine Serum (FBS) (Thermo Fisher Scientific) and 1% Penicillin/Streptomycin. To investigate the effect of surface topography, passage 5 hMSCs were seeded at 5000 cells/cm² density and cultured for the designated times in a humidified incubator with 5% CO_2 at 37 °C. Adipose-derived human mesenchymal stem cells (AD-hMSCs) were purchased from Lonza. AD-hMSCs were cultured on MEM Alpha GlutaMAX, no nucleosides (Gibco) supplemented with 10% FBS, 0.2 mM ascorbic-acid-2-phosphate (ASAP), and 10 U/mL Penicillin/Streptomycin. Cells were grown at 37°C in a humid atmosphere at 5% CO_2. Rat tenocytes were isolated from the hind limbs of 23 weeks old Cyp1a2ren strain rats after euthanization considering their surplus status from the breeding program. Upon cell isolation, tenocytes were expanded in a cell culture medium of Dulbecco's modified Eagle's medium (DMEM, Sigma-Aldrich) supplemented with 10% FBS,

100 U/ml penicillin/streptomycin. To investigate the effect of surface topography, passage 4 tenocytes were seeded at 5000cells/cm² density and cultured for the designated times in a humidified incubator with 5% CO_2 at 37 °C. Bovine chondrocytes were isolated from bovine articular cartilage from the metacarpo/tarsophalangeal joint, provided as a slaughterhouse material, by using an overnight digestion protocol. In brief, the digestion solution containing chondrocyte medium (high-glucose DMEM (Gibco), 10% FBS (Sigma-Aldrich), 100 U/ml Penicillin/Streptomycin (Thermo Fisher Scientific)), 0.01% hyaluronidase, and 0.15% collagenase II. Passage 2 chondrocytes was used in this study. HeLa cells (ATTC CRM-CCL-2™, 70012009) were cultivated in high-glucose DMEM with pyruvate (Gibco), 10% FBS (Sigma-Aldrich), 100 U/ml Penicillin/Streptomycin (Thermo Fisher Scientific). HeLa cells were used at passage 9. Human monocytes were isolated using CD14 Microbeads human (BD, 130-050-201) from peripheral blood mononuclear cells (PBMCs). CD14+ cells were seeded 104 cell/mL using complete RPMI 1640 medium containing 10% FBS (Sigma-Aldrich), 100 U/ml Penicillin/Streptomycin.

Pharmaceutical reagents exposure

Rat tenocytes were seeded on tendon imprints at the seeding density of 5,000 cells/cm² in a basic medium, after 24 hours basic medium is replaced with a new basic medium supplemented with Y-27632 (Selleckchem), CCG-203971 (Sigma-Aldrich) and Blebbistatin (Sigma-Aldrich) at the final concentration of 10 µM. Cells were fixed after 24 hours for staining. hMSCs were seeded on Topo1018 surface topographies at the seeding density of 5,000 cells/cm² in basic medium supplemented with manganese (II) chloride ($MnCl_2$) (Sigma-Aldrich) at the final concentration of 2mM to activate integrins, Paclitaxel (Sigma-Aldrich) at the final concentration of 1 µM to stabilizes microtubule arresting, Parbendezole (Bio-Connect B.V) at the final concentration of 4 µM to inhibit the microtubule assembly. We also added RGD peptides Gly-Arg-Gly-Asp-Ser-Pro and Gly-Arg-Gly-Asp-Ser-Pro-Lys (Sigma-Aldrich) to block integrin activation, Gly-Arg-Ala-Asp-Ser-Pro (Sigma-Aldrich) as a negative control. Cells were exposed to pharmaceutical reagents for 4 hours.

Microarray analysis and transcriptional profiling

Transcriptomics data for tenocytes are downloaded from ArrayExpress (https://www.ebi.ac.uk/arrayexpress/). Raw data belonging to "E-MTAB-4800 - Transcriptomic profiling of chondrocytes and tenocytes in de- and re-differentiation relative to native tissue[67]" was downloaded and processed in the online portal arrayanalysis.org. P-values were corrected for multiple testing using the Benjamini and Hochberg method. Genes were considered differentially expressed when a corrected p-value below 0.05 was reached. In order to identify all the differentially expressed genes, a Venn's diagram tool was used. Next, pathway over-representation analysis was

performed *via* ConsensusPathDB (CPDB)[68] to identify the gene ontology (GO) identifiers of selected genes with background list containing all measured genes to improve the statistical evaluation of the pathways. To cluster genes with their GO identifiers, ToppCluster was used. Obtained data were imported to CytoScape to modify the network for further visualizations. Pathways with a false discovery rate-corrected p-value <0.05 were considered significant.

Scanning electron microscopy (SEM)

Rat tenocytes were cultured at as described above and fixed in 2.5 % glutaraldehyde (Fisher Scientific) at room temperature for one hour. Then, they were washed with distilled water 3 times 10 minutes, dehydrated in 25%, 50%, 75%, 90%, and 100% ethanol for 15 minutes each, and incubated in 100% ethanol for additional 15 minutes. Next, samples were dried in Hexamethyldisilazane (HMDS) (Sigma-Aldrich) for 1 hour. Prior to imaging, samples were coated with 5 nm gold-palladium and imaged using a scanning electron microscope (SEM) (FEI Quanta 3D FEG Dual Beam).

Immunofluorescent staining

Rat tenocytes and human mesenchymal stem cells cultured on tendon imprints and Topo1018 surface were fixed at designated time points with 4% paraformaldehyde in PBS for 20 minutes, and washed with PBS twice to remove remaining fixative. Next, samples were permeabilized with 0.1% Triton X-100 in PBS for 10 minutes. The samples were incubated with 1:100 Horse Serum (HS) in PBST (PBS with 0.2% Triton X-100 and 0.5% Bovine Serum Albumin (BSA)) for 60 minutes and washed with PBST. The samples were incubated overnight with monoclonal mouse IgG1 for vinculin (Sigma, V9131, 1:200) diluted in PBST and subsequently washed three times with PBST. The samples were then incubated with 1:200 Goat anti-mouse IgG conjugated with Alexa488 (Molecular Probes, A21121) and 1:200 Phalloidin 647 (Sigma) in PBS-T for 1.5 hour. Afterwards, the imprints were washed three times with PBST, whereafter they were incubated for 30 minutes with 1:50 DAPI in PBS-T. The DAPI solution was removed and the samples were washed three times with PBS. Then, the samples were mounted on a glass slide with Mowio and kept at 4oC until imaging.

Human mesenchymal stem cells cultured on binary micropatterns were washed with phosphate-buffered saline (PBS) and fixed with 3.7% paraformaldehyde (Sigma-Aldrich) for 10 min at room temperature. After washing three times, cells were permeabilized with 0.01% Triton X-100 and blocked with 3% BSA in PBT (PBS + 0.02% Triton-X-100, 0.5% BSA) for 1 h. Afterward, cells were incubated with the primary antibodies dissolved in PBT for overnight at 4 °C. Cells were washed three times and incubated with a specific secondary goat antibody conjugated to Alexa Fluor 647 and/or Alexa Fluor 488 (1:400; ThermoFisher), together with Phalloidin conjugated to Alexa Fluor 568 (1:250; ThermoFisher) in PBT for 1 h. After washing, the nucleus

was counterstained with Hoechst 33258 (1:1000) for 10 min. After washing three times, surfaces were mounted on glass cover slides with mounting media (Dako). All washing steps were performed with PBT. Primary antibodies used in this study were: mouse anti human-YAP1 antibody (1:200; Santa Cruz, SC-101199) and rabbit anti human-paxillin antibody (1:200; Abcam; ab32084).

Sir-Actin live imaging

In order to visualize live actin organization, SiR-actin Kit (Spriochrome, CY-SC001) was used by following manufacturer's instructions. Briefly, after letting tenocytes to adhere on tendon imprints and flat surface for two hours, we replaced the culture medium with culture medium enriched with final concentration of 100nM of SiR-actin probe and 1nM of verapamil. Images were taken in every 10 minutes with Leica DMI8 microscope for 40 hours. During imaging, the cells inside in a humidified tissue culture chamber at 37°C with 5% CO_2.

Imaging and data analysis

Focal adhesion imaging was performed with a confocal microscope (Leica TCS SP5X). Images were taken at 63X magnification. Focal adhesion length was measured by using ImageJ by using *measure* plugin. Cell shape was analyzed through CellProfiler 3.1.8[69] employing custom-made pipelines. Briefly, after correction of illumination of the three channels, the nuclei were identified as Primary Objects by Global Minimum Cross Entropy thresholding from the DAPI image channel. Subsequently, cell shape was determined as Secondary Object by propagating and again applying Global Minimum Cross Entropy thresholding from the Phalloidin image channel. For both channels, missegmented artifacts were removed by adapting the arbitrary threshold on nuclei and cell size. Following this, the cytoplasm was identified as Tertiary Object by removing the nuclei shape from the total cell shape. After enhancing and masking the vinculin channel, the focal adhesions were identified as Primary Objects again. These structures were captured by Otsu Adaptive thresholding of the enhanced and masked vinculin channel. The object's size and shape were determined. Figures are prepared in InkSpace and graphs are prepared by using GraphPad Prism version 8.0 (GraphPad Software, Inc., San Diego, CA).

Statistical analysis

All statistical analysis was performed by using GraphPad Prism version 8.0 (GraphPad Software, Inc., San Diego, CA). Two-way analysis of variance (ANOVA) was performed to determine the statistical significance in Fig.2, Fig.3 and Fig.4. One-way ANOVA was used performed to determine the statistical significance Fig.6, Fig.7, Fig.8 and Fig.10. Student's t-test was carried out for Fig. 9. Significance set at $p < 0.05$ to determine the significance between means. All quantitative data represented in this study are based on

biological triplicates unless stated otherwise. Microarray p-values were corrected for multiple testing using the Benjamini and Hochberg method. Genes with a corrected p-value below 0.05 were considered differentially expressed.

References

1. Weiss, P. Experiments on cell and axon orientation in vitro. J Exp Zool. **1**, 353, 1945.

2. Campbell, R.D., and Marcum, B.A. Nematocyte migration in hydra: evidence for contact guidance in vivo. J Cell Sci . **41**, 33 LP, 1980.

3. Bettinger, C.J., Orrick, B., Misra, A., Langer, R., and Borenstein, J.T. Microfabrication of poly (glycerol–sebacate) for contact guidance applications. Biomaterials . **27**, 2558, 2006.

4. Vasilevich, A.S., Vermeulen, S., Kamphuis, M., Roumans, N., Eroumé, S., Hebels, D.G.A.J., et al. On the correlation between material-induced cell shape and phenotypical response of human mesenchymal stem cells. Sci Rep . 2020.05.13.093641, 2020.

5. Robotti, F., Bottan, S., Fraschetti, F., Mallone, A., Pellegrini, G., Lindenblatt, N., et al. A micron-scale surface topography design reducing cell adhesion to implanted materials. Sci Rep . **8**, 10887, 2018.

6. Dalby, M.J., Riehle, M.O., Sutherland, D.S., Agheli, H., and Curtis, A.S.G. Use of nanotopography to study mechanotransduction in fibroblasts – methods and perspectives. Eur J Cell Biol . **83**, 159, 2004.

7. Cassidy, J.W., Roberts, J.N., Smith, C.A., Robertson, M., White, K., Biggs, M.J., et al. Osteogenic lineage restriction by osteoprogenitors cultured on nanometric grooved surfaces: The role of focal adhesion maturation. Acta Materialia Inc., **10**, 651, 2014.

8. Baharloo, B., Textor, M., and Brunette, D.M. Substratum roughness alters the growth, area, and focal adhesions of epithelial cells, and their proximity to titanium surfaces. J Biomed Mater Res - Part A. **74**, 12, 2005.

9. Wang, N., Naruse, K., Stamenović, D., Fredberg, J.J., Mijailovich, S.M., Tolić-Nørrelykke, I.M., et al. Mechanical behavior in living cells consistent with the tensegrity model. Proc Natl Acad Sci U S A. **98**, 7765, 2001.

10. Ingber, D.E. Tensegrity I. Cell structure and hierarchical systems biology. J Cell Sci. **116**, 1157, 2003.

11. Prager-Khoutorsky, M., Lichtenstein, A., Krishnan, R., Rajendran, K., Mayo, A., Kam, Z., et al. Fibroblast polarization is a matrix-rigidity-dependent process controlled by focal adhesion mechanosensing. Nat Cell Biol. **13**, 1457, 2011.

12. Pelham, R.J., and Wang, Y. Cell locomotion and focal adhesions are regulated by substrate flexibility. Proc Natl Acad Sci . **94**, 13661 LP, 1997

13. Fusco, S., Panzetta, V., Embrione, V., and Netti, P.A. Crosstalk between focal adhesions and material mechanical properties governs cell mechanics and functions. Acta Biomater . **23**, 63, 2015.

14. Abagnale, G., Sechi, A., Steger, M., Zhou, Q., Kuo, C.C., Aydin, G., et al. Surface Topography Guides Morphology and Spatial Patterning of Induced Pluripotent Stem Cell Colonies. Stem Cell Reports. **9**, 654, 2017.

15. Bershadsky, A.D., Kozlov, M., and Geiger, B. Adhesion-mediated mechanosensitivity: a time to experiment, and a time to theorize. Curr Opin Cell Biol. **18**, 472, 2006.

16. Legerstee, K., Geverts, B., Slotman, J.A., and Houtsmuller, A.B. Dynamics and distribution of paxillin, vinculin, zyxin and VASP depend on focal adhesion location and orientation. Sci Rep. **9**, 1, 2019.

17. Thievessen, I., Thompson, P.M., Berlemont, S., Plevock, K.M., Plotnikov, S. V., Zemljic-Harpf, A., et al. Vinculin-actin interaction couples actin retrograde flow to focal adhesions, but is dispensable for focal adhesion growth. J Cell Biol. **202**, 163, 2013.

18. Von Erlach, T.C., Bertazzo, S., Wozniak, M.A., Horejs, C.M., Maynard, S.A., Attwood, S., et al. Cell-geometry-dependent changes in plasma membrane order direct stem cell signalling and fate. Nat Mater. Springer US, **17**, 237, 2018.

19. Beijer, N.R.M., Nauryzgaliyeva, Z.M., Arteaga, E.M., Pieuchot, L., Anselme, K., van de Peppel, J., et al. Dynamic adaptation of mesenchymal stem cell physiology upon exposure to surface micropatterns. Sci Rep. Springer US, **9**, 1, 2019.

20. Jansen, K.A., Atherton, P., and Ballestrem, C. Mechanotransduction at the cell-matrix interface. Semin. Cell Dev. Biol. Elsevier Ltd, pp. 75–83, 2017.

21. English, A., Azeem, A., Spanoudes, K., Jones, E., Tripathi, B., Basu, N., et al. Substrate topography: A valuable in vitro tool, but a clinical red herring for in vivo tenogenesis. Acta Materialia Inc., **27**, 3, 2015.

22. McNamara, L.E., McMurray, R.J., Biggs, M.J.P., Kantawong, F., Oreffo, R.O.C., and Dalby, M.J. Nanotopographical Control of Stem Cell Differentiation. J Tissue Eng. SAGE Publications Ltd STM, **1**, 120623, 2010.

23. Yao, L., Bestwick, C.S., Bestwick, L.A., Maffulli, N., and Aspden, R.M. Phenotypic drift in human tenocyte culture. Tissue Eng. **12**, 1843, 2006.

24. Vermeulen, S., Vasilevich, A., Tsiapalis, D., Roumans, N., Vroemen, P., Beijer, N.R.M., et al. Identification of topographical architectures supporting the phenotype of rat tenocytes. Acta Biomater. Acta Materialia Inc., **83**, 277, 2019.

25. Dede Eren, A., Vasilevich, A., Eren, E.D., Sudarsanam, P., Tuvshindorj, U., de Boer, J., et al. Tendon-derived biomimetic surface topographies induce phenotypic maintenance of tenocytes in vitro. Tissue Eng Part A . 2020. Available

26. Younesi, M., Islam, A., Kishore, V., Anderson, J.M., and Akkus, O. Tenogenic

Induction of Human MSCs by Anisotropically Aligned Collagen Biotextiles. Adv Funct Mater. **24**, 5762, 2014.

27. Kishore, V., Bullock, W., Sun, X., Van Dyke, W.S., and Akkus, O. Tenogenic differentiation of human MSCs induced by the topography of electrochemically aligned collagen threads. Biomaterials . Elsevier Ltd, **33**, 2137, 2012.

28. Dede Eren, A., Sinha, R., Deniz, E., Huipin, Y., Gulce-iz, S., Valster, H., et al. Decellularized Porcine Achilles Tendon Induces Anti-inflammatory Macrophage Phenotype In Vitro and Tendon Repair In Vivo. J Immunol Regen Med . Elsevier, **8**, 100027, 2020.

29. Vermeulen, S., Roumans, N., Honig, F., Carlier, A., Hebels, D.G.A.J., Eren, A.D., et al. Mechanotransduction is a context-dependent activator of TGF-β signaling in mesenchymal stem cells. Biomaterials. **259**, 2020.

30. Younesi, M., Islam, A., Kishore, V., Anderson, J.M., and Akkus, O. Tenogenic Induction of Human MSCs by Anisotropically Aligned Collagen Biotextiles. Adv Funct Mater. 5762, 2014.

31. Sit, S.T., and Manser, E. Rho GTPases and their role in organizing the actin cytoskeleton. J Cell Sci. **124**, 679, 2011.

32. Vicente-Manzanares, M., Ma, X., Adelstein, R.S., and Horwitz, A.R. Non-muscle myosin II takes centre stage in cell adhesion and migration. Nat Rev Mol Cell Biol . **10**, 778, 2009.

33. Madhurakkat Perikamana, S.K., Lee, J., Ahmad, T., Kim, E.M., Byun, H., Lee, S., et al. Harnessing biochemical and structural cues for tenogenic differentiation of adipose derived stem cells (ADSCs) and development of an in vitro tissue interface mimicking tendon-bone insertion graft. Biomaterials. **165**, 79, 2018.

34. Xu, B., Song, G., Ju, Y., Li, X., Song, Y., and Watanabe, S. RhoA / ROCK , Cytoskeletal Dynamics , and Focal Adhesion Kinase are Required for Mechanical Stretch-Induced Tenogenic Differentiation of Human Mesenchymal Stem Cells. J Cell Physiol. 2722, 2011.

35. Maharam, E., Yaport, M., Villanueva, N.L., Akinyibi, T., Laudier, D., He, Z., et al. Rho/Rock signal transduction pathway is required for MSC tenogenic differentiation. Bone Res. **3**, 2015.

36. Dede Eren, A., Eren, E.D., Wilting, T.J.S., de Boer, J., Gelderblom, H., and Foolen, J. Self-agglomerated collagen patterns govern cell behaviour. Sci Rep. **11**, 1516, 2021.

37. Hulshof, F.F.B., Papenburg, B., Vasilevich, A., Hulsman, M., Zhao, Y., Levers, M., et al. Mining for osteogenic surface topographies: In silico design to in vivo osseo-integration. Biomaterials . Elsevier Ltd, **137**, 49, 2017.

38. Tojkander, S., Gateva, G., and Lappalainen, P. Actin stress fibers - Assembly,

dynamics and biological roles. J Cell Sci. **125**, 1855, 2012.

39. Brum, A.M., Van De Peppel, J., Van Der Leije, C.S., Schreuders-Koedam, M., Eijken, M., Van Der Eerden, B.C.J., et al. Connectivity Map-based discovery of parbendazole reveals targetable human osteogenic pathway. Proc Natl Acad Sci U S A. **112**, 12711, 2015.

40. Cox, T.R., and Erler, J.T. Remodeling and homeostasis of the extracellular matrix: implications for fibrotic diseases and cancer. Dis Model &amp; Mech . **4**, 165 LP, 2011.

41. Engler, A.J., Sen, S., Sweeney, H.L., and Discher, D.E. Matrix Elasticity Directs Stem Cell Lineage Specification. Cell . **126**, 677, 2006.

42. Mueller, A.J., Tew, S.R., Vasieva, O., and Clegg, P.D. A systems biology approach to defining regulatory mechanisms for cartilage and tendon cell phenotypes. Nature Publishing Group, 1, 2016.

43. Dede Eren, A., Sinha, R., Eren, E.D., Huipin, Y., Gulce-Iz, S., Valster, H., et al. Decellularized Porcine Achilles Tendon Induces Anti-inflammatory Macrophage Phenotype In Vitro and Tendon Repair In Vivo. J Immunol Regen Med . Elsevier, **8**, 100027, 2020.

44. Le, B.Q., Vasilevich, A., Vermeulen, S., Hulshof, F., Stamatialis, D.F., van Blitterswijk, C.A., et al. Micro-Topographies Promote Late Chondrogenic Differentiation Markers in the ATDC5 Cell Line. Tissue Eng Part A **23**, 458, 2017.

45. Curtis, A.S.G. the Mechanism of Adhesion of Cells To Glass. J Cell Biol. **20**, 199, 1964.

46. Pierres, A., Benoliel, A.-M., Touchard, D., and Bongrand, P. How Cells Tiptoe on Adhesive Surfaces before Sticking. Biophys J. **94**, 4114, 2008.

47. Ramirez-San Juan, G.R., Oakes, P.W., and Gardel, M.L. Contact guidance requires spatial control of leading-edge protrusion. Mol Biol Cell. American Society for Cell Biology (mboc), **28**, 1043, 2017.

48. Sales, A., Holle, A.W., and Kemkemer, R. Initial contact guidance during cell spreading is contractility-independent. Soft Matter . The Royal Society of Chemistry, **13**, 5158, 2017.

49. Davidson, P.M., Özçelik, H., Hasirci, V., Reiter, G., and Anselme, K. Microstructured Surfaces Cause Severe but Non-Detrimental Deformation of the Cell Nucleus. Adv Mater . John Wiley & Sons, Ltd, **21**, 3586, 2009.

50. Vassey, M.J., Figueredo, G.P., Scurr, D.J., Vasilevich, A.S., Vermeulen, S., Carlier, A., et al. Immune Modulation by Design: Using Topography to Control Human Monocyte Attachment and Macrophage Differentiation. Adv Sci . John Wiley & Sons, Ltd, **7**, 1903392, 2020.

51. Tong, W.Y., Shen, W., Yeung, C.W.F., Zhao, Y., Cheng, S.H., Chu, P.K., et al. Functional replication of the tendon tissue microenvironment by a bioimprinted substrate and the support of tenocytic differentiation of mesenchymal stem cells. Biomaterials . Elsevier Ltd, **33**, 7686, 2012.

52. Romero, S., Le Clainche, C., and Gautreau, A.M. Actin polymerization downstream of integrins: Signaling pathways and mechanotransduction. Biochem J. **477**, 1, 2020.

53. Abagnale, G., Steger, M., Nguyen, V.H., Hersch, N., Sechi, A., Joussen, S., et al. Surface topography enhances differentiation of mesenchymal stem cells towards osteogenic and adipogenic lineages. Biomaterials . Elsevier Ltd, **61**, 316, 2015.

54. Yang, L., Gao, Q., Ge, L., Zhou, Q., Warszawik, E.M., Bron, R., et al. Topography induced stiffness alteration of stem cells influences osteogenic differentiation. Biomater Sci. **8**, 2638, 2020.

55. Chen, D., Magnuson, V., Hill, S., Arnaud, C., Steffensen, B., and Klebe, R.J. Regulation of integrin gene expression by substrate adherence. J Biol Chem . Â© 1992 ASBMB. Currently published by Elsevier Inc; originally published by American Society for Biochemistry and Molecular Biology., **267**, 23502, 1992.

56. Balcioglu, H.E., van Hoorn, H., Donato, D.M., Schmidt, T., and Danen, E.H.J. The integrin expression profile modulates orientation and dynamics of force transmission at cell-matrix adhesions. J Cell Sci. **128**, 1316, 2015.

57. Elosegui-Artola, A., Bazellières, E., Allen, M.D., Andreu, I., Oria, R., Sunyer, R., et al. Rigidity sensing and adaptation through regulation of integrin types. Nat Mater. **13**, 631, 2014.

58. Seong, J., Tajik, A., Sun, J., Guan, J.-L., Humphries, M.J., Craig, S.E., et al. Distinct biophysical mechanisms of focal adhesion kinase mechanoactivation by different extracellular matrix proteins. Proc Natl Acad Sci . **110**, 19372 LP, 2013.

59. Cai, W.J., Li, M.B., Wu, X., Wu, S., Zhu, W., Chen, D., et al. Activation of the integrins α5β1 and αvβ3 and focal adhesion kinase (FAK) during arteriogenesis. Mol Cell Biochem. **322**, 161, 2009.

60. Schiller, H.B., Hermann, M.R., Polleux, J., Vignaud, T., Zanivan, S., Friedel, C.C., et al. β 1 - And α v -class integrins cooperate to regulate myosin II during rigidity sensing of fibronectin-based microenvironments. Nat Cell Biol. Nature Publishing Group, **15**, 625, 2013.

61. Lamers, E., te Riet, J., Domanski, M., Luttge, R., Figdor, C.G., Gardeniers, J.G.E., et al. Dynamic cell adhesion and migration on nanoscale grooved substrates. Eur Cell Mater. **23**, 182, 2012.

62. Puech, P.-H., Taubenberger, A., Ulrich, F., Krieg, M., Muller, D.J., and Heisenberg, C.-P. Measuring cell adhesion forces of primary gastrulating cells from zebrafish using atomic force microscopy. J Cell Sci. **118**, 4199, 2005.

63. Sawyer, A.A., Hennessy, K.M., and Bellis, S.L. Regulation of mesenchymal stem cell attachment and spreading on hydroxyapatite by RGD peptides and adsorbed serum proteins. Biomaterials . **26**, 1467, 2005.

64. Chalut, K.J., and Paluch, E.K. The Actin Cortex: A Bridge between Cell Shape and Function. Dev Cell . **38**, 571, 2016.

65. Engl, W., Arasi, B., Yap, L.L., Thiery, J.P., and Viasnoff, V. Actin dynamics modulate mechanosensitive immobilization of E-cadherin at adherens junctions. Nat Cell Biol. England, **16**, 587, 2014.

66. Zhao, Y., Truckenmüller, R., Levers, M., Hua, W.-S., de Boer, J., and Papenburg, B. High-definition micropatterning method for hard, stiff and brittle polymers. Mater Sci Eng C. **71**, 558, 2017.

67. Mueller, A.J., Tew, S.R., Vasieva, O., Clegg, P.D., and Canty-Laird, E.G. A systems biology approach to defining regulatory mechanisms for cartilage and tendon cell phenotypes. Sci Rep. Nature Publishing Group, **6**, 1, 2016.

68. Kamburov, A., Wierling, C., Lehrach, H., and Herwig, R. ConsensusPathDB--a database for integrating human functional interaction networks. Nucleic Acids Res. 2008/10/21. Oxford University Press, **37**, D623, 2009.

69. Carpenter, A.E., Jones, T.R., Lamprecht, M.R., Clarke, C., Kang, I.H., Friman, O., et al. CellProfiler: image analysis software for identifying and quantifying cell phenotypes. Genome Biol. **7**, R100, 2006.

Chapter VII

Decellularized porcine Achilles tendon induces anti-inflammatory macrophage phenotype in vitro and tendon repair in vivo

Decellularized tissues and organs from animal sources are widely used in regenerative medicine and tissue engineering. However, in tendon tissue engineering there is limitation not only in terms of tissue source -allografts and autografts- but also standardization of decellularization techniques. The goal of this study is to decellularize porcine Achilles tendon to be used as an off-the-shelf product for tendon reconstruction. We describe a novel, mild decellularization strategy which retains the biochemical and biomechanical characteristics of native tendon upon decellularization. We further show that decellularized tendon sections *in vitro* induce tenogenic differentiation in stem cells and anti-inflammatory response in naïve macrophages. Upon implantation in an Achilles tendon defect in rabbits, we observed that decellularized tendons integrated with the host tissue without signs of tissue rejection or encapsulation. Together, we demonstrate that decellularized tendons produced with our new protocol bear a great potential for tendon tissue regeneration.

Chapter VI

Introduction

Tendon injury is one of the most common types of musculoskeletal injuries, which is associated with intrinsic and extrinsic factors including age, gender, and obesity as well as with sport-related or other rigorous physical activities [1]. Due to its poor blood supply [2], low cell density [3–5], and low regenerative capacity [5], natural tendon healing results in the formation of scar tissue, impaired structural integrity and mechanical strength. As a consequence, the healed tendon is more susceptible to re-injury [6]. Treatment of tendon injury includes physiotherapy, anti-inflammatory drugs, painkillers or surgery yet the net outcome is ineffective as patients suffer from a substantial decrease in personal productivity [7]. In surgery, the damaged tendon is replaced with autografts, allografts, or natural extracellular matrix (ECM) derived grafts [8–10]. Autografts are limited in number, dimension and sites of harvest, and lead to donor site morbidity [10,11]. Allografts are limited in terms of available healthy donors as well as the potential of causing an inflammatory response in the host and can be expensive [12–14]. There are commercial xenogenic scaffolds available, however not yet of tendon origin but instead dermis, intestinal submucosa and pericardium [15]. The use of these scaffolds are unfortunately not without complications such as rerupture, postoperative edema, aggravated pain and decreased range of motion [15]. In addition, synthetic polymers such as a poly-glycolic acid (PGA), poly-lactic glycolic acid (PLGA) or polysaccharides such as chitosan or various collagen derivatives have been used for tendon reconstructions [16]. However, due to the complex ECM structure, composition, and mechanical properties; no biomaterials have yet progressed beyond in vitro or early in vivo evaluation [17]. Within the last few decades, researchers have applied decellularized tissues for tissue regeneration, due to their inductive nature which makes them a strong candidates for clinical application[18–20]. Decellularized tissues such as dermis, small intestine, pericardium and heart valves harvested from allogenic or xenogeneic sources are commercially available and have been used in the clinic for various applications including soft tissue regeneration and valve replacements [21]. Similarly, demineralized bone matrix has been used for decades as a bone graft substitute. Although decellularized non-tendon tissues are being used in tear repairs or provide support, decellularized tendons from xenogeneic sources to be used in tendon orthopaedic applications are not available [22]. Therefore, the aim of this study is to develop and validate a protocol towards an off-the-shelf product for tendon and ligament reconstruction.

Several protocols describe decellularization of a whole tendon or tendon sections, and involve physical and/or chemical disruption of cellular components and use different tendon sources [23–27]. Special attention is given on *in vitro* and *in vivo* characterization of decellularized tissue in order to prove that material can be used as an off-the-shelf product. ECM structure and composition [23–32] after decellularization is important and

should be similar to the native tissue to retain the mechanical properties typical of tendon tissue. Moreover, decellularized tissue should be cytocompatible, support the invasion of tissue-resident cells after implantation, and support tenogenic differentiation [31]–[37]. Decellularized allogeneic and xenogeneic tissues may even induce an immunogenic response favouring tissue remodelling [38]. Keane *et al* used decellularized porcine small intestine produced with three different methods and investigated host response in terms of macrophage polarization profile [39]. Their results indicate that effective decellularization resulted in M_2 macrophages, which is associated with constructive tissue remodelling [39]. Even though challenging, producing decellularized tendons while preserving ECM structure and composition, allowing recellularization in absence of an anti-inflammatory response in the host material is a major step towards a clinically applicable tendon graft [40]. Therefore, we formulated a mild but robust decellularization protocol as illustrated in Fig.1 and demonstrated that decellularized tendons were devoid of DNA yet retained important biochemical and biomechanical properties. The decellularized tendons we produced can support *in vitro* and *in vivo* cell viability and tissue formation. In addition, the produced decellularized tendons were shown to induce an anti-inflammatory macrophage phenotype.
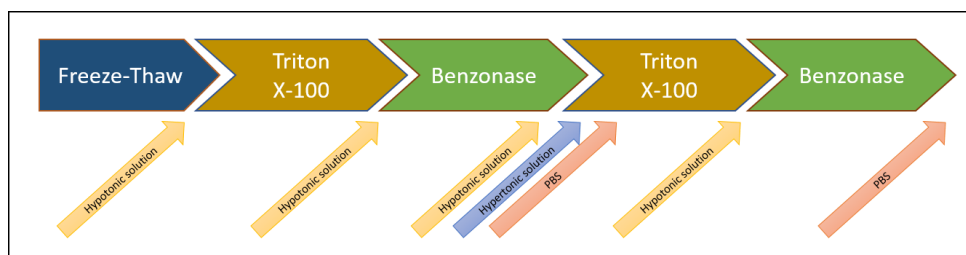
Figure 1. Decellularization protocol. After *freeze-thaw cycles, tissues were incubated with Triton X-100 and Benzonase. In between every step, tissues were washed with hypotonic or hypertonic solutions to achieve cell lysis. The final step consisted of a five-day long washing step of tendons in PBS.*

Results

Gross structure, DNA content and biochemical properties of tendon after decellularization

To evaluate remaining DNA after decellularization, we visualized nuclei in decellularized and native tissue using Hematoxylin & Eosin (H&E) and 4', 6-diamidino-2-phenylindole staining (DAPI). In native tissue sections, we observed nuclei in both H&E (Fig.2A) and DAPI stained sections (Fig.2C).Cells were aligned between the crimp of the collagenous extracellular matrix (ECM) and more densely packed in the endotenon regions (Fig.2A). In decellularized tissue sections, we observed no nuclei

with both stains (Fig.2B, D). Next, we quantified the DNA content of both tissues. Native tendon contained 814 ± 14 ng/mg DNA per tissue dry weight, which was significantly reduced to 34 ± 13 ng/mg (Student t-test, p<0.0001) per tissue dry weight after decellularization, which is below the threshold set by decellularization criteria. Finally, gel electrophoresis demonstrated that in decellularized samples, DNA fragments were not observable; however, high molecular weight DNA was observed in DNA isolated from native tissue (Supplementary Figure S1). Together, we conclude that our novel protocol was successful in decellularization of tendon tissue.

Both tissue structure and biochemical composition should be maintained as much as possible to act as a tissue-instructive scaffold. We noted that the pink colour of ECM coming from eosin staining was lighter in decellularized tissue, indicating loss of ECM proteins. Alcian Blue staining showed glycosaminoglycan (GAG) staining in native tendon sections throughout the tissue section, but more pronounced in the endotenon region (Fig.2E). Decellularization resulted in less prevalent staining of GAGs compared to native tendons sections (Fig.2F). Picro Sirius Red Stain was used to stain all collagens in native and decellularized tendon ECM and we observed collagen type I in red, and type III in green under polarized light (Fig.2G, H). We observed a slight colour difference in collagen I and collagen III between native and decellularized tendon. Next, we quantified total GAG and collagen in native and decellularized tendons. Total GAG content was 6.9 ± 0.6 µg/mg and statistically significantly reduced to 3.2 ± 0.2 µg/mg (p<0.0001, student t-test) following decellularization, confirming our histological observations. For the total hydroxyproline content, an indicator of collagen content, of native tendons was 33.0 ± 8.7 µg/mg and increased to 40.9 ± 5.9 µg/mg following decellularization, which was however not statistically significantly different (Student t-test, p>0.05). Here, we conclude that decellularization has no effect on collagen composition and structure in tendon ECM; however, GAG content significantly decreased.

Tendon has a unique tissue structure with bundles of collagen fibres aligned along the tissue forming unique crimp structures. We observed a similar crimp pattern of collagen fibre in both native (Fig.3A) and decellularized (Fig.3B) tissues using scanning electron microscopy. At higher magnification, we observed the alignment of collagen fibres along the tissue as shown in figure 3C, D. Biochemical and histological examination thus demonstrates mild effects on the biochemical composition of decellularized tendons, but intact structure.
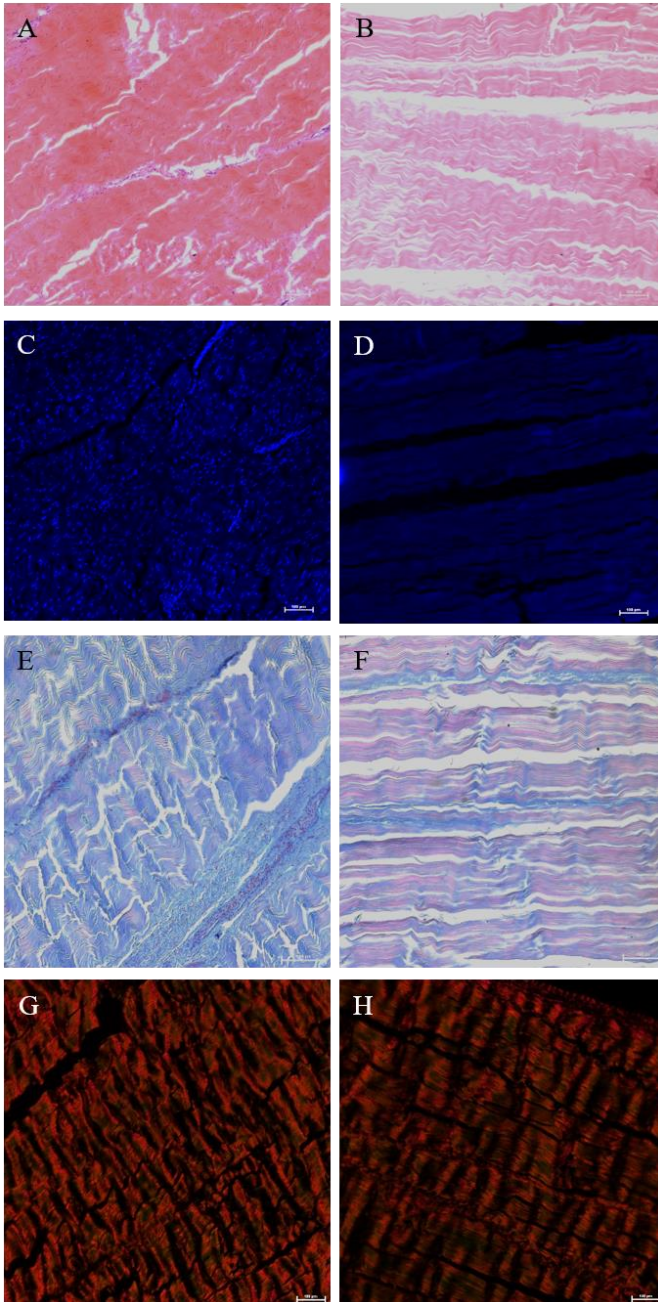
Figure 2. Loss of nuclear components and alterations in tendon composition following decellularization. *Histological sections of native (A, C, E & G) decellularized (B, D, F & H) were stained with nuclear stainings H&E (A,B) and DAPI (C,D), alcian blue staining (E,F) for GAGs and picro sirius red stain (G,H) for collagen type I and type III. In nuclear stainings, no nuclei are observed on decellularized sections (B, D). In native sections, nuclei are observed in H&E staining (purple) (A) and blue colour in DAPI staining (blue) (C). In alcian blue stain, GAGs are stained in blue and nuclei are stained in pink/red colour. In native tendon (E), GAGs and nucleus staining is visible. However, decellularization results in a visible colour change of GAGs and no nuclei are observed (F). Picro sirius red staining, which dyes type I collagen red and type III in green exhibit a slight colour change after decellularization (G, H). Scale bar indicates 100µm.*

Mechanical properties of tendon after decellularization

To assess the mechanical properties after decellularization we subjected decellularized and native tendon tissues to uniaxial tensile testing in a biodynamic chamber in which samples were incubated in PBS during the whole test period (Supplementary figure 2). Both ends of the samples were embedded in epoxy resin to limit slippage from the clamps during tensile testing (S2. C-E). Unfortunately, slippage was still observed at high strains and samples were thus not tested completely until failure. The stress-strain plots revealed a discrepancy (S2. F,G) between the decellularized (DPT) and native (NTP) group, likely due to sample deformation upon re-hydration. Primarily this resulted in varying toe regions (S2. F,G) between samples. Still, all stress-strain curves displayed a linear region, devoid of slippage, the elastic moduli could be quantified. The elastic modulus of the NPT group (22.1 ± 12.0 MPa) was significantly higher ($p < 0.05$, Welch test) compared to the DPT group (9.2 ± 10.2 MPa) (S2. H).
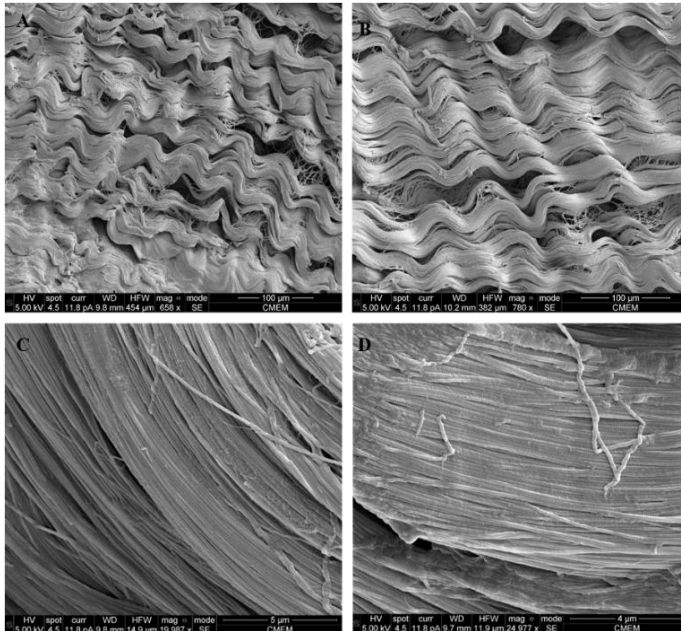
Figure 3. Preserved tissue ultrastructure. *SEM micrographs of native (A, C) and decellularized (B, D) tendon sections. At lower magnifications, similar crimp patterning on native (A) and decellularized (B) tissue is observed. Similarly, at higher magnifications (C, D) alignment of collagen fibers was reserved after decellularization (D).*

Decellularized tendons are cytocompatible

To assess *in vitro* cytocompatibility of decellularized tendons, we seeded hMSCs on decellularized tendon sections and measured the release of lactose dehydrogenase 24 hours after seeding (Fig.4). Cells cultured in tissue culture plastic in basic medium were used as a negative control, and as a positive control, we added lysis buffer to cells cultured on tissue culture plastic. LDH release was significantly different between positive control and negative control, whereas no significant difference between

negative control and hMSCs cultured on decellularized tendon sections was observed (Fig.4A). Here, we conclude that decellularized tendon sections do not have a noticeable cytotoxic effect.

To further investigate cell viability, we cultured hMSCs on decellularized tendon sections for 6 hours, 1, 3 and 7 days and labelled live cells with calcein and dead cells with ethidium bromide (Fig.4B). After 6 hours, we observed attachment of hMSCS to decellularized tendon sections with very few dead cells (Fig.4B). At later time points, cells displayed a high rate of proliferation and were viable (Fig.4B). We observed only a few dead cells in all replicates for each time point. Interestingly, calcein stain showed that even at the earliest time point (6 hours) cells aligned along the tissue (Fig. 4B).
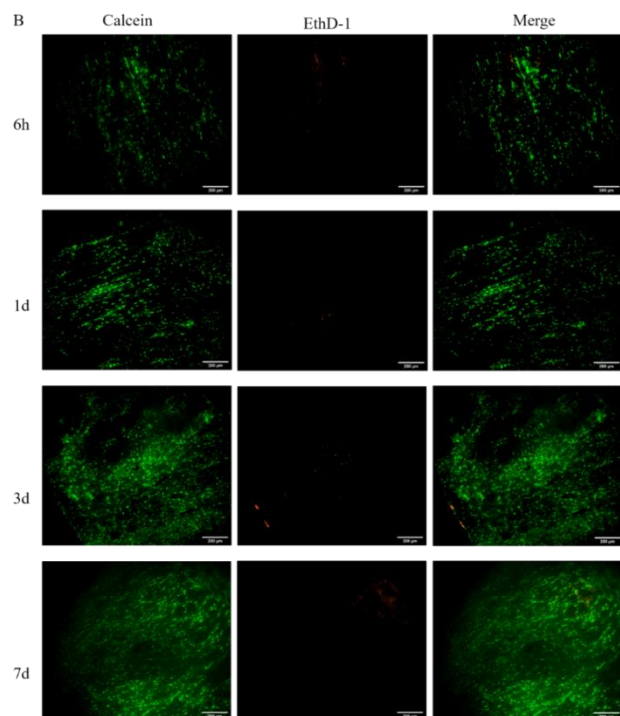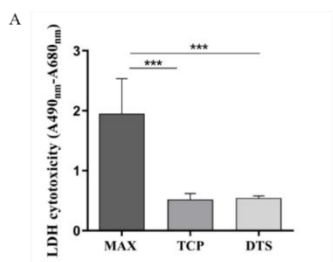
Figure 4. Induction of cell viability of decellularized tendon sections (A) Absorbance measurement of LDH release. hMSCs cultivated on decellularized tendon sections released the same amount of LDH with hMSCs cultivated on tissue culture plate with the basic medium. (B) Fluorescence microscopy images of hMSCs cultured on the 300µm thick of decellularized tendon sections at 6 hours, 1 day, 3 days, and 7 days stained with LIVE/DEAD stain. Live cells stained in green (calcein AM) and dead cells stained in red (EthD-1). At early time points (6 hours) cellular attachment started and over 7 days, a high percentage of viable cells with very few dead cells are observed. Scale bar indicates 100µm. (MAX=maximum LDH release, TCP=Tissue culture plate, DTS=Decellularized tendon section. (***indicates a p-value of<0.001)

Decellularized tendon sections induce a tenocyte-like morphology and support differentiation of hMSCs towards tenogenic lineage

To study the effect of decellularized tendon sections on tenogenic differentiation, we investigated morphology and gene expression of hMSCs for 7 days. At day 1, both nuclei (blue) and cytoskeleton (red) of hMSCs started to align between collagen fibres and took the shape of collagen crimps (Fig.5A). From day 1 to day 4, we observed an increase in the number of cells, while cells retained an elongated shape (Fig.5A). Nuclear aspect ratio at day 1 (1.67 ± 0.41) significantly increased to 1.91 ± 0.96 at day 4 (p<0.05, student t-test). At day 7, the surface of decellularized tendon section was covered with elongated hMSCs (Fig. 5A) and nuclear aspect ratio (1.89 ± 0.59) remained similar to day 4 . Additionally, the orientation of the cellular stress fiber network of the hMSCs was calculated. At day 1 and day 4, stress fibers displayed a strong anisotropy -18.26 ± 13.62° at day 1 and -20.37 ± 10.74 ° at day 4 and strickly followed the collagen fiber direction (S3. D,E) At day 7, orientation of the cellular stress fiber network was -6.68 ± 8.75 ° (S3. F).

To investigate the effect of the decellularized tendon on the expression of tenogenic marker genes, hMSCs were cultured on the decellularized tendon and at day 1, day 4 and day 7 qPCR was performed on the following genes: *SCX, TNMD, MKX, EGR-1 and COL1A1*(Fig.5B-F). As control surfaces, tissue culture plastic was left uncoated (TCP) or coated with rat tail collagen type I (CC). Expression of *SCX*, which is a tenocyte specific transcription factor, was significantly upregulated on decellularized tendon sections (DTS) compared to TCP conditions at day 1, but similar at day 4 and day 7 (Fig. 5B). Expression of *TNMD*, which is a mature tenocyte marker, was statistically upregulated at day 1 in DTS conditions compared to TCP and significantly upregulated compared to CC and TCP at day 4 (Fig. 5C). However, at day 7, *TNMD* expression decreased and was similar to CC and DTS conditions. *MKX*, a transcription factor which controls tenocyte differentiation and cell homeostasis, was significantly upregulated in CC condition compared to TCP and DPT at day 1 and significantly upregulated in CC conditions competed to DTS day 7 (Fig. 5D). *EGR-1* is a zinc finger transcription factor early growth response 1 and was shown it involve in the differentiation of stem cells towards tenogenic lineage. Expression of *EGR-1* (Fig. 5E) was not changed over the 7 days in hMSCs cultured on DTS and reduced in TCP. *COL1A1* is one of the main ECM genes expressed in tenocytes, and its expression did not show a significant change for 7 days in DTS condition yet its expression was significantly downregulated compared to the CC condition at day 1 and day 4 (Fig. 5E). Based on these results, we can conclude that culturing hMSCs on DPTs improved

tenogenic differentiation, especially when compared to tissue culture plastic at early time points.
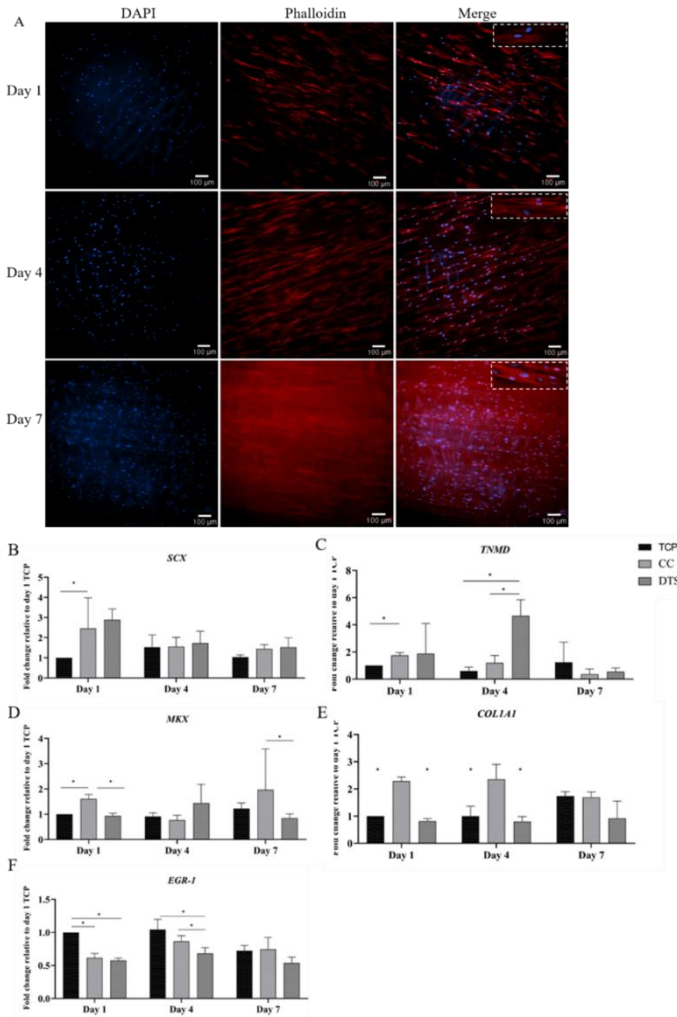
Figure 5. Promotion of tenogenic phenotype and differentiation on decellularized tendon sections *(A) Fluorescence microscopy images of hMSCs cultured on the 300µm thick of decellularized tendon sections at 1 day, 3 days, and 7 days stained with DAPI (nuclei, blue) and Phalloidin-AF488 (F-actin, red). At day 1, nuclei and cytoskeleton of hMSCs adopted the direction of the collagen fibres. At day 4, cells proliferated and aligned between collagen fibres. At day 7, cell kept proliferating and covered the surface of decellularized tendon section. Scale bar indicates 100µm. (B-F) Tendon-related gene expression of hMSCs cultured on TCP, CC and DTS. Expression of SCX was significantly increased at day 1, gradually decreased at DTS condition, and was stable under CC and TCP conditions. (B) Expression of TNMD at day 4 compared to TCP and CC but reduced at day 7. (D) Expression of MKX was significantly higher at day 4 in CC compared to TCP and DTS and showed a similar expression profile at day 7. (E) Expression of COL1A1 was significantly higher at day 1 and day 4 in CC condition compared to CC and DTS. (F) Expression of EGR-1 was highest day day 1 and day 4 but reduced at day 7. In DPT and CC conditions, expression of EGR-1 remained same. Relative gene expression was calculated by normalizing the data to TCP day 1, using 18SRNA as a*

housekeeping gene. (TCP=Tissue culture plate, CC=Collagen coated surface, DTS=Decellularized tendon section). (*indicates a p-value of <0.05, ** indicates a p-value of <0.01).

Decellularized tendons induce anti-inflammatory phenotype in macrophages

Assessment of macrophage polarization towards pro- or anti-inflammatory phenotype is another aspect for the characterization of decellularized tendons. We differentiated the THP-1 macrophage cell line into M_0 macrophages, Then, we either exposed M_0 macrophages with IFNγ and LPS to polarize them towards an M_1 (pro-inflammatory) phenotype, or with IL-4 to polarize them into M_2 (anti-inflammatory) phenotype, and used these cells as positive controls for macrophage polarization. In order to assess the response of M_0 macrophages to decellularized tendons, we cultured them on DTSs for 24 hours (M_{DPT}) and calculated the fold changes relative to M_0 (Fig.6). *MCP-1, CD68, CCR7, TNF-a* and *IL-6* were significantly less in both M_2, M_{DPT} and M_0 groups compared to M_1 (Fig. 6A). On the other side, expression of anti-inflammatory markers *CD200R1, CD206, CD163* and *IL-10* in the M_{DPT} group showed similar expression profile with those in M_2 group (Fig. 6B). Thus, decellularized tendon sections induce an anti-inflammatory (M_2) phenotype in macrophages.
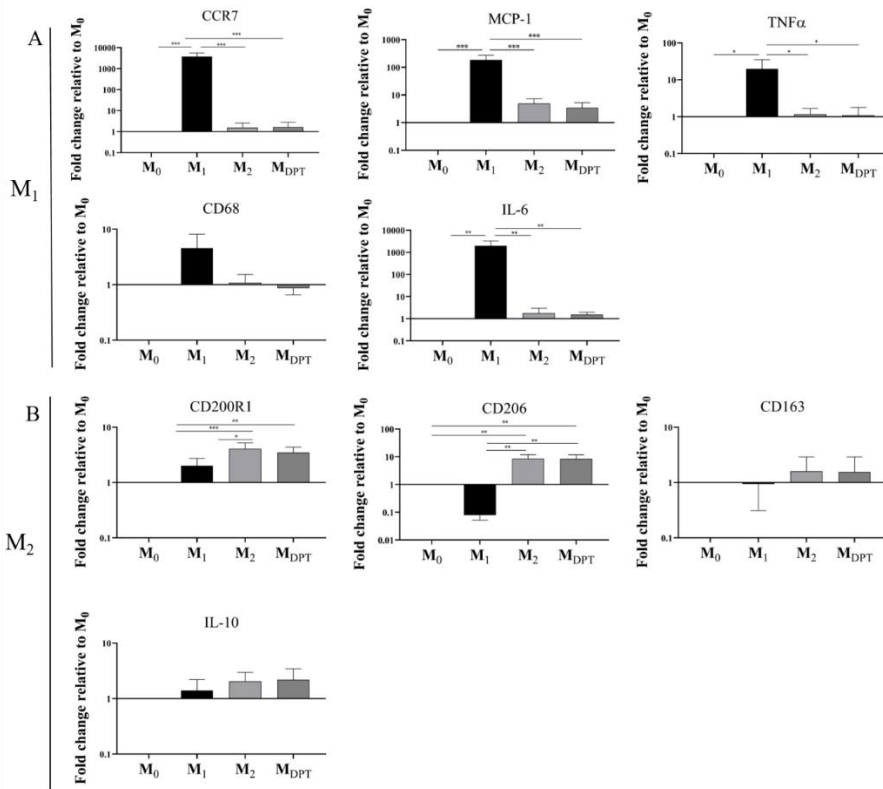
Figure 6. In vitro macrophage polarization of THP-1 cells cultured on decellularized tendon sections for 24 hours. *Gene expression of THP-1 cells treated with IFNγ + LPS (pro-inflammatory, M_1), IL-4 (anti-inflammatory, M_2), DPT (M_{DPT}) and M_0 to assess the expression of pro-inflammatory marker genes MCP-1, CD68, CCR7, TNF-a and IL-6. (A) Expression of M_1 marker genes is significantly higher in both M_2 and M_{DPT} indicating that M_{DPT} does not induce a pro-inflammatory phenotype. (B) Expression of CD206 and CD200R1 is significantly higher for both marker genes in groups M_2 and M_{DPT} compared to M_1 and M_0 indicating that M_{DPT} induces an anti-inflammatory phenotype. Relative gene expression was calculated by normalizing the data to M_0 values, using GAPDH as a housekeeping gene. (* indicates a p-value of <0.05, ** indicates a p-value of <0.01, *** indicates a p-value of <0.001).*

Decellularized tendon induces efficient tissue formation *in vivo*

We investigated the *in vivo* performance of decellularized tendons (DT) by implanting them into a 10 × 3 mm rabbit patellar tendon defect. As a control group, we implanted autologous tendon (AT) from one knee into the defect that we created (Supplementary figure 2). After 6 weeks, we collected tissues and stained them with H&E (Fig.7A, D), Pico Sirius red (Fig.7B, E) and Alcian blue (Fig.7D, F) to histologically examine the

response of the host to implants in terms of cellularity and collagen fibre organization. In general, our results indicated no tissue rejection or encapsulation and the interphase between the implant and host tissue was not clear. H&E and Alcian blue staining of DT indicated cellular infiltration from the host (Fig.7A, C). Based on cell shape, we propose that these cells are tenocytes located between collagen fibres, aligned in the loading direction. In addition, the shape of the cells that repopulated the decellularized tendons, displayed an elongated shape similar to that of the host cells. Moreover, the presence of blood vessels was not observed. Sirius red staining which gives type I collagen a red colour and a green colour to type III collagen under polarized light demonstrated that both at the host (H), DT and AT, the main type of collagen is type I (Fig.7B, E). Alcian blue staining (Fig.7C, F) showed GAGs was recovered in decellularized tendon tissue after implantation. To conclude, our results indicate that GAGs, which are lost after decellularization, are restored and implanted tissue is repopulated with host cells.
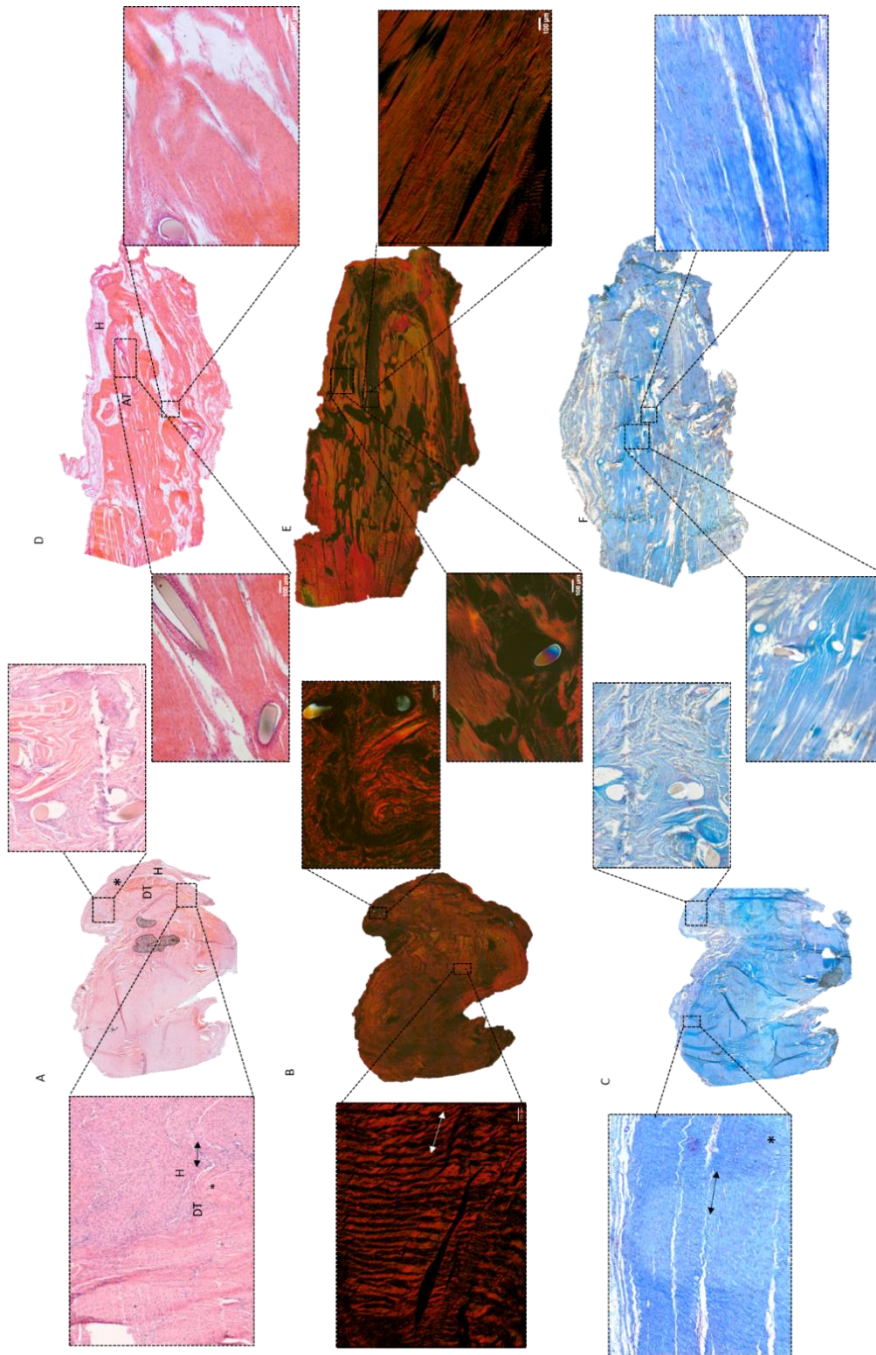
Figure 7. In vivo performance of decellularized tendon in rabbit patellar tendon at 6 weeks after surgery. *(A-F) Histological evaluations of H&E stained decellularized tendon (DT) with autologous patellar tendon transplantation from the contralateral leg (AT) as control. (A-*

C) H&E, picro sirius red (collagen staining) and alcian blue staining (GAG staining) of DT implanted tendon show that decellularized tendons are invaded by host (H) tenocytes. Both tenocytes and collagen fibres aligned towards the loading direction (A&C). Pico Sirius red staining is imaged with polarized light under which collagen type I is observed in red, collagen type II is observed in green. Staining results indicate that at the meeting point of host and DT, collagen remodelling is ongoing and collagen type I is dominating the collagenous part of the ECM (B). (D-F) H&E picro sirius red and alcian blue stainings of AT tendon show that implanted tendon is capable of bearing mechanical loads. (D&F). Scale bar indicates 100μm. Arrows indicate the loading direction, asterisks indicate tenocytes and boxes indicate randomly selected areas to be magnified for viewing cells and suture sites. Dashed circles represent incision sites. (DT=Decellularized tendon, H=Host, AT= Autologous tendon)

Discussion

Criteria of biological materials to be used in clinics have been described in a number of official documents. For instance, according to American Food and Drug Administration (FDA) "Regulatory Considerations for Human Cells, Tissues, and Cellular and Tissue-Based Products: Minimal Manipulation and Homologous Use" regulations, transplanted tissue should be able to perform basic functions of replaced tissue. Furthermore, European Union Commission Regulation number 722/2012 states many rules such as reduction, elimination or removal of infectious agents, risk analysis and risk management, slaughtering and processing controls, the contact area, its the surface type for the use of animal source products as medical devices [41]. In the light of these, engineered animal tissues or derivatives to be used as graft material should induce host cell migration and infiltration, should be sterile and be able to bear the mechanical forces that replaced tissue is exposed to after implantation. For many years, natural ECM derived from different tissues or organs have been successfully used in the clinic. For instance, allogenic bone grafts have been used by surgeons for the past 50 years and the demineralized bone matrix is a readily available and popular form of bone graft substitute [42,43]. Similarly, *in situ* tissue engineering approaches have been used in the clinic for the reconstruction of several tissues including the larynx, and for trachea and finger reconstructions [44,45]. Xenogenic source tissues such as porcine small intestinal submucosa or bovine dermis, but not tendon itself, are used as reinforcements in tendon-related orthopaedics [46]. In this manuscript, we engineered a decellularized porcine tendon and propose that it can be clinically applied for tendon replacement or repair.

Our decellularization protocol, using a combination of physical, chemical and enzymatic methods, enabled decellularization of tendon and did not grossly affect tissue structure

although its biochemical composition changed slightly due to the decellularization procedure. Similar results have been described in the literature, where it is stated that decellularization alters both mechanical and biochemical properties of decellularized tissues such as tendons and aortic valves [21,47]. Based on the results of *in vivo* experiments, we can claim that there's no rejection or encapsulation of implanted tissue, and decellularized tissue is re-populated with host cells and biochemical properties are recovered after implantation. In line with this, it has been reported that the *in vitro* macrophage response to implanted materials is strongly correlated with tissue remodelling outcome. Thus, macrophage polarization assays in the characterization of the materials to be used in clinics is highly convenient to predict the host response to the material [48,49]. We tested the influence of decellularized tendon sections on macrophage polarization *in vitro* and we observed that decellularized tendon sections induced an M_2 phenotype, which is a regulatory, alternatively activated, anti-inflammatory phenotype which is favourable for tissue remodelling [14,50]. Supporting this result, Keane *et al* showed that decellularized porcine small intestinal ECM showed smaller M_1/M_2 ratio [39]. This is supported by our histological data in which we observe that GAG staining, which was reduced after decellularization, recovered to normal levels after 6 weeks. The different structure that we observe between host tendon and decellularized tendon might result from the fact that two different animals (porcine versus rabbit) and different tendons (Achilles versus patellar tendon) were used. Another outstanding question regarding the mechanical stability and strength of the decellularized tendon is the durability of the suture points, as one of the main reasons for the failure of current techniques is overloaded sutures [51]. We can claim that, as after 6 weeks of implantation tissue was still intact, it will endure longer time points and integrate with the whole tissue, in other words, the interface between the host and implanted tissue can hardly be recognized, which is an indicator for proper integration and likely mechanical integrity.

In order to preserve mechanical and biochemical properties, our decellularization strategy can be optimized in terms of time or methods used such as enzymes or detergents, or the size of the tendon to be decellularized. Not all tendon injuries require a whole tendon replacement; it could be a segmental defect or a tendon tear, hence the graft material needed for repair is different. Another challenge in tendon repair with a graft is that although surgery is an option, there's no gold standard to be used as xenogenic graft material [4,52–54] Especially, the repair of rotator cuff (RC) injuries is a particular challenge as surgery often includes removal of the biceps tendon that otherwise gets impinged. Dermal grafts are mainly used in RC surgeries for preventing impingement but not for repair [55]. As the risk of injuring rotator cuff tendon increases with ageing and given the current treatment methods, a new strategy can be implemented [56,57]. Considering this, our method can be implemented to

decellularization of bone-tendon grafts for RC reconstructions or decellularization of other connective tissues such as anterior cruciate ligament (ACL) for ACL reconstructions. In parallel to this, our research group also applied the same protocol for bone-patellar tendon-bone (BPTB) decellularization to create a graft material for ACL reconstruction.

In vitro assessment on bioactivity performance of decellularized tendon showed that they were not cytotoxic, allowed attachment and proliferation and induced tenogenic differentiation of hMSCs. However, we did not observe cell infiltration on day 7, which is one of the challenges of recellularization of the decellularized tendon owing to its dense structure [47]. *In vivo* results showed that within 6 weeks, the decellularized tendon was repopulated with host cells. Repopulation after *in vivo* implantation can be explained by the exposure the mechanical stimulation. Here, we can speculate that as mechanical forces stimulated tendon fibroblasts, more cells from the host were attracted to the new, empty scaffold.. The infiltrated cells had an elongated shape and oriented in the axis of mechanical stimulation. Gene expression results also confirmed that *in vitro,* decellularized tendons induce an upregulation in the early tenogenic marker *SCX and mature tenocyte marker TNMD.*Collagen type I is the main collagen type in tendon ECM.Cultivating mesenchymal stem cells on decellularized tendon sections resulted in stable gene expression of collagen type I for 7 days *in vitro.* This results can be explained by the fact that not only a collagen-rich environment but also an aligned collagen fibre structure in DTS may decrease collagen I synthesis. In agreement with these results, Yang *et al* demonstrated that expression of *COL1A* remains similar in a 2D and 3D collagen enriched environments, whereas a tendon ECM and non-collagen coated 2D environment results in higher expression [58]. This indicates that decellularized tendons carry enough biochemical and topographical ECM cues to stem cells cultivated on them.

In translation perspective, there are two questions to be addressed before we can use the decellularized tendon clinically: 1) which animal model and which tendon tissue should we use to demonstrate efficacy of the tendon graft? In our study, we selected rabbit patellar tendon owing to its similarity with human patellar tendon in terms of mechanical loading. However, sheep could be a better animal model based on closer biomechanical and mechanical properties to human [51,59]. Porcine is another candidate as the healing process is similar to humans [60]. 2) What is the method to map the usability of the product and reduce the cost? This requires collaboration and coordination between research laboratories and clinics. Also, targeting the particular problem for each tendon and designing experimental approaches based on that would increase the efficiency, reduce cost and likelihood of failures. In commercialization perspective, tendon grafts are challenging for several reasons. In order to completely replace a ruptured tendon, decellularized tendon graft must be able to bear very large and

impulsive forces and stresses during even modest activities of daily living. Considering this, repair of each injury in particular tendon tissue could be unique; hence it is difficult to propose one model of the decellularized tendon as a general graft. However, in terms of augmenting repairs and replacements, it is less challenging as scaffold does not need to resist such large mechanical loads from bone to muscle. Therefore, depending on the need of repairing the injury, our method can be optimized and applied.

While with this study we characterized decellularized tendons extensively for its potential use for tendon tissue repair, we will first focus on pre-clinical efficiency. Production of a pain-free, functional tendon is the prime target, so animal behaviour such as gait pattern in the knees can be monitored right from the moment of implantation. In addition to this, in order to get more insight on the time needed for the graft to fully integrate with the host animal, longer time points such as 2 months, 6 months and 12 months need to be monitored.

Conclusion

In this study, we produced a simple but robust protocol to decellularize porcine Achilles tendon and characterized it in many aspects that can be used not only in the characterization of decellularized tissues but also any biological material. We demonstrate that decellularized tendons support stem cell proliferation, induce early tenogenic differentiation and induce macrophages towards a tissue remodelling phenotype. Furthermore, *in vivo* experiments showed that 6 weeks after implantation, decellularized tendons integrate with host tendon without showing signs of tissue rejection or encapsulation. These findings are essential in terms of standardization of not only the decellularized tendons but also tendon-bone or bone-ligament-bone sections in the reconstruction of musculoskeletal defects.

Materials and Methods

Tissue harvest and storage

Porcine Achilles tendons were obtained from crossbreeds of Great Yorkshire and Dutch land pigs aged between 6-8 months old and between 85-95 kg of weight (Compaxo Meat B.V, the Netherlands). Achilles' tendons were transported under conditioned circumstances (4°C) in sealed plastic bags within 24 hours of slaughter. Muscle, fat, bone-like tissues, synovial sheath, and para-tenon were aseptically dissected and the remaining tendon was cut into 4-cm segments and stored at -80°C until further processing.

Preparation of decellularized tendon slices

Frozen tendons were cut into 2-3 cm long sections and freeze-thawed five times in liquid nitrogen and 37°C phosphate buffered saline (PBS) (Sigma-Aldrich), respectively,

then incubated for 48 hours in distilled water at room temperature. Next, samples were incubated in Tris-EDTA (VWR) buffer (pH 7.6) containing 1% Triton 100-X (VWR) for 48 hours at room temperature. After another 24 of wash in distilled water at room temperature, samples were incubated in Benzonase (2U/ml) (Sigma-Aldrich) in 50mM Tris / 1mM MgCl$_2$ (Sigma-Aldrich) at pH 7.6 for 24 hours at 37°C. This step is followed by 30 minutes wash in distilled water at room temperature, 3 hours incubation in 2.7mM EDTA pH 7.6 at 37°C, and 50mM Tris /1.5M NaCl (VWR) (pH 7.6) overnight incubation at room temperature. Next day, samples were incubated in PBS for 30 minutes and 70% ethanol (EtOH) prepared in PBS at room temperature. This was followed by 72 hours of incubation in PBS. Next, samples were incubated in Tris-EDTA buffer pH 7.6 containing 1% Triton 100-X for 48 hours at room temperature, washed in distilled water at room temperature for 24 hours, incubated in Benzonase (2U/ml) in 50mM Tris plus 1mM MgCl2 at pH 7.6 for 24 hours at 37°C and finally washed in PBS at 4°C for 5 days. Figure 1 summarizes the decellularization protocol. Samples were incubated on a rotator shaker, 40 mL solutions were used changed every day unless stated otherwise. Samples are stored at -80°C until further usage.

Determination of total DNA content

DNA in decellularized (N=6) and native samples (N=6) was measured with CyQUANT™ Cell Proliferation Assay Kit (Thermo Fisher Scientific). Briefly, frozen tendons were thawn to room temperature and cut into smaller pieces. Next, samples were freeze-dried for at least 24 hours at -55°C and frozen again in liquid nitrogen. Next, 10 mg samples were lysed with Proteinase K (Sigma-Aldrich) in Tris/EDTA buffer at a final concentration of 1 mg/ml for 48 hours at 56°C. 100 µl digested DNA sample and 400 µl of cell lysis buffer at 0.01 mg/ml final concentration were mixed and incubated at room temperature for one hour. Finally, 100 µl of each sample and DNA standards (4 µg/ml, 2 µg/ml 1 µg/ml, 0.5 µg/ml, 0.25 µg/ml and 0 µg/ml dilution) were transferred into a 96 well plate and mixed with 100 µl 2x GR-dye solution. Samples were incubated for 15 minutes in the dark and fluorescence at emission wavelength 520 nm, excitation 480 nm was measured. Data were normalized to scaffold dry weight, obtained prior to digestion. To determine the remaining DNA fragment size, 2 µg of extracted DNA from each sample were loaded onto a 2% agarose gel (Thermo Fisher Scientific) containing SYBR Safe DNA gel stain (Thermo Fisher Scientific) and visualized with Biorad-ChemidocTM MP imaging system using the 1 Kb Plus DNA Ladder (Thermo Fisher Scientific) as a reference.

Determination of collagen content

The total collagen content of decellularized (N=3) and native samples (N=3) was measured using the Hydroxyproline Assay Kit (Sigma-Aldrich). Briefly, frozen tendons were freeze-dried for at least 24 hours at -55°C. Next, samples were cut into a constant

weight and hydrolyzed in 4M HCl for 4 hours at 120°C. 10μl of each sample was transferred to a 96-well plate and evaporated under vacuum overnight. Next, 100μl of the Chloramine T/Oxidation Buffer Mixture was added to each sample and standards and incubated at room temperature for 5 minutes. Next, 100μl of the Diluted DMAB Reagent was added to each sample and standards and incubated for 90 minutes at 60°C. Absorbance was measured at 560 nm. Readings were corrected by subtracting the blank value from all readings. The amount of hydroxyproline present in the samples was calculated based on the standard curve. Data were normalized to scaffold dry weight, obtained prior to digestion.

Determination of glycosaminoglycan content

Glycosaminoglycan content of decellularized (N=3) and native samples (N=3) was measured using the dimethylene blue (DMMB) assay. Briefly, frozen tendons were cut into smaller pieces and freeze-dried for at least 24 hours at -55°C. Samples were cut into a constant weight and digested in papain (Sigma-Aldrich) digestion buffer [140 μg per ml in 5 mM L-cysteine hydrochloride (Sigma-Aldrich) plus 5mM Na_2EDTA (VWR)] for 16 hours at 60°C with agitation. 40μl of standards (chondroitin sulfate sodium salt from shark cartilage (Sigma, C4384)) and test samples were transferred to 96-well plate and mixed with 150 μl of 1,9-dimethylene blue solution (DMMB) and incubated 2 minutes at room temperature. Absorbance was measured sequentially at wavelengths 540 nm and 595 nm and the readings were subtracted one another (540-595). Concentrations of the samples were calculated based on the data from the standard curve. Data were normalized to scaffold dry weight, obtained prior to digestion.

Histology and immunohistochemistry

Decellularized and native samples were fixed in 10% (v/v) neutral buffered formalin (Sigma-Aldrich) for 48 hours at room temperature. Next, samples were incubated in 70% ethanol for 1 hour, 95% ethanol for another hour and in absolute ethanol for 4 hours. Then, samples were twice incubated in Xylene for 1 hour. Finally, samples were embedded in Paraplast X-TRA (Sigma Aldrich) at 58°C for 1 hour, twice and incubated at room temperature. Embedded samples were sectioned at 10 μm thickness by using a microtome.

Hematoxylin & eosin and DAPI staining

Sections of native and decellularized tissues were deparaffinized in Histo Clear (Baker), decreasing ethanol series and finally incubated in distilled water for 4 minutes each. Next, samples were incubated in Weigert's iron hematoxylin solution (Sigma-Aldrich) for 1 minute, washed in tap water and distilled water for 3 minutes, incubated in eosin (Sigma-Aldrich) for 30 seconds, and washed again. Finally, samples were dehydrated in increasing series of ethanol, Histo Clear and mounted in DPX mounting medium

(Sigma Aldrich). For DAPI staining, after deparaffinization, the samples were incubated with 4',6-diamidino-2-phenylindole dihydrochloride (DAPI) (Sigma-Aldrich) for 5 minutes, dehydrated and mounted.

Alcian blue stain

Alcian blue was used to stain glycosaminoglycans. Briefly, sections of native and decellularized tissues were deparaffinized in Histo Clear (Baker), decreasing ethanol series and finally incubated in distilled water for 4 minutes each. Next, sections were incubated in 3% acetic acid solution (VWR) before they have incubated in 1% Alcian blue solution [Alcian Blue-8GX (Sigma Aldrich) dissolved in 3% Acetic Acid] for 30 minutes at room temperature. After rinsing in 3% acetic acid, tap water, and distilled water, sections were stained with 0. 1% Nuclear Fast Red Solution for 5 minutes, dehydrated in increasing series of ethanol, Histo Clear (Sigma Aldrich) and mounted in DPX mounting medium (Sigma Aldrich).

Picro Sirius Red stain

Picro Sirius Red Stain Kit (Connective Tissue Stain) (Abcam) was used to stain collagen. Briefly, sections of native and decellularized tissues were deparaffinized in Histo Clear (Baker), decreasing ethanol series and finally incubated in distilled water for 4 minutes in each. Next, samples were incubated in Picro-Sirius Red Solution for one hour. Then, tissue sections were rinsed in 0.5% acetic acid twice and rinsed in absolute ethanol. Finally, sections were dehydrated in increasing series of ethanol, Histo Clear (Sigma Aldrich) and mounted in DPX mounting medium (Sigma Aldrich).

Scanning Electron Microscopy

Samples were fixed in 2% glutaraldehyde (Fisher Scientific) in 0.1M sodium cacodylate trihydrate (Sigma-Aldrich) buffer prepared in PBS pH 7.4 at room temperature for one hour. Next, samples were washed with 0.1M sodium cacodylate trihydrate buffer for 3 times 10 minutes and dehydrated in 25%, 50%, 75%, 90%, and 100% EtOH for 15 minutes each and incubated in 100% ethanol for additional 15 minutes. Next, samples were dried in hexamethyldisilazane (HMDS) (Sigma Aldrich) overnight and covered with 5 nm gold-palladium and imaged using a scanning electron microscope (FEI Quanta 3D FEG Dual Beam).

Tensile testing of native and decellularized samples

Native (N=2) and decellularized (N=2) tendons were longitudinally cut into 4-6 pieces and imaged using a Nikon SMZ25 stereomicroscope to determine their cross-sectional areas. Tissue ends were embedded in an epoxy resin (Innotec Topfix) to prevent sample slippage from tensile test clamps, often observed due to cross-sectional thinning upon elongation. Upon epoxy curing, samples were incubated in PBS at room temperature overnight and tensile tests were carried out in PBS at room temperature. A TA

Electroforce 3200 mechanical tester with a Biodynamic Chamber accessory (allowing for testing in fluid environments) was used to conduct the tests. A 450 N load cell was used. Samples were elongated at 1% strain/s (mover velocity in mm/sec was adjusted for each sample based on the length of the stretchable part between the resin embedded ends) and the force and the displacement were recorded. The elastic moduli of the samples were determined by calculating the slope of the linear regions of the stress-strain curves, beyond the toe region.

Preparation of tendon sections for cell culture

Frozen decellularized tendons were embedded in Optimal Cutting Temperature (OCT, Sakura) compound and fixed to the cutting base plate of a cryotome and longitudinally sectioned into tendon slices with a thickness of 300 μm and washed with PBS, snap-frozen in liquid nitrogen and freeze-dried for at least 24 hours. Dry decellularized tendon sections were cut into the size of the surface area of a well plate of interest and incubated in 70% ethanol for 1 hour. Remaining ethanol was removed and samples were dried in sterile conditions. Next, samples were washed in sterile PBS for two times, half an hour at room temperature, and one time at 37°C for half an hour. The day before the experiment started, samples were incubated in culture media, overnight at 37°C in 5% CO_2.

Cell culture, viability and cytotoxicity assay

Bone marrow aspirate was obtained from a donor (D210, female/74 years old) who were undergoing total hip replacement surgery and had given informed consent. Nucleated cells were counted from the aspirate and seeded at a density of 500 000 cells cm^{-2} in hMSC proliferation medium consisting Minimal Essential Media alpha (α-MEM) containing (Thermo Fisher Scientific) 10% fetal bovine serum (FBS) (Sigma-Aldrich), 100 U/ml Penicillin/Streptomycin (Thermo Fisher Scientific), and 20 mM L-Ascorbic acid with an additional 1 ng mL^{-1} basic fibroblast growth factor (Neuromics) at 37°C in a humidified tissue culture chamber with 5% CO_2. The hMSCs obtained after the first trypsinization (Trypsin-EDTA (0.05%), Fisher Scientific) were seeded at a density of $2x10^5$ cells/cm^2 in Minimal Essential Media alpha (α-MEM) containing (Thermo Fisher Scientific) 10% fetal bovine serum (FBS) (Sigma-Aldrich), 100 U/ml Penicillin/Streptomycin (Thermo Fisher Scientific), and 20 mM L-Ascorbic acid at 37°C in a humidified tissue culture chamber with 5% CO_2. Cell viability was qualitatively assessed for a week (6 hours, 1 day, 4 days and 7 days) with LIVE/DEAD™ Viability/Cytotoxicity Kit (Thermo Fisher Scientific) assay. Briefly, cell-seeded tendon sections were washed with PBS two times and incubated in 2 μM Calcein AM and 6 μM ethidium homodimer (EthD-1) in serum-free α-MEM with nucleosides and without phenol red (Thermo Fisher Scientific) for 30 minutes at 37°C in the dark and washed with the medium twice.

Cytotoxicity assay was performed by measuring lactate dehydrogenase (LDH) release using the Pierce LDH Cytotoxicity Assay Kit (Thermo Fisher Scientific). Briefly, hMSCs were cultured on decellularized tendon sections at a density of $2x10^5$ cells/cm² in Minimal Essential Media alpha (α-MEM) (Thermo Fisher Scientific) containing 10% fetal bovine serum (FBS) (Sigma-Aldrich), 100U/ml Penicillin/Streptomycin (Thermo Fisher Scientific), and 20 mM L-Ascorbic acid (ASAP) at 37°C in a humidified tissue culture chamber with 5% CO_2 for 24 hours. Then, to measure the maximum LDH activity, 10X Lysis Buffer was added and incubated at 37°C, 5% CO_2 for 45 minutes. Next, 50µL of each sample medium (cells cultured on basic medium as a negative control, cells cultured on decellularized tendon sections and maximum LDH activity group as a positive control) were transferred to a new well plate and mixed with 50µL of Reaction Mixture, incubated at room temperature for 30 minutes protected from light. Finally, 50µL of Stop Solution was added and absorbance was measured at wavelength 490nm and 680nm. To determine LDH activity, we subtracted the 680nm absorbance value (background) from the 490nm absorbance value. Culture plates were coated with rat tail collagen I (Gibco) based on the vendor's protocol. Briefly, 1 mg/ml of rat tail collagen tail was coated and incubated at 37°C, 5% CO_2 overnight, and wells were washed with PBS three times.

Macrophage culture and polarization

The human monocytic cell line THP-1 (Sigma-Aldrich) was cultured in Roswell Park Memorial Institute (RPMI) 1640 medium (A10491-0, Gibco), supplemented with FBS (10% v/v, Bovogen) and penicillin/streptomycin (1% P/S v/v; Lonza, Basel, Switzerland, DE17-602E) in 37°C, 5% CO_2. In order to induce macrophage differentiation, 300,000 cells/ml were incubated in culture medium with 50 ng/ml of 12-myristate13-acetate (PMA). After 24 hours, adherent macrophages were washed with PBS and incubated in fresh media for 48 hours to acquiesce. Macrophages were cultured for 24 hours in following conditions for further assessment: RPMI medium supplemented with 10% FBS and 1% P/S with 20 ng/ml IFNγ and 100 ng/ml LPS to promote an M_1 phenotype, RPMI medium supplemented with 10% FBS and 1% P/S with 20 ng/ml IL-4 to promote an M_2 phenotype and on decellularized tendon sections with RPMI medium supplemented with 10% FBS and 1% P/S resulting in a M_{DPT} phenotype.

RNA isolation and quantitative PCR (RT-qPCR)

RNA of each sample was isolated with the protocol described in the RNeasy Mini Kit (QIAGEN) or TRIsol™ Reagent. Reverse transcription was carried out based on the protocol provided by iScript™ Select cDNA Synthesis Kit (Bio-Rad). qPCR was performed by using iQ SYBR Green Supermix (Bio-Rad). Briefly, iQ SYBR Green Supermix (2x), forward and reverse primers (at 300nM final concentration), cDNA

(100ng final concentration) and nuclease-free water were mixed for a total of 10 μl reaction volume. qPCR run was performed by using the Bio-Rad CFX manager. The expression of target genes (*MCP-1, CD68, CCR, TNF-a, IL-6 ,CD200R, CD206, CD163 and IL-10*) in macrophage polarization experiments was normalized to glyceraldehyde 3-phosphate dehydrogenase (GAPDH) gene as a housekeeping gene. The expression of target genes (*SCX, COL1A1, TNMD, MKX*) in tenogenic differentiation was normalized to RNA18S as a housekeeping gene. Relative gene expression was calculated with the ΔΔ Ct formula. Primer sequence of target genesare listed in Table 1.

Sterilization and in vivo biocompatibility of decellularized samples

Animal experiments were performed in the animal centre of Sichuan University with the permission of the local ethics committee for laboratory animal (Sichuan Laboratory Animal Management Committee) and two adult female New Zealand rabbits were used. The rabbits were anaesthetized with intravenous pentobarbital sodium (30 mg/kg) and surgically operated under general sterile condition. A longitudinal incision was made on the knee and the subcutaneous tissue was divided to expose the patellar tendon. A 10 × 3 mm size defect (length × width) was made in the middle third of the tendon. The implant (10 × 3 mm) was bundled up with 4-0 nylon suture at the two ends and was sutured to the host tendon at the four corners using 4-0 nylon suture. Following the implantation, the wound was closed by 4-0 nylon suture. Using the same implantation procedure, the tendon harvested from one knee was bundled and implanted in the other knee of the sampled animal as an autologous control. Penicillin was intramuscularly injected for 3 consecutive days to prevent infection. Six weeks later, the rabbits were sacrificed by intravenous administration of a lethal dose of pentobarbital sodium and the implants were collected with surrounding tissues. The samples harvested were fixed in 10% formalin and subjected to paraffin embedding for histological evaluation.

Image analysis

Aspect ratio of the nuclei was calculated by using ImageJ. Briefly, images were treasholded and analysed by using *Analyze Particles* option for which measurements were selected to *Shape descriptions*. Directionality of actin fibers was measured by using *Directionality* section in the *Analyse* command.

Statistical analysis

All statistical analysis was performed using GraphPad Prism version 8.0 (GraphPad Software, Inc., San Diego, CA). Student's t-test, one-way and two-way analysis of variance (ANOVA) was carried out with significance set at $p < 0.05$ to determine the significance between means. For multiple comparison tests, the Tukey procedure was applied.

References

1. Xu, Y., and Murrell, G.A.C. The basic science of tendinopathy. Clin Orthop Relat Res. **466**, 1528, 2008.

2. Fenwick, S.A., Hazleman, B.L., and Riley, G.P. The vasculature and its role in the damaged and healing tendon. Arthritis Res. **4**, 252, 2002.

3. Docheva, D., Müller, S.A., Majewski, M., and Evans, C.H. Biologics for tendon repair. Adv Drug Deliv Rev . Elsevier B.V., **84**, 222, 2015.

4. Fan, W., Michael, N., and Denitsa, D. Tendon injuries: basic science and new repair proposals. Gen Orthop. **2**, 211, 2017.

5. Kuo, C.K., Marturano, J.E., and Tuan, R.S. Novel strategies in tendon and ligament tissue engineering: Advanced biomaterials and regeneration motifs. Sport Med Arthrosc Rehabil Ther Technol. 1, 2010.

6. Zumstein, M.A., Lädermann, A., Raniga, S., and Schär, M.O. The biology of rotator cuff healing. Orthop Traumatol Surg Res. Elsevier Masson SAS, **103**, S1, 2017.

7. Ricchetti, E.T., Aurora, A., Iannotti, J.P., and Derwin, K.A. Scaffold devices for rotator cuff repair. J Shoulder Elb Surg. Elsevier Ltd, **21**, 251, 2012.

8. Huang, X., Huang, G., Ji, Y., Ao, R.G., Yu, B., and Zhu, Y.L. Augmented Repair of Acute Achilles Tendon Rupture Using an Allograft Tendon Weaving Technique. J Foot Ankle Surg. Elsevier Ltd, **54**, 1004, 2015.

9. Lui, P.P.Y. Tendinopathy in diabetes mellitus patients—Epidemiology, pathogenesis, and management. Scand J Med Sci Sport. **27**, 776, 2017.

10. Lovati, A.B., Bottagisio, M., and Moretti, M. Decellularized and Engineered Tendons as Biological Substitutes: A Critical Review. Stem Cells Int. **2016**, 2016.

11. Cheng, C.W., Solorio, L.D., and Alsberg, E. Decellularized tissue and cell-derived extracellular matrices as scaffolds for orthopaedic tissue engineering. Biotechnol Adv . Elsevier Inc., **32**, 462, 2014.

12. Hampson, K., Forsyth, N., El Haj, A., and Maffulli, N. Tendon Tissue Engineering, chapter 3. Top Tissue Eng vol 4 Eds N Ashammakhi, RReis F Chiellini. **4**, 2008.

13. Moshiri, A., and Oryan, A. Role of tissue engineering in tendon reconstructive surgery and regenerative medicine: Current concepts, approaches and concerns. Hard Tissue. **1**, 1, 2012.

14. Mantovani, A., Biswas, S.K., Galdiero, M.R., Sica, A., and Locati, M. Macrophage plasticity and polarization in tissue repair and remodelling. J Pathol. **229**, 176, 2013.

15. Chen, J., Xu, J., Wang, A., and Zheng, M. Scaffolds for tendon and ligament repair: Review of the efficacy of commercial products. Expert Rev Med Devices. **6**, 61, 2009.

16. Schulze-Tanzil, G., Al-Sadi, O., Ertel, W., and Lohan, A. Decellularized Tendon Extracellular Matrix—A Valuable Approach for Tendon Reconstruction? Cells. **1**, 1010, 2012.

17. Wang, S., Wang, Y., Song, L., Chen, J., Ma, Y., Chen, Y., et al. Decellularized tendon as a prospective scaffold for tendon repair. Mater Sci Eng C. Elsevier B.V., **77**, 1290, 2017.

18. Keane, T.J., Swinehart, I.T., and Badylak, S.F. Methods of tissue decellularization used for preparation of biologic scaffolds and in vivo relevance. Methods. Elsevier Inc., **84**, 25, 2015.

19. Cheng, C.W., Solorio, L.D., and Alsberg, E. Decellularized tissue and cell-derived extracellular matrices as scaffolds for orthopaedic tissue engineering. Biotechnol Adv . Elsevier Inc., **32**, 462, 2014.

20. Parmaksiz, M., Dogan, A., Odabas, S., Elçin, A.E., and Elçin, Y.M. Clinical applications of decellularized extracellular matrices for tissue engineering and regenerative medicine. Biomed Mater. **11**, 2016.

21. Crapo, P.M., Gilbert, T.W., and Badylak, S.F. An overview of tissue and whole organ decellularization processes. Biomaterials. Elsevier Ltd, **32**, 3233, 2011.

22. Commission, T.H.E.E. 9.8.2012. **2012**, 3, 2012.

23. Youngstrom, D.W., Barrett, J.G., Jose, R.R., and Kaplan, D.L. Functional Characterization of Detergent-Decellularized Equine Tendon Extracellular Matrix for Tissue Engineering Applications. PLoS One. **8**, 2013.

24. Roth, S.P., Glauche, S.M., Plenge, A., Erbe, I., Heller, S., and Burk, J. Automated freeze-thaw cycles for decellularization of tendon tissue - a pilot study. BMC Biotechnol. BMC Biotechnology, **17**, 1, 2017.

25. Xing, S., Liu, C., Xu, B., Chen, J., Yin, D., and Zhang, C. Effects of various decellularization methods on histological and biomechanical properties of rabbit tendons. Exp Ther Med. **8**, 628, 2014.

26. Ning, L.J., Zhang, Y., Chen, X.H., Luo, J.C., Li, X.Q., Yang, Z.M., et al. Preparation and characterization of decellularized tendon slices for tendon tissue engineering. J Biomed Mater Res - Part A. **100 A**, 1448, 2012.

27. Deeken, C.R., White, A.K., Bachman, S.L., Ramshaw, B.J., Cleveland, D.S., Loy, T.S., et al. Method of preparing a decellularized porcine tendon using tributyl phosphate. J Biomed Mater Res - Part B Appl Biomater. **96 B**, 199, 2011.

28. Yin, Z., Chen, X., Zhu, T., Hu, J.J., Song, H.X., Shen, W.L., et al. The effect of decellularized matrices on human tendon stem/progenitor cell differentiation

and tendon repair. Acta Biomater. 2013.

29. Balogh, D.G., Biskup, J.J., O'Sullivan, M.G., Scott, R.M., Groschen, D., Evans, R.B., et al. Biochemical, histologic, and biomechanical characterization of native and decellularized flexor tendon specimens harvested from the pelvic limbs of orthopedically normal dogs. Am J Vet Res. **77**, 388, 2016.

30. Cartmell, J.S., and Dunn, M.G. Effect of chemical treatments on tendon cellularity and mechanical properties. J Biomed Mater Res. **49**, 134, 2000.

31. Vavken, P., Joshi, S., and Murray, M.M. TRITON-X is most effective among three decellularization agents for ACL tissue engineering. J Orthop Res. **27**, 1612, 2009.

32. Burk, J., Erbe, I., Berner, D., Kacza, J., Kasper, C., Pfeiffer, B., et al. Freeze-Thaw Cycles Enhance Decellularization of Large Tendons. Tissue Eng Part C Methods. **20**, 276, 2014.

33. Jones, G., Herbert, A., Berry, H., Edwards, J.H., Fisher, J., and Ingham, E. Decellularization and Characterization of Porcine Superflexor Tendon: A Potential Anterior Cruciate Ligament Replacement. Tissue Eng Part A. **23**, 124, 2017.

34. Zhang, J., Li, B., and Wang, J.H.C. The role of engineered tendon matrix in the stemness of tendon stem cells in vitro and the promotion of tendon-like tissue formation in vivo. Biomaterials. Elsevier Ltd, **32**, 6972, 2011.

35. Schmitt, T., Fox, P.M., Woon, C.Y., Farnebo, S.J., Bronstein, J.A., Behn, A., et al. Human flexor tendon tissue engineering: In vivo effects of stem cell reseeding. Plast Reconstr Surg. **132**, 567, 2013.

36. Il Lee, K., Soo Lee, J., Tak Kang, K., Bock Shim, Y., Sik Kim, Y., Woong Jang, J., et al. In Vitro and In Vivo Performance of Tissue-Engineered Tendons for Anterior Cruciate Ligament Reconstruction. Am J Sports Med. 036354651875972, 2018.

37. Omae, H., Yu, L.S., An, K.N., Amadio, P.C., and Zhao, C. Engineered tendon with decellularized xenotendon slices and bone marrow stromal cells: an in vivo animal study. J Tissue Eng Regen Med. 238, 2011.

38. Badylak, S.F. Decellularized allogeneic and xenogeneic tissue as a bioscaffold for regenerative medicine: Factors that influence the host response. Ann Biomed Eng. **42**, 1517, 2014.

39. Keane, T.J., Londono, R., Turner, N.J., and Badylak, S.F. Consequences of ineffective decellularization of biologic scaffolds on the host response. Biomaterials. **33**, 1771, 2012.

40. Schulze-Tanzil, G., Al-Sadi, O., Ertel, W., and Lohan, A. Decellularized Tendon Extracellular Matrix—A Valuable Approach for Tendon Reconstruction? Cells.

1, 1010, 2012.

41.   Zhang, C.-H., Jiang, Y.-L., Ning, L.-J., Li, Q., Fu, W.-L., Zhang, Y.-J., et al. Evaluation of Decellularized Bovine Tendon Sheets for Achilles Tendon Defect Reconstruction in a Rabbit Model. Am J Sports Med. 036354651878751, 2018.

42.   Roberts, T.T., and Rosenbaum, A.J. Bone grafts, bone substitutes and orthobiologics. Organogenesis . **8**, 114, 2012.

43.   Pacaccio, D.J., and Stern, S.F. Demineralized bone matrix: Basic science and clinical applications. Clin Podiatr Med Surg. **22**, 599, 2005.

44.   Omori, K., Tada, Y., Suzuki, T., Nomoto, Y., Matsuzuka, T., Kobayashi, K., et al. Clinical application of in situ tissue engineering using a scaffolding technique for reconstruction of the larynx and trachea. Ann Otol Rhinol Laryngol. **117**, 673, 2008.

45.   Inada, Y., Morimoto, S., Moroi, K., Endo, K., and Nakamura, T. Surgical relief of causalgia with an artificial nerve guide tube: Successful surgical treatment of causalgia (Complex Regional Pain Syndrome Type II) by in situ tissue engineering with a polyglycolic acid-collagen tube. Pain. **117**, 251, 2005.

46.   Parmaksiz, M., Dogan, A., Odabas, S., Elçin, A.E., and Elçin, Y.M. Clinical applications of decellularized extracellular matrices for tissue engineering and regenerative medicine. Biomed Mater. **11**, 2016.

47.   Liao, J., Joyce, E.M., and Sacks, M.S. Effects of decellularization on the mechanical and structural properties of the porcine aortic valve leaflet. Biomaterials. **29**, 1065, 2008.

48.   Brown, B.N., Ratner, B.D., Goodman, S.B., Amar, S., and Badylak, S.F. Macrophage polarization: An opportunity for improved outcomes in biomaterials and regenerative medicine. Biomaterials. Elsevier Ltd, **33**, 3792, 2012.

49.   Brown, B.N., Sicari, B.M., and Badylak, S.F. Rethinking regenerative medicine: A macrophage-centered approach. Front Immunol. **5**, 1, 2014.

50.   Novak, M.L., and Koh, T.J. Macrophage phenotypes during tissue repair. J Leukoc Biol. **93**, 875, 2013.

51.   Shearn, J.T., Kinneberg, K.R.C., Dyment, N.A., Marc, T., Kenter, K., Wylie, C., et al. Tendon Tissue Engineering: Progress, Challenges, and Translation to the Clinic. 2013.

52.   Dickinson, M., and Wilson, S.L. A Critical Review of Regenerative Therapies for Shoulder Rotator Cuff Injuries. SN Compr Clin Med. SN Comprehensive Clinical Medicine, **1**, 205, 2019.

53.   Zheng, Z., Lipman, K., Wang, C., Ting, K., and Soo, C. Tendinopathy: injury, repair, and current exploration. Drug Des Devel Ther. **Volume 12**, 591, 2018.

54. Yang, G., Rothrauff, B.B., and Tuan, R.S. Tendon and Ligament Regeneration and Repair: Clinical Relevance and Developmental Paradigm Guang. **99**, 203, 2014.

55. Wall, K.C., Toth, A.P., and Garrigues, G.E. How to Use a Graft in Irreparable Rotator Cuff Tears: A Literature Review Update of Interposition and Superior Capsule Reconstruction Techniques. Curr Rev Musculoskelet Med. Current Reviews in Musculoskeletal Medicine, **11**, 122, 2018.

56. Wani, Z., Abdulla, M., Habeebullah, A., and Kalogriantis, S. Rotator cuff tears: Review of epidemiology, clinical assessment and operative treatment. Trauma (United Kingdom). **18**, 190, 2016.

57. Yamamoto, A., Takagishi, K., Osawa, T., Yanagawa, T., Nakajima, D., Shitara, H., et al. Prevalence and risk factors of a rotator cuff tear in the general population. J Shoulder Elb Surg . Journal of Shoulder and Elbow Surgery Board of Trustees, **19**, 116, 2010.

58. Yang, G., Rothrauff, B.B., Lin, H., Gottardi, R., Alexander, P.G., and Tuan, R.S. Enhancement of tenogenic differentiation of human adipose stem cells by tendon-derived extracellular matrix. Biomaterials. Elsevier Ltd, **34**, 9295, 2013.

59. Tapper, J.E., Fukushima, S., Azuma, H., Sutherland, C., Marchuk, L., Thornton, G.M., et al. Dynamic in vivo three-dimensional (3D) kinematics of the anterior cruciate ligament/medial collateral ligament transected ovine stifle joint. J Orthop Res. **26**, 660, 2008.

60. Murray, M.M., Magarian, E., Zurakowski, D., Ph, D., and Braden, C. Bone-to-bone Fixation Enhances Functional Healing of the Porcine Anterior Cruciate Ligament Using a Collagen-Platelet Composite. **26**, 1, 2011.

Supplementary figures
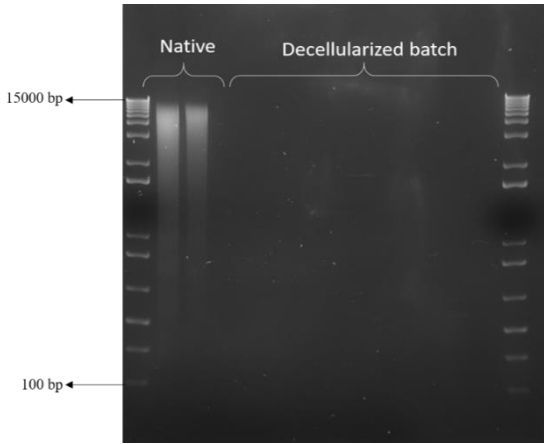
Supplementary Figure S1: Length of DNA fragment. *The size of DNA fragments isolated from decellularized and native tendon. Remaining DNA fragments in decellularized tissue was not observable. DNA isolated from native tissue have intact DNA, which appeared as a smear in the agarose gel.*
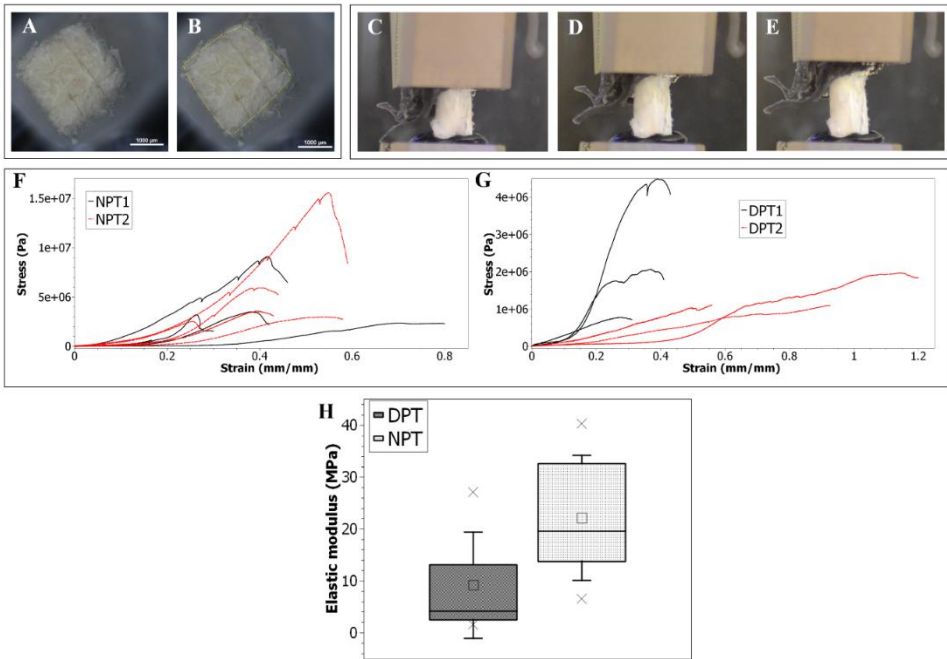
Supplementary Figure S2: Representative images of mechanical tests and stress-strain plots. *(A-E) Mechanical tests were carried out on longitudinal sections obtained from ~1cm long pieces of lyophilized porcine tendons. The cross sectional areas were measured from stereomicroscope images (A) by drawing a polygon around the area using ImageJ (B). The ends of the samples were embedded in epoxy resin to prevent slipping from clamps during tensile testing (C-E). Results displayed large variations between stress-strain plots (F,G). From the linear region of the stress-strain curves,*

the elastic modulus was calculated. (H) Box plot result showing first, second and third quartiles with crosses marking the maximum and minimum values. Results indicated a significant difference in modulus based on a Welch t-test between native and decellularized tissues (p-value 0.04) (NPT=Native tendon, DPT=Decellularized tendon).
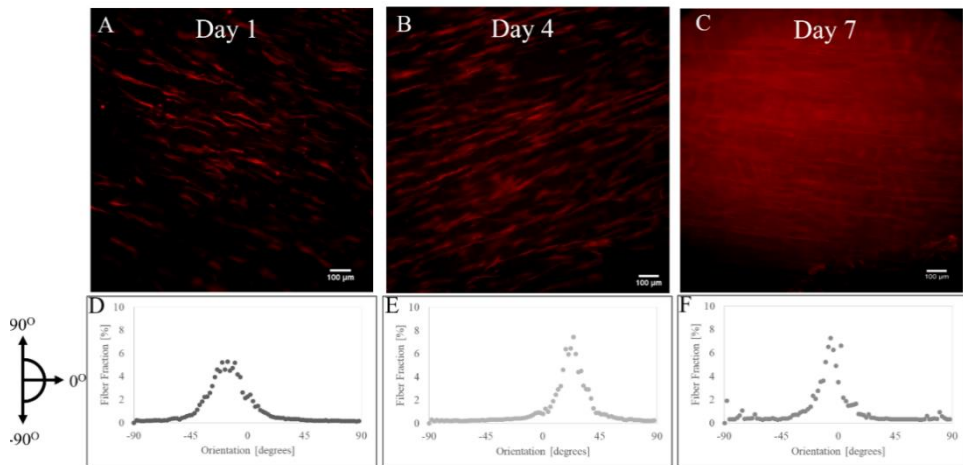
Supplementary Figure S3: Directionality analysis of hMSCs cultured on decellularized tendon sections and directionality analysis of cytoskeleton. (A-C) Representative images f hMSCs cultuted on DTS for day 1 (A), day 4 (B) and day 7 (C). (D-F) Stress fiber directionality of hMCSs at day 1 (-18.26 ± 13.62°) was even more strongly anisotropic at day day 4 (-20.37 ± 10.74°) and day 7 (-6.86 ± 10.74°).
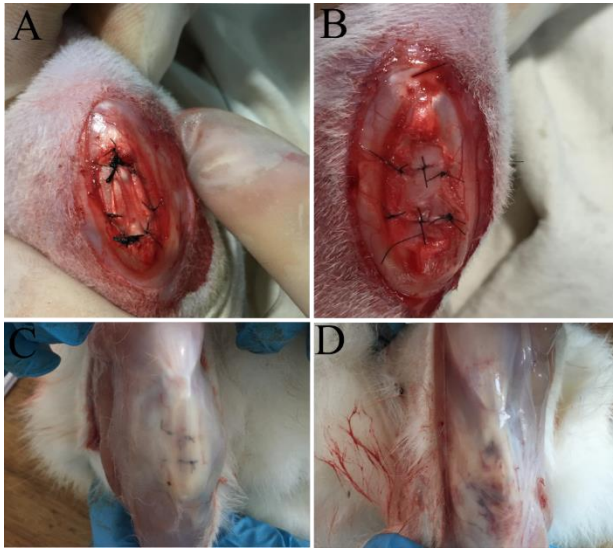
Supplementary Figure S4: Subcutaneous view of the patellar tendon site, before and after implantation of the decellularized and autologous tendon in the surgically produced rabbit patellar tendon defect. *(A) Image of the decellularized tendon (DT) implemented in the rabbit patellar tendon within the 10 × 3 mm incision site. (B) Image of the autologous tendon that was harvested from one knee and implanted in the contralateral knee of the animal as control. (C) Image of the rabbit knee, 6 weeks after implantation of the DT graft. (D) Image of the rabbit knee, 6 weeks after implantation of the AT graft.*

Chapter VIII

General Discussion

They say the history we know begins when ancient Sumerians of Mesopotamia invented the cuneiform. Being the pioneers of many things that we use today, such as wheels, maps, the fundamentals of mathematics and astronomy, they also created the foundation of regenerative medicine. It is documented on Sumerian tablets that between 2100–2000 BC, honey was used as a treatment for wound healing[1]. Since then, humans kept on developing new applications in regenerative medicine as much as technology allows. In 1794 autologous skin grafting and in 1881 cadaveric skin grafting had started, however, it was not until 1952 that cryopreservation of tissue had started to store collected tissues and only in 1987 the term "Tissue engineering" joined the modern medicine and science literature[2]. Thanks to the accumulation of scientific experience and knowledge, today, we are developing new biomaterials that our ancestor would not have imagined, and frankly, they would be dumbfounded to see what we have achieved. By following the footsteps of ancient Sumerians, I too used nature as a source for inspiration and created "Nature-inspired biomaterials" to be used in tendon tissue engineering, which are documented in this thesis.

Recapitulation of main findings

As we obtain more information about human physiology, and advancements in biological and material science, we are getting better at producing biomimetics for regenerative medicine. Variations of synthetic and natural polymers are used as a backbone to make materials with varying biochemical and biophysical properties. Of the available synthetic or natural polymers, collagen steps forward as it is the main structural protein in the connective tissues, as well as other tissues and thus can be used as a joker biomimetic material [3]. In particular, in tendon tissue engineering, collagen receives the lion's share in both *in vivo* and *in vitro* applications[4] as tendon tissue is predominantly composed of collagen[5]. 3D collagen gels[6,7], coating surfaces with soluble collagen[8,9], creating surface topography with collagen[10–13] are different ways of mimicking tendon's collagen nature. In this thesis, in **chapter IV**, we also created surface topographies that are formed by the self-agglomeration of collagen. The surface topographies we obtained are special in many ways. First, the topography in the concentric rings induced elongated cell morphology that tenocytes *in vivo* have. Second, cells experienced the collagen itself as a biochemical cue. Third, formation of three distinct regions upon evaporation with respect to topographical architecture can resemble the heterogeneity that we also have *in vivo*. Although it is arguable that how much of the *in vivo* experience that we can provide tenocytes *in vitro* (considering that tenocytes in the tendon are in limited access to supplies and oxygen, constant exposure to mechanical stimulation and cocktail of growth factors and enzymes), it is valuable to give tenocytes the best we can *in vitro*.

Another way of creating a tendon biomimetic is creating tissue itself or surface topographies with the help of certain technologies, such as 3D printing[14] or electrospinning[15,16]. These methods can enable fine-tuning the biophysical properties (e.g. surface topography, stiffness etc.) and chemical composition. In particular, the advancements in 3D printing technology led researchers to fabricate tissues with complex architectures, such as heart or cartilage, *via* layer-by-layer construction. However, due to the limitations of the printability of biocompatible polymers, such as melting temperature and viscosity, as well as the needle size, fiber dimensions can only be around a few hundred micrometers. This, in particular, is a limiting factor for tendon tissue as the hierarchal fiber organization is around 10-50 μm, and fibril diameters are at nano level[17]. Therefore, laser-assisted bioprinting or inkjet bioprinting are better selections to increase spatial resolution as they could give 10μm resolution and despite their pros, they induce lower cell viability and density[18]. Here, electrospinning is more advantageous as spatial resolution with it can be reduced to tens of micrometers or even nanoscale. Nonetheless, both techniques require specialized equipment, expensive materials and specific protocols that can limit their application in tissue engineering.

As illustrated in **chapter V** and **chapter VI**, we used a simple soft-embossing technique that only requires everyday-lab types of equipment, such as oven or glass microscopy slides. One might argue that the drawback of our technique is standardization. That is, new PDMS from new tendons are prepared after several use of mother PDMS mold to maintain the quality of tendon imprints. However, in theory and in practice, using different tendons to make imprints does not affect the readout. Furthermore, the graft materials from animal or human resources are not their identical replicates. Therefore, maybe in *in vitro* tissue engineering research, we need to loosen the "standardization" belt and give some space to variability in material properties within a certain range. From a translational point of view, the limitation of this technique, though, is that we have only tested polystyrene imprinting from PDMS, but not other biodegradable polymers that have been used in tissue engineering applications. Collagen and silk can be interesting candidates as they have been actively used in tendon regenerative medicine. However, material properties, such as glass transition temperature, of these materials has to be studied more in detail and further optimizations have to be adjusted.

A great number of *in vitro* platforms had established to prove the concept that tenocyte phenotype is correlated with spindle-shaped cell morphology. This is a very important point, as it has been demonstrated by other groups[19–21] -as well as in **chapter V** and our other published work[22]- that tenocytes rapidly dedifferentiate, and pushing cells into an elongated shape recovers dedifferentiated tenocyte phenotype and induce differentiation of stem cells to tenogenic lineage. In fact, as we emphasize in **chapter V** that expression of tenocyte marker genes is positively correlated with cell elongation and negatively correlated with cell area.

Undoubtedly, aspect ratio, as it indicates cell elongation (or spindle-shape), is an important parameter to describe tenocyte shape both *in vivo* and *in vitro*. However, the cell area *in vitro* also indicates cell phenotype with respect to its spreading and tension. Essentially, the more spread the cell, the more tension occurs in the cell to manage attachment. However, in *in vivo,* cell spreading, hence, cell area is lower. Tension also reflects on the focal adhesion (FA) area and length as well as stress fibers. Therefore, smaller cells with fewer stress fibers and smaller FAs is another description to define tenocyte phenotype, as we discussed in **chapter II** and **chapter VI**. However, the cell-biomaterial interface is a complex contact point where the biochemical and biophysical cues from ECM are translated by integrins and focal adhesions to actin cytoskeleton to give a biological response. Although it sounds very straightforward, the story of the organization of actin cytoskeleton and its reflection on the cell phenotype is rather an incomplete picture, especially for tenocytes. One example is the Rho/ROCK/SRF signaling, as we discuss in **chapter II** and **chapter VI**. Considering the way we define tenocyte phenotype with respect to its shape and the cytoskeletal organization does not

really fit with the activity of Rho/ROCK/SRF signaling as described in above-mentioned chapters. Therefore, we need more data to elucidate the regulation of tenocyte phenotype *via* signal transduction pathways. One suggestion can be performing transcriptomics and proteomics experiments in tenocytes possessing different shapes and performing detailed pathway and gene network analysis. As we described in **chapter III**, omics tool preserve a lot of information waiting to be unearthed.

There are different attempts to modulate a healthy tenocyte phenotype *in vitro* (e.g. mechanical stretching, altering biophysical properties of the culture conditions etc.) and thanks to the lessons we learned from these studies, we are getting closer to find alternatives for tendon grafts. So far, using natural (e.g. silk, collagen, chitosan etc) or synthetic polymers (e.g. polylactic acid (PLA), polyglycolic acid (PGA), polylactic-co-glycolic acid (PLGA) etc.) or composite materials have been on the rise in *in vivo* research[4] as they can also be compatible with the above mentioned technologies. However, in clinics, selection of a candidate material is tricky as allografts and autografts are already the golden standards and orthopedic surgeons, as well as patients, have to have good reasons to switch to another potential product.

Therefore, as described in **chapter VII**, in order to produce a graft material to be used in tendon tissue engineering, instead of mimicking the nature, we used the nature itself, the tendon, to create a sense of familiarity in the patient's and surgeon's head as the replacing product is still a tendon. Secondly, in order to create reliability and trustworthiness, we used a highly-accepted process called decellularization[23] and created an acellular tendon by washing out its cells and some proportion of its ECM components. In fact, the very concept of decellularization is fascinating. In analogy, decellularization is selling your house to someone else and taking some of the furniture with you. Finally, we characterized our decellularized tendons in various aspects: biochemically, biomechanically, *in vitro* and *in vivo* biocompatibility to demonstrate the potential of decellularized tendons in regenerative medicine.

Decellularized tissues are already in use in the clinics and have a variety of applications including wound healing, atrial and ventricle repair, pericardial and thoracic wall replacement. For tendon tissue regeneration, GraftJacket® and Allopatch HD™ offer commercial products prepared by the decellularization of human dermis ECM, which has been approved for clinical use by the FDA in 2014 and used in rotator cuff repair[24]. Several other companies are in the market and offer decellularized porcine dermis and intestine submucosa (Conexa™ and CuffPatch™) for Achilles tendon and rotator cuff repair and reinforcement[24]. However, the issue with the current applications is that they are not of tendon origin, hence, may lack the biochemical composition and biomechanical properties that are required for the injured tendon. As mentioned in **chapter I** and **chapter II**, for the maintenance of tendon homeostasis, mechanical

stimulation is very critical and most tendon injuries originate from excessive loading. Another issue with the current tendon grafts is the origin of the tendon. Human materials (both autografts and allografts) are expensive and limited in access. However, there are millions of tendons available as a byproduct of the food industry. Therefore, from a sustainability point of view, once prepared properly, characterized thoroughly both *in vitro* and *in vivo,* xenograft decellularized tendon can be the new golden standard.

Future directions

In this thesis, with the concept of "nature-inspired" in mind, we introduce different methodologies to create surface topographies to manipulate cell shape, investigate cell-biomaterial interface and produce a biomaterial that has a potential to be used in tendon tissue engineering. The data that we report answers several questions regarding tenocyte and tendon physiology, however; it also creates more questions than it answered.

Firstly, in general, when we think about tissue engineering and regenerative medicine, animal source tissues or synthetic/natural polymers come to mind. However, a growing amount of research now demonstrates the potential of plant-based tissue engineering[25–30]. For instance cellulose and alginate are among the most frequently used plant-based polymers and have been demonstrated to be biocompatible in both *in vitro* and *in vivo* studies[28]. In the context of tendon tissue engineering, decellularized celery can promote tenocyte phenotype *in vitro*[31] and scaffolds –with respect to their size and mechanical properties- can withstand the physiological loads that a palmaris longus is exposed to[31]. There are certain aspects that plant-based tissue engineering can become superior to animal-based tissue engineering. Firstly, plants have a very complex tissue organization (porosity, fiber density, network structure etc.) and topographical landscape. This complexity can be used as an advantage to explore their capability to manipulate cell behavior. Secondly, their availability and absence of ethical concerns compared to animal-based materials can make the preference easier. Finally, cross-reactivity that occurs with animal-based tissues can be overcome with plant-based tissues owing to their inherent resistance to degradation in human body, though, long term effects of such non-degradable materials have to be elucidated.

Secondly, as briefly described above, the soft embossing method has great potential to make biomimetics. Indeed, the protocol has to be optimized for the potential polymer of interest, such as melting temperature or duration of embossing. For tissues, such as tendon, that has a uniform topographical order; imprinting surface topography is a great step to create a biomimetic material. More interestingly, in the degenerated tendon, compared to healthy tissue, there is a drastic difference in tissue organization and surface topography, which can be imprinted on a PDMS (with our current method) or other polymers that are more pronounced in the degenerated tendon (such as GAGs or

collagen type III). With this, a tendinopathy model can be created *in vitro* to elucidate the dynamics between healthy and degenerated tendon. Furthermore, the replication of enthesis, which is the bone-tendon end of the tendon, *in vitro* can enable future research to understand this interface better.

The relevance of mechanotransduction in the regulation of tenocyte phenotype cannot be overstated as tenocytes are highly mechanosensitive cells and their fate is highly correlated with their morphology. Therefore, the mechanotransduction pathways that are affected by the cell shape are among the hot topics in tendon research. Rho/ROCK/SRF signaling, for instance, is one of these pathways, as described in **chapter II** in detail, yet we still have to unravel their involvement in steering tenocyte phenotype. This can help us to create biomaterials or small molecules that could target activation (or inhibition) of these pathways and maybe allow *in situ* interference to the injury site. One of the most efficient ways of obtaining such comprehensive information is using transcriptomics or proteomics tools.

The future of tendon tissue engineering can follow the footsteps of regenerative medicine. Essentially, the health of a tendon is influenced by age, smoking, gender or drugs and furthermore the nature of each injury can be different and may need to have a different approach for treatment. Given the various methods to create decellularized tissues with varying sizes and mechanical properties, situation of each patient can be assessed individually and implant can be produced for the need. In fact, with the right technology, similar to stem cell therapies, tendon therapies can be provided. This technology can be a *washing machine* that requires a tendon and the detergents or more like an imprinting machine that creates an implant in the surgery room. For this to happen, clinics and research laboratories should join their power.

References

1. Broughton, G.I.I., Janis, J.E., and Attinger, C.E. A Brief History of Wound Care. Plast Reconstr Surg . **117**, 2006.

2. Berthiaume, F., Maguire, T.J., and Yarmush, M.L. Tissue engineering and regenerative medicine: History, progress, and challenges. Annu Rev Chem Biomol Eng. **2**, 403, 2011.

3. Cen, L., Liu, W., Cui, L., Zhang, W., and Cao, Y. Collagen Tissue Engineering: Development of Novel Biomaterials and Applications. Pediatr Res. **63**, 492, 2008.

4. Alshomer, F., Chaves, C., and Kalaskar, D.M. Advances in Tendon and Ligament Tissue Engineering: Materials Perspective. Bandyopadhyay, A., ed. J Mater. Hindawi, **2018**, 9868151, 2018.

5. Fan, W., Michael, N., and Denitsa, D. Tendon injuries: basic science and new repair proposals. Gen Orthop. **2**, 211, 2017.

6. Garvin, J., Qi, J., Maloney, M., and Banes, A.J. Novel System for Engineering Bioartificial Tendons and Application of Mechanical Load. Tissue Eng . Mary Ann Liebert, Inc., publishers, **9**, 967, 2003.

7. Feng, Z., Tateishi, Y., Nomura, Y., Kitajima, T., and Nakamura, T. Construction of fibroblast–collagen gels with orientated fibrils induced by static or dynamic stress: toward the fabrication of small tendon grafts. J Artif Organs . **9**, 220, 2006

8. Chen, X., Wang, Z., Qin, T.-W., Liu, C.-J., and Yang, Z.-M. Effects of micropatterned surfaces coated with type I collagen on the proliferation and morphology of tenocytes. Appl Surf Sci . **255**, 368, 2008.

9. Mazzocca, A.D., McCarthy, M.B., Arciero, C., Jhaveri, A., Obopilwe, E., Rincon, L., et al. Tendon and bone responses to a collagen-coated suture material. J Shoulder Elb Surg . **16**, S222, 2007. A

10. Yang, S., Shi, X., Li, X., Wang, J., Wang, Y., and Luo, Y. Oriented collagen fiber membranes formed through counter-rotating extrusion and their application in tendon regeneration. Biomaterials. **207**, 61, 2019.

11. Younesi, M., Islam, A., Kishore, V., Anderson, J.M., and Akkus, O. Tenogenic Induction of Human MSCs by Anisotropically Aligned Collagen Biotextiles. Adv Funct Mater. **24**, 5762, 2014.

12. Kishore, V., Bullock, W., Sun, X., Scott, W., Dyke, V., and Akkus, O. Tenogenic differentiation of human MSCs induced by the topography of electrochemically aligned collagen threads. Biomaterials . Elsevier Ltd, **33**, 2137, 2012.

13. Islam, A., Younesi, M., Mbimba, T., and Akkus, O. Collagen Substrate Stiffness Anisotropy Affects Cellular Elongation, Nuclear Shape, and Stem Cell Fate

toward Anisotropic Tissue Lineage. Adv Healthc Mater. **5**, 2237, 2016.

14. Jiang, X., Wu, S., Kuss, M., Kong, Y., Shi, W., Streubel, P.N., et al. 3D printing of multilayered scaffolds for rotator cuff tendon regeneration. Bioact Mater. **5**, 636, 2020.

15. Chainani, A., Hippensteel, K.J., Kishan, A., Garrigues, N.W., Ruch, D.S., Guilak, F., et al. Multilayered Electrospun Scaffolds for Tendon Tissue Engineering. Tissue Eng Part A . Mary Ann Liebert, Inc., publishers, **19**, 2594, 2013.

16. Orr, S.B., Chainani, A., Hippensteel, K.J., Kishan, A., Gilchrist, C., Garrigues, N.W., et al. Aligned multilayered electrospun scaffolds for rotator cuff tendon tissue engineering. Acta Biomater . **24**, 117, 2015.

17. Harvey, A.K., Thompson, M.S., Cochlin, L.E., Raju, P.A., Cui, Z., Cornell, H.R., et al. Functional Imaging of Tendon. 1, 2009.

18. Placone, J.K. Addressing present pitfalls in 3D printing for tissue engineering to enhance future potential. AIP Publishing LLC, **010901**, 2020.

19. Mueller, A.J., Tew, S.R., Vasieva, O., and Clegg, P.D. A systems biology approach to defining regulatory mechanisms for cartilage and tendon cell phenotypes. Nature Publishing Group, 1, 2016.

20. Yao, L., Bestwick, C.S., Bestwick, L.A., Maffulli, N., and Aspden, R.M. Phenotypic drift in human tenocyte culture. Tissue Eng. **12**, 1843, 2006.

21. Mazzocca, A.D., Chowaniec, D., McCarthy, M.B., Beitzel, K., Cote, M.P., McKinnon, W., et al. In vitro changes in human tenocyte cultures obtained from proximal biceps tendon: Multiple passages result in changes in routine cell markers. Knee Surgery, Sport Traumatol Arthrosc. **20**, 1666, 2012.

22. Vermeulen, S., Vasilevich, A., Tsiapalis, D., Roumans, N., Vroemen, P., Beijer, N.R.M., et al. Identification of topographical architectures supporting the phenotype of rat tenocytes. Acta Biomater. **83**, 2019.

23. Gilbert, T.W., Sellaro, T.L., and Badylak, S.F. Decellularization of tissues and organs. Biomaterials. **27**, 3675, 2006.

24. Parmaksiz, M., Dogan, A., Odabas, S., Elçin, A.E., and Elçin, Y.M. Clinical applications of decellularized extracellular matrices for tissue engineering and regenerative medicine. Biomed Mater. **11**, 2016.

25. Indurkar, A., Pandit, A., Jain, R., and Dandekar, P. Plant based cross-linkers for tissue engineering applications. J Biomater Appl. SAGE Publications Ltd STM, 0885328220979273, 2020.

26. Jahangirian, H., Azizi, S., Rafiee-Moghaddam, R., Baratvand, B., and Webster, T.J. Status of Plant Protein-Based Green Scaffolds for Regenerative Medicine Applications. Biomolecules. MDPI, **9**, 619, 2019.

27. Campuzano, S., Mogilever, N.B., and Pelling, A.E. Decellularized Plant-Based Scaffolds for Guided Alignment of Myoblast Cells. bioRxiv. 2020.02.23.958686, 2020.

28. Jovic, T.H., Kungwengwe, G., Mills, A.C., and Whitaker, I.S. Plant-Derived Biomaterials: A Review of 3D Bioprinting and Biomedical Applications. Front. Mech. Eng. . p. 19, 2019.

29. Indurkar, A., Pandit, A., Jain, R., and Dandekar, P. Plant-based biomaterials in tissue engineering. Bioprinting. **21**, e00127, 2021.

30. Iravani, S., and Varma, R.S. Plants and plant-based polymers as scaffolds for tissue engineering. Green Chem . The Royal Society of Chemistry, **21**, 4839, 2019.

31. Negrini, N.C., Toffoletto, N., Farè, S., Altomare, L., and Berry, H.E. Plant Tissues as 3D Natural Scaffolds for Adipose , Bone and Tendon Tissue Regeneration. **8**, 1, 2020.

Summary

N ature, undoubtedly, is the best engineer. It provides an enormous amount of information concerning how cells, tissues and organs form, organize and communicate with each other inharmony. Ergo, throughout the scientific journey of humankind, scientists are constantly inspired by nature to produce materials to reflect nature's genial way of working for human use. For example in industry, highly flexible and deformable properties of octopus became a muse to develop adaptive robotics. Similarly, through inspiration from the surface topography of plant leaves, materials that can reduce particle adhesion or that have self-cleaning and anti-pollution properties were created. In regenerative medicine, application of bio-inspired tissue engineering approach roots back to 1970s when Dr W.T Green used spicules of bone as a tool to mimic cartilage tissue. Ever since, we scientists are heartened by what nature has to offer and not only create solutions to treat pathogenic or dysfunctioning tissues but also try to understand the roots of the problem.

In this thesis, by taking nature as a guide, we aim to develop materials to be used in tendon tissue engineering and further understand the cell-biomaterial interactions concerning cell shape to control cell behaviour. We used **chapter I** to briefly introduce tendon tissue and the tenocyte phenotype cycle and highlighted the motivation of this thesis, which is developing materials to be used in tendon tissue engineering *in vivo* and materials that can mimic *in vivo* tenocyte phenotype *in vitro* to elucidate how tenocyte shape is linked with its phenotype. In **chapter II**, we elaborated the concept of tenocyte phenotype cycle as *"Loop of phenotype"* and elaborated on the role of tenocyte cell shape in healthy and damaged tendon *in vivo*. We further elaborated on how cell shape is manipulated *via in vitro* tools, through which mechanisms the information on cell shape is reflected in downstream phenotypical responses that affect both cell-extracellular matrix and, in return, cell shape. Ultimately, we discussed how this

information can be translated into clinical applications to generate new approaches for tendon tissue engineering. We used **chapter III** to discuss the relevance of omics tools (transcriptomics, proteomics etc.) to investigate cell-biomaterial interactions en route to engineering new biomaterials or explore new potentials of the existing biomaterials.

In **chapter IV**, we did our first attempt to mimic nature. By using the self-agglomeration process of collagen molecules as a starting point, we managed to create three distinct surface topographies to manipulate tenocyte shape and orientation. We elaborated on the impact of cell shape on cell phenotypical markers by making a tendon-biomimetic *in vitro* that possesses native tendon topography obtained *via* soft embossing technology in **chapter V**. Ultimately, this method allowed us to obtain a *plastic tendon* that can be used to alter tenocyte shape, expression of its marker genes and proliferation capacity, and allow tenocytes to experience *in vivo* stimuli during *in vitro* culture. We explored the involvement of cell shape on the regulation of integrin signalling and focal adhesion maturation in **chapter VI**, to have a better understanding of the *Loop of Phenotype*. As a final experimental chapter, we used **chapter VII** to directly apply what nature has provided to find a biomaterial to be used in tendon tissue engineering. For this reason, we adopted the decellularization approach to obtain decellularized tendon.

In summary, this thesis provides new aspects on how to use nature itself to manipulate cell shape and overall cell phenotype and their relation with focal adhesion maturation, which elucidates an important parameter of the mechanisms of mechanotransduction. In **chapter VIII**, we discussed the translational aspect of our findings and their (dis)advantages and encouraged to looking into nature when seeking inspiration.

Samenvatting

D e natuur is zonder enige twijfel de beste ingenieur. Ze bevat enorm veel informatie waarmee ze de vorm, organisatie en communicatie van cellen, weefsels en organen in harmonie orkestreert. Ergo, gedurende de hele wetenschappelijke reis van de mensheid zijn wetenschappers constant door de natuur geïnspireerd om materialen te produceren die de ingenieuze manier van werken van de natuur weerspiegelen. Zo vormden in de industrie de zeer flexibele en vervormbare eigenschappen van de octopus een bron van inspiratie voor de ontwikkeling van adaptieve robotica. Ook de fascinerende oppervlaktetopografie van plantenbladeren stimuleerde onze creativiteit om materialen te ontwikkelen die de aanhechting van deeltjes verminderen of die zelfreinigende en anti-vervuilende eigenschappen hebben. In de regeneratieve geneeskunde gaat de toepassing van bio-geïnspireerde *tissue engineering* terug tot de jaren '70, toen dr. W.T. Green de spicula van bot gebruikte als instrument om kraakbeenweefsel na te bootsen. Sindsdien worden wij wetenschappers bemoedigd door wat de natuur te bieden heeft en creëren we niet alleen oplossingen voor de behandeling van pathogene of niet functionerende weefsels, maar proberen we ook de problemen die we tegenkomen bij de wortel aan te pakken. In dit proefschrift zijn we, door de natuur als leidraad te nemen, op zoek gegaan naar materialen die gebruikt kunnen worden voor peesweefsel *engineering* en wilden we daarnaast de cel-biomateriaal interacties die de celvorm beïnvloeden beter begrijpen om zo het gedrag van de cellen te kunnen controleren. We hebben **hoofdstuk I** gebruikt om het peesweefsel en de fenotypecyclus van tenocyten kort te introduceren. We benadrukten daarin ook onze motivatie voor dit proefschrift, namelijk het ontwikkelen van: *a)* materialen die gebruikt kunnen worden in tendon tissue engineering *in vivo* en *b)* materialen die het *in vivo* tenocyt fenotype kunnen nabootsen in *in vitro* omstandigheden, met als uiteindelijk doel om te verduidelijken hoe de tenocytvorm verbonden is met het fenotype. In **hoofdstuk I** hebben we de tenocyt fenotype cyclus verder onderzocht als een "*looping* fenotype" en zijn we dieper ingedoken op de rol die

de vorm van tenocyten heeft in gezond en beschadigd peesweefsel *in vivo*. We onderzochten ook hoe de celvorm kan worden gemanipuleerd met *in vitro* technieken en identificeerden daarnaast enkele mechanismen waarmee de celvorm invloed uitoefent op een aantal fenotypische reacties die uiteindelijk de *downstream* extracellulaire matrix beïnvloeden. Die matrix kan op zijn beurt weer de vorm van de cel beïnvloeden. Tot slot hebben we in dit hoofdstuk besproken hoe deze nieuw verkregen informatie kan worden vertaald naar klinische toepassingen om nieuwe benaderingen voor peesweefsel *engineering* te ontwikkelen. **Hoofdstuk III** hebben we gebruikt om de relevantie van omics tools (transcriptomics, proteomics, etc.) te bespreken om cel-biomateriaal interacties te onderzoeken die mogelijk de weg kunnen banen naar nieuwe *engineered* biomaterialen of naar nieuwe toepassingen voor bestaande biomaterialen. In **hoofdstuk IV** hebben we een eerste poging gedaan om de natuur na te bootsen. Door het zelfagglomeratieproces van collageenmoleculen als uitgangspunt te nemen, zijn we erin geslaagd drie verschillende oppervlaktetopografieën te maken waarmee de vorm en oriëntatie van tenocyten gemanipuleerd kan worden. In **hoofdstuk V** hebben we de impact van de celvorm op de celfenotypische markers onderzocht door *in vitro* met behulp van *soft embossing* een pees-*biomimetic* te creëren die een pees-eigen topografie bezit. Uiteindelijk heeft deze methode ons in staat gesteld een plastic pees te synthetiseren die gebruikt kan worden om de vorm van de tenocyten, de expressie van *marker* genen en het proliferatievermogen te veranderen. Het maakt het bovendien mogelijk voor tenocyten om *in vivo* stimuli te ervaren tijdens *in vitro* celkweek. In **hoofdstuk VI** hebben we het effect van de celvorm op de regulatie van integrine-signalering en *focal adhesion maturation* onderzocht, om een beter inzicht te krijgen in het "*looping* fenotype". In het laatste experimentele deel van dit proefschrift, **hoofdstuk VII**, maakten we gebruik van een decellularisatie-techniek om van echte pezen geïsoleerd uit paarden een biomateriaal te creëren dat gebruikt kan worden in peesweefsel *engineering*. Samenvattend biedt dit proefschrift nieuwe inzichten in hoe we de celvorm en het celfenotype kunnen manipuleren en het vergroot ons begrip van hun relatie met *focal adhesion maturation*, wat resulteerde in de ontdekking van een belangrijk aspect van mechanotransductie. In het laatste **hoofdstuk VIII** reflecteerden we daarom op deze bevindingen, bespraken we mogelijkheden voor translatie naar de kliniek en de bijbehorende voor- en nadelen, en moedigden we onderzoekers aan om zich tot de natuur te wenden bij het zoeken naar inspiratie.

Özet

D oğa hiç şüphesiz ki en iyi mühendis ve bize hücrelerin, dokuların ve organların nasıl oluştuğu ve birbirleriyle nasıl bir uyum içinde haberleştiği konusunda muazzam miktarda bilgi veriyor. İnsanlığın bilimsel tarihi süresince, bilim insanları sürekli doğadan ilham alıp, doğanın genel çalışma seklini yansıtan malzemeler üretip insan kullanımına sunulmuştur. Örneğin, bir ahtapotun esnek ve bicimi bozulabilen yapısı ayarlanabilir robotik çalışmalarında kullanılan köpüğe ilham vermiştir. Yine benzer bir şekilde, bitki yapraklarının yüzey topografisinden ilham alınarak parçacık yapışmasını azaltan, kendi kendini temizleyen, kirlenme karşıtı özellikleri olan malzemeler üretilmiştir. Biyolojiden esinlenen doku mühendisliğinin rejeneratif tip alanında kullanılması 1970'lerde Dr. W.T Green'in kemik sivri uçlarını kıkırdağı taklit etmek için bir araç olarak kullanması ile baslamistir. O zamandan beri doğanın sundukları bilim insanlarını çalışmayan ya da sorunlu dokuları iyileştirmek için ve bu sorunların temelini anlayabilmek için yüreklendirmiştir

Tezimde doğayı rehber alarak, tendon doku mühendisliğinde kullanılmak üzere malzeme geliştirmeyi ve aynı zamanda hücrelerle biyomalzeme arasındaki ilişkiyi hücre seklini manipüle ederek, hücre sekli ve genel fenotipi arasındaki ilişkiyi çalışmayı amaçladık. **Bölum I**'i tendon dokusunu ve tenosit fenotip döngüsünü tanıtmak, tezimin konusunu sizlere aktarmak için kullandım. **Bölum II**'de, tenosit fenotip döngüsü kavramını "fenotip döngüsü" olarak detaylandırdık ve tenosit hücrelerinin şekillerinin yaşayan koşullarda sağlıklı ve hasarlı tendon üzerindeki rolünü detaylandırdık. Daha sonra, hücre şekillerinin laboratuvar ortamındaki araçlarla nasıl değiştirildiğine, hücre seklinin bilgisinin hangi aşağı akis işleyiş ile hücre ve hücre matrisi arasındaki etkileşimi ve hücrenin kendi şeklini etkileyen fenotip cevaplara aktarıldığını detaylandırdık. Nihayetinde bu bilgilerin nasıl tendon mühendisliğinde yeni yaklaşımlar geliştirmek amaçlı klinik uygulamaya dönüştürücü olabileceğinden bahsettik. **Bölum III**'u omics araçlarının (transcriptomics, proteomics vb) hücre ve biyomalzeme arasındaki etkileşimlerin araştırılmasındaki yerini ve bunun yeni biyomalzemelerin

tasarlanmasında veya hali hazırda bulunan biyomalzemelerin yeni potansiyellerinin bulunmasında nasıl kullanılabileceğini tartışmak için kullandık. **Bölüm IV**'de doğayı taklit etmekteki ilk cabamızı yaptık. Kolajen moleküllerinin kendi kendine yığılma surecini başlangıç noktası olarak alarak tenositlerin seklini ve yönelimlerini değiştirmek için 3 farklı yüzey topografyası üretmeyi başardık. Hücre seklinin hücre fenotip belirteçlerine etkisini laboratuvar ortamında yumuşak kabartma tekniğini kullanarak yerli tendon topografisini sahiplenen tendon-biyomimetiği yaparak nasıl çalıştığımıza **Bölüm V**'de bahsettik. Nihayetinde bu teknik bizim tenosit seklini, belirteç genlerinin ifadesini ve çoğalma yetisini etkilemekte kullanılabilecek plastik tendon üretmemizi ve tenositlerin yasayan koşullardaki uyarıcıları laboratuvar ortamındaki kültürde deneyimlemelerini sağladı. "Fenotip döngüsünü daha iyi anlayabilmek için **Bölüm VI'da** hücre seklinin Integrin sinyal yolak kontrolündeki ve fokal adezyon olgunlaşmasındaki rolünü inceledik. Son deneysel bolum olan **Bölüm VI** de doğanın sağladıklarını tendon dokusu mühendisliğinde doğrudan biyomalzeme olarak kullanılması için yazdık. Bu sebeple, hucresizlestirilmiş tendon elde etmek için hücresizleştirme yöntemini kullandık. Son olarak **Bölüm VII'**de sonucları ve genecek fırsatlarini tartistik.

Özetle, bu tez doğanın kendisini nasıl hücrelerin şekillerini ve genel olarak fenotiplerini etkilemek için kullanabileceğimiz ve bunun mekanotransduksiyon işleyişinde önemli bir parametre olan fokal adezyon olgunlaşmasındaki rolüne yeni bakış açıları getirmektedir. Son bolümde bulgularınızın klinik alanına çeviri yönünü ve avantaj ve dezavantajlarını tartışıp, ilham arayışı içerisinde olduğunda doğaya dönülüp bakmayı cesaretlendirdik.

Acknowledgements

First and foremost, I would like to begin with thanking all the rats and pigs whose tendons enabled the production of the data presented in this thesis.

🦅

When I started my PhD four years ago, one of the PhD students who was finishing his thesis told me that "I remember being in your position, you would not believe how fast these four years will pass". Of course, I believed him because they said the same thing for high school, university, and even kindergarten! What I did not expect is that it felt like more than four years (I salute you Albert Einstein). In so many ways, scientifically, emotionally, awarenessly (not a word), I am a different person; and for this, I would like to thank everyone who is present or passed in transit in my life from the bottom of my heart.

🦅

During my Master degree, there was only one experiment that I had to do: Western blot. For two years, 5 days a week I did western blots. All of my friends were doing the cool stuff (qPCRs, stainings, SEMs, TEMs etc.), but I stuck with western blots and occasional qPCRs and some stainings. I remember, I felt very diffident about it because I thought "Who would hire someone who only knows western blot?". Well, **Jan de Boer** did! So **Jan**, thank you for giving a neuroscientist, who was butchering zebrafish brains more often than an Albert Hein butcher, butchering pigs and cows to feed an average Dutch person with 77 kg of meat per year (true stat, you can Google), a chance to butcher tendons from pigs and rats and to show her the awesomeness of being a scientist! I always say, "Once you survive work discussion meetings with Jan, the rest of the presentations you give anywhere else is just a picnic" (except for PhD defence...), so thank you for challenging me. Finally, thank you for always encouraging my unconventional way of making science and heartening me to follow my craziness. I don't think any other supervisor would be that patient with my too-out-of-box ideas. May the force always be with you.

Dear **Jasper**, I think I am one of the lucky PhD students who got to be supervised by you and I don't know what I did to deserve that. I learned a lot from your patience, political correctness (and incorrectness), and the importance of having "me" time. I am looking forward to making the ultimate tendon/ACL with you. I hope your future student will be as awesome as I was (though I would not be optimistic about that…). Thank you for the awesome 4 years!

My female role models; dear **Aurélie**, you are an amazing person and I am genuinely sad that I did not get to spend more time with you. You taught me so many things in only one and a half years. Thank you a million times to the PhD gods for allowing me to get to know you. Dear **Patricia**, the funniest person I know, I will ALWAYS remember the time you only grabbed your laptop after the fire alarm ans subsequent hotel evacuation. This was a great lesson for me: data comes before all! Thank you for this and other memorable moments. Many more to come!

I would also like to thank the assessment committee, **Prof. Dr. Carlijn Bouten**, **Prof. Dr. Cornelis Storm**, **Dr. Pieter Emans**, **Prof. Dr. Stephen Badylak** and **Dr. Bert van Rietbergen** for their time and critical assessment of this thesis.

Of all the people I have met in the past four years, **Dr. Steven Albert Vermeulen** is one of the most special people. He is my tendon buddy, sci-fi nerd buddy, constantly-editing-my-manuscripts buddy, teaching-me-almost-everything-I-learned-in-my-PhD buddy, the-one-who-almost-made-me-cry-after-reading-his-thesis acknowledgement buddy. I am so happy that I got to spend this journey with you. I am also incredibly proud of the scientist you are. However, I am not thanking you for making me feel like crap because of your 'hardworkness' and my 'not-so-hardworkness', and making me look like a full-diaper. I wanted to say I will miss you but I see you everywhere, so please stop shooting videos. I wish you all the happiness and beer in the world!

Dear BiS crew: **Sultan**, you became my *Can Yoldasi* in this *issiz memleket*. You are one of the people that I genuinely say "what would I do without her", so thank you for taking my hand and walking with me in this journey. Iyki varsin kalp kalp. **Phani**, first of all, I made my peace with your intimate bromance with Deniz. Cool. Cool cool cool cool. I remember the day that I interviewed with you and then we walked to the train station together and I offered you a cigarette. But I don't remember whether you took it or not because smoking kills brain cells. Good that we quit. Thanks bro for being with me in this journey. I am so

glad that I had a colleague, nej, I have a friend like you. I hope you won't cry out of laughter while reading these but cry because I am leaving. Will miss you bro! **Memo**, I wish you were here in the past four years, we could have had a lot of fun other than doing KFC at home. I am very sorry to corrupt a nice guy like you, but as I always say "*icinde var kardesim ben nabayim*". I am so glad to know you and get to call you a life-time-friend. Wish you all the happiness kalp kalp kalp. **Burcu**, **Alex**, **Nusrat**, **Jorge**, **Katinka**, **Roel**, **Miguel** and awesome master students: I am grateful for the beautiful time that we spent together! I hope life will only bring you laughter and occasional tears because of that laughter.

My dear **Elizabeth**, I think the reason that I ended up in The Netherlands was because I was destined to meet you and become your ultimate GalPal. You are my hero, my Royal Family guide, my English Teacher, my artist. I hope life will give you an endless number of musical instruments, tea, and lots of Turkish food (together)!

My amazing friends at BMT! **Cas**, you are a great office friend and a perfect guide to Dutch political system! Thank you for all the lessons! **Tara**, I am so going to miss our chats that are exclusively about our amazing PhD and how blessed we are! **Sana**, thank you for introducing me to the best food in the world and all the good "gossips" that we shared! **Martijn**, **Dylan**, **Suzanne**, **Ester**, **Tamar**, **Jonnick**, **Cansu**, **Hans Martin**, **Larissa**, **Celien**, **Dewy**, **Marloes**, **Michelle**, **Jan-Willem** and **Bregje**, thank you for being amazing lab and office mates.

❦

To my cBiTE family: **Hebelz**, I have so many words but *I have no money*. Thank you for welcoming me with the warmest heart to cBiTE and for showing me the best place in the whole Netherlands, *nee*, the world: Efteling and making me part of your gang. You are an awesome human being and I am so glad to know you. And my name is Aysegul not Ayse. **Marloes**, the woman of laughter, you are the happiest person I know. Please tell me, what is your secret? **Pascal**, thank you for being my personal doctor in a country where seeing a doctor is itself a challenge. I am so glad that we are still friends after me sending you some disgusting health-related pictures. It is good that you will be an eye doctor because I am getting old and I guess I will need a personal eye doctor in the *foreseeable* future. **Saïd**, ma brother from another mother! You are an awesome, kind person, but also the only person in the whole world who eats a ginger as if it is nothing. Will miss you a lot!!! **Urnaa**, you are my safe-zone in MERLN. When I was angry at someone/something (which happened more often than it

should), I used to come to you and express myself in the best way in Turkish, and you listened to me without any complaints. Thank you for that. Also, you and Emre made the cutest baby girl and I really think she should be a model. Please consider this pleaseeeeee. **Nadia**, **Nick** and **Jasia**, thank you for the great memories and I wish you all the happiness in the world! To my **MERLN** family: **Fiona**, my love! **Afonz**, ma brothaaaaa! **Zarina**, the-most-beautiful-woman-that-ever-existed! I wish for a world where we could all be together forever.

Other amazing people in my life! **Zeynep**, *dayı*! *Nereden nereye be*! I vividly remember the day we were shouting "Dayi, naptin" at each other in a random park in Stockholm, and you were taking care of me when I was sick in Maastricht. I hope you never let me go! **Esin**, canim danom. Sen olmasan ben gercekten yok olurdum, inflak ederdim, lablardan kalirdim, cuzdanimi/telefonumu kirk kere kayip ederdim. Hayatima anlam katiyosun danom, seni cok seviyorum. **Ozgus**, **Burcu** ve **Onur**, tez zamanda doktoranizi bitirip klube katilmanizi temenni ediyorum. **Seren** ve **Gokhan**, siz benim icin cowsunuz. Ayni hizaya gelmeye calisan 7'lersiniz. Siyah 13 sunuz. Bi kere gelsin abi hayatimiz kurtulursunuz. James Bondsunuz. Cilt bakimimsiniz. Jocko'msunuz. Iyki varsiniz. So long GBs!

Deniz, sana her baktigim an "Kiz seni alan yasadi, dertlerini de bosadi, mest oldum vallahi jest oldum ooo" caliyor kafamda. Tabii bir de hep soruyorum kendime, bu cocuk gunesi gulusune nasil sigdiriyor diyorum, cunku kalbimi collere donduruyor. Sensiz bu hayat rulete oturup surekli oynadigin sayinin yanindaki sayinin cikmasi gibi olurdu. Seni cok seviyorum Denkom! Iyki benimsin!

Canim **Annem, babam**; bana caliskanligi, ahlaki, dogruyu yanlisi ayirabilmeyi, haksizliga sesimi cikartmayi, herzaman pozitif ve mutlu olmayi, hayatta guclu olmayi ogrettiginiz icin ve mukemmel karadeniz genleri size minnettarim. Canim babam, senin egitime verdigin onem, benim ve ablalarimin bu kadar bagimsiz ve guclu birer Kadin olmamizi sagladi, ve bunu icin dunyada yeterince tesekkur yok. *Dunyanin en iyi babasi sensin*. Canim annem, senin yemek yapma becerilerini alamadim, ama caliskanligi, durustlugu, hosgorulu olmayi ver HER ZAMAN mutlu ve positif olmayi senden ogrendim. Iyki benim annemsin. **Abi**, **Elif**, **Habis**, sizinle buyumek ve sizden ogrenmek ve **Hakan'a** eziyet etmek beni dunyanin en sansli insani yapti! Sizi cok seviyorum!

Curriculum Vitae

Aysegul was born in February 12ᵗʰ , 1991 in Turkey. During high school years, her interest grew into science; therefore, she majored in Biology, Physics, Chemistry and Mathematics. In 2010, she moved to Ankara to study Biological Sciences in Middle East Technical University where she obtained more knowledge regarding various aspects of Biology. She did an internship at University of North Carolina at Chapel Hill in United States of America to explore applications of the theoretical knowledge regarding protein-DNA interactions. However, Aysegul found neuroscience, in particular, more interesting. Therefore, in 2015, she started her Master's studies in Neuroscience at Bilkent University in Ankara. Her Master research was on investigating the differences of the expression of certain synaptic proteins in male/female and young/old zebrafish. She obtained Master's degree in January 2017.

Meanwhile, Aysegul grew interest in translation aspect of science, and in particular, tissue engineering. Subsequently, in February 2017, Aysegul started as a PhD student in MERLN under supervision of Professor Jan de Boer on the Tendon Therapy Train project aiming to find biomaterials to be used in tendon tissue engineering. Within her 4 years of PhD journey, Aysegul moved from Maastricht University to Eindhoven University of Technology to complete her PhD studies. In the past 4 years, Aysegul involved in several projects and collaborations that aims to study cell-biomaterial interactions by creating nature-inspired biomaterials. In this context, she worked on the development of decellularized tendons and ACL from porcine and human origin as well as *nature inspired in vitro* tools to explore cell shape.

List of publications

Steven Vermeulen, Aliaksei Vasilevich, Dimitrios Tsiapalis, Nadia Roumans, Pascal Vroemen, Nick RM Beijer, **Aysegul Dede Eren**, Dimitrios Zeugolis, Jan de Boer. Identification of topographical architectures supporting the phenotype of rat tenocytes. *Acta Biomaterialia*, 2019

Ana I Gonçalves, Dominika Berdecka, Márcia T Rodrigues, **Aysegul Dede Eren**, Jan de Boer, Rui L Reis, Manuela E Gomes. Evaluation of tenogenic differentiation potential of selected subpopulations of human adipose-derived stem cells. *Journal of Tissue Engineering and Regenerative Medicine*, 2019

Aysegul Dede Eren, Ravi Sinha, Egemen Deniz Eren, Yuan Huipin, Sultan Gulce-Iz, Henriette Valster, Lorenzo Moroni, Jasper Foolen, Jan de Boer. Decellularized Porcine Achilles Tendon Induces Anti-inflammatory Macrophage Phenotype *In Vitro* and Tendon Repair *In Vivo. Journal of Immunology and Regenerative Medicine*, 2020

Aysegul Dede Eren, Aliaksey Vasilevich, E Deniz Eren, Phanikrishna Sudarsanam, Urandelger Tuvshindorj, Jan De Boer, Jasper Foolen. Tendon-derived biomimetic surface topographies induce phenotypic maintenance of tenocytes *in vitro. Tissue Engineering Part A*, 2020

Tara C Schmitz, **Aysegul Dede Eren**, Janne Spierings, Jan de Boer, Keita Ito, Jasper Foolen. Solid-phase silica-based extraction leads to underestimation of residual DNA in decellularized tissues. *Xenotransplantation*, 2020

Steven Vermeulen, Nadia Roumans, Floris Honig, Aurélie Carlier, Dennie GAJ Hebels, **Aysegul Dede Eren**, Peter Ten Dijke, Aliaksei Vasilevich, Jan de Boer. Mechanotransduction is a context-dependent activator of TGF-β signaling in mesenchymal stem cells. *Biomaterials*, 2020

Aysegul Dede Eren[¥], E Deniz Eren[¥], Twan JS Wilting[¥], Jan de Boer, Hanneke Gelderblom, Jasper Foolen. Self-agglomerated collagen patterns govern cell behaviour. *Scientific Reports*, 2021

[¥]Authors contributed equally

Liangliang Yang[¥], Sara Pijuan-Galito[¥], Hoon Suk Rho[¥], Aliaksei S Vasilevich[¥], **Aysegul Dede Eren**[¥], Lu Ge, Pamela Habibović, Morgan R Alexander, Jan de Boer, Aurélie

List of publications

Carlier, Patrick van Rijn, Qihui Zhou. High-Throughput Methods in the Discovery and Study of Biomaterials and Materiobiology. *Chemical Reviews*, 2021

¥Authors contributed equally

Steven Vermeulen, Floris Honig, Aliaksei Vasilevich, **Aysegul Dede Eren,** Nadia Roumans, Aurelie Carlier, Manuel Romero, Paul Williams, Jorge Alfredo Uquillas, Jan de Boer. Expanding Biomaterial Surface Topographical Design Space through Natural Surface Reproduction. *Advanced Materials,* 2021

Aysegul Dede Eren, Steven Vermeulen, Tara C. Schmitz, Jasper Foolen, Jan de Boer. The loop of phenotype: dynamic reciprocity links tenocyte morphology to tendon tissue homeostasis. *Under review, Biomaterials*

Aysegul Dede Eren, Amy W.A. Lucassen, Urandelger Tuvshindorj, Roman Truckenmüller, Stefan Giselbrecht, Deniz Eren, Mehmet Orhan Tas, Phanikrishna Sudarsanam, Jan de Boer. Cells dynamically adapt to surface geometry by remodelling their focal adhesions and actin cytoskeleton. *In preparation*

Egemen Deniz Eren, Wouter Nijhuis, Freek van der Weel, **Aysegul Dede Eren**, Sana Ansari, Paul Bomans, Heiner Friedrich, Ralph Sakkers, Harrie Weinans, Gijsbertus de With. Multiscale hierarchical bone organization in a case of osteogenesis imperfecta type IV compared to control bone. *In preparation*